UNIVERSITA' DEGLI STUDI DI PARMA

DIPARTIMENTO DI CHIMICA GENERALE ED INORGANICA,
CHIMICA ANALITICA, CHIMICA FISICA

Ph.D. Thesis in Chemical Sciences

Synthesis and Characterization of Zwitterionic Metallates and Molecular Clusters

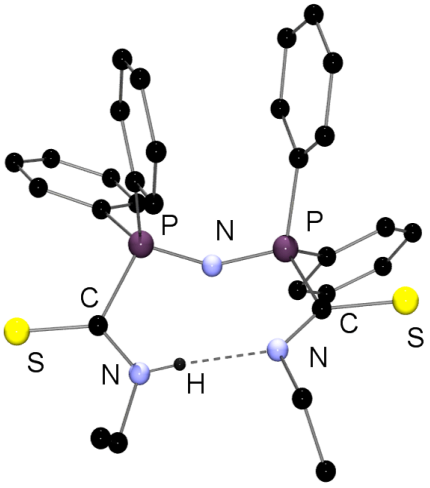

Advisor

Prof. Daniele Cauzzi

Ph.D. candidate

Dr. Massimiliano Delferro

2006 – 2008

Contents

To Daniela and Giorgio,

1

General Introduction

Zwitterionic compounds are defined by the on-line IUPAC Compendium of Chemical Terminology[1] as "Neutral compounds having formal unit electrical charges of opposite sign". However, zwitterionic metal complexes need a more detailed description, which has been given by Remi Chauvin in his review concerning zwitterionic organometallates.[2] Indeed, couples of opposite charges may be easily evidenced in the Lewis structures although it is often possible to define resonance forms in which all the atoms are neutral. In this case the molecule cannot be called *zwitterion*. In addition, single positive and negative charges can be delocalized over a group of atoms, as carboxylate groups in amino acids and betaines. Single, nonpolymeric, neutral molecules containing more than one charge couple[3] may be generally called "multizwitterions," different from polyzwitterions, which refers to polymers containing zwitterionic chain substituents.[4] If further positive or negative charges are present, ionic molecules can be called zwitterion-cations or zwitterion-anions in order to distinguish them from ordinary ions.[5]

As a consequence of the charge separation, a very strong molecular electric dipole moment is observed depending on the distance between the charges barycenters. This strong dipole and ambiphilicity allow these "neutral ions" to be applied in a wide range of fields. Molecular zwitterions or zwitterionic polymers are studied as stationary phases[6] or eluents[7] in liquid chromatography, as drugs,[8] and as NLO chromophores.[9] As far as zwitterionic coordination compounds are concerned, their most important and outstanding application is in metallocene catalyzed Ziegler-Natta polymerization[10] or even as carriers for membranes.[11]

Zwitterionic metal complexes can be prepared following different strategies, the most common being as follows: (a) by reaction of zwitterionic ligands with metal species[12] (b) by generating the charge separation upon coordination;[13] and (c) by association of a positive (or negative) metal center with an oppositely charged ligand maintaining the charge separation.[14] In addition, zwitterionic complexes can be divided in two main categories; the most common one regroups complexes in which the metal center bears the formal positive charge, while the second comprises the still uncommon "zwitterionic metallates" whose metal center is formally negative.

Since the 1870s, the reaction of PEt_3 with EtNCS is know as a route to obtain ethyl isocynide (Figure 1). In this reaction, the transfer of a sulfur atom from the NCS group to the phosphorus center is responsible for the formation of the corresponding phosphano-sulfide ($Et_3P{=}S$) and EtNC. In fact, in the reaction $PR'_3 + RNCS = R'_3PS + RNC$, a zwitterionic

intermediate is formed, which is, in turn, dissociated in R'$_3$PS and RNC. This process is believed to proceed by the formation of a three-membered C-P-S non-zwitterionic ring (Scheme 1).[15]

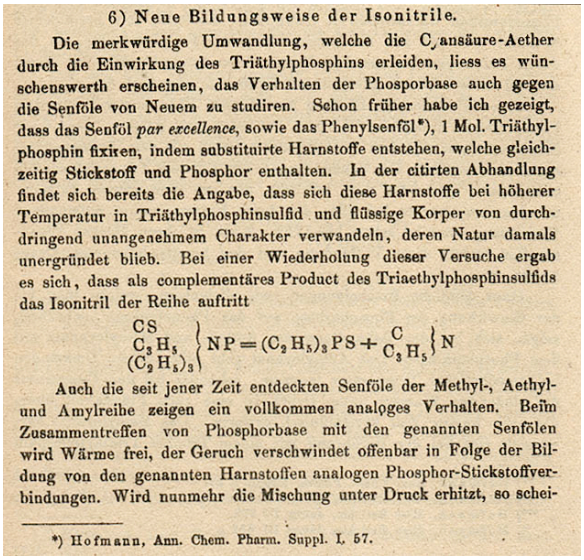

6) Neue Bildungsweise der Isonitrile.

Die merkwürdige Umwandlung, welche die Cyansäure-Aether durch die Einwirkung des Triäthylphosphins erleiden, liess es wünschenswerth erscheinen, das Verhalten der Phosporbase auch gegen die Senföle von Neuem zu studiren. Schon früher habe ich gezeigt, dass das Senföl *par excellence*, sowie das Phenylsenföl*), 1 Mol. Triäthylphosphin fixiren, indem substituirte Harnstoffe entstehen, welche gleichzeitig Stickstoff und Phosphor enthalten. In der citirten Abhandlung findet sich bereits die Angabe, dass sich diese Harnstoffe bei höherer Temperatur in Triäthylphosphinsulfid und flüssige Korper von durchdringend unangenehmem Charakter verwandeln, deren Natur damals unergründet blieb. Bei einer Wiederholung dieser Versuche ergab es sich, dass als complementäres Product des Triaethylphosphinsulfids das Isonitril der Reihe auftritt

$$\left.\begin{matrix} CS \\ C_3H_5 \\ (C_2H_5)_3 \end{matrix}\right\} NP = (C_2H_5)_3PS + \left.\begin{matrix} C \\ C_3H_5 \end{matrix}\right\} N$$

Auch die seit jener Zeit entdeckten Senföle der Methyl-, Aethyl- und Amylreihe zeigen ein vollkommen analoges Verhalten. Beim Zusammentreffen von Phosphorbase mit den genannten Senfölen wird Wärme frei, der Geruch verschwindet offenbar in Folge der Bildung von den genannten Harnstoffen analogen Phosphor-Stickstoffverbindungen. Wird nunmehr die Mischung unter Druck erhitzt, so schei-

*) Hofmann, Ann. Chem. Pharm. Suppl. I. 57.

Die dem Schwefelkohlenstoff-Additionsprodukt analogen, von A. W. Hofmann entdeckten, gelben Additionsprodukte mit Senfölen[1]) entsprechen zweifellos der ersteren von den beiden möglichen Formeln:

I. $(C_2H_5)_3P(S)C:N.C_6H_5$ II. $(C_2H_5)_3P(N.C_6H_5)C:S$

[1]) Ann. d. Chem. Suppl. I, 36 u. 57.

Figure 1. *Chem. Ber.*, 1870 and 1907

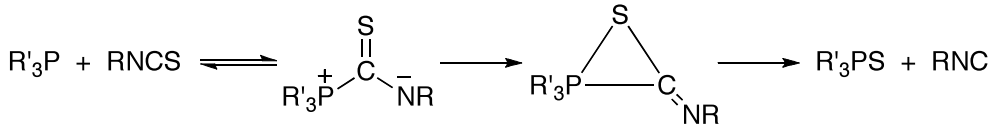

Scheme 1. Addition reaction of alkylphosphanes to isothiocyanates and subsequent transformation in phosphano-sulfide and isocyanide.

Similar reactions of R_3P with CS_2 give zwitterionic adducts R_3PCS_2, whose ligating properties have been reviewed.[12]

Data reported in the literature indicates that only alkylsubstituted phosphanes, R_3P, or phosphanoamines, $(R'_2N)_xR''_{(3-x)}P$, which contain P-N bonds, can react with isothiocyanates. The zwitterion formation is an equilibrium depending on R, R', and the solvent, and it is initiated by a nucleophilic attack of the phosphorus center on the carbon atom of the heterocumulene group.[16,17] The higher nucleophilic character of the P atom in phosphanoamines is due to the N lone pair delocalization, evidenced in $Ph_2PNHPPh_2$

(diphenylphosphineamine, PNP) by the planarity of the P-NH-P system.[18]

Four kinds of products can be obtained in the reaction of PNP with RNCS, depending on R, the temperature, and the PNP/RNCS molar ratio (Scheme 2).

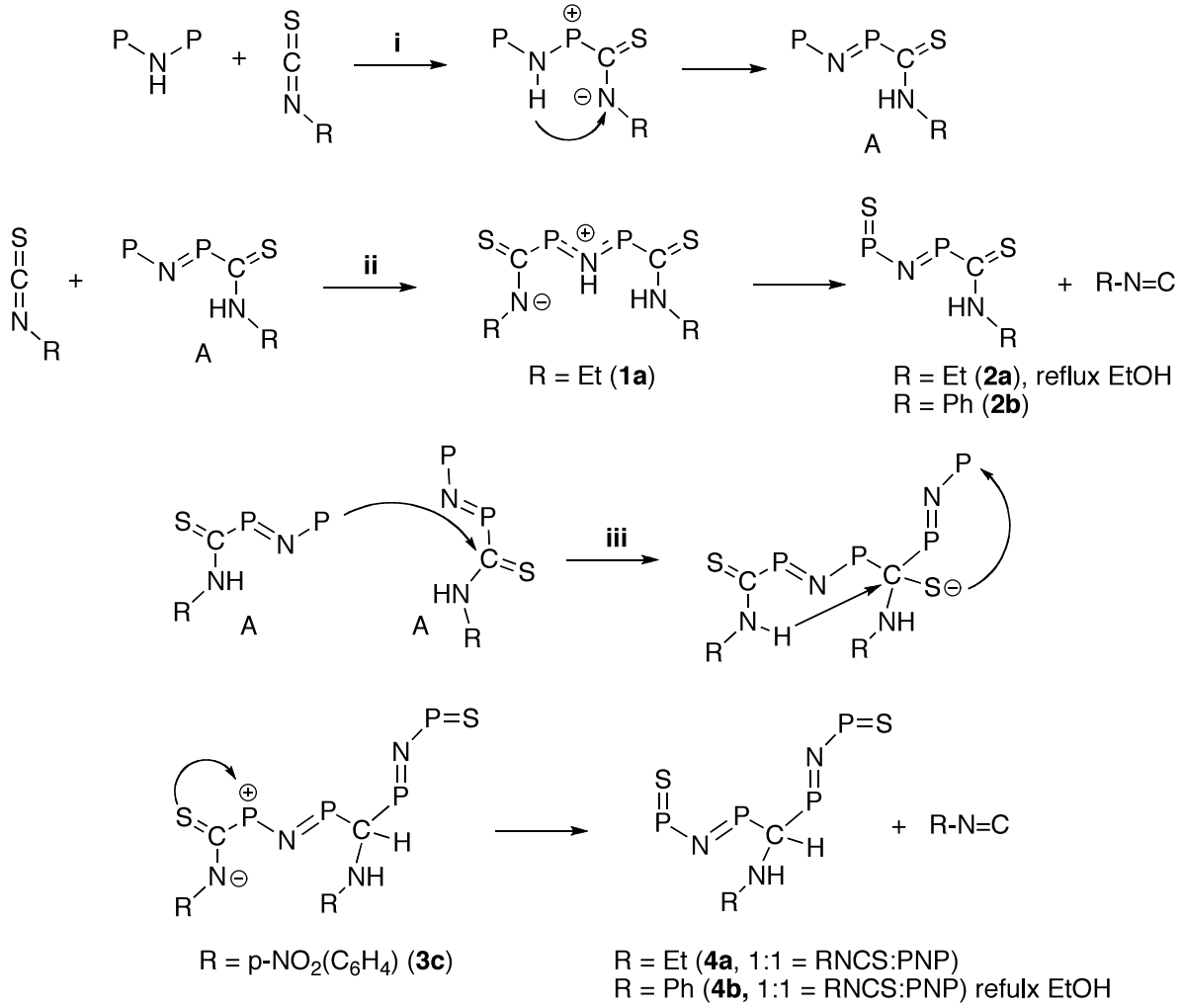

Scheme 2.

Reaction **i** represents the primary attack of PNP on RNCS giving the proposed intermediate A, via a proton migration. Intermediate A cannot be isolated because of the reactivity of its free P atom, which is able to react further with RNCS (pathway **ii**) or with another A molecule (pathway **iii**) on the electrophilic CS group. Along pathway **ii**, the zwitterionic compound **1** is obtained, which, in turn, can rearrange to afford quantitatively compound **2** and an isocyanide molecule. Along pathway **iii**, two molecules of A react with each other through the attack of the tertiary phosphorus of one molecule on the PC(S)N carbon atom of the second one. The resulting intermediate undergoes an S-atom transfer from the C-S group

to the free P atom, probably through the formation of a C,P,N,P,S five-membered ring. After the S-atom transfer, the C atom is formally negative and can accept the thioamidic proton which migrates from N to C, leading to the formation of a zwitterionic N-C(S)P^+ "arm" (compound **3**). An isocyanide molecule can be finally released by rearrangement of **3** into **4**, in the same way as the rearrangement of **1** to **2**. In compound **2**, the formation of the P=S group from the PC(S)N zwitterionic arm with the release of a RNC molecule depends on the temperature. When R = Ethyl, compound **1a** (HEtSNS, Figure 2) is obtained in high yield (100%) in EtNCS neat.

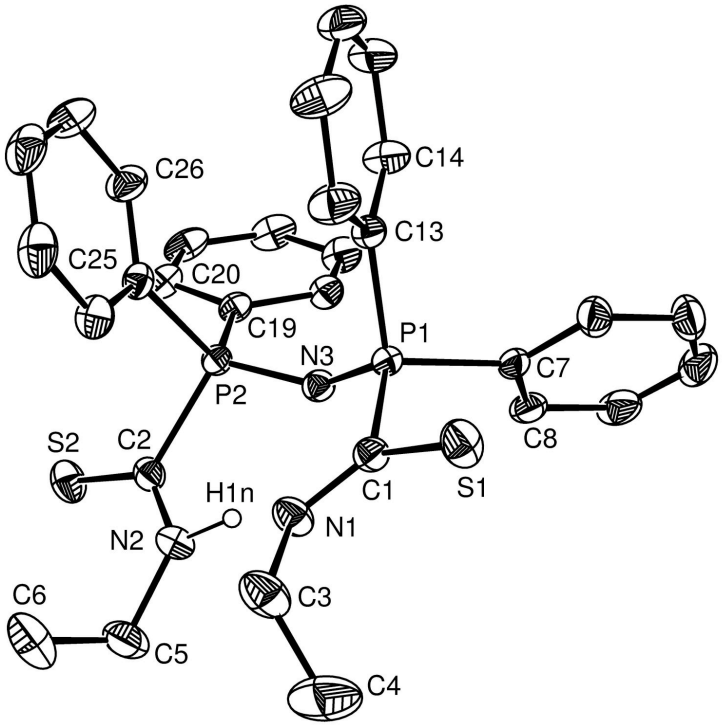

Figure 2. Ortep Plot of **1a**. Thermal ellipsoids are drawn at 30% probability level. H atoms are omitted for clarity, except for H1n.

Compound **2a** can be obtained almost quantitatively (50% after recrystallization) by reacting PNP and EtNCS (1:2 ratio) in refluxing ethanol, or by refluxing an ethanol solution of compound **1a** (Figure 3).

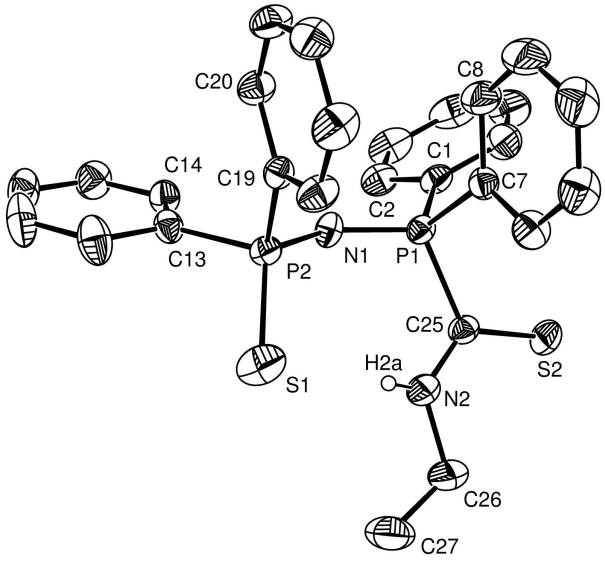

Figure 3. Ortep Plot of **2a**. Thermal ellipsoids are drawn at 30% probability level. H atoms are omitted for clarity, except for H2a.

When R = Et and the ratio of PNP/EtNCS is 1:1, compound **4a** can be obtained (20–30% yield, together with **1a**, **2a** and unreacted PNP), whereas formation of compound **3a** is not observed (Figure 4).

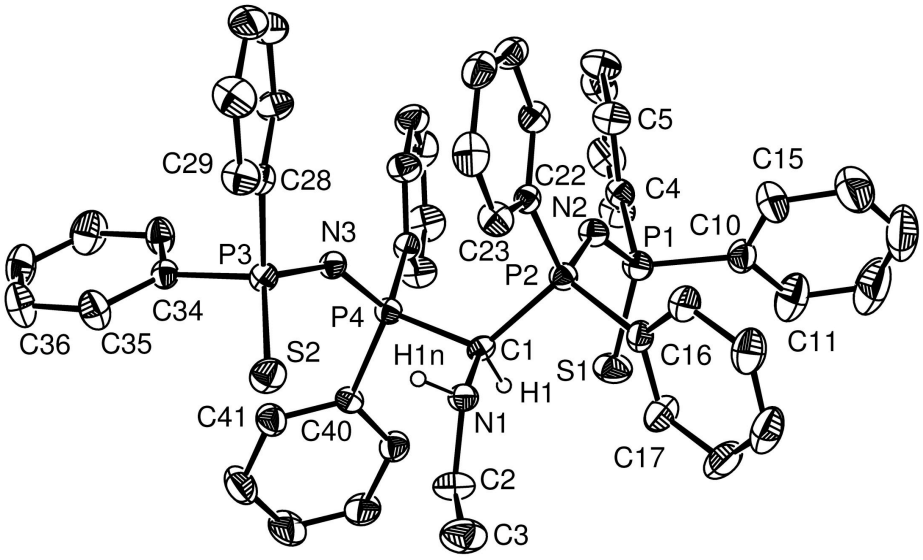

Figure 4. Ortep Plot of **4a**. Thermal ellipsoids are drawn at 30% probability level. H atoms are omitted for clarity, except for H1 and H1n.

When R = Ph and the PNP/ PhNCS ratio is 1:2, the transformation of **1b** to **2b** occurs at lower

temperatures, and only compound **2b** is obtained (Yield > 85%). When the PNP/PhNCS ratio is 1:1, compounds **4b** is obtained. When R = *p*-$NO_2(C_6H_4)$, only the formation of **3c** is observed regardless of the temperature or the PNP/PhNCS ratio (Figure 5).

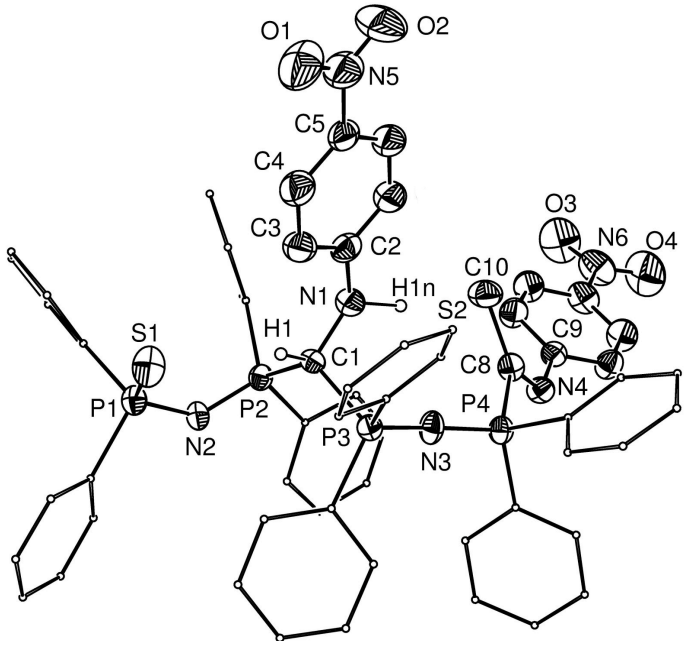

Figure 5. Ortep Plot of **4b**. Thermal ellipsoids are drawn at 30% probability level. H atoms are omitted for clarity, except for H1 and H1n.

Only when R = *p*-$NO_2(C_6H_4)$ is the reaction driven towards the formation of a single zwitterionic product that is stable with respect to the subsequent P=S group and p-$NO_2(C_6H_4)$NC formation. Apparently, the resonance effect of the *p*-$NO_2(C_6H_4)$ group stabilizes the negative charge on the N atom.

The reactivity of RSNS (R = Me, Et) was studied towards M(I) salts (M = Cu, Ag and Au, Scheme 3).

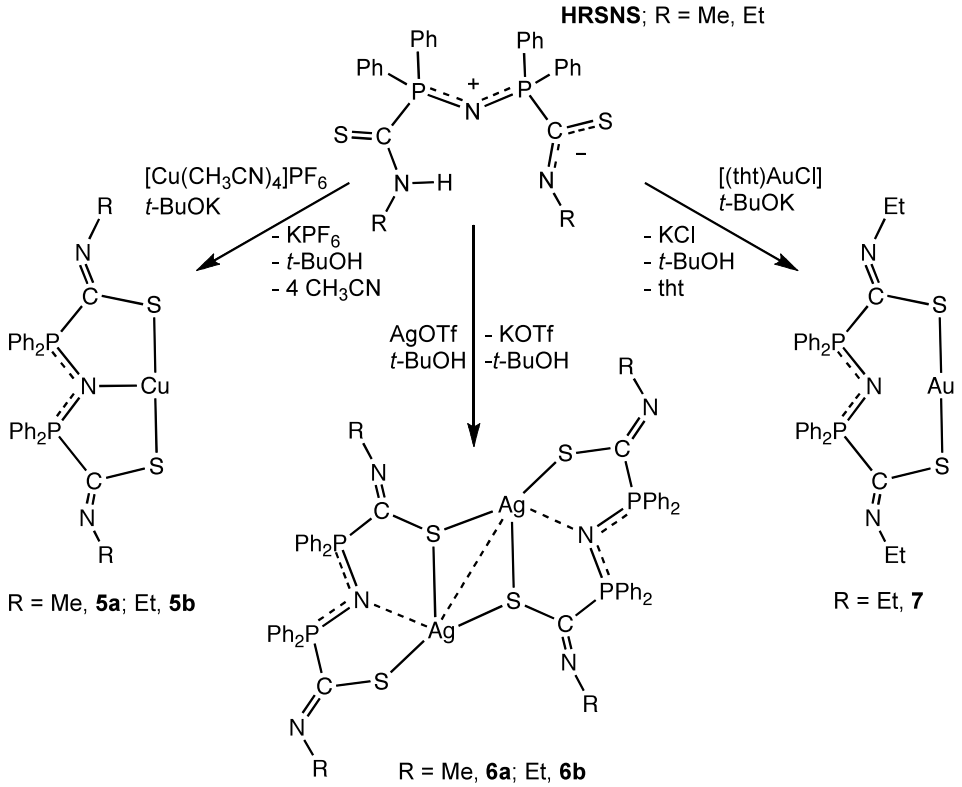

Scheme 3.

The reaction of $[Cu(MeCN)_4][PF_6]$ with HRSNS in a 1:1 molar ratio, in presence of a base *t*-BuOK afforded [Cu(RSNS)] (R = Me, **5a;** R = Et**, 5b**, Figure 6) in quantitative yields.

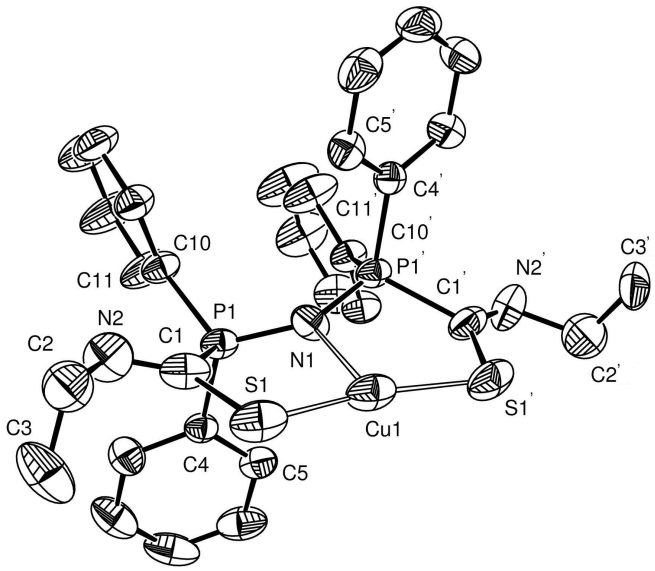

Figure 6. Ortep Plot of **5b**. Thermal ellipsoids are drawn at 30% probability level. H atoms are omitted for clarity.

Complex **5b** displayed a crystallographically imposed C_2 symmetry, the two fold axis passing through the Cu1 and N1 atoms. The PNP system maintains geometric parameters comparable to those found for the free ligand. The formal negative and positive charges are located over the copper and the two phosphorous atoms, respectively. The two fused penta-atomic Cu, S, C, P, N rings are formed by five different atoms. The $[\text{-}Ph_2PNPPh_2\text{-}]^+$ cationic group can be associated with the classical $[Ph_3PNPPh_3]^+$ cation (PPN^+). Indeed, as evidenced by the bent geometry of the P-N-P group of PPN^+, the nitrogen may *potentially* coordinate a metal centre through the N atom lone pair, even though it has never been found coordinating. In the case of the $RSNS^-$ complexes, the $[\text{-}Ph_2PNPPh_2\text{-}]^+$ coordination is forced by the *S,S* chelation that brings N1 in the good geometry.

The reaction of HRSNS with AgOTf and *t*-BuOK ($OTf^- = CF_3SO_3^-$), afforded complexes [Ag(RSNS)] (R = Me, **6a;** R = Et, **6b**, Figure 7) in quantitative yields.

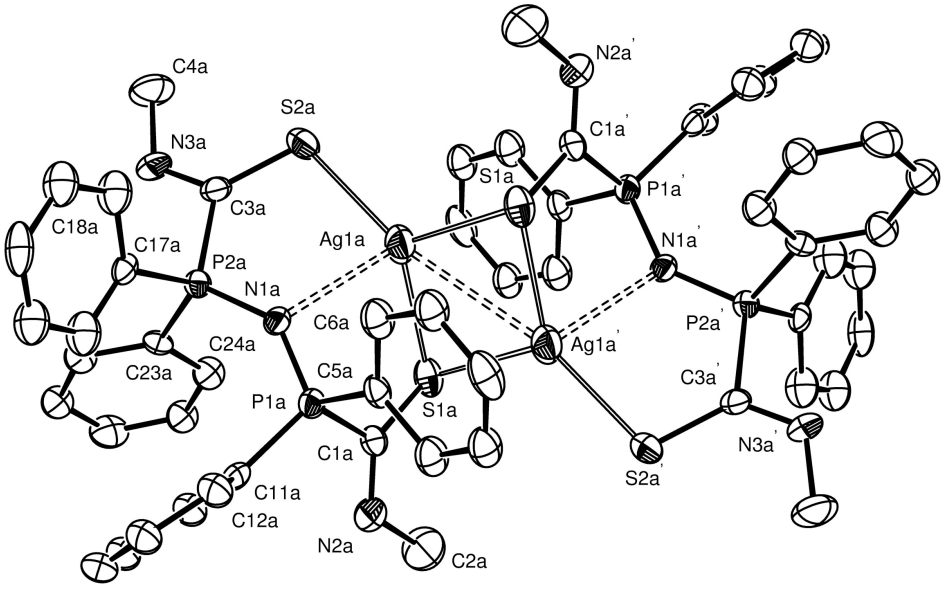

Figure 7. Ortep Plot of **6b**. Thermal ellipsoids are drawn at 30% probability level. H atoms are omitted for clarity

The ligand coordinates to the metal centres through the sulphur atoms, found one in terminal and one in bridging modality, in such a way that a four membered planar Ag_2S_2 ring is formed. The two independent molecules show remarkable structural differences. In fact, the Ag1A-Ag1A′ distance is longer than the Ag1B-Ag1B′ one [3.125(2) and 2.997(2) Å, respectively], while the Ag1A-N1A distance is shorter than the analogue Ag1B-N1B one

[2.635(6) Å and 2.721(6) Å, respectively]. Moreover, the distances between Ag1A and Ag1B from the planes defined by P1A, N1A, P2A and P1B, N1B, P2B are 1.271(1) and 1.907(1) Å, respectively. This data indicate that the more the Ag···Ag separation is short, the more the Ag···N one is long (and *vice versa*); therefore, in complex **6a** the Ag···N interactions may exists. The sum of the bond angles of N1A and N1B (354.74(8)° and 347.49(8)°) differ significatively from that observed in compound **5b**, indicating a less pronounced sp^2 character for the nitrogen atoms also due to the weaker coordination interaction.

The NMR data suggests that the dimer dissociates in solution at room temperature, as deduced by their ^{31}P NMR spectra: **6a** and **6b** display a narrow singlet in the typical range for coordinated $RSNS^-$, instead of two signals expected for the dimer. In addition, in the ^1H spectrum of **6b**, the methylene groups are equivalent and resonate as doublet of quartets, being coupled also with the methyl protons.

Reaction of [(tht)AuCl] (tht = tetrahydrothiophene) with HEtSNS and *t*-BuOK afforded compound [Au(EtSNS)] (**7**), whose crystal structure is shown in Figure 8.

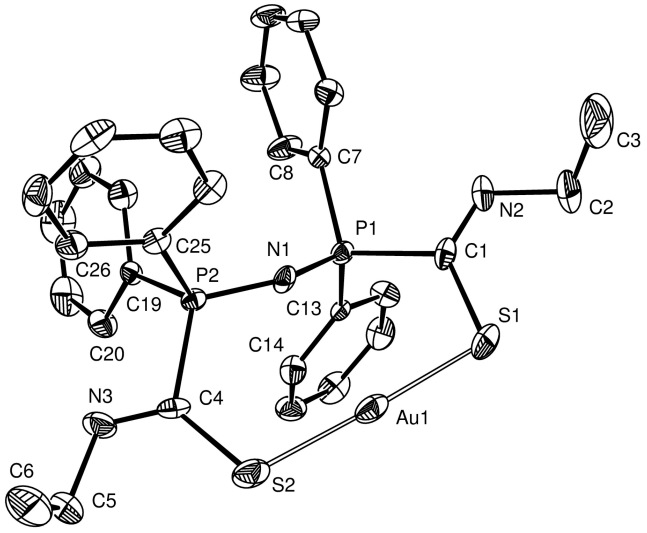

Figure 8. Ortep Plot of **7**. Thermal ellipsoids are drawn at 30% probability level. H atoms are omitted for clarity.

Complex **7** can be considered a classical 14 electrons linear AuL_2 complex. On the other hand, linear Au^I chelates displaying a 180° bite angle are rather rare, most involving diphosphine and polysulphide ligands, and being, to the best of our knowledge, all ionic.[19]
The mononuclear complexes **5a, 5b** and **6a, 6b** behave as metalloligands. The negative charge density on the S-M-S groups induces reactivity towards metal cations. Indeed, addition of M^I

species (M = Ag, Cu) resulted in the assembly of multinuclear cationic clusters with formation of sulphur bridges. The 3:2 reactions of complexes **5a** and **5b** with suitable Cu^{I} or Ag^{I} salts afforded quantitatively $[Cu_2\{Cu(RSNS)\}_3][PF_6]_2$ (R = Me, **8a**; R = Et, **8b**) and $[Ag_2\{Cu(RSNS)\}_3][A]_2$ (R = Et, A = OTf, **9a**; R = Me, A = OTf, **9b**; R = Et, A = BF_4, **9c**), respectively, as shown in Scheme 4. In the same way, complexes **6a** and **6b** reacted with suitable Ag^{I} salts yielding $[Ag_2\{Ag(RSNS)\}_3][A]_2$ (R = Me, A = PF_6, **10a**; R = Et, A = OTf, **10b**). Reaction of complexes **6b** with $[Cu(MeCN)_4]PF_6$ did not give the expected $[Cu_2\{Ag(RSNS)\}_3][PF_6]_2$ cluster.

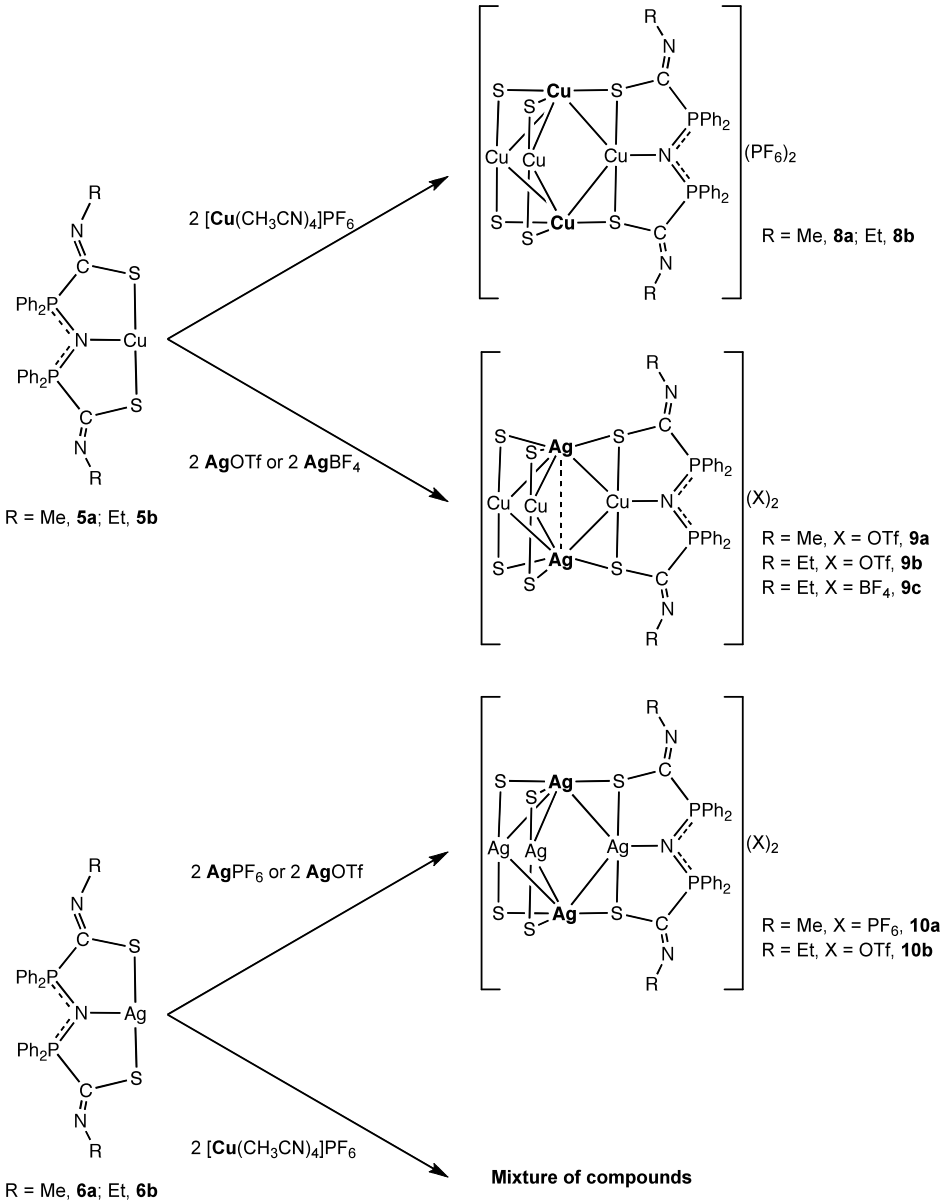

Scheme 4.

Metalloligand cationic compounds are formed by three [M(RSNS)] units joined together by two M′ atoms (M **=** M′ = Cu for **8**, M = Cu, M′ = Ag for **9,** M = M′ = Ag for **10**). The metal centres define a trigonal bipyramidal $M_3M'_2$ *core*, with the M′ atoms in the axial positions.

Looking at the formal charge distribution, they can be regarded as tri-zwitterionic, di-cationic pentanuclear clusters. Views of the crystal structures of clusters **8a**, **9c**, **10a** are depicted in Figures 9, 10 and 11.

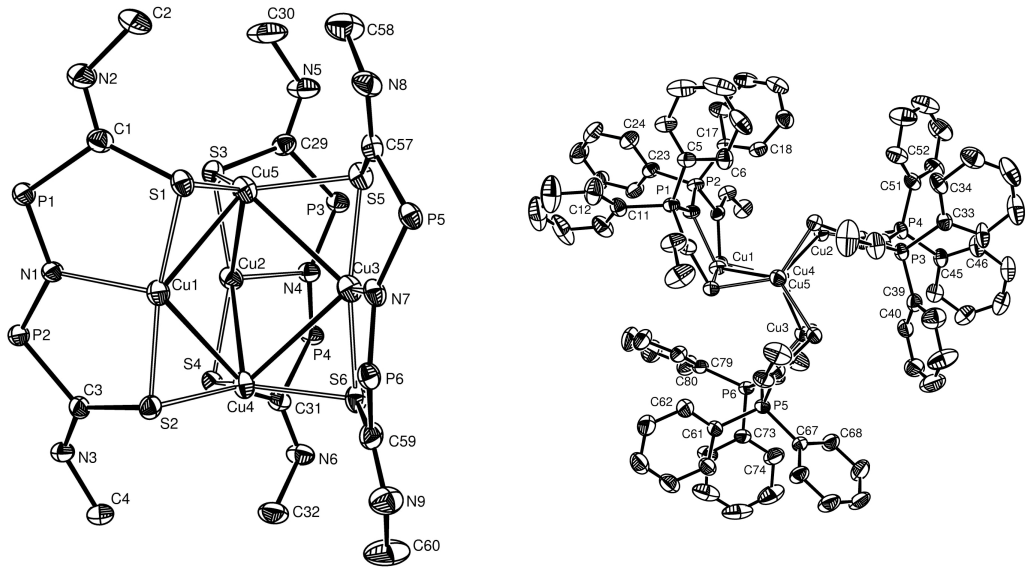

Figure 9. Ortep Plot of **8a**. Thermal ellipsoids are drawn at 30% probability level. H atoms and the two PF_6 are omitted for clarity.

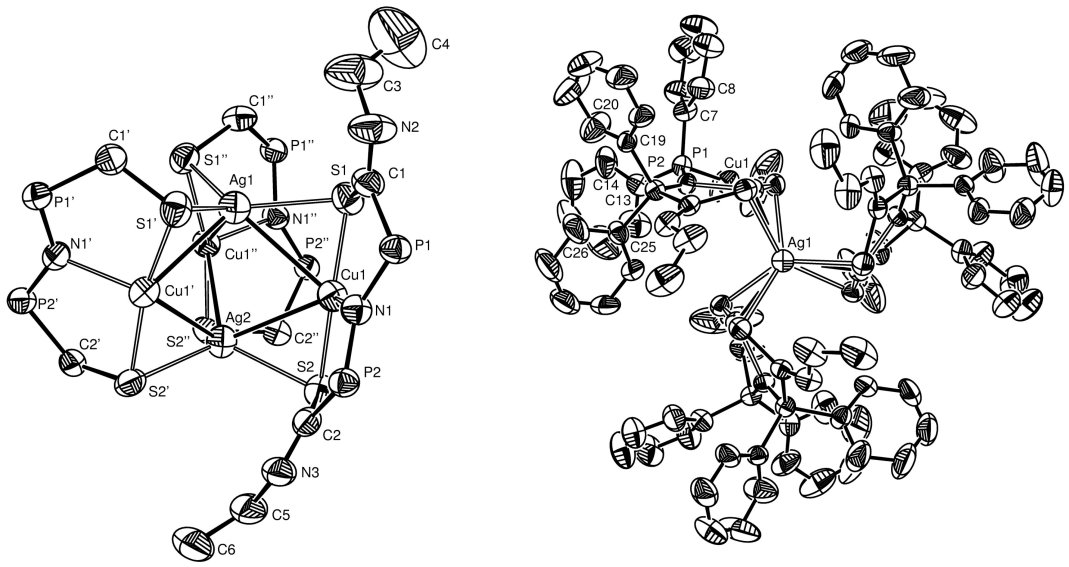

Figure 10. Ortep Plot of **9c**. Thermal ellipsoids are drawn at 30% probability level. H atoms, phenyl groups and the two BF_4 are omitted for clarity.

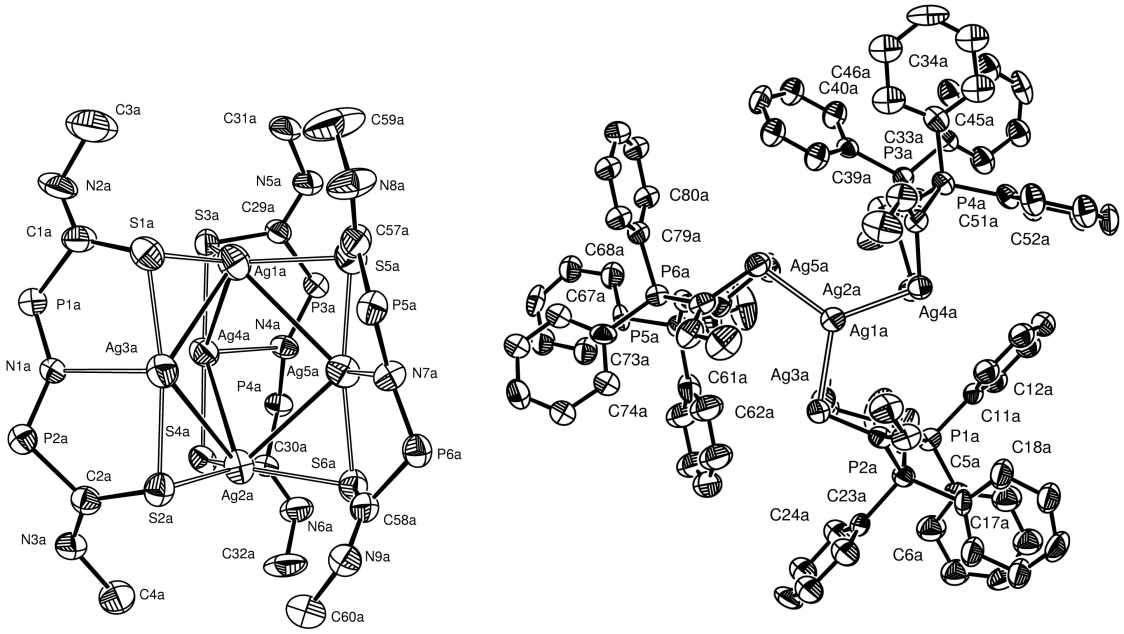

Figure 11. Ortep Plot of **10a**. Thermal ellipsoids are drawn at 30% probability level. H atoms, phenyl groups and the two PF_6 are omitted for clarity.

For all the three structures, the ligand′s sulfur atoms bridge the M′-M bonds. Each nitrogen of the P-N-P groups coordinates to a M atom. All the [M(RSNS)] unities are tilted in the same direction with respect to the relative M′, M, M′ plane.

It is noteworthy that the *core* geometry of cluster **9c** differs significatively from cluster **8a** and **10a**. A distortion of the bipyramid is observed, being the two M′ axial atoms much closer. An interaction probably exists between the two Ag atoms, being the Ag···Ag distance 3.149(7) Å.

Although few examples of Cu_5[20] and Ag_5[21] clusters bearing these types of metal *cores* have been already reported, these are the first cases in which the cage supports positive charges. Cluster **9c** represents one of the rare examples of complexes displaying an Ag-Cu bond. Surprisingly, molecules containing the Cu-Ag interaction are very rare, whereas Cu-Au and Ag-Au bonds are rather common. Only four structurally defined molecules bearing the aforementioned bond are reported in the literature.[22]

The formation of pentanuclear multi-zwitterionic clusters (**8**, **9** and **10**) suggested that any combination of M(RSNS) and M^I (M = Cu, Ag) could lead to the assembly of clusters with desired compositions and geometries. However, the 3:2 reaction of complex [Ag(EtSNS)] (**6b**) with $[Cu(MeCN)_4]PF_6$ did not give rise to the expected $[Cu_2\{Ag(EtSNS)\}_3][PF_6]_2$ cluster but to a mixture of species, of which $[Ag_2\{Cu(EtSNS)\}_3]^{2+}$ resulted the major one, as detected

by ESI-MS analyses and confirmed by means of ^{31}P NMR spectroscopy. The formation of the cluster with inverted metal ratio (Ag_2Cu_3 instead of Ag_3Cu_2) can be explained by the $RSNS^-$ ligand exchange:

$$[Ag(RSNS)] + Cu^+ = [Cu(RSNS)] + Ag^+$$

Several $[M_2\{M'(RSNS)\}_3]^{2+}$ cations (M = Ag, Cu; M′ = Ag, Cu) were detected in the ESI-MS spectrum of the crude product.

The reaction ratio between the complex M(RSNS) and the M^I ion can be different from 3:2. In fact, reaction of [Ag(EtSNS)] (**2b**) with AgOTf in a 1:1 molar ratio led quantitatively to the formation of $[Ag_2\{Ag(RSNS)\}_2(OTf)_2]$ (**11**), a bis-zwitterion. A view of its crystal structure is shown in Figure 13.

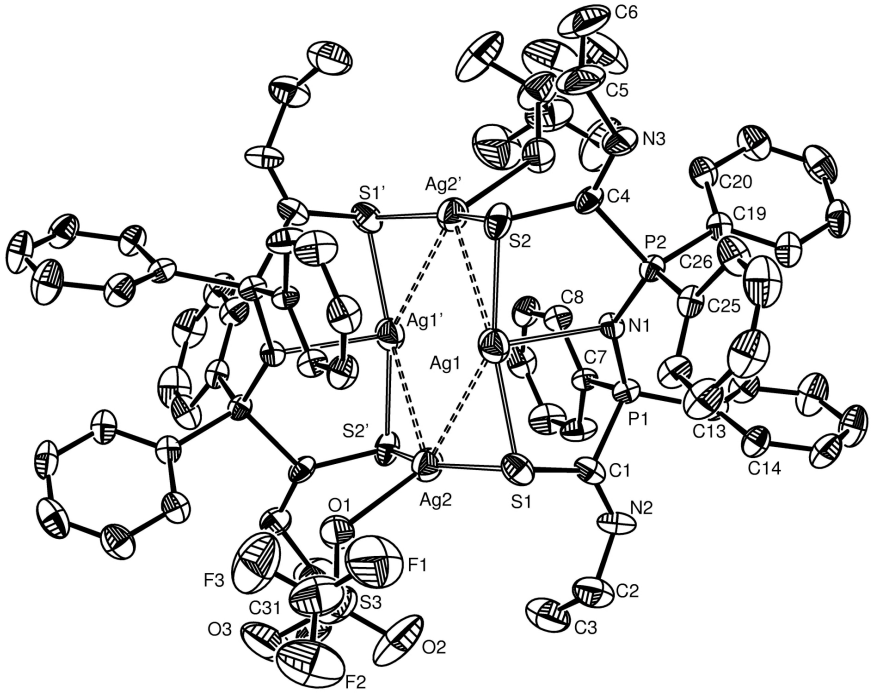

Figure 13. Ortep Plot of **11**. Thermal ellipsoids are drawn at 30% probability level. H atoms are omitted for clarity.

When complex **11** is reacted, in a 1:1 ratio, with complex **6b**, cluster $[Ag_2\{Ag(EtSNS)\}_3][OTf]_2$ (**10b**) is quantitatively formed, as depicted in Scheme 5.

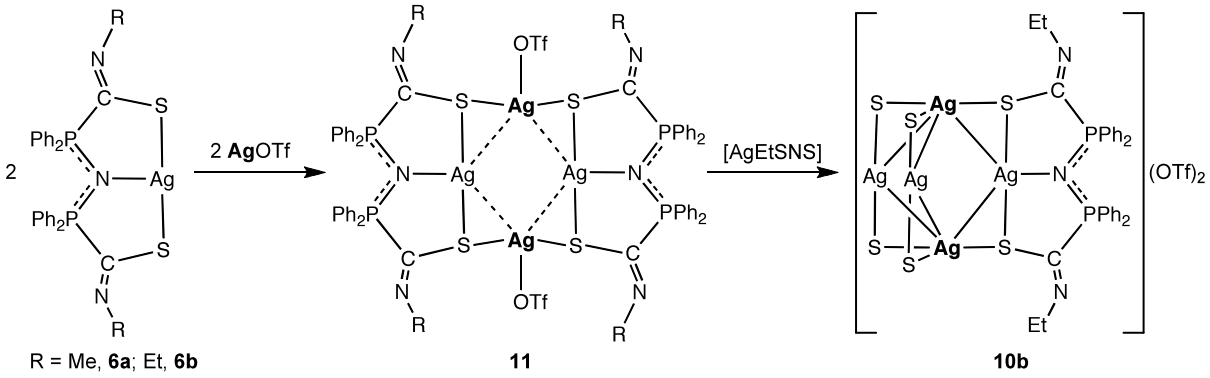

Scheme 5. For clarity, only one of the three ligand molecule is completely shown for cluster **6**; for the other two, only the S bridging atoms have been evidenced

Since complex **11** is an intermediate species in the assembly of cluster **10b**, it is possible to hypothesize a analogous planar Cu_4 intermediates in the formation of **8a** and **8b** and Cu_2Ag_2 ones for **9a**, **9b**, **9c**. In the case of Ag^I, the coordinating OTf anion may stabilize the tetranuclear species, allowing its isolation. Cluster **10b** can be thus assembled following three different strategies: a) 5:3 reaction of AgOTf with HEtSNS in the presence of a base such as *t*-BuOK, b) 3:2 reaction of complex **6b** with AgOTf and c) 1:1 reaction of complex **10b** with complex **6b**.

1.1 References

[1] www.iupac.org/publications/compendium/index.html.

[2] R. Chauvin, *Eur. J. Inorg. Chem.* **2000**, *4*, 577-591.

[3] a) D. C. Finnen, A. A. Pinkerton, *Acta Cryst.* **1997**, *C53*, 1455-1457. b) I. Karame, M. L. Tommasino, R. Faure, B. Fenet, M. Lemaire, *Chem. Lett.* **2004**, *33(2)*, 178-179.

[4] A. B. Lowe, C. L. McCormick, *Chem. Rev.* **2002**, *102(11)*, 4177-4189.

[5] D. Gudat, *Top. Curr. Chem.* **2004**, *232*, 175-212.

[6] P. N. Nesterenko, P. R. Haddad, *Anal. Sci.* **2000**, *16(6)*, 565-574.

[7] Z. Yan, L. Yanyan, J. S. Fritz, P. R. Haddad, *J. Chromatogr. A* **2003**, *1020(2)*, 259-264.

[8] A. Pagliara, P. A. Carrupt, G. Caron, P. Gaillard, B. Testa, *Chem. Rev.* **1997**, *97*, 3385-3400.

[9] a) V. M. Geskin, C. Lambert, J. L. Bredas, *J. Am. Chem. Soc.* **2003**, *125(50)*, 15651-15658. b) C. Lambert, S. Stadler, G. Bourhill, C. Bräuchle, *Angew. Chem., Int. Ed.* **1996**, *35(6)*, 644-646.

[10] a) W. E. Piers, *Chem. Eur. J.* **1998**, *4(1)*, 13-18. b) E. Gerhard, *Chem. Commun.* **2003**, *13*, 1469-1476. c) J. Strauch, G. Erker, G. Kehr, R. Frohlich, *Angew. Chem., Int. Ed.* **2002**, *41*, 2543-2546.

[11] H. Lee, D. B. Kim, S. H. Kim, H. S. Kim, S. J. Kim, D. K. Choi, Y. S. Kang, J. Won, J. *Angew. Chem., Int. Ed.* **2004**, *43(23)*, 3053-3056.

[12] A. Galindo, D. Miguel, J. Perez, *Coord. Chem. Rev.* **1999**, *193*, 643-690.

[13] H. Schmidbaur, *Angew. Chem., Int. Ed.* **1983**, *22*, 907-927.

[14] a) B. Ronig, H. Schulze, I. Pantenburg, L. Wesemann, *Eur. J. Inorg. Chem.* **2005**, *(2)*, 314-320. b) J. C. Thomas, J. C. Peters, *J. Am. Chem. Soc.* **2003**, *125(29)*, 8870-8888.

[15] a) A. W. Hofmann, *Berichte der Deutschen Chemischen Gesellschaft*, **1870**, *3*, 761. b) A. Hantzsch, H. Hibbert, *Chem. Ber*. **1907**, *40*, 1511.

[16] L. Engel, O. Dahl, *Acta Chem. Scand*. **1974**, *9*, B28.

[17] K. Akiba, T. Yoneyama, H. Hamada, N. Inamoto, *Bull. Chem. Soc. Japan.,* **1976**, *49(7)*, 1970.

[18] N. Noth, E. Fluck, *Z. Naturforsch., B: Chem. Sci*. **1984**, 39, 744.

[19] a) W. H. Chan, T. C. W. Mak, C. M. Che, *J. Chem. Soc., Dalton Trans.* **1998,** 2275-2276. b) B. Heuer, S. J. A. Pope, G. Reid, *Polyhedron* **2000***, **19***,** 743-749. c) A. M. Gibson, G. Reid, *J. Chem. Soc., Dalton Trans.* **1996**, 1267-1274.

[20] a) I. G. Dance, *Chem. Commun*. **1976**, 68-69. b) A. Eichhofer, D. Fenske, W. Holstein, *Angew. Chem*. **1993**, *32*, 242-245. c) M. Hakansson, H. Eriksson, A. B. Ahman, S. Jagner, *J. Organomet. Chem*. **2000**, *595*, 102-108. d) P. G. Edwards, R. W. Gellert, M. W. Marks, R. Bau, *J. Am*. *Chem. Soc*. **1982**, *104*, 2072-2073. e) A. Heine, D. Stalke, *Angew. Chem*. **1993**, *32*, 121-122.

[21] a) O. M. Abu-Salah, A. R. A. Al-Ohaly, Z. F. Mutter, *J. Organomet. Chem.* **1990**, *389(3)*, 427-34. b) G. A. Bowmaker, L. C. Tan, *Aust. J. of Chem*. **1979**, *32(7)*, 1443-52.

[22] a) M. J. Freeman, M. Green, A. G.Orpen, I. D. Salter, F. G. A. Stone, *Chem. Commun* **1983**, 1332-1334. b) O. M. Abu-Salah, M. S. Hussain, E. O. Schlemper, *Chem. Commun,* **1988**, 212-213. c) J. P. Fackler Junior, C. A. Lopez, R. J. Staples, Suning Wang, R. E. P.Winpenny, R. P. Lattimer, *Chem. Commun.* **1992**, 146-148. d) C. J. Shorrock, Bao-Yu Xue, P. B. Kim, R. J. Batchelor, B. O. Patrick, D. B. Leznoff, *Inorg. Chem.* **2002***, 41***,** 6743-6753.

2

A study on the coordinative versatility of the zwitterionic *S,N,S* ligand $EtNHC(S)Ph_2P{=}NPPh_2C(S)NEt$ in its anionic, neutral and cationic forms. Determination of absolute pK_a values in CH_2Cl_2 of Rh^I complexes.

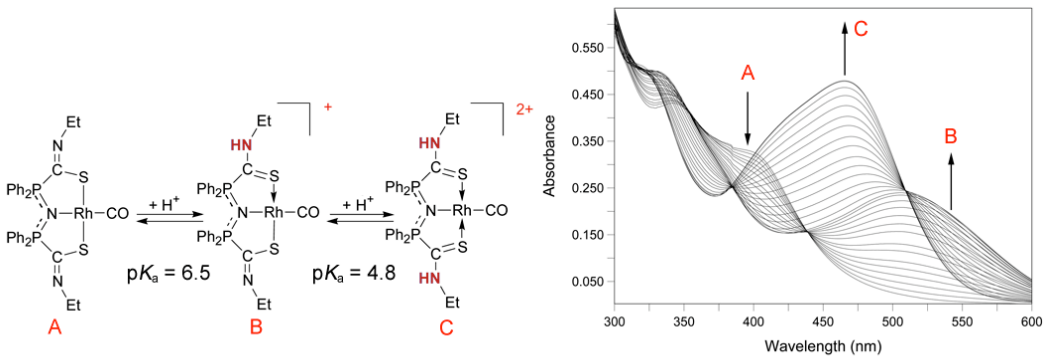

The coordination properties of $EtNHC(S)Ph_2P{=}NPPh_2C(S)$-NEt (HEtSNS) towards Rh(I) species derived from $[Rh(CO)_2Cl]_2$ and $[Rh(cod)Cl]_2$ (cod = 1,5-cyclooctadiene) were studied. This ligand is an amphoteric zwitterion, which forms the H_2EtSNS^+ cation upon protonation and the $EtSNS^-$ dianion-cation upon deprotonation. All three forms coordinate to metal centers. Their geometrical versatility allows many coordination fashions: *S*-monodentate, *S,S*-bidentate (with a bite angle spanning from 90 to 180°), *S,N,S*-tridentate, *N,N,N*-tridentate and *S,S*-bridging, as determined by X-ray diffraction methods. The [Rh(CO)EtSNS] complex is a biprotic base; its conjugated acids are $[Rh(CO)HEtSNS]^+$ and $[Rh(CO)H_2EtSNS]^{2+}$, and their pKa values were determined in dichloromethane solutions. In this triad of compounds, which are geometrically similar, the Rh(I) metal center features variable charge density as confirmed by the νCO infrared absorption frequency.

2.1 Introduction

The $EtSNS^-$ acts as an *S*,*N*,*S*-tridentate or *S*,*S*-bidentate ligand towards M(I) species (M = Rh[1] and Cu, Ag, Au[2]). The $[\text{-}Ph_2PNPPh_2\text{-}]^+$ nitrogen atom can be coordinated as in [Rh(CO)(EtSNS)] and [Cu(EtSNS)] and it weakly interacts with the metal center in $[Ag(EtSNS)]_2$, or it can be not coordinated as in the case of [Au(EtSNS)]. The $[\text{-}Ph_2PNPPh_2\text{-}]^+$ group is reminiscent of the classical bis(triphenylphosphine)iminium cation $[Ph_3PNPPh_3]^+$ (PPN^+) whose N atom, as evidenced by its bent geometry, may coordinate a metal center, although this behavior has never been observed.[3] We became interested in studying also the coordination properties of HEtSNS and H_2EtSNS^+. Their reactivity towards Rh^I species derived from $[Rh(CO)_2Cl]_2$ and $[Rh(cod)Cl]_2$ (cod = 1,5 cyclooctadiene) is reported. Acid–base properties of complex [Rh(CO)(EtSNS)] are discussed together with a general method for the determination of absolute pK_a values in dichloromethane.

2.2 Experimental

2.2.1 General procedures

All manipulations were carried out at room temperature in the air or, when necessary, under nitrogen atmosphere by standard Schlenk techniques; *t*BuOK, EtNCS, $[Rh(cod)Cl]_2$, $[Rh(CO)_2Cl]_2$, $AgPF_6$, AgOTf (OTf = CF_3SO_3), HOTf, HPF_6 (60% aqueous solution) and NaH were purchased and used as received (Aldrich and Fluka). The solvents was dried and distilled by standard techniques. $Ph_2PNHPPh_2$ (dppa),[4] HEtSNS,[1] $(H_2EtSNS)Cl$,[1] [Rh(CO)(EtSNS)],[1] $[Rh(CH_3CN)_2(CO)_2]X$ and $[Rh(THF)_2(CO)_2]X$ (X = PF_6, OTf)[5] were prepared as described elsewhere. Elemental analyses were carried out on a Carlo Erba EA1108 microanalyzer. FTIR spectra (4000-400 cm^{-1}) were recorded on a Nicolet Nexus spectrophotometer equipped with a Smart Orbit HATR accessory (diamond crystal). ^1H NMR (300.13 MHz, TMS) and $^{31}P\{^1H\}$ NMR (161.98 MHz, external reference 85% H_3PO_4) spectra were recorder on Bruker instruments (AC300 Avance and AMX400, respectively) using deuterated solvents ($CDCl_3$, CD_2Cl_2, DMSO-d_6 and CD_3OD). The solid state $^{31}P\{^1H\}$ NMR–MAS spectra were recorded on a Bruker Avance 300 MHz operating at a frequency of 121.57 MHz, equipped with a MAS 4 mm ^1H–X probe. Sample rotation was set at 1010 Hz.

$NH_4H_2PO_4$ was used as external reference (0 ppm), and PF_6^- (–144 ppm) as internal secondary one. A Micromass Quattro LC triple quadrupole instrument equipped with an electrospray interface (Masslynx v. 3.4 software) was used for ESI–MS data collection and processing. The nebulizing gas (nitrogen, 99.999% purity) and the desolvation gas (nitrogen, 99.998% purity) were delivered at a flow-rate of 80 and 500 l/h, respectively. ESI–MS analyses were performed by operating the mass spectrometer in positive ion (PI) mode, acquiring mass spectra over the scan range *m/z* 100–2800, using a step size of 0.1 Da and a scan time of 2.7 sec. The interface operating parameters were: source temperature 70 °C, desolvation temperature 70 °C, ESI(+) capillary voltage 3.0 kV, cone voltage 15 V, rf lens 0.3 V. Absorption spectra in the range 300-600 nm were recorded with a Perkin Elmer Lambda 25 spectrophotometer using matched quartz cells of 1 cm pathlength and dichloromethane as reference.

2.2.5 Synthesis of [Na(EtSNS)]

A suspension of NaH (0.043 g, 1.79 mmol) in THF (20 mL) was added to a solution of HEtSNS (0.500 g, 0.89 mmol) in THF (20 mL) under nitrogen. The resulting suspension was stirred for 1 h. Unreacted NaH was removed via filtration. Evaporation of the solvent afforded [Na(EtSNS)] as a white powder (Yield 97%). [Na(EtSNS)] was recrystallized by slow evaporation of a CH_2Cl_2/hexane solution, yielding $[Na(EtSNS)H_2O]_2$. ^{1}H NMR (DMSO-d_6): δ = 8.0-7.2 (m, 20H, Ph), 3.42 (qd, 4H, -*CH*$_2$CH$_3$, ^3J(H,H) = 7.2 Hz, ^4J(H,P) = 5.0 Hz), 0.99 (t, 6H, -CH$_2$*CH*$_3$, ^3J(H,H) = 7.2 Hz) ppm. ^{31}P{^{1}H} NMR (DMSO-d_6): δ = 7.2 (s) ppm. $C_{30}H_{30}N_3P_2NaS_2$ (581.65): calcd. C 61.95; H 5.20, N 7.22, S 11.03; found C 62.31, H 5.31, N 7.25, S 10.87.

2.2.6 Synthesis of $(H_2EtSNS)PF_6$

Solid HEtSNS (0.073 g, 0.13 mmol) was dissolved in CH_2Cl_2 (10 mL) resulting in a yellow solution; a solution of HPF_6 (60% in H_2O, 0.2 mL, 2.4 mmol) was added and the reaction mixture was vigorously shaken. The aqueous phase was removed and the resulting organic phase was dried with anhydrous Na_2SO_4 and evaporated under reduced pressure to obtain $(H_2EtSNS)PF_6$ as a yellow powder (Yield 98%). ^{1}H NMR ($CDCl_3$): δ = 12.8 (s, 2H; N-H), 8.0-7.3 (m, 40H; Ph), 4.05 (qd, 4H, -*CH*$_2$CH$_3$, ^3J(H,H) = 7.2 Hz, ^4J(H,P) = 7 Hz), 1.41 (t, -

CH_2CH_3, ^3J(H,H) = 7.2 Hz) ppm. $^{31}P\{^1H\}$ NMR ($CDCl_3$): δ = 13.3 (s) ppm. $C_{30}H_{32}F_6N_3P_3S_2$ (705.64): calcd. C 51.06, H 4.57, N 5.95, S 9.09; found: C 52.03, H 4.62, N 6.15, S 9.54.

*2.2.7 Synthesis of [Rh(cod)(S,S-EtSNS)] (**1**)*

Solid $[Rh(cod)Cl]_2$ (0.100 g, 0.203 mmol) and HEtSNS (0.226 g, 0.406 mmol) were dissolved in 10 mL of CH_2Cl_2. A solution of *t*BuOK (0.046 g, 0.406 mmol) in 2 mL of MeOH was then added and the reaction mixture stirred for 30 min. The volatiles were evaporated and the resulting yellow powder was redissolved in 5 mL of CH_2Cl_2. KCl was removed via filtration. Evaporation of the solvent afforded [Rh(cod)(*S,S*-EtSNS)] (**1**) as yellow powder (Yield 85%). Complex **1** could be recrystallized by layering hexane onto a CH_2Cl_2 solution. ^1H NMR ($CDCl_3$): δ = 7.8-7-2 (m, 20H, Ph), 3.9-3.7 (m, 4H, -CH=CH-, cod; m, 4H, -CH_2CH_3), 1.87 (br, 4H, -C*H*H-, cod), 1.52 (m, 4H, -CH*H*-, cod), 1.18 (t, 6H, -CH_2CH_3) ppm. $^{31}P\{^1H\}$ NMR ($CDCl_3$): δ = 9.7 (s) ppm. $C_{38}H_{42}N_3P_2RhS_2$ (769,74): calcd. C 59.29, H 5.50, N 5.46, S 8.33; found C 59.11, H 5.64, N 5.29, S 8.16.

*2.2.8 Synthesis of [{Rh(cod)}$_2$(μ-S,S-EtSNS)]OTf (**2**)*

A solution of AgOTf (0.077 g, 0.30 mmol) in THF (10 mL) was added dropwise to a solution of $[Rh(cod)Cl]_2$ (0.075 g, 0.15 mmol) in THF (10 mL). The resulting reaction mixture was stirred at room temperature for 10 min. Solid AgCl was removed via filtration. To the solution, complex **1** (0.115 g, 0.15 mmol) was added and the purple reaction mixture was stirred for 1 h. Evaporation of the volatiles yielded [{Rh(cod)}$_2$(*μ-S,S*-EtSNS)]OTf (**2**) as a purple powder (Yield 76%). The complex can be recrystallized by layering hexane onto a THF solution, affording violet crystals of **2**·½THF. ^1H NMR ($CDCl_3$): δ = 7.7-7.2 (m, 20H; Ph) , 4.20 (dq, 4H; -CH_2CH_3, ^3J(H,H) = 7.2 Hz, ^4J(H,P) = 4.2 Hz), 4.23 (br, 4H; -CH=CH-, cod), 3.73 (s, 4H; -CH=CH-, cod), 2.42 (br, 8H; -C*H*H-, cod), 1.95 (m, 8H; -CH*H*-, cod), 1.45 (t, 6H; -CH_2CH_3, ^3J(H,H) = 7.2 Hz) ppm. $^{31}P\{^1H\}$ NMR ($CDCl_3$): δ = 17.9 (s) ppm. $C_{47}H_{54}F_3N_3O_3P_2Rh_2S_3$ (1129.90): calcd. C 49.96, H 4.82, N 3.72, S 8.51; found C 50.12, H 4.83, N 3.63, S 8.74. MS (ESI^+, CH_2Cl_2): *m/z* (%) = 980.26 (100) $[M]^+$.

*2.2.9 Reaction of **1** with [Rh(cod)Cl]$_2$. Solution formation of [{Rh(cod)}$_2$(μ-S,S-EtSNS)]Cl (**3**)*

A solution of $[Rh(cod)Cl]_2$ (0.024 g, 0.097 mmol) in CH_2Cl_2 (10 mL) was added to a solution of 1 (0.150 g, 0.195 mmol) in CH_2Cl_2 (10 mL). The resulting orange reaction mixture

was stirred for 10 min. Methanol (40 mL) was added and the solution color turned to purple. Evaporation of the solvent yielded the starting mixture of the reagents. The same reaction was performed in CD_3OD in order to obtain NMR data for **3**: ^{1}H NMR (CD_3OD): δ = 7.5-7.2 (m, 20H; Ph), 4.21 (m, 4H; -C*H*$_2$CH$_3$, m, 4H, -CH=CH-, cod), 3.7 (s, 4H; -CH=CH-, cod), 2.40 (s, 8H; -CH*H*-, cod), 1.95 (m, 8H; -C*H*H-, cod), 1.45 (t, 6H; -CH$_2$C*H*$_3$) ppm. ^{31}P{^{1}H} NMR (CD_3OD): δ = 17.1 (s) ppm. MS (ESI$^+$, CH_2Cl_2): *m/z* (%) = 980.26 (100) [M]$^+$.

*2.2.10 Synthesis of [Rh(cod)(S-HEtSNS)Cl] (**4**)*

A solution of HEtSNS (0.145 g, 0.26 mmol) in CH_2Cl_2 (20 mL) was added to a solution of [Rh(cod)Cl]$_2$ (0.064 g, 0.13 mmol) in CH_2Cl_2 (10 mL). The red reaction mixture was stirred for 10 min. Evaporation of the solvent yielded [Rh(cod)(S-HEtSNS)Cl] (**4**) as a yellow powder (Yield 92%) which could be recrystallized by layering hexane onto a CH_2Cl_2 solution. In solution, compound **4** was found to be in equilibrium with [Rh(cod)(S,S'-HEtSNS)]Cl (**4a**). **4**: ^{1}H NMR ($CDCl_3$): δ = 11.37 (s, br, N-H), 7.7-7.2 (m, Ph), 4.15 (m, br, -CH=CH-, cod), 4.00 (m, br, -CH$_2$CH$_3$), 3.93 (m, br, -CH$_2$CH$_3$), 3.63 (m, br, -CH=CH-, cod), 2.13 (s, br, -CHH-, cod), 1.48 (m, -CHH-, cod), 1.27 (t, -CH$_2$CH$_3$, ^{3}J(H,H) = 6 Hz) ppm; signals of compound **4a** (except for NH group) were underimposed to signals of compound **4** thus affecting peak integration.^{31}P{^{1}H} NMR ($CDCl_3$): δ = 11.1 (d, *J*(P,P) = 15.9 Hz), 10.5 (d *J*(P,P) = 15.9 Hz) ppm. $C_{38}H_{43}ClN_3P_2RhS_2$ (806.21): calcd. C 56.61, H 5.38, N 5.21, S 7.95; found C 57.46, H 5.46, N 5.37, S 8.10. **4a**: ^{31}P{^{1}H} NMR ($CDCl_3$): δ = 12.4 (s, integral ratio with respect to complex **4** = 1:10) ppm. ^{1}H NMR ($CDCl_3$): δ = 12.82 (s, br, N-H) ppm.

2.2.11 Reaction of [Rh(CO)$_2$Cl]$_2$ with HEtSNS

A solution of HEtSNS (0.280 g, 0.50 mmol) in CH_2Cl_2 (10 mL) was added under nitrogen to [Rh(CO)$_2$Cl]$_2$ (0.097 g, 0.25 mmol) dissolved in 15 mL of CH_2Cl_2. The solution color changed rapidly from yellow to red. Stirring was continued for 2 h and the volatiles were removed under vacuum, affording a red-orange powder. Three compounds (namely [Rh(CO)$_2$(*S*-EtSNS)Cl], [H$_2$EtSNS][Rh(CO)$_2$Cl$_2$] (**5**) and [Rh(CO)(EtSNS)]) were spectroscopically identified as the major components of the crude product. Crystals of compound **5** were obtained by layering hexane onto a solution of the crude product. ^{31}P{^{1}H} NMR ($CDCl_3$): δ = 16.85 (s, integration 0.75, [Rh(CO)(EtSNS)]), 13.30 (s, integration 1, compound **5**), 12.90 (d, ^{2}*J*(P,P) = 15.2 Hz, integration 0,12), 11.44 (d, ^{2}*J*(P,P) = 15.2 Hz,

integration 0.12, [Rh(CO)$_2$(*S*-EtSNS)Cl]) ppm. FTIR (Diamond crystal HATR, cm^{-1}): ν_{CO} = 2071, 1992.

*2.2.12 Synthesis of [H$_2$EtSNS][Rh(cod)Cl$_2$] (**6**)*

Solid (H$_2$EtSNS)Cl (0.242 g, 0.406 mmol) was added to a solution of [Rh(cod)Cl]$_2$ (0.100 g, 0.203 mmol) in CH_2Cl_2 (20 mL). The resulting orange reaction mixture was stirred for 10 min. Evaporation of the volatiles afforded [H$_2$EtSNS][Rh(cod)Cl$_2$] (**6**) as an orange powder (Yield 92%). The salt can be recrystallized by layering hexane onto its CH_2Cl_2 solution. ^{1}H NMR ($CDCl_3$): δ = 12.70 (s, br, 2H, N-H); 7.6-7.1 (m, 20H, Ph); 4.18 (m, br, 8H, -*CH*$_2$CH$_3$ and -CH=CH-), 2.48 (m, br, 4H, -C*H*H-, cod), 1.73 (m, br, 4H, -CH*H*-, cod), 1.49 (t, 6H, -CH$_2$*CH*$_3$, ^{3}*J*(H,H) = 7.05 Hz) ppm. ^{31}P{^{1}H} NMR ($CDCl_3$): δ = 13.6 (s) ppm. $C_{38}H_{44}Cl_2N_3P_2RhS_2$ (842,67): calcd. C 54.16, H 5.26, N 4.99, S 7.61; found C 54.49, H 5.18, N 5.01, S 7.73.

*2.2.13 Synthesis of [Rh(CO)(S,N,S-H$_2$EtSNS)][Rh(CO)$_2$Cl$_2$]$_2$ (**7**)*

A solution of (H$_2$EtSNS)Cl (0.100 g, 0.17 mmol) in CH_2Cl_2 (10 mL) was added under nitrogen to a solution of [Rh(CO)$_2$Cl]$_2$ (0.099 g, 0.255 mmol) in CH_2Cl_2 (10 mL). Stirring was continued for 2 h and the solution color turned to dark-red. Evaporation of the volatiles afforded [Rh(CO)(*S,N,S*-H$_2$EtSNS)][Rh(CO)$_2$Cl$_2$]$_2$ (**7**) as a red microcrystalline powder (Yield 91%). ^{1}H NMR (DMSO-d$_6$): δ = 11.08 (s, br, 2H, N-H); 7.9-7.3 (m, 20H, Ph); 4.15 (dd, 4H, -*CH*$_2$CH$_3$, ^{3}*J*(H,H) = 6.3 Hz, ^{4}*J*(H,P) = 6.3 Hz), 1.25 (t, 6H, -CH$_2$*CH*$_3$) ppm. ^{31}P{^{1}H} NMR ($CDCl_3$): δ = 38.2 (s) ppm. $C_{35}H_{32}Cl_4N_3P_2O_5Rh_3S_2$ (1151.26): calcd. C 36.51, H 2.80, N 3.65, S 5.57; found C 36.39, H 2.86, N 3.54, S 5.71. MS (ESI$^+$, CH_2Cl_2): *m/z* (%) = 691.6 (100) [M]$^+$. FTIR (Diamond crystal HATR, cm^{-1}): ν_{CO} = 2074 (s, ν_{CO}[Cl$_2$Rh(CO)$_2$]$^-$), 1998 (s, ν_{CO}[Cl$_2$Rh(CO)$_2$]$^-$), 2014 (m, sh, ν_{CO} Rh–CO).

*2.2.14 Synthesis of [Rh(CO)(S,N,S'-HEtSNS)]PF$_6$ (**8**)*

A solution of HEtSNS (0.280 g, 0.50 mmol) in CH_2Cl_2 (10 mL) was added under nitrogen to a solution of [Rh(CH$_3$CN)$_2$(CO)$_2$]PF$_6$ (0.193 g, 0.50 mmol) in CH_2Cl_2 (10 mL). Stirring was continued for 2 h and the solution color turned to violet-red. Evaporation of the volatiles afforded [Rh(CO)(*S,N,S'*-HEtSNS)]PF$_6$ (**8**) as a red microcrystalline powder (Yield 89%). The complex can be recrystallized by layering pentane onto a THF solution of **8**

affording red crystals of **8** · 2THF. ^{1}H NMR (DMSO-d_6): δ = 11.0 (s, br, 1H, N-H); 7.7-7.4 (m, 20H, Ph); 3.67 (m, 4H, -*CH*$_2$CH$_3$), 1.16 (t, 6H, -CH$_2$*CH*$_3$) ppm. ^{31}P{^{1}H} NMR ($CDCl_3$): δ = 35.0 (s), 19.9 (s) ppm. $C_{31}H_{31}F_6N_3P_3ORhS_2$ (835.55): calcd. C 44.56, H 3.74, N 5.03, S 7.67; found C 44.45, H 3.69, N 4.96, S 7.58. MS (ESI$^+$, CH_2Cl_2): *m/z* (%) = 690.6 (100) [M]$^+$. FTIR (Diamond crystal HATR, cm^{-1}): ν_{CO} = 1979.

*2.2.15 Synthesis of [Rh(CO)(S,N,S'-H$_2$EtSNS)](PF$_6$)$_2$ (**9**)*

A solution of [Rh(CH$_3$CN)$_2$(CO)$_2$]PF$_6$ (0.193 g, 0.50 mmol) in CH_2Cl_2 (10 mL) was added under nitrogen to a solution of (H$_2$EtSNS)PF$_6$ (0.352 g, 0.50 mmol) in CH_2Cl_2 (15 mL). Stirring was continued for 2 h and the solution color turned to red. Evaporation of the volatiles afforded [Rh(CO)(*S,N,S*-H$_2$EtSNS)](PF$_6$)$_2$ (**9**) as an orange microcrystalline powder (Yield 88%). ^{1}H NMR (DMSO-d_6): δ = 11.1 (s, br, 2H, N-H); 7.8-7.4 (m, 20H, Ph); 4.15 (m, 4H, -*CH*$_2$CH$_3$), 1.18 (t, 6H, -CH$_2$*CH*$_3$) ppm. ^{31}P{^{1}H} NMR ($CDCl_3$): δ = 38.2 (s) ppm. $C_{31}H_{32}F_{12}N_3P_4ORhS_2$ (981.52): calcd. C 37.93, H 3.29, N 4.28, S 6.53; found C 37.55, H 3.21, N 4.15, S 6.38. MS (ESI$^+$, CH_2Cl_2): *m/z* (%) = 691.6 (100) [M]$^+$. FTIR (Diamond crystal HATR, cm^{-1}): ν_{CO} = 2013.

*2.2.16 Synthesis of [Rh(CO)(S,N,S'-HEtSNS)](OTf) (**10**)*

A solution of [Rh(CH$_3$CN)$_2$(CO)$_2$]OTf (0.200 g, 0.37 mmol) in CH_2Cl_2 (10 mL) was added under nitrogen to a solution of HEtSNS (0.215 g, 0.37 mmol) in CH_2Cl_2 (15 mL). Stirring was continued for 2 h and the solution color turned to red. Evaporation of the volatiles afforded compound [Rh(CO)(S,N,S-HEtSNS))]OTf as an orange microcrystalline powder (Yield 87%). ^{1}H NMR (DMSO-d_6): δ = 11.0 (s, br, 1H, N-H); 7.7-7.4 (m, 20H, Ph); 3.67 (m, 4H, -CH$_2$CH$_3$), 1.16 (t, 6H, -CH$_2$CH$_3$) ppm. ^{31}P{^{1}H} NMR ($CDCl_3$): δ = 35.0 (s), 19.9 (s) ppm. $C_{32}H_{31}F_3N_3O_4P_2RhS_3$ (839.65): calcd. C 45.77, H 3.72, N 5.00, S 11.45; found C 45.62, H 3.69, N 4.97, S 11.39. MS (ESI$^+$, CH_2Cl_2): *m/z* (%) = 690.6 (100) [M]$^+$. FTIR (Diamond crystal HATR, cm^{-1}): ν_{CO} = 1977.

*2.2.17 Synthesis of [Rh(CO)(S,N,S'-H$_2$EtSNS)](OTf)$_2$ (**11**)*

In a Schlenk tube and under nitrogen, a solution of [Rh(CO)(EtSNS)] (0.200 g 0.29 mmol) in 10 mL of chloroform was treated with 10 mL of a water solution of HOTf in large excess with respect to the rhodium precursor. The yellow solution turned orange-red and a

precipitate formed which was separated by decanting. The two liquid phases were separated, and the organic one dried, giving an orange red solid. The two solids were recrystallized from hot methanol affording compound $[Rh(CO)(S,N,S\text{-}H_2EtSNS)](OTf)_2$ as an orange microcrystalline powder (Yield 90%). ^1H NMR ($CDCl_3$): δ = 11.1 (s, br, 2H, N-H); 7.8-7.4 (m, 20H, Ph); 4.15 (m, 4H, $-CH_2CH_3$), 1.18 (t, 6H, $-CH_2CH_3$) ppm. $^{31}P\{^1H\}$ NMR (DMSO-d_6): δ = 38.2 (s) ppm. $C_{33}H_{32}F_6N_3O_7P_2RhS_4$ (989.73): calcd. C 40.04, H 3.26, N 4.24, S 12.96; found C 39.97, H 3.23, N 4.19, S 12.89. MS (ESI^+, CH_2Cl_2): *m/z* (%) = 691.6 (100) $[M]^+$. FTIR (Diamond crystal HATR, cm^{-1}): ν_{CO} = 2011.

2.2.18 UV-Visible Titration

The spectra of reference complexes [Rh(CO)(EtSNS)], [Rh(CO)(HEtSNS)]OTf and $[Rh(CO)(H_2EtSNS)](OTf)_2$ were recorded in *ca*. $1x10^{-3}$ M dichloromethane solutions (Respectively, Figure S1, S2 and S3 of the Appendix 1). Purity was previously checked by ^1H NMR, $^{31}P\{^1H\}$ NMR, and elemental analysis. A dichloromethane stock solution of [Rh(CO)(EtSNS)], *ca*. $7x10^{-3}$ M, was prepared by weight and diluted to *ca*. $1x10^{-4}$ M for the UV–Visible titration. KOH aqueous solutions (*ca*. 0.2 M) were prepared by diluting concentrated Merck Titrisol ampoules and standardised with the reported procedures.[6]

The titrant solution of HOTf (*ca*. $15x10^{-3}$ M) was prepared by dissolving pure triflic acid (15 µl) in 10 mL of CH_2Cl_2 with the addition of 150 µl of reagent grade methanol. Its titre was determined by titrating a suspension of 2 mL of a dichloromethane solution in water with the standard KOH solution, using phenolphthalein as indicator. Thirty UV–visible spectra were collected at different acid : complex ratios (range between 0 and 2.2) by the addition of 25 µL of titrant at each step (concentration of [Rh(CO)(EtSNS)] = $1x10^{-4}$ M, V_0 = 50 mL). The spectroscopic data were processed to calculate the protonation constants (pK_a) by means of the program SPECFIT 32 using the molar absorbance values of the pure protonated complexes as fixed parameters.[7] The wavelength range taken into account in the calculations was limited to 380–600 nm, where the complexes shown major variations in their absorption spectra. The distribution diagram was calculated and plotted using the program HYSS.[8]

2.2.19 X-ray Data Collection, Structure Solution, and Refinement

The intensity data of all compounds were collected at room temperature on a Bruker AXS Smart 1000[9a] single crystal diffractometer equipped with an area detector using a

graphite monochromated Mo Ka radiation (λ = 0.71073 Å). Crystallographic and experimental details of the structures are summarized in Table 1. When necessary, an empirical correction for absorption was made. The structures were solved by Patterson and Fourier methods and refined by full-matrix least-squares procedures (based on F_o^2)[9b] first with isotropic thermal parameters and then with anisotropic thermal parameters in the last cycles of refinement for all the non-hydrogen atoms. The hydrogen atoms were introduced into the geometrically calculated positions and refined *riding* on the corresponding parent atoms except for the amidic hydrogen atoms and those of the water molecule in $[Na(EtSNS)H_2O]_2$ which were localized in the $2F_o$-F_c map and refined isotropically. In $(H_2EtSNS)PF_6$ one of the two ethyl groups and PF_6 anion was found disordered in two position; in **2**·½THF the THF molecule was found disordered around the two fold axis and in **8**·2THF the PF_6 anion was found disordered in two positions.

Table 1 Crystal Data and Structure Refinement for $[Na(EtSNS)H_2O]_2$, $(H_2EtSNS)PF_6$, **1**, **2**·½THF, **4**, **5**, **6**, **7** and **8**·2THF

	$[Na(EtSNS)H_2O]_2$	**$(H_2EtSNS)PF_6$**	**1**	**2**·THF
formula	$C_{60}H_{64}N_6Na_2O_2P_4S_4$	$C_{30}H_{32}F_6N_3P_3S_2$	$C_{38}H_{42}N_3P_2Rh_1S_2$	$C_{49}H_{58}F_3N_3O_{3.5}P_2Rh_2S_3$
FW	1199.27	705.62	769.72	1165.92
crystal system	monoclinic	monoclinic	triclinic	monoclinic
space group	*C*2/*c*	$P2_1/c$	*P*-1	*C*2/*c*
a, Å	22.444(5)	15.213(1)	10.512(1)	32.825(1)
b, Å	14.903(4)	21.324(2)	11.562(1)	12.820(1)
c, Å	20.869(5)	21.006(2)	16.799(2)	24.689(1)
α, deg	90	90	97.63(2)	90
β, deg	117.12(1)	91.94(2)	102.87(2))	103.46(1)
γ, deg	90	90	109.26(2)	90
V, Å^3	62133	6811(1)	1831(1)	10104(9)
Z	4	8	2	8
D_{calcd}, g cm^{-3}	1.282	1.376	1.396	1.533
F(000)	2512	2912	796	4768
crystal size (mm^3)	0.18 x 0.19 x 0.10	0.10 x 0.09 x 0.08	0.30 x 0.10 x 0.10	0.23 x 0.19 x 0.12
μ cm^{-1}	3.16	3.56	6.98	8.96
rflns collected	33448	91636	19758	52978
rflns unique	6788	19135	7950	10464
rflns observed [$I>2\sigma(I)$]	4444	8955	6616	6053
parameters	362	910	430	647
R indices	R1 = 0.0469	R1 = 0.0447	R1 = 0.306	R1 = 0.0506
[$I>2\sigma(I)$]	wR2 = 0.1045	wR2 = 1090	wR2 = 0.0824	wR2 = 0.1222
R indices	R1 = 0.0939	R1 = 0.1129	R1 = 0.0394	R1 = 0.0907
(all data)	wR2 = 0.1204	wR2 = 0.1281	wR2 = 0.0862	wR2 = 0.1301

	4	**5**	**7**	**8**·2THF
formula	$C_{38}H_{43}Cl_1N_3P_2Rh_1S_2$	$C_{32}H_{32}Cl_2N_3O_2P_2Rh_1S_2$	$C_{35}H_{32}Cl_4N_3O_5P_2Rh_3S_2$	$C_{39}H_{47}F_6N_3O_3P_3Rh_1S_2$
FW	806.17	790.48	11541.23	979.74
crystal system	triclinic	monoclinic	monoclinic	monoclinic
space group	*P*-1	$P2_1/c$	$C2/c$	$P2_1/c$
a, Å	10.302(4)	15.909(4)	22.011(5)	20.678(8)
b, Å	13.579(5)	11.255(3)	14.479(4)	9.443(2)
c, Å	14.391(5)	20.474(5)	13.225(4)	23.131(6)
α, deg	80.86(5)	90	90	90
β, deg	78.57(5)	93.95(5)	92.98(5)	93.43(2)
γ, deg	74.99(5)	90	90	90
V, Å^3	1894(1)	3657(2)	4209(2)	4508(1)
Z	2	4	4	4
D_{calcd}, g cm^{-3}	1.414	1.436	1.817	1.444
F(000)	832	1608	2272	2008
crystal size (mm^3)	0.11 x 0.10 x 0.10	0.11 x 0.10 x 0. 90	0.12 x 0.11 x 0.10	0.20 x 0.16 x 0.15
μ cm^{-1}	7.47	8.47	16.35	6.41
rflns collected	34377	24575	22300	65699
rflns unique	12047	8403	4801	10437
rflns observed [$I>2\sigma(I)$]	8529	5448	3204	6665
parameters	453	411	246	572
R indices	R1 = 0.0337	R1 = 0.0343	R1 = 0.0264	R1 = 0.0380
[$I>2\sigma(I)$]	wR2 = 0.0713	wR2 = 0.0801	wR2 = 0.0393	wR2 = 0.0887
R indices	R1 = 0.1129	R1 = 0.0622	R1 = 0.0600	R1 = 0.0707
(all data)	wR2 = 0.0828	wR2 = 0.0888	wR2 = 0.0434	wR2 = 0.0997

[a]R1 = $\Sigma||F_o|-|F_c||/\Sigma|F_o|$. wR2 = $[\Sigma[w(F_o^2-F_c^2)^2]/\Sigma[w(F_o^2)^2]]$

2.3 Results and Discussion

2.3.1 Acid-base properties of HEtSNS

The thioamidyl moiety of HEtSNS can be protonated with acids as HCl or HPF_6, forming the respective salts, while deprotonation of HEtSNS can be achieved with NaH (Scheme 1).

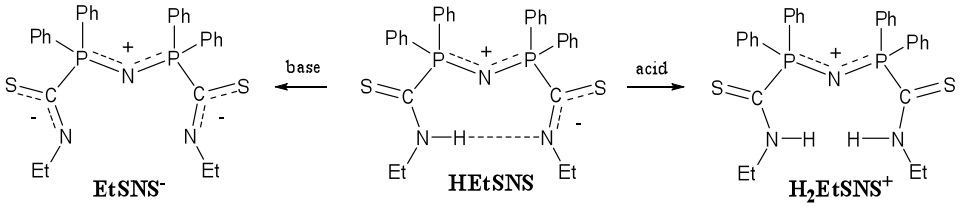

Scheme 1. Lewis structures and formal charge distribution of HEtSNS and its deprotonated ($EtSNS^-$) and protonated (H_2EtSNS^+) forms.

Single crystals of $(H_2EtSNS)PF_6$ (yellow) and $[Na(EtSNS)H_2O]_2$ (colorless) were obtained. Views of their crystal structures are reported in Figures 1. Selected bond distances

and angles are listed in Table 2 and compared to those previously reported for HEtSNS[1] and to those of the complexes described herein.

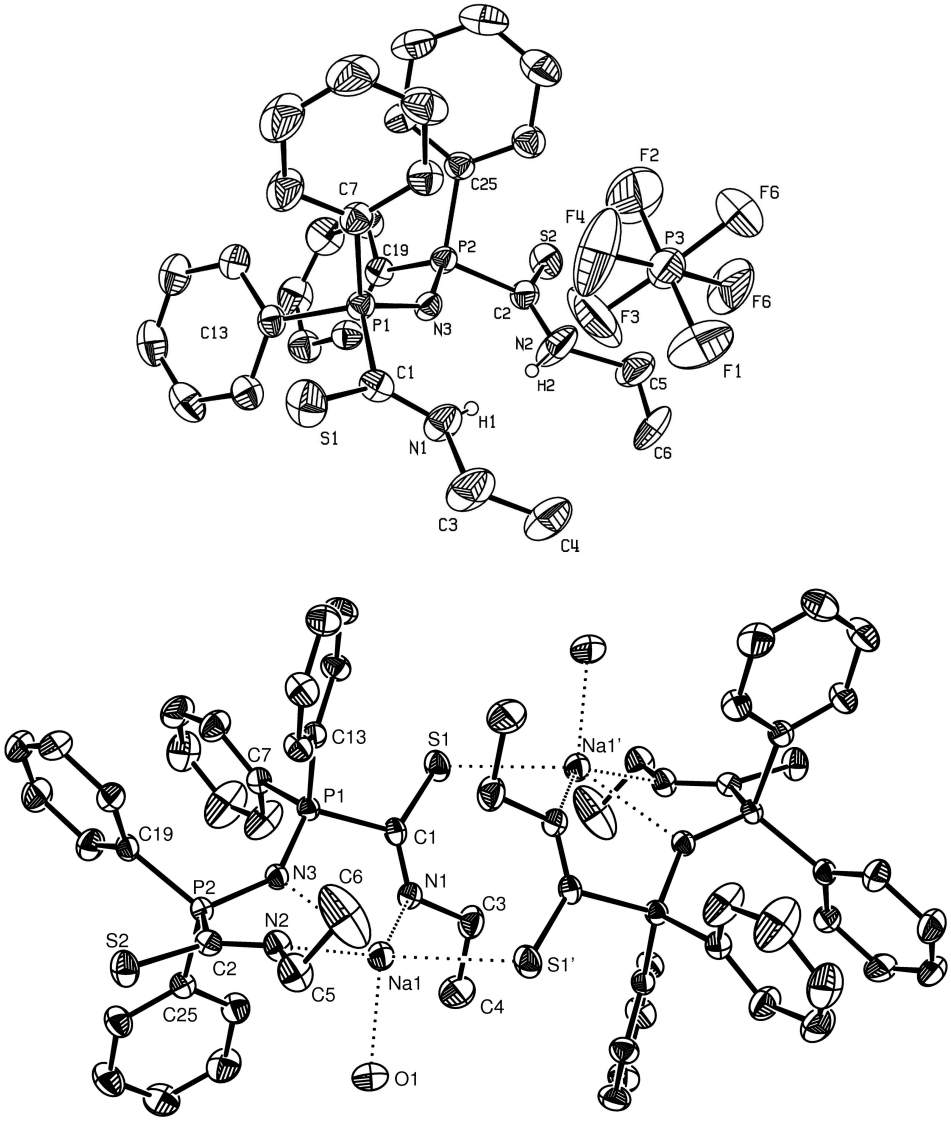

Figure 1. ORTEP plots of the molecular structures of $(H_2EtSNS)PF_6$ and $[Na(EtSNS)H_2O]_2$. Thermal ellipsoids are drawn at 30% probability level. H atoms are omitted for clarity. Only one of the two crystallographic independent $(H_2EtSNS)PF_6$, units is depicted.

In the crystals of $(H_2EtSNS)PF_6$, two independent H_2EtSNS^+/PF_6^- couples are present and display similar geometrical parameters. The N1···N2 separation of 4.315(3) Å is larger than that of HEtSNS [2.856(8) Å],[1] the latter featuring an intramolecular hydrogen bond (Scheme 1). Differently from HEtSNS, the P–N–P system is coplanar with the two thioamidic groups

[maximum deviation from the mean plane defined by C1, N1, S1, C2, N2, S2, P1, N3, P2 = 0.104 Å], probably due to a bifurcated (on the donor atom) hydrogen bonding of the type N1–H···N3···H–N2 (H1···N3 and H2···N3 distances: 2.396(1) and 2.418(1)Å). The presence of an interaction with the N3 lone pair is also suggested by the P–N–P angle, which is significantly narrower than those of HEtSNS and $[Na(EtSNS)H_2O]_2$.

The hydrated dimeric salt $[Na(EtSNS)H_2O]_2$ crystallized in the air by evaporation of a CH_2Cl_2/hexane solution of [Na(EtSNS)]. Each Na^+ cation interacts with the three nitrogen atoms of $EtSNS^-$ (Na–N3, Na–N1, Na–N2 distances: 2.592(2), 2.478(2), 2.503(3) Å, respectively) and with the oxygen atom of a water molecule (Na–Ow separation: 2.277(3) Å). The two units are connected by S···Na interactions (Na–S1' distance is 2.893(1) Å) resulting in a distorted square pyramidal geometry around Na^+ ions. It is worthy to note that sulfur–bridged complexes of alkaline metals are far less common than their oxygen-containing counterparts.[10]

Solid Na(EtSNS) is not stable towards hydrolysis. When left in the air it reacts with water vapor, transforming to HEtSNS. The presence of coordinated water in the crystals of $[Na(EtSNS)H_2O]_2$ seems to indicate that the dimerization results in a much lower reactivity towards hydrolysis. When a sample of Na(EtSNS) was dissolved in *d*-chloroform, spontaneous re-transformation in H(D)EtSNS was monitored by $^{31}P\{^1H\}$ NMR over a period of ca. two hours, the 8.0 ppm signal of colorless Na(EtSNS) being replaced by that of yellow HEtSNS at 8.4 ppm.[11] The initial observation of a sharp singlet (regardless of the temperature) suggested that, in this solution, the salt is present in its monomeric form. On the contrary, monomeric NaEtSNS is stable in DMSO solution. Also in this case, only a sharp singlet was observed in the $^{31}P\{^1H\}$ NMR spectrum in DMSO-d_6 (δ = 7.2 ppm) and even the addition of a large excess of water did not result in the formation of HEtSNS (δ = 13.8 ppm). This stabilizing effect is probably stemming from the interaction of Na^+ with DMSO, through the oxygen atom.[12]

In $(H_2EtSNS)PF_6$, $[Na(EtSNS)H_2O]_2$ and HEtSNS the P1–N3 and P2–N3 bond distances are rather similar while variations can be evidenced in the C–S and C–N distances. As expected, the protonation of the thioamidyl group results in the lengthening of the corresponding C–N bonds and in shorter C–S distances; the same behavior is observed in the complexes described herein.

Table 2. Selected bond lengths (Å) and angles (°).

	$[Na(EtSNS)H_2O]_2$	**HEtSNS**	**$(H_2EtSNS)PF_6$**	**1**	**4**	**6**
P1–N3	1.576(2)	1.584(2)	1.596(1)	1.5810(18)	1.5832(18)	1.580(2)
P2–N3	1.585(2)	1.575(2)	1.599(1)	1.5798(18)	1.5721(17)	1.591(3)
P1–C1	1.845(2)	1.841(2)	1.843(2)	1.831(3)	1.829(2)	1.843(3)
P2–C2	1.843(2)	1.858(2)	1.837(2)	1.840(2)	1.852(2	1.833(3)
C1–S1	1.713(2)	1.690(2)	1.650(2)	1.747(3)	1.747(2)	1.631(3)
C2–S2	1.705(3)	1.660(2)	1.638(2)	1.744(2)	1.656(2)	1.639(3)
C1–N1	1.276(3)	1.297(3)	1.302(3)	1.269(3)	1.266(3)	1.305(4)
C2–N2	1.284(3)	1.314(3)	1.291(3)	1.269(3)	1.303(3)	1.314(4)
S1–Rh1	-	-	-	2.3457(7)	2.3614(15)	-
S2–Rh1	-	-	-	2.4047(6)	-	-
P1–N3–P2	140.8(1)	140.3(3)	132.9(1)	136.2(1)	140.25(10)	136.7(2)

	[Rh(CO)(EtSNS)]	**7**	**8**
P1–N3	1.643(2)	1.619(1)	1.625(2)
P2–N3	1.643(2)	1.619(1)	1.613(2)
P1–C1	1.851(5)	1.825(2)	1.823(3)
P2–C2	1.851(5)	1.825(2)	1.827(3)
C1–S1	1.764(5)	1.673(2)	1.742(3)
C2–S2	1.764(5)	1.673(2)	1.679(3)
C1–N1	1.288(7)	1.307(3)	1.279(3)
C2–N2	1.288(7)	1.307(3)	1.315(4)
S1–Rh1	2.367(2)	2.298(1)	2.315(1)
S2–Rh1	2.367(2)	2.298(1)	2.314(1)
N–Rh	2.159(2)	2.115(3)	2.126(2)
P1–N3–P2	134.3(3)	139.75(30)	133.3(2)

2.3.2 Coordination properties and geometrical versatility of $EtSNS^-$, HEtSNS and H_2EtSNS^+.[13]

Reaction of HEtSNS with $[Rh(cod)Cl]_2$ in the presence of *t*BuOK. The reaction of HEtSNS and $[Rh(cod)Cl]_2$ in the presence of a stoichiometric amount of *t*BuOK (Scheme 2) yields [Rh(cod)(*S*,*S*–EtSNS)] (**1**) in quantitative yields. A view of its molecular structure is depicted in Figure 3.

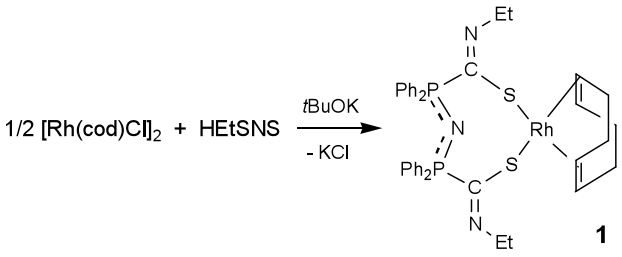

Scheme 2

In complex **1**, $EtSNS^-$ chelates the metal centre through both sulfur atoms, forming an 8-membered ring. The distorted square planar coordination is completed by a chelating cod molecule. The S1–Rh1–S2 angle of 92.90(2)° is dramatically narrower than that observed in the *S*,*S*–chelated complex [Au(EtSNS)],[2] in which the coordination over the metal centre is almost linear [S1–Au1–S2 = 177.73(6)°].

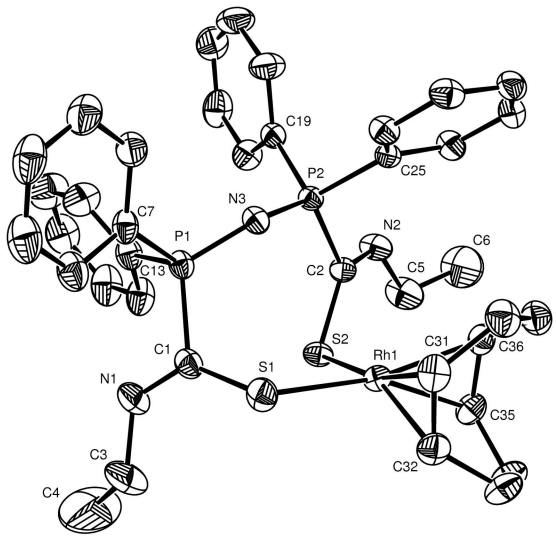

Figure 3. ORTEP plot of the molecular structure of **1**. Thermal ellipsoids are drawn at 30% probability level. H atoms are omitted for clarity.

An intermediate geometry was found in dimer $[Ag(EtSNS)]_2$ [mean value of the S–Ag–S angles = 136.6(1)°].[14] The structural flexibility of $EtSNS^-$ allows the ligand to comply with the coordination requests of the different metal centres. In **1**, the charge separation is conserved so that this complex belongs to the category of zwitterionic metallates.[15]

Reaction of HEtSNS with $[Rh(CO)_2Cl]_2$ in the presence of *t*BuOK. The reaction of HEtSNS and $[Rh(CO)_2Cl]_2$ in the presence of a stoichiometric amount of *t*BuOK results in the quantitative formation of [Rh(CO)(EtSNS)]. This compound was previously reported as the

product of the reaction between NaEtSNS and $[Rh(CO)_2Cl]_2$.[1b] In the same work, $[Rh(CO)_2(S,N–EtSNS)]$ was proposed as intermediate product of the reaction (evidenced by FTIR spectrophotometry). In view of the isolation of compound **1**, we now propose $[Rh(CO)_2(S,S–EtSNS)]$ to be the actual intermediate, as shown in Scheme 3.

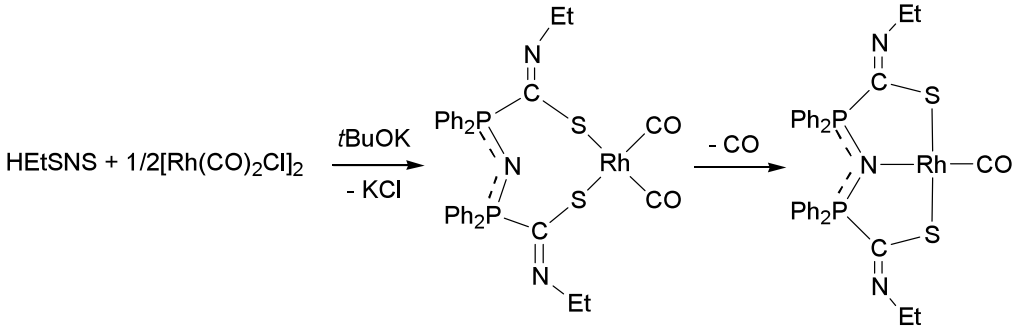

Scheme 3

Complex **1** undergoes cyclooctadiene substitution by bubbling CO in dichloromethane solution, at room temperature and atmospheric pressure, transforming quantitatively to [Rh(CO)(EtSNS)].

A Rh_2 dinuclear complex. Reaction of **1** with $[Rh(cod)(THF)_2]OTf$ results in the formation of the purple dinuclear compound $[\{Rh(cod)\}_2(\mu–S,S–EtSNS)]OTf$ (**2**). An ORTEP plot of the structure of $[\{Rh(cod)\}_2(\mu–S,S–EtSNS)]^+$ in **2**·½THF is reported in Figure 4.

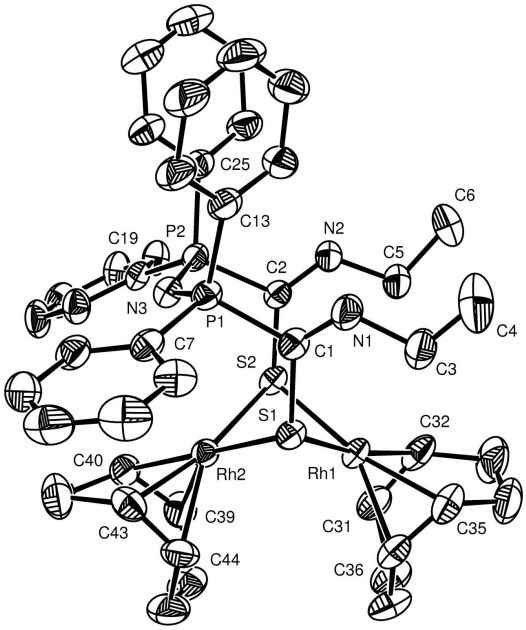

Figure 4. ORTEP plot of the molecular structure of the cation of **2** in **2**·½THF. Thermal ellipsoids are drawn at 30% probability level. H atoms are omitted for clarity. Selected distances [Å] and angles [°]: P1–N3 1.591(4), P2–N3 1.587(4), P1–C1 1.834(5), P2–C21.829(5), C1–S1 1.786(5), C2–S2 1.790(5), C1–N1 1.244(6), C2–N2 1.250(6), S1–Rh1 2.417(1), S2–Rh1 2.400(1), S1–Rh2 2.369(1), S2–Rh2 2.407(2), Rh1–Rh2 2.942(1), P1–N3–P2 128.0(3).

Dinuclear complex **2** can be seen as an adduct between **1** and the fragment $[Rh(cod)]^+$. Both sulfur atoms of $EtSNS^-$ bridge the metal centres forming a Rh_2S_2 core, rather common for dithiolate complexes.[16] The Rh–S bond lengths range from 2.369(1) Å for Rh2–S1 to 2.417(1) Å for S1–Rh1. The ligand geometry differs from that observed in compound **1**, emphasizing its geometrical versatility. In particular, the P1, C1, S1, N1 and P2, C2, S2, N2 mean planes are almost orthogonal in **1** [88.2(1)°] while in **2** they are almost parallel [19.2(4)°].

A similar reaction, between **1** and $[Rh(cod)Cl]_2$, carried out in chlorinated solvents, did not afford the expected dinuclear complex $[\{Rh(cod)\}_2(\mu\text{–}S,S\text{–EtSNS})]Cl$ (**3**), analogous to **2**, as evidenced by the $^{31}P\{^1H\}$ NMR spectra in which only the signal of **1** (9.7 ppm, $CDCl_3$) was visible.

On the other hand, **3** was quantitatively formed when methanol was used as solvent, as confirmed by $^{31}P\{^1H\}$ NMR and the ESI–MS spectrum, showing the expected $(M–Cl)^+$ peak at 980.26 *m/z*. The assembly of **3** was monitored using $^{31}P\{^1H\}$ spectroscopy by addition of known quantities of CH_3OH into a stoichiometric solution of **1** and $[Rh(cod)Cl]_2$ in CD_2Cl_2 ($CD_2Cl_2/CH_3OH \approx 5$). Any attempt to obtain **3** in the solid state failed: re-formation of **1** and

$[Rh(cod)Cl]_2$ was observed upon solvent removal. Moreover, only crystals of the two precursors could be separated by any crystallization method that was tried. This equilibrium strongly depends on the dielectric properties of the solvent but also on the ionic strength of the solution, since upon addition of $(Et_4N)PF_6$, assembly of **3** can be achieved in $CHCl_3$.

Reaction of HEtSNS with [Rh(cod)Cl]$_2$. Complex [Rh(*S*–HEtSNS)(cod)Cl] (**4**), in which HEtSNS behaves as monodentate, was prepared by reacting HEtSNS with $[Rh(cod)Cl]_2$ (Scheme 4).

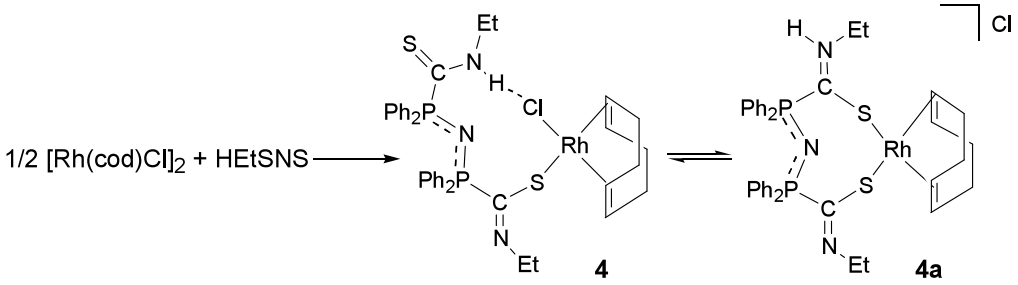

Scheme 4

In the $^{31}P\{^1H\}$ NMR of **4** in *d*-chloroform, two sets of peaks are present. Two doublets (δ = 11.1 (d), 10.5 (d) ppm; ^2J(P,P) = 15.9 Hz) can be assigned to **4** while a singlet at 12.4 ppm suggests the presence of a second species, probably isomer [Rh(*S*,*S*'–HEtSNS)(cod)]Cl (**4a**), which may be in slow equilibrium with **4** (integral ratio **4**/**4a** ≈ 10, see spectrum in Figure S1 of the Appendix 1). In complex **4a**, HEtSNS could behave as an *S*,*S* chelating ligand, similarly to what observed in **1**.

Isomer **4a** is only present in solution, since the HATR infrared spectrum of the crude powder obtained by evaporation of the reaction solvent, was found superimposable to the spectrum of a single crystal of **4**. In the ^1H NMR spectra, two broad N–H signals can be observed at 11.4 and 12.8 ppm, (assigned to **4** and **4a**, respectively). In the solid state structure of **4**, HEtSNS is coordinated through the sulfur atom of the thioamidyl group, a chloride and a chelating cod being bound to the Rh atom. A N2H3n···Cl interaction is present, forming a 10-membered pseudo-ring (Figure 5).

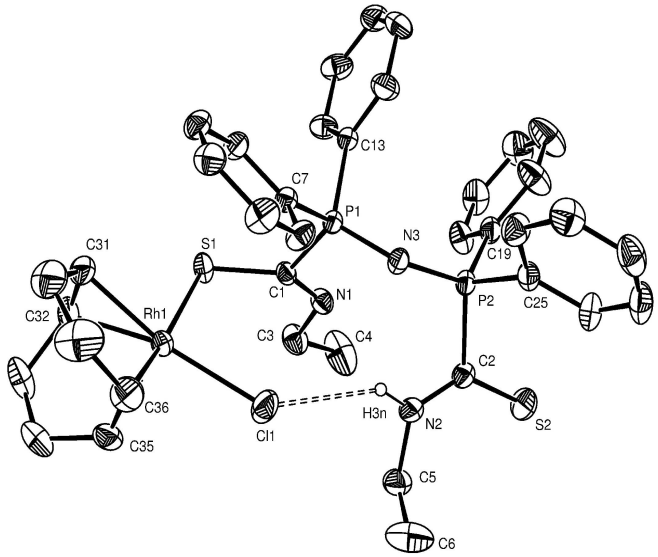

Figure 5. ORTEP plot of the molecular structure of **4**. Thermal ellipsoids are drawn at 30% probability level. H atoms are omitted for clarity.

As evidenced by *in situ* $^{31}P\{^{1}H\}$ NMR, when *t*BuOK was added to a $CDCl_3$ solution of **4**, compound **4a** was first, quickly and completely consumed, slowly followed by deprotonation of compound **4**. Both reactions converged to the formation of [Rh(cod)(*S*,*S*–EtSNS)] (**1**, singlet at 9.7 ppm).

This fast reactivity is in agreement with the proposed structure of **4a** whose formula can be written as **1**·HCl. When methanol was added to a chloroform solution of **4** (Scheme 5), the solution color instantly changed from yellow to purple. The $^{31}P\{^{1}H\}$ NMR suggested the formation of H_2EtSNS^+ along with the dinuclear compound **3** (13.3 and 17.9 ppm respectively).

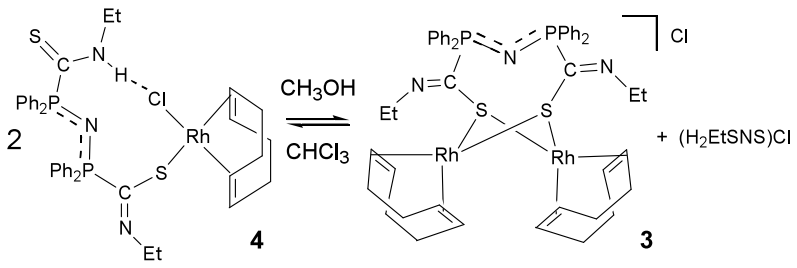

Scheme 5. Solvent dependent equilibrium for complex **3** and **4**.

This equilibrium, which implies the autoprotonation reaction:

$$2\ HEtSNS \rightarrow H_2EtSNS^+ + EtSNS^-$$

is somehow similar to the formation of **3** in methanol, confirming that the cationic dinuclear entity $[\{Rh(cod)\}_2(\mu\text{–}S,S\text{–}EtSNS)]^+$ is favored in polar solvents. Moreover, the attempt to perform a chloride abstraction from **4** using AgOTf, with the aim of obtaining a *S,S'*–HEtSNS chelated complex analogous to **4a** failed, resulting in the formation of $[\{Rh(cod)\}_2(\mu\text{–}S,S\text{–}EtSNS)]OTf$ (**2**).

Reaction of HEtSNS with $[Rh(CO)_2Cl]_2$. In the reaction of HEtSNS with $[Rh(CO)_2Cl]_2$ in dichloromethane (Scheme 6), three products are formed, as detected by $^{31}P\{^1H\}$ NMR.

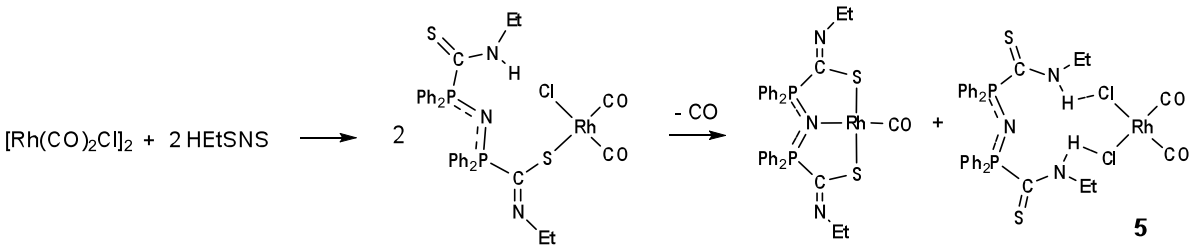

Scheme 6.

The main products of the reaction correspond to the *S,N,S* tridentate complex [Rh(CO)(EtSNS)] (16.6 ppm) and to $[H_2EtSNS]^+[Rh(CO)_2Cl_2]^-$ (**5**) (13.3 ppm). Two low intensity doublets at 11.9 and 11.4 ppm ($^2J_{PP}$ = 15.2 Hz) suggest the formation of monodentate complex $[Rh(CO)_2(S\text{–}HEtSNS)Cl]$, analogous to **4**, as intermediate minor product. Compound **5** was separated by crystallization and its molecular structure determined by X-ray diffraction (see Figure S2 of the Appendix 1) and it displays geometrical parameters analogous to those observed for compound **6** (*vide infra*). The cation in compound **5** stems from the protonation reaction of HEtSNS due to the scavenging of HCl liberated in the formation of [Rh(CO)(EtSNS)]. The chloride was found coordinated by the Rh atom of anion $[Rh(CO)_2Cl_2]^-$. The reaction is probably driven by the stability of the *S,N,S* tridentate complex [Rh(CO)(EtSNS)]. Complex $[Rh(CO)_2(S\text{–}HEtSNS)Cl]$ can be regarded as the first reaction product, successively yielding **5** and [Rh(CO)(EtSNS)].

Reaction of $(H_2EtSNS)X$ (X = Cl, PF_6) with $[Rh(cod)Cl]_2$. The reactivity of $(H_2EtSNS)X$ (X = Cl, PF_6) depends on the coordinative properties of the anion. The reaction of $(H_2EtSNS)Cl$ with $[Rh(cod)Cl]_2$ yielded $[H_2EtSNS][Rh(cod)Cl_2]$ (**6**). A view of its molecular structure, determined by X-ray diffraction methods, is reported in Figure 6.

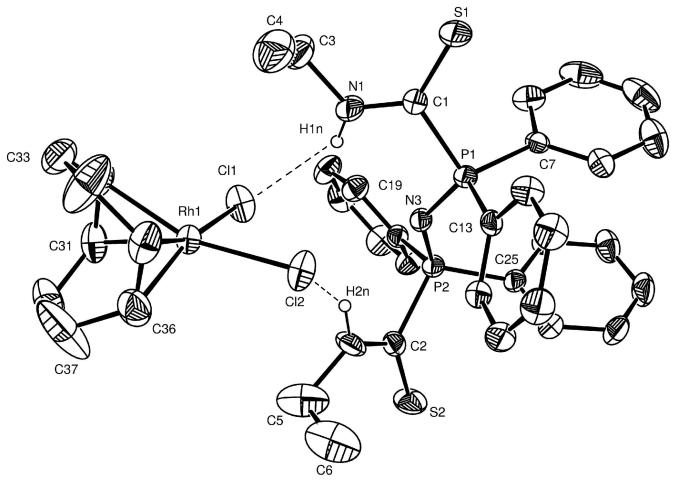

Figure 6. ORTEP plot of the molecular structure of **6**. Thermal ellipsoids are drawn at 30% probability level. H atoms are omitted for clarity.

In the crystal structure, bond lengths and angles of H_2EtSNS^+ are similar to those observed for $(H_2EtSNS)PF_6$, except for the P–N–P angle which is slightly bigger [**6**: 136.7(2)°; $(H_2EtSNS)PF_6$: 132.9(1)°, 133.9(1)°] and the value of the C1–P1–P2–C2 torsion angle (*circa* 1° for $(H_2EtSNS)PF_6$ and 91° for **6**). The cation–anion interaction features two H···Cl contacts as depicted in Figure 6. Being the positive charge located on the P–N–P system, this interaction is reminiscent of the anion coordination by neutral thioureas and ureas.[17] No reaction was observed between $(H_2EtSNS)PF_6$ and $[Rh(cod)Cl]_2$. The cation H_2EtSNS^+ is thus unable to open the chloride bridge of the dimeric precursor and coordinate to the Rh centre (see below for the coordination properties of H_2EtSNS^+).

Reaction of $(H_2EtSNS)X$ (X = Cl, PF_6) with $[Rh(CO)_2Cl]_2$. Although **6** can be quantitatively prepared by the aforementioned reaction of $(H_2EtSNS)Cl$ with ½ $[Rh(cod)Cl]_2$, a similar reaction pathway can not be followed for the synthesis of **5**.

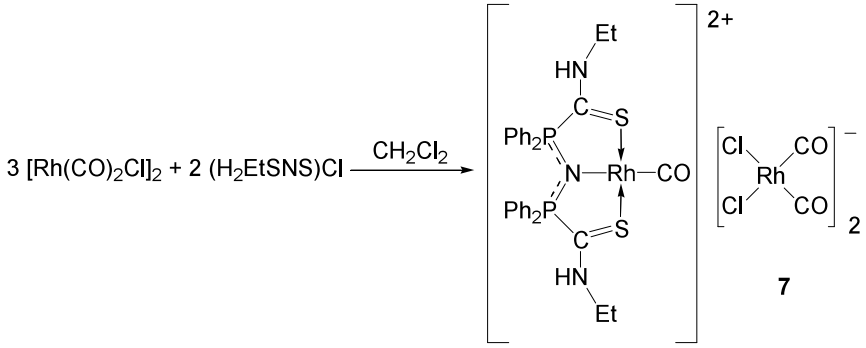

Scheme 7.

The reaction of $(H_2EtSNS)Cl$ with $[Rh(CO)_2Cl]_2$ in CH_2Cl_2 afforded $[Rh(CO)(S,N,S–H_2EtSNS)][Rh(CO)_2Cl_2]_2$ (**7**); two unreacted $(H_2EtSNS)Cl$ were also observed, by $^{31}P\{^1H\}$ NMR. The coordination of the Cl^- liberated in the formation of $[Rh(CO)(S,N,S–H_2EtSNS)]^{2+}$ afforded the two chloro-rhodates $[Rh(CO)_2Cl_2]^-$ and, due to the formation of a new coordination site by the loss of a CO molecule, the cation H_2EtSNS^+ could act as ligand for a $Rh(CO)^+$ group. A more convenient preparation of **7** was achieved by reacting $(H_2EtSNS)Cl$ with $[Rh(CO)_2Cl]_2$ in a 2 : 3 ratio (Scheme 7). A view of its structure, determined by X-ray diffraction methods, is reported in Figure 7.

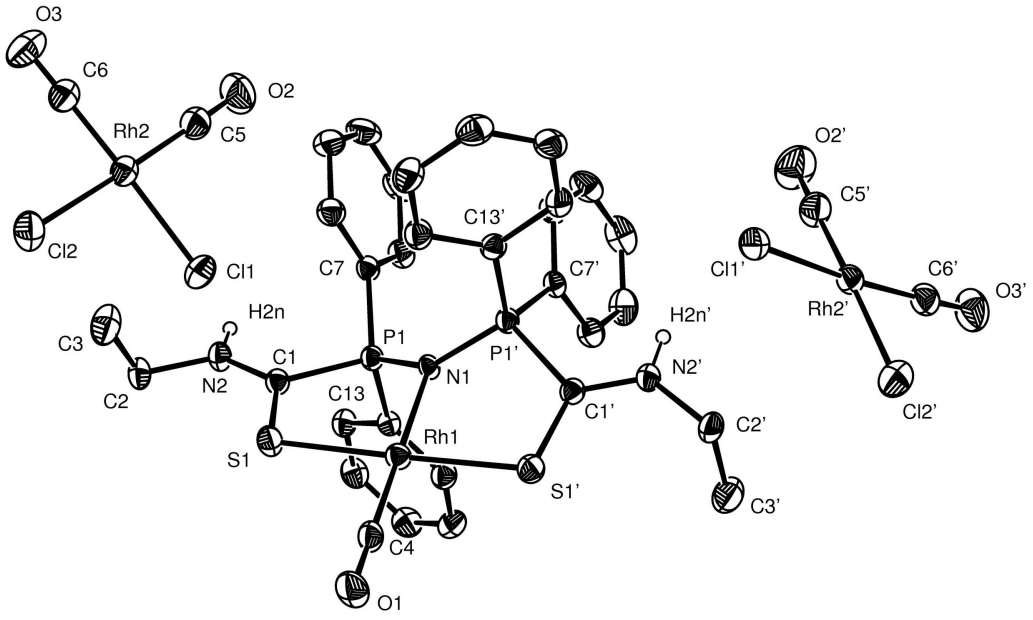

Figure 7. ORTEP plot of the molecular structure of **7**. Thermal ellipsoids are drawn at 30% probability level. H atoms are omitted for clarity. Symmetry transformation used to generate equivalent atoms: 1 – x, y, ½ – z.

The formation of **7** suggested that other stable protonated derivatives of [Rh(CO)(EtSNS)] could be obtained (Scheme 8). Indeed, [Rh(CO)(*S*,*N*,*S*'–HEtSNS)]PF_6 ([Rh(CO)(EtSNS)] · HPF_6, **8**) was synthesized by protonation of [Rh(CO)(EtSNS)] with an equimolar amount of HPF_6 or by complexation of $[Rh(CO)_2(MeCN)_2]PF_6$ with HEtSNS. In a similar manner, [Rh(CO)(*S*,*N*,*S*–H_2EtSNS)]$(PF_6)_2$ ([Rh(CO)(EtSNS)] · $2HPF_6$, **9**) was prepared by protonation of [Rh(CO)(EtSNS)] with two equimolar amounts of HPF_6 or by reacting $[Rh(CO)_2(MeCN)_2]PF_6$ with $(H_2EtSNS)PF_6$. The latter reaction is an example of complex formation by reacting a cationic ligand and a cationic metal fragment, not frequent in coordination chemistry.[18] The cations of **7** and **9**, [Rh(CO)(*S*,*N*,*S*–H_2EtSNS)]$^+$, are identical. Single crystals of **8**·2THF were obtained. Its structure is depicted in Figure 8.

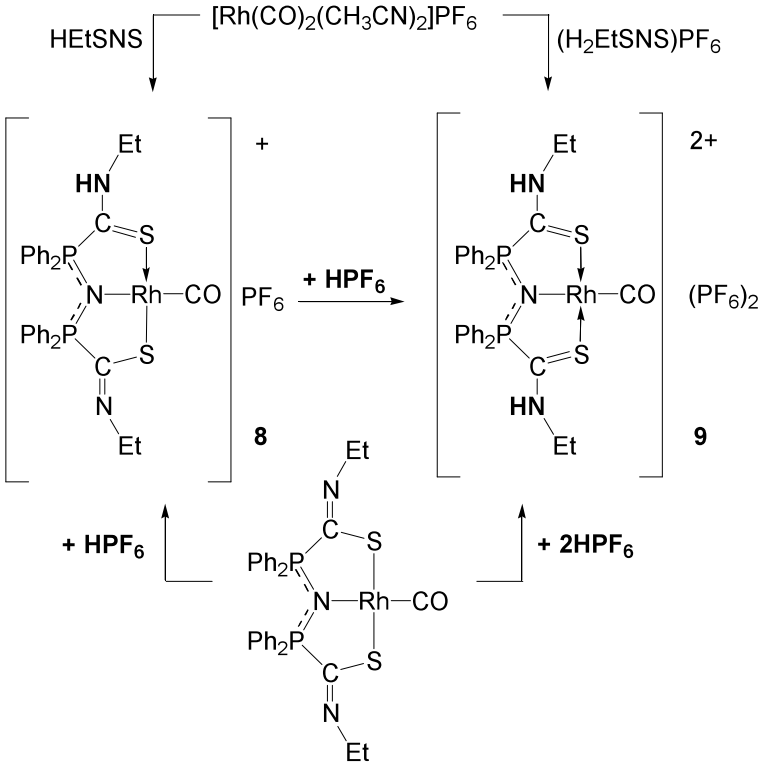

Scheme 8. Formation of complexes **8** and **9** by protonation of [Rh(CO)EtSNS] and direct complexation of $[Rh(CO)]^+$ species.

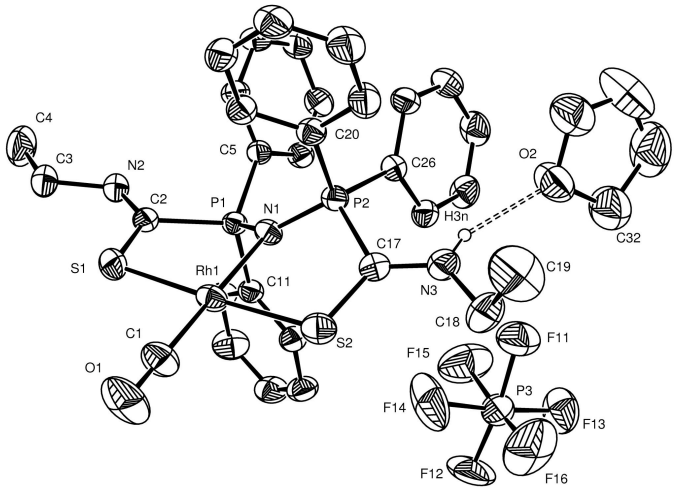

Figure 8. ORTEP plot of the molecular structure of **8**·THF in **8**·2THF. Thermal ellipsoids are drawn at 30% probability level. H atoms are omitted for clarity. The second THF molecule was not involved in direct interactions with the complex and is omitted for clarity.

It is worthy to note that in **7**, **8** and [Rh(CO)(EtSNS)] the coordination geometry is almost identical. The ligands correspond to, respectively, cationic H_2EtSNS^+, neutral–zwitterionic HEtSNS and dianionic–cationic $EtSNS^-$. In the solid state infrared HATR spectra of the complexes [Rh(CO)(EtSNS)], **8** and **9**, the CO stretching frequency increases (1951, 1979, and 1996 cm^{-1} respectively in the solid state; 1968, 1994 and 2017 cm^{-1} respectively in CH_2Cl_2 solution), suggesting that the protonation of [Rh(CO)(EtSNS)] results in a decreased electron density on the metal centre and thus in a weaker Rh→CO back donation.[19] The P–N distances in **7** and **8** are slightly shorter than those of [Rh(CO)(EtSNS)], as well as the P–C ones. Since the protonation of HEtSNS does not affect the P–N–P system (see Table 2), this small change could stem from a variation of the ligating properties of the thioamidyl/thioamidic groups. In fact, the Rh–S bond length increases in the **7**, **8**, [Rh(CO)(EtSNS)] series, in turn affecting the P–N–P system through the metal centre. The thioamidyl fragment, more thiolato in character, is a stronger donor than the thioamidic group of thione character. The Rh–N distance is slightly shorter in the protonated species, probably influenced by the lower electron density on the Rh atom. The ^{31}P chemical shift is strongly affected by the protonation: [Rh(CO)(EtSNS)] shows a sharp singlet at 16.6 ppm ($CDCl_3$) while in **9** the two equivalent P atoms resonate at 38.2 ppm. The $^{31}P\{^1H\}$ NMR data recorded in *d*-chloroform for **8** shows two sharp singlets (35.0 and 19.9 ppm), assigned respectively to the P atoms bound to the thioamidic and thioamidyl coordinated functions[20] suggesting the

absence of fast proton exchange. The solid state ^{31}P NMR of compound **8** was recorded and the two peaks (36.1 and 24.1 ppm) were observed. As a reference, in the solid state NMR spectrum of HEtSNS, two singlets are found at 8.1 (thioamidic) and 2.6 ppm (thioamidyl), showing that Rh coordination exerts a strong influence on the chemical shift of the P atoms. The formal Lewis structures depicted in Scheme 8 are in agreement with this observation and with the bond distances discussed above. The thioamidic groups can be considered neutral in **8** and **9**; the *formal* charge on the Rh atom is negative in [Rh(CO)(EtSNS)], neutral in **8**, positive in **9**. The Mulliken atomic net charge for complex [Rh(CO)(EtSNS)] (-0.150, -0.157, -0.177 in gas, cyclohexane and THF respectively) was calculated by DFT methods.[1a] A positive charge is always shared by the two P atoms.

Protonation reaction of complex 1. The protonation behaviour of complex **1** using HCl or HOTf doesn't parallel the one of [Rh(CO)EtSNS]; change of the ligand coordination geometry was observed, as depicted in Scheme 9. When one equivalent of HCl was used, S–monodentate HEtSNS was formed and the chloride anion substituted a sulfur atom in the coordination sphere of Rh, yielding complexes **4** and **4a**. With two equivalents of HCl, cation H_2EtSNS^+ formed, the second chloride anion entered in the coordination sphere of Rh, and complex **6** was obtained. When HOTf was used the formation of **2** was observed, together with one equivalent of H_2EtSNS^+. The different reactivity is apparently due to the lower stability of the bidentate complex with respect to the tridentate [Rh(CO)EtSNS].

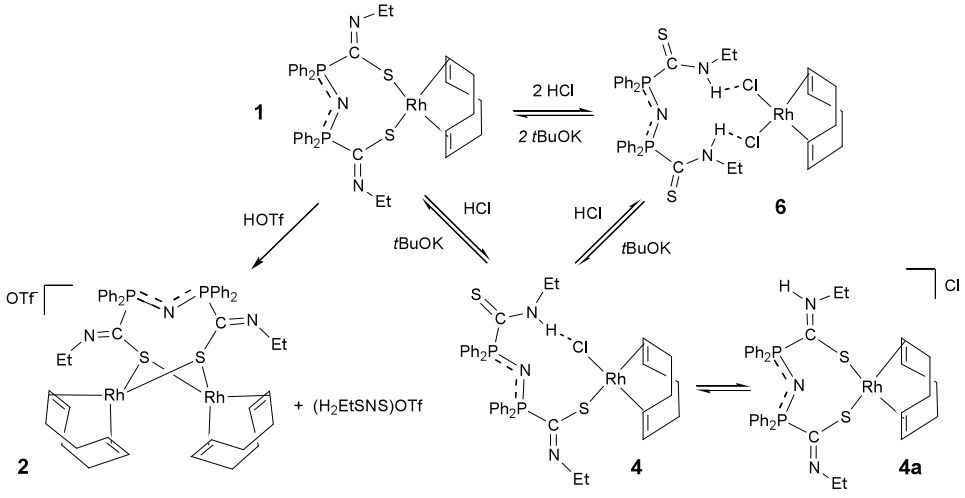

Scheme 9. Acid–base reactions for complex **1**

2.3.3 Acid–base properties of [Rh(CO)(EtSNS)]

Protonation equilibria of [Rh(CO)(EtSNS)] were studied by means of spectroscopic UV–Visible titration in CH_2Cl_2, using a solution of HOTf in a 1.5% mixture of methanol in dichloromethane.[21] Under these conditions it was assumed that HOTf is completely dissociated and acts as a superacid,[22a] so that the concentration of H^+ can be considered equal to the analytical concentration of the acid added (the methanol is present to allow the triflic acid to completely dissolve and to level HOTf to $CH_3OH_2^+$).[22b] These circumstances allow for the determination of the pK_a in this solvent on an absolute scale. In the literature, protonation equilibria of ligands and complexes in CH_2Cl_2 were studied by means of proton exchange reactions using $HP(Cy)_3^+$ (Cy = cyclohexyl) as weak acid, for which a pK_a = 9.7 was established by literature convention.[23] This pK_a scale, however, represents a relative pK_a ladder which should be rescaled to the real $HP(Cy)_3^+$ acidity constant.[24] The employment of triflic acid as titrant, dissolved in CH_2Cl_2 with small amounts of methanol, allows for a direct evaluation of protonation equilibria, in a similar way as studying the protonation equilibria in water by means of fully dissociated HCl.

In the titration of [Rh(CO)(EtSNS)] with triflic acid three very well defined isosbestic points were detected: one at 438 nm for acid to complex ratios from 0 to 1, and two at 509 and 385 nm for acid to complex ratios from 1 to 2 (Figure 9). These results are in agreement with the expected diprotic nature of $[Rh(CO)(H_2EtSNS)]^{2+}$ and the presence of two distinct protonation processes involving [Rh(CO)(EtSNS)].

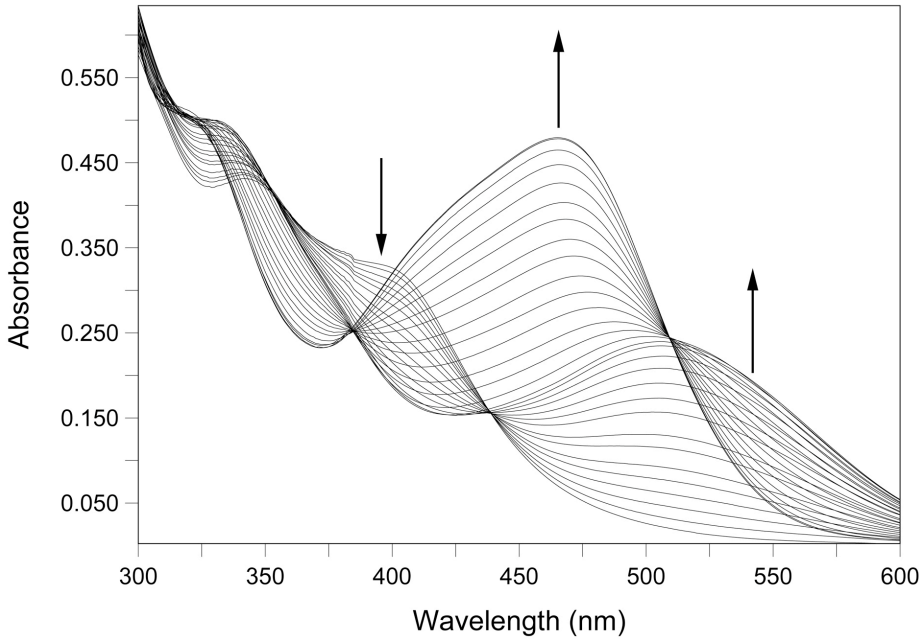

Figure 9. Experimental UV–Visible spectra (300–600 nm) for the titration of [Rh(CO)(EtSNS)] with HOTf in CH_2Cl_2.

Two pK_a values of 4.8(4) and 6.5(3) ($\sigma = 4.11 \cdot 10^{-2}$) were determined for the dissociation processes:

$$[Rh(CO)(H_2EtSNS)]^{2+} \leftrightarrows [Rh(CO)(HEtSNS)]^{+} + H^{+}$$

$$[Rh(CO)(HEtSNS)]^{+} \leftrightarrows [Rh(CO)(EtSNS)] + H^{+}$$

A representative distribution diagram for the $[Rh(CO)(H_2EtSNS)]^{2+}$ complex is shown in Figure 10 (UV-Vis spectra of pure samples of [Rh(CO)(EtSNS)], [Rh(CO)(EtSNS)] · HOTf and [Rh(CO)(EtSNS)] · 2HOTf are reported in Appendix 1). Recently, a similar acid–base behavior was observed for Pd complexes of thioamidic SNS pincer ligands but protonation constants were not determined.[25] Unfortunately, although the protonation equilibria of several complexes were investigated in the last decade[22, 23] the dissociation constants were all referenced to the $HP(Cy)_3^+$ standard, and no direct comparison with those values is possible. Titration of HEtSNS by UV-Vis was not possible due to the absence of suitable variation in the absorption spectra. The titration was performed monitoring the protonation by ^{31}P NMR. In these conditions, the basicity of the ligand is too high for p*K* determination.

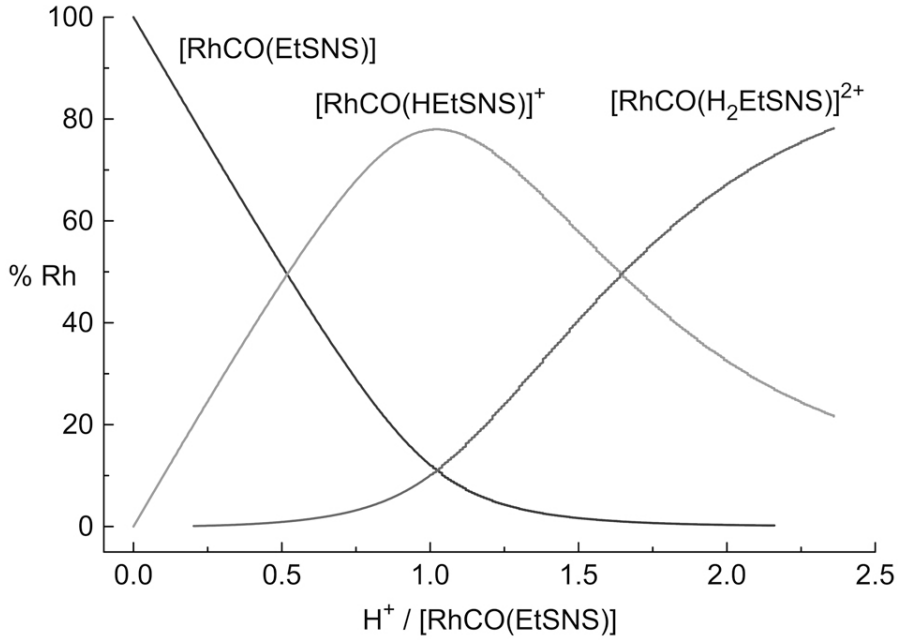

Figure 10. Distribution diagram for the titration of [Rh(CO)(EtSNS)] (C_{Rh} = 1x10^{-4} M).

2.4 Conclusions

The zwitterionic ligand HEtSNS is amphoteric and possesses ligating properties in all of its three forms: zwitterionic–neutral, zwitterionic–anionic and cationic. This work, together with previous results, evidenced its geometrical versatility which allows the following coordination fashions: *S*–monodentate (compound **4**) eight-membered chelating *S*,*S*–bidentate with 180° bite-angle ([Au(EtSNS)][2]) or 90° bite-angle (compound **1**), *S*,*N*,*S*–bischelating ([Rh(CO)EtSNS][1], [Cu(EtSNS)][2]), *N*,*N*,*N*–tridentate coordination in [Na(EtSNS)H_2O]$_2$, in which monodentate *S*–coordination is also found. The S atoms are also able to bridge as in clusters described in Ref. 2, and in dinuclear complex **2**. In the case of [Rh(cod)]$^+$ precursors, the coordination geometry and complex nuclearity in solution are strongly dependent on the polarity of the solvent. Noteworthy, HEtSNS, $EtSNS^-$ and H_2EtSNS^+ show the same *S*,*N*,*S* coordinating properties towards the cationic metal species [Rh(CO)]$^+$ (compounds [Rh(CO)EtSNS], **7**, **8** and **9** respectively). Protonated complexes can be prepared also by reaction of acids with [Rh(CO)EtSNS], whose two pK_a have been determined in CH_2Cl_2 solution. The protonation causes a change in the electron density on the Rh atom, as

evidenced by the stretching vibration of the coordinated CO molecule, which could be exploited in tuning its catalytic properties, for instance in reactions involving oxidative addition on the metal centre.

2.5 References

[1] a) M. Asti, R. Cammi, D. Cauzzi, C. Graiff, R. Pattacini, G. Predieri, A. Stercoli, A. Tiripicchio, *Chem. Eur. J.* **2005***, 11* (11)*,* 3413–3419. b) [Rh(CO)(EtSNS)]: ^{1}H NMR (300 MHz, $CDCl_3$, 25 °C, TMS): δ = 7.48–7.26 (m, 20H; Ph), 3.75 (qd, ^{3}J(H,H) = 7.2, ^{4}J(H,P) = 3.9 Hz, 4H; CH_2), 1.19 ppm (t, ^{3}J(H,H) = 7.2 Hz, 6H; CH_3); ^{31}P{^{1}H} NMR (400 MHz, $CDCl_3$, 25 °C): d = 16.6 ppm (s). FTIR (Diamond crystal HATR, cm^{-1}): ν_{CO} = 1951.

[2] R. Pattacini, L. Barbieri, A. Stercoli, D. Cauzzi, C. Graiff, M. Lanfranchi, A. Tiripicchio, L. Elviri, *J. Am. Chem. Soc*. **2006,** *128* (3), 866–876.

[3] In more than one thousand structures of metal compounds, containing the PPN^{+} cation, found in the Cambridge Crystallographic Data Base, the shortest distance is reported in: P. G. Jones, *Z. Kristallogr.* **1995**, *210*, 375.

[4] P. Bhattacharyya, J. D. Woollins, *Polyhedron* **1995**, *14* (23/24), 3367–3388.

[5] J. A. Osborn, R. Schrock, *J. Am. Chem. Soc*. **1971**, *93* (12), 3089–3091.

[6] F. Dallavalle, G. Folesani, R.Marchelli, G. Galaverna, *Helv. Chim. Act,* **1994**, *77*, 1623–1630.

[7] R. A. Binstead, B. Jung, A. D. Zuberbühler, SPECFIT Global Analysis System, Version 3.0, Spectrum Software Associates, Marlborough (MA, U.S.A.), **2004**.

[8] L. Alderighi, P. Gans, A. Ienco, D. Peters, A. Sabatini,; A. Vacca, *Coord. Chem. Rev.* **1999**, *184*, 311–318.

[9] a) *SMART Software Users Guide*, Version 5.1; Bruker Analytical X-ray Systems: Madison, WI, **1999**. b) *SAINT Software Users Guide*, Version 6.0; Bruker Analytical X-ray Systems: Madison, WI, **1999**. G. M. Sheldrick, *SADABS*; Bruker Analytical X-ray Systems, Madison, WI, **1999**. G. M. Sheldrick, *SHELXL-97*, Program for crystal structure refinement; University of Göttingen: Germany, **1997**

[10] a) U. Englich, S. Chadwick, K. Ruhlandt–Senge, *Inorg. Chem.* **1998**, *37* (2), 283–293. b) M. Niemeyer, P. P. Power, *Inorg. Chem.* **1996,** *35* (25), 7264–7272.

[11] Differently from CH_2Cl_2, solvent used for the crystallization, it is known that $CHCl_3$ may contain amounts of HCl produced by exposure to light and oxygen. D. G. Hill, *J. Am. Chem. Soc*. **1932,** *54*, 32–40.

[12] a) B. W. Maxey, A. I. Popov, *J. Inorg. Nucl. Chem.*, **1970**, *32* (3), 1029–1032. b) L. Matilainen, M. Leskelae, M. Klinga, *J. Chem. Soc. Chem. Comm,* **1995**, (4), 421–422.

[13] The overall reactivity towards $[Rh(cod)Cl]_2$, solvent-dependent equilibria and the reaction of complex **1** with CO are depicted in Scheme S1 and S2 of the supplementary material

[14] The mean value between 180° and 90°(respectively found in [Au(EtSNS)] and in **1**) is 135° as found in $[Ag(EtSNS)]_2$.

[15] R. Chauvin, *Eur. J. Inorg. Chem*., **2000**, *4*, 577–591.

[16] for recent examples see: a) V. Miranda–Soto, J. J. Perez–Torrente, L. A. Oro, F.J. Lahoz, M. L. Martin, M. Parra–Hake, D. B. Grotjahn, *Organometallics* **2006**, *25* (18), 4374–4390. b) S. Cai, G. X. Jin, *Organometallics* **2005**, *24* (22), 5280–5286. c) J. A. Camerano, M. A. Casado, M. A. Ciriano, C. Tejel, L. A. Oro, *Dalton Trans.* **2005**, *18*, 3092–3100.

[17] V. Amendola, M. Bonizzoni, D. Esteban–Gomez, L. Fabbrizzi, M. Licchelli, F. Sancenon, A. Taglietti, *Coord. Chem. Rev.* **2006**, *250* (11+12), 1451–1470.

[18] a) V. L. Goedken, M. L. Vallarino, J. V. Quagliano, *Inorg. Chem.* **1971**, *10*(12), 2682–2685. b) D. D. J. W. Mercer, H. A. Jenkins, *Inorg. Chim. Acta* **2007**, *360*(9), 3091–3098.

[19] S. C. Van der Slot, J. Duran, J. Luten, C. Paul, J. Kamer, P. W. N. M. Van Leeuwen, *Organometallics* **2002**, *21* (19), 3873–3883.

[20] L. Boubekeur, S. Ulmer, L. Ricard, N. Mézailles, P. Le Floch, *Organometallics,* **2006***, 25* (2)*,* 315–317.

[21] During the titration, 30 additions of 25 μL of HOTf dissolved in CH_2Cl_2/CH_3OH, were made to 50 mL of solution of [Rh(CO)EtSNS] in neat dichloromethane. In this condition, the final quantity of methanol in the titrated solution is negligible (0,02%).

[22] a) T. Fujinaga, I. Sakamoto, *J. Electroanal. Chem*. **1977**, *85*, 185–201. b) J. Bessiere, P. Gagne, *Teintex* **1978**, *43*(1), 5–12. c) R. L. Benoit, D. Figeys, *Can. J. Chem*. **1991**, *69*(12), 1985–1988.

[23] a) C. A. Streuli, *Anal. Chem.,* **1960**, *32*(8), 985–987. b) G. Jia, R. H. Morris, *J. Am. Chem. Soc*. **1991**, *113*(3), 875–883. c) R. H. Morris, *Chem. Eur. J.* **2007**, *13*, 3796–3803.

[24] T. Li, A. J. Lough, C. Zuccaccia, A. Macchioni, R. H. Morris, *Can. J. Chem*. **2006**, *84*(2), 164–175.

[25] R. A. Begum, D. Powell, K. Bowman–James, *Inorg. Chem,* **2006**, *45* (3), 964–966.

3

Oxidative Addition of Iodomethane to Charge-tuned Rh^{I} Complexes

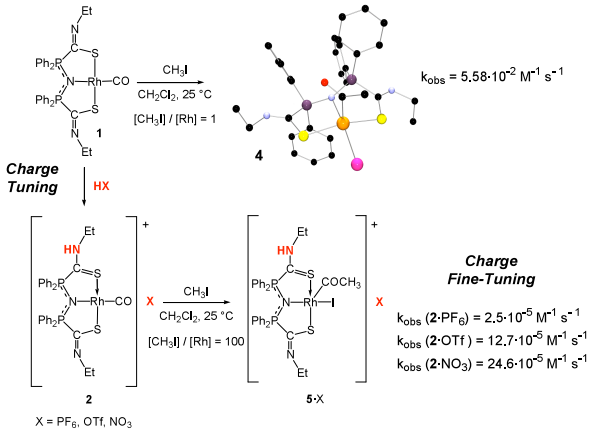

The zwitterionic Rh^{I} monocarbonyl complex [Rh(EtSNS)(CO)] (**1**, EtSNS = EtNC(S)Ph_2P=NPPh_2C(S)NEt$^-$) was reacted with iodomethane in dichloromethane, yielding the stable acetyl-Rh^{III} complex [Rh(EtSNS)($COCH_3$)I] (**4**). Complex **4** was characterized in solution and in the solid state by X-Ray diffraction analysis. The rate constant of the reaction [5.48 (7) x 10^{-2} M^{-1} s^{-1} at 25 °C CH_2Cl_2] and the activation parameters $\Delta H^{\ddagger}$ [28(3) kJ mol^{-1}] and $\Delta S^{\ddagger}$ [-173(10) J mol^{-1} K^{-1}] were determined, confirming a nucleophilic addition mechanism. The rate constant was obtained by monitoring the acetylic product by ^{1}H NMR, under second-order conditions ([Rh] / [CH_3I] = 1). Complex **1** can be mono- and bi-protonated with HX (X = PF_6, OTf, NO_3), forming [Rh(HEtSNS)(CO)]X (**2**·X) and [Rh(H_2EtSNS)(CO)]X_2 (**3**·X_2) respectively. A decrease of the calculated DFT Mulliken atomic population is observed along the series **1** > **2** > **3** in accordance with the variation of the coordinated CO stretching frequency. Compounds **2**·X were also reacted with iodomethane forming complexes [Rh(HEtSNS)($COCH_3$)I]X (**5**·X), stable in solution for a short time, that transform by deprotonation in **4** and in unidentified decomposition products. The rate constants were determined under pseudo first-order conditions due to the lower reactivity [**2**·NO_3 = 24.6 (6) x 10^{-5} M^{-1} s^{-1}; **2**·OTf = 12.7 (3) x 10^{-5} M^{-1} s^{-1}; **2**·PF_6 = 2.50 (6) x 10^{-5} M^{-1} s^{-1}]. The activation parameters for **2**·PF_6 were also determined. The influence of the counterion could be explained assuming that the different non metal-coordinated anions form hydrogen bonding with the NH group of **2**·X, that in turn causes a variation of the electron density on the Rh centre. A good correlation between the CO stretching frequencies and the rate constants was observed. The experimental rate constant for complex **1** is one order of magnitude higher than the one calculated using the linear regression function obtained for the **2**·X series (experimental = 5.48 x 10^{-2} M^{-1} s^{-1}; calculated = 1.29 x 10^{-3} M^{-1} s^{-1}), pointing out that the monoprotonated complexes react more slowly than expected. Both steric and electronic effects were examined and held responsible of this reduced reactivity. Complexes **3**·X_2 reacted too slowly, yielding complex **4** and unidentified decomposition products, hindering the determination of the rate constants.

3.1 Introduction

It is established, by experiment and calculation, that oxidative addition of methyl iodide to square-planar rhodium(I) carbonyl complexes proceeds *via* a nucleophilic mechanism, where the rate determining step shows a S_N2 transition state.[1] Consequently, if the reactivity is not strongly moderated by steric effects, due to bulky substituents or ligand orientation that hinder the space above *and* below the Rh coordination plane,[2] higher reaction rates are found for complexes with high electron density on the Rh center, which behaves as a nucleophile towards the carbon atom of CH_3I. The value of the IR stretching frequency of coordinated CO is taken as an indicative measure of the electron density on the Rh atom, and a qualitative correlation between the electronic density, the CO frequency and the reaction rate is possible (as a rule of thumb, faster kinetics are observed for complexes with a CO frequency of about 1990 cm^{-1} or lower). However, Haynes *et al*.[3] suggest that similar complexes with sensibly different CO stretching frequency, namely *trans*-$[Rh(CO)(PPh_3)_2I]$ and [Rh(CO)(dppe)I] (dppe = 1,2-bis(diphenylphosphino)ethane; ν(CO) = 1981 and 2011 cm^{-1} respectively), might be expected to have similar electron density on the Rh center. In our opinion, this shows that the Rh electron density is not only dependent on the kind of donor atoms in the ligands, but also on their orientation and geometry, and that this density is indeed reflected by the CO stretching frequency. Nonetheless, in different complexes with the same donor atoms and the same coordination geometry, the CO stretching frequency can be used, with confidence, as a measure of the electronic densities.

The rhodate complex $[Rh(CO)_2I_2]^-$ (the "Monsanto" catalyst)[4] is taken as reference in comparing kinetic constant values; to now, the highest ones have been determined for carbonyl complexes containing bis(imino)carbazolide[5] and N-heterocyclic carbene[6] ligands. It can be assumed that for geometrically analogous complexes whose CO stretching frequency are equal, the electron density on the Rh atom is the same and the variation of the sterics of ligand substituents allows the observation of steric effects alone.[7] For Rh^I carbonyl complexes, the oxidative addition is often followed by the migratory CO insertion, forming an acetyl complex. This reaction seems faster when steric demand is high[8,9] but slower for high electron density complexes.[10] Apparently, rate-enhancing electronic effects in the migratory CO insertion are observed when strong π-donor ligands are used.[11] In this chapter we report kinetic and thermodynamic studies of the oxidative addition of iodomethane to the

zwitterionic metallate[12] [Rh(EtSNS)(CO)][13] (**1**) and its protonated derivatives:[14] [Rh(HEtSNS)(CO)]X (**2**·X) and [Rh(H_2EtSNS)(CO)]X_2 (**3**·X_2) [X = PF_6, OTf, NO_3; EtSNS = EtNC(S)Ph_2P=NPPh_2C(S)NEt^-].[15] In the case of [Rh(EtSNS)(CO)], ^{1}H NMR was useful to obtain real second-order kinetic parameters, while in most literature cases, pseudo-first order rate constants were determined.[16] In the case of the mono-protonated compounds 2·X, a quantitative correlation between their CO stretching frequency with different counterion and the kinetic constant was observed, showing a long-range electronic effect due to the different hydrogen bonding acceptor properties of the anion. The bi-protonated complexes were found, as expected, to react very slowly.

3.2 Experimental

3.2.1 General procedures

All operations were carried out under nitrogen athmosphere using standard Schelnk techniques. Methyl iodide (Aldrich) and dichloromethane were distilled from calcium hydride. [(Rh(CO)EtSNS],[13] [Rh(CO)(HEtSNS)]X and [Rh(CO)(H_2EtSNS)]$(X)_2$ (X = PF_6, OTf)[14] and [Rh(CH_3CN)$_2$(CO)$_2$]NO_3[17] were prepared as described elsewhere. HNO_3 (65%) and [Rh(CO)$_2$Cl]$_2$ (Aldrich) were used as supplied. Elemental analyses were carried out on a Carlo Erba EA1108 microanalyzer. FTIR spectra (4000-400 cm^{-1}) were recorded on a Nicolet Nexus spectrophotometer equipped with a Smart Orbit HATR accessory (diamond crystal and ZnSe). IR cell: CaF_2 windows, 0.5 mm path length. ^{1}H NMR (300.13 MHz, TMS) spectra were recordered on Bruker 300 Avance, ^{31}P{^{1}H} NMR (161.98 MHz, external reference 85% H_3PO_4) and ^{103}Rh NMR (12.65 MHz, the absolute ^{103}Rh frequency was determined by relating it to the reference frequency Ξ = 3.16 MHz), spectra were recordered on Bruker AMX400, using deuterated solvents ($CDCl_3$, CD_2Cl_2 and CD_3OD). All solid-state NMR spectra were recorded on a Bruker Avance II 400 operating at 400.23 and 100.65 MHz for ^{1}H and ^{13}C, respectively. All spectra have been recorded at room temperature with a spinning speed of 12-14 kHz. Cylindrical 4 mm o.d. zirconia rotors with sample volume of 120 μL were employed. A standard ramp cross-polarization pulse sequence were used with a contact time of 5 ms, a ^{1}H 90° pulse of 3.35 ms, recycle delays of 10 sec and a number of 264-1000 transients. A two pulse phasemodulation (TPPM) decoupling scheme was used with an rf field of 75 kHz. ^{13}C chemical shifts were referenced via the resonance of solids HMB (hexa-methyl benzene,

methyl signal at 17.4 ppm). A Micromass Quattro LC triple quadrupole instrument equipped with an electrospray interface (Masslynx v. 3.4 software) was used for ESI–MS data collection and processing. The nebulizing gas (nitrogen, 99.999% purity) and the desolvation gas (nitrogen, 99.998% purity) were delivered at a flow-rate of 80 and 500 l/h, respectively. ESI–MS analyses were performed by operating the mass spectrometer in positive ion (PI) mode, acquiring mass spectra over the scan range *m/z* 100-2800, using a step size of 0.1 Da and a scan time of 2.7 sec. The interface operating parameters were: source temperature 70 °C, desolvation temperature 70 °C, ESI(+) capillary voltage 3.0 kV, cone voltage 15 V, rf lens 0.3 V.

*3.2.2 Preparation of [Rh(CO)(HEtSNS)]NO_3 (**2**·NO_3).*

A solution of $[Rh(CH_3CN)_2(CO)_2]NO_3$ (0.200 g, 0.26 mmol) in CH_2Cl_2 (10 mL) was added under nitrogen to a solution of HEtSNS (0.148 g, 0.26 mmol) in CH_2Cl_2 (15 mL). Stirring was continued for 2 hs and the solution color turned to red. Evaporation of the volatiles afforded compound [Rh(CO)(HEtSNS)]NO_3 (**2**·NO_3) as a red microcrystalline powder (Yield 87%). Anal. Calcd. for $C_{31}S_2H_{31}O_4N_4P_2Rh$ (*M* = 752.59): C 49.47; H 4.15; N 7.44; S 8.52. Found: C 49.30; H 4.12; N 7.40; S 8.49. ^{1}H NMR (CD_2Cl_2): δ = 10.5 (s, br, 1H, N-H); 7.7-7.4 (m, 20H, Ph); 3.67 (m, br, 4H, -$CH_2$$CH_3$), 1.16 (t, 6H, -$CH_2CH_3$, $^3J_{H,H}$ = 7.2 Hz) ppm. $^{31}P\{^1H\}$ NMR (CD_2Cl_2): δ = 35.2 (s), 25.1 (s) ppm. ESI-MS [MeOH solution: *m/z* (rel. int., formula)]: 690.6 (100%, $[Rh(CO)(HEtSNS)]^+$). FTIR (Diamond crystal HATR, cm^{-1}): ν_{CO} = 1968s; (CH_2Cl_2, cm^{-1}): ν_{CO} = 1989s.

*3.2.3 Preparation of [Rh(CO)(H_2EtSNS)]$(NO_3)_2$ [**3**·$(NO_3)_2$].*

In a Schlenk tube and under nitrogen, a solution of [Rh(EtSNS)(CO)] (0.200 g 0.29 mmol) in 10 mL of CH_2Cl_2 was treated with 10 mL of a water solution of HNO_3 (5 M) in large excess with respect to the rhodium precursor and the yellow solution turned orange. The two liquid phases were separated, and the organic one dried, giving an orange red solid. The solid was recrystallized from hot methanol affording compound [Rh(CO)(H_2EtSNS)]$(NO_3)_2$ [**3**·$(NO_3)_2$] as an orange microcrystalline powder (Yield 92%). Anal. Calcd. for $C_{31}H_{32}N_5O_7P_2RhS_2$ (815.61): C 45.65, H 3.95, N 8.57, S 7.86. Found C 45.48, H 3.91, N 8.52, S 7.83. ^{1}H NMR (CD_2Cl_2): δ = 10.4 (s, br, 2H, N–H); 7.7–7.4 (m, 20H, Ph); 3.82 (m, 4H, -CH_2CH_3, $^3J_{H,H}$ = 7.2 Hz), 1.27 (t, 6H, -CH_2CH_3, $^3J_{H,H}$ = 7.2 Hz) ppm. $^{31}P\{^1H\}$ NMR (CD_2Cl_2): δ = 41.1 (s) ppm.

ESI–MS [MeOH solution: *m/z* (rel. int., formula)]: 691.6 (100%, $[Rh(CO)(H_2EtSNS)]^{2+}$). FTIR (Diamond crystal HATR, cm^{-1}): ν_{CO} = 1986s; (CH_2Cl_2, cm^{-1}): ν_{CO} = 2008s.

3.2.4 Reaction of [Rh(EtSNS)(CO)] with CH_3I.

Methyl iodide (0.014 g, 0.98 mmol) was added to a solution of [Rh(EtSNS)(CO)] (0.068 g, 0.98 mmol) in CH_2Cl_2 (10mL). The resulting red reaction mixture was stirred for 3 hs. Evaporation of the solvent afforded compound [Rh(EtSNS)($COCH_3$)I] (**4**) as a red powder. (Yield: 91%). The complex could be recrystallized by layering hexane onto a CH_2Cl_2 solution of crude product at -20 °C affording red crystals of [Rh(EtSNS)($COCH_3$)I] (**4**). Anal. Calcd. for: $C_{32}H_{33}IN_3OP_2RhS_2$ (*M* = 831.51): C 46.22; H 4.00; N 5.05; S 7.71. Found: C 46.12; H 3.97; N 4.99; S 7.66. ^{1}H NMR (CD_2Cl_2): δ = 7.60-7.30 (m, 20H, Ph); 3.79 (m, br, 4H, -*CH_2*CH_3), 2.80 (s, 3H, $COCH_3$); 1.23 (t, 6H, -CH_2*CH_3*, $^3J_{H,H}$ = 7.1 Hz) ppm. $^{31}P\{^1H\}$ NMR (CD_2Cl_2): δ = 27.4 (s) ppm. CP-MAS ^{13}C NMR: d = 210.8 (s, CO), 181.5 (d, $^1J_{C,P}$ = 151 Hz, C=N), 175.9 (d, $^1J_{C,P}$ = 161 Hz, C=N), 137.2-120.9 (m, Ph), 51.8 (s, -*CH_2*CH_3), 49.1 (s, -*CH_2*CH_3 + $COCH_3$), 15.0 (s, -CH_2*CH_3*), 12.1 (s, -CH_2*CH_3*) ppm. FTIR (Diamond crystal HATR, cm^{-1}): ν_{CO} = 1709s [Rh^{III}C(O)Me]; (CH_2Cl_2, cm^{-1}): ν_{CO} = 1712s [Rh^{III}C(O)Me].

3.2.5 Reaction of [Rh(CO)(HEtSNS)]X (X = PF_6, OTf, NO_3) with CH_3I.

Methyl iodide was added to a solution of [Rh(HEtSNS)(CO)]X (X = PF_6, OTf, NO_3) ([CH_3I]/[Rh] = 100) in CH_2Cl_2 (10 mL). The reactions were monitored by FTIR spectrophotometry (CaF_2 windows, 0.5 mm path-length) until the absorption of the νCO of the starting materials were completely absent. The crude solutions were chromatographed by preparative TLC silica plate (CH_2Cl_2/Hexane = 8/2), affording the monoprotonated Rh^{III}-acetyl complexes [Rh(HEtSNS)($COCH_3$)I]X (**5**·X, X= PF_6, OTf, NO_3), **4** and unidentified products. **5**·PF_6: $^{31}P\{^1H\}$ NMR (CD_2Cl_2): δ = 44.5 (s), 23.2 (s) ppm. FTIR (CH_2Cl_2, cm^{-1}): νCO = 1725s [Rh^{III}C(O)Me]. **5**·OTf: $^{31}P\{^1H\}$ NMR (CD_2Cl_2): δ = 44.3 (s), 23.6(s) ppm. FTIR (CH_2Cl_2, cm^{-1}): ν_{CO} = 1721s [Rh^{III}C(O)Me]. **5**·NO_3: $^{31}P\{^1H\}$ NMR (CD_2Cl_2): δ = 44.1 (s), 23.9(s) ppm. FTIR (CH_2Cl_2, cm^{-1}): ν_{CO} = 1717s [Rh^{III}C(O)Me].

3.2.6 X-ray Data Collection, Structure Solution, and Refinement.

The intensity data of compound **4** were collected at room temperature on a Bruker AXS Smart 1000[18] single crystal diffractometer equipped with an area detector using a graphite

monochromated Mo Ka radiation (λ = 0.71073 Å). Crystallographic and experimental details of the structure is summarized in Table 1. An empirical correction for absorption was made. The structure was solved by direct methods and refined by full-matrix least-squares procedures (based on F_o^2)[19] first with isotropic thermal parameters and then with anisotropic thermal parameters in the last cycles of refinement for all the non-hydrogen atoms. The hydrogen atoms were introduced into the geometrically calculated positions and refined *riding* on the corresponding parent atoms.

Table 1. Summary of Crystallographic Data for **4**

	4
formula	$C_{32}H_{33}IN_3OP_2RhS_2$
FW	831.52
crystal system	monoclinic
space group	*P21/n*
T, K	293
a, Å	10.220(1))
b, Å	17.102(2)
c, Å	19.943(2)
β, deg	99.151(2)
V, Å^3	3441.5(6)
Z	4
D_{calcd}, g cm^{-3}	1.605
F(000)	1656
crystal size, mm^3	0.11 x 0.13 x 0.10
μ, cm^{-1}	16.37
rflns collected	42555
rflns unique	8298
rflns observed [$I>2\sigma(I)$]	5383
parameters	379
R indices [$I>2\sigma(I)$]	R1 = 0.0372 (wR2 = 0.0902)
R indices (all data)	R1 = 0.0670 (wR2 = 0.0998)

[a]$R1 = \Sigma||F_o|-|F_c||/\Sigma|F_o|$. $wR2 = [\Sigma[w(F_o^2-F_c^2)^2]/\Sigma[w(F_o^2)^2]]$

3.2.7 Kinetic Experiments

The kinetics of the oxidative addition of CH_3I to the complexes **1**, **2**·X (X = PF_6, OTf, NO_3) were studied by ^{1}H NMR in CD_2Cl_2. For the complexes **1** and **2**·PF_6, the reaction rates of the oxidative addition were determined at different temperatures.

Samples for the kinetic measurements of the complexes (C_{Rh} 1.57-1.98 10^{-2} M) were prepared by weighting an appropriate amount of the recrystallized complex and dissolving its in CD_2Cl_2 (*ca.* 0.6 mL) in a sealed NMR tube. Second order conditions for the neutral **1** complex (C_{Rh} / C_{CH3I} = 1-4.3) were obtained by adding a proper amount (20-60 μL) of a *ca.* 1 M CH_3I

solution in CD_2Cl_2 to the complex solution. Pseudo-first-order conditions for **2**·X (X = PF_6, OTf, NO_3) complexes (C_{Rh} / C_{CH3I} = 100) were obtained by adding a proper amount (ca. 80 μL) of neat CH_3I to the complex solution. The precise concentration of CH_3I in the tube was obtained by referencing the integrals of the CH_3 group of CH_3I and the acetyl complex to the integral of the CH_3 groups of the complex (used as internal standard) in the first collected spectrum. Spectra were collected as single FID acquisition at intervals of 30-60 s (**1**) and 45-180 s (**2**·X) making use of a dedicated Bruker MULTIZG program. Time zero offsets ($t_{first\ spectrum}$ - $t_{reactants\ mixing}$) for any kinetic run were 90-120 s. Spectra collection lasted up to 2 h.

For each kinetic run, the NMR spectrum collected prior to CH_3I addition was used as reference spectrum. Measurements were performed in the temperature range 273.16-298.16 K for **1** (4 experiments), and 280.16-298.16 K for **2**·PF_6 (3 experiments). Temperature was controlled by the dedicated Bruker TopSpin software function.

Processing of the spectra (30-50 for each kinetic run) was performed by using MestreNova, and all integrals were normalized using the TMS or solvent peaks (CH_2Cl_2 in CD_2Cl_2). Calculations of the kinetic constants were performed processing the integrals of the signals of the reactants and the products *vs*. time using the SPECFIT 32 software.[20] For **1**, both the variation of the acetyl CH_3 signal (2.80 ppm) and the disappearance of the CH_3I signal (2.20 ppm) were take into account in the calculations, while for the monoprotonate complexes only the appearance of the acetyl CH_3 signal (2.80 ppm) was considered (C_{MeI} constant in pseudo-first-order conditions). Integrals were correlated to the CH_3I and acetyl complex concentrations considering that $I_{MeI\ or\ complex} = I^*\cdot$[$CH_3I$ or complex], where I^* is the calculated integral for a CH_3 group at 1 M concentration as obtained from the spectrum collected prior to CH_3I addition {$I^* = I_{2x(Me)} / (2\cdot[Rh])$}. A second-order and both a second-order and a pseudo-first-order fitting functions were used to process the spectra for **1** and **2**·X (X = PF_6, OTf, NO_3) complexes, respectively.

For **1**, best fit was obtained using a second-order reaction function. For the monoprotonate complex, best fit was obtained using either one second-order or one pseudo first-order functions. For the latter complex, a good fitting was obtained only using the spectra collected within 15 min after reagents mixing. After this time, a marked deviation from the calculated fitting function was obtained, indicating the occurrence of a second subsequent reaction after this reaction time. For all complexes, the fitting for the acyl complex signal was obtained with

a single function, indicating that the migratory CO insertion is faster than the oxidative addition step.

The second-order rate constants determined for complexes **1** and **2**·PF_6 as a function of the temperature were processed to obtain the activation $\Delta H^{\ddagger}$ and $\Delta S^{\ddagger}$ parameters by means of the Eyring function $k = (\varkappa T/h)\cdot\exp(-\Delta H^{\ddagger}/RT)\cdot\exp(\Delta S^{\ddagger}/R)$, where k is the rate constant at temperature T, $\varkappa$ is the Boltzmann's constant, h the Planck's constant and R the gas constant. A non-linear least-square algorithm implemented in SPSS 14.0 software was used for the calculations.

Each kinetic run was repeated at least twice to check reproducibility, the k_2 (for **1**) and k_{obs} (for **2**·OTf, **2**·PF_6 and **2**·NO_3,) values given being averaged values with the component measurements deviating from each other by ≤ 5%. The error in temperature was assumed to be 1 K.

3.2.8 Computational details

The geometries of all minimums were optimized in the gas phase at density functional theory (DFT) level by means of hybrid B3LYP functional.[21] The geometries were optimized in gas phase with 6-31g** basis set on H, C, N, O, P and S atoms and Lanl2DZ basis and pseudopotential on Rh developed by Hay and Wadt (BS-0). This last uses a semicore double-ζ contraction scheme for the heavy elements such as Rh. A more wide basis set has been used to evaluate the pseudopotential effects on some molecular properties, substituting the Lanl2DZ functions and potential with complete dgdzvp functions (BS-I).[22] All the simulations were performed both in the gas phase and solution by means of Polarizable Continuum Model (PCM). The continuum were built in CH_2Cl_2 environment and standard PCM energies were computed with UA0 cavity model. Thermochemical analysis has been performed on all the minimum and no imaginary frequencies were found. Accurate energy calculation has been performed at same level with tight SCF criteria on the wavefunction. Mulliken population analysis[23] study were performed at each calculation level. The MO rendering was performed with the cubegen utility provided in the Gaussian03 package. All the calculations has been performed with Gaussian03 and gdv package.[24]

3.3 Results and Discussion

As previously reported,[13,14] the *S,N,S*-κ^3 complex [Rh(EtSNS)(CO)] (**1**) can be prepared by reaction of HEtSNS with $[Rh(CO)_2Cl]_2$ in the presence of *t*-BuOK or by bubbling CO in a solution of the *S,S*-κ^2 complex [Rh(EtSNS)(cod)] (cod = 1,5-cyclooctadiene). During these reactions, the unstable *S,S*-κ^2 intermediate $[Rh(EtSNS)(CO)_2]$ was observed, monitoring the solution reaction by FTIR (νCO: 2075, 2009 cm^{-1}). The coordination of the nitrogen atom raises the electron density of the Rh, as inferred from the lower CO stretching frequency of **1** [νCO (CH_2Cl_2): 1967 cm^{-1}]. Compound **1** is a biprotic base and can be protonated affording cationic species $[Rh(HEtSNS)(CO)]^+$ (**2**) and $[Rh(H_2EtSNS)(CO)]^{2+}$ (**3**) in which protons bind to the nitrogen atoms of the thioamidyl functions [pK_a in CH_2Cl_2 = 6.5(3) and 4.8(4)][14] (Scheme 1). Compound **3** can be conveniently prepared by using an excess of acid, while **2** is obtained by mixing **1** and **3** in 1:1 molar ratio.

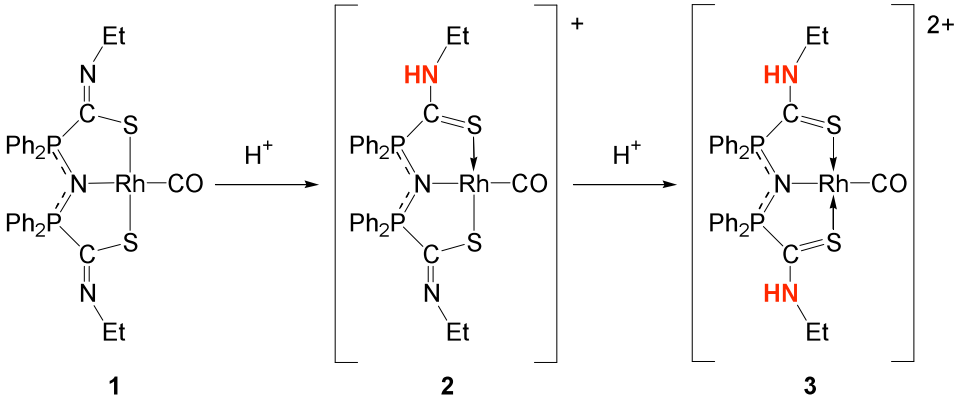

Scheme 1. Formation of the mono-cationic complex **2** and the di-cationic complex **3** by protonation of the zwitterionic complex **1**.

The electronic distribution varies dramatically, as evidenced by the C-S and C-N bond distances[14] and by the $^{31}P\{^1H\}$ NMR chemical shift values (Table 1). In the case of **2**·X (X = PF_6, OTf, NO_3), two ^{31}P resonances are present,[14] suggesting that proton exchange is very slow (exchange can be fast, i. e. when X = CF_3COO^-; δ = 27.9 ppm, unpublished results). In turn, protonation influences the electron density on the Rh(CO) system, as reflected by the infrared CO stretching frequencies (Table 2).

Table 2. νCO stretching (CH_2Cl_2 solution and HATR-ZnSe crystal) and relevant ^1H NMR, $^{31}P\{^1H\}$ NMR and ^{103}Rh NMR chemical shifts of **1**, **2**·X, and **3**·X_2 (X = PF_6, OTf, NO_3).

	1	**2**·NO_3	**2**·OTf	**2**·PF_6	**3**·$(NO_3)_2$	**3**·$(OTf)_2$	**3**·$(PF_6)_2$
νCO (HATR, ZnSe, cm^{-1})	1953	1968	1977	1979	2006	2011	2013
νCO (CH_2Cl_2, cm^{-1})	1967	1989	1992	1994	2008	2013	2017
^1H NMR (N*H*, CD_2Cl_2, ppm)	-	10.5	10.8	11.0	10.4	10.6	11.1
$^{31}P\{^1H\}$ NMR (CD_2Cl_2, ppm)	16.6	35.2-25.1	36.7-22.1	36.7-19.9	41.1	39.3	38.2
^{103}Rh NMR (CD_2Cl_2, ppm)	-6886	-	-	-6888	-	-	-6901[a]

a: in CD_2Cl_2/CD_3OD (1:1 ratio)

The Mulliken populations for the Rh atom was calculated at the BS-0 level for **1**, **2** and **3** in the gas phase and varies from -0.338 a.u. to -0.263 a.u. (Table 3), showing that the protonation of one thioamidic function induces a 13% decrease in the electronic population for the mono-protonation and a 22% decrease for the bi-protonation (a decreasing of 8% and 16% respectively has been found in solution symulation). This decrease in the calculated population is in agreement with the trend found experimentally for the CO stretching frequencies.

Table 3. Mulliken populations (a.u.) for selected atoms, in the gas phase and in solution (PCM, CH_2Cl_2) for **1**, **2** and **3**. For compound **2**, the protonation is on the N1 atom [B3LYP/BS-0//B3LYP/BS-0; BS-0=6-31g** + Lanl2DZ(Rh)].

Gas Phase										
	Rh	**S1**	**S2**	**N1**	**N2**	**N3**	**C**	**O**	**P1**	**P2**
1	-0.338	-0.055	-0.055	-0.381	-0.381	-0.820	0.313	-0.271	0.937	0.937
2	-0.294	0.087	0.0095	-0.409	-0.373	-0.823	0.315	-0.229	0.899	0.922
3	-0.263	0.137	0.134	-0.417	-0.417	-0.825	0.311	-0.188	0.905	0.903
CH_2Cl_2										
	Rh	**S1**	**S2**	**N1**	**N2**	**N3**	**C**	**O**	**P1**	**P2**
1	-0.395	-0.116	-0.120	-0.358	-0.376	-0.835	0.302	-0.280	0.939	0.940
2	-0.361	-0.074	0.097	-0.348	-0.420	-0.836	0.324	-0.264	0.934	0.904
3	-0.331	0.132	0.123	-0.402	-0.413	-0.827	0.337	-0.239	0.908	0.912

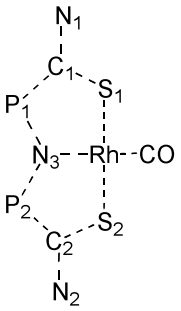

A more detailed calculation has been carried out at BS-I level, both in the gas and solution phase, to confirm the BS-0 data. The results are consistent with the abovementioned trend (see Table S1 of the Appendix 2).

The ^{103}Rh NMR chemical shifts are very similar for **1**, **2**·PF_6 and **3**·$(PF_6)_2$ (Table 1). Nevertheless, ^{103}Rh shielding seems to be mainly dependent on the kind of coordinated atoms and on the coordination geometry, both identical in our case.[25]

The νCO stretching in complexes **2**·X, and **3**·X_2 (X = PF_6, OTf, NO_3) is slightly different (Table 1). As shown by the value of the ^{1}H NMR (CD_2Cl_2) chemical shift of the NH group, the anion interacts with the cation through hydrogen bonding (Table 1). The NH values of mono- and di-protonated complexes move, as expected, downfield along the series NO_3 (coordinating), OTf (less coordinating) and PF_6 (non coordinating) in good correlation with the variation of the CO stretching. The more coordinating anion lowers the positive charge on the Rh centre through the hydrogen bonding, causing the decreasing of the CO stretching value and suggesting that the Rh electron density can be fine-tuned by changing the anion.

*3.3.1 Reaction of [Rh(EtSNS)(CO)] (**1**) with CH_3I.*

Treatment of **1** with a stoichiometric amount of CH_3I in CH_2Cl_2 at 25 °C resulted in the quantitative formation of the stable Rh^{III} acetyl-complex [Rh(EtSNS)($COCH_3$)I] (**4**) characterized in solution and in the solid state (Scheme 2).

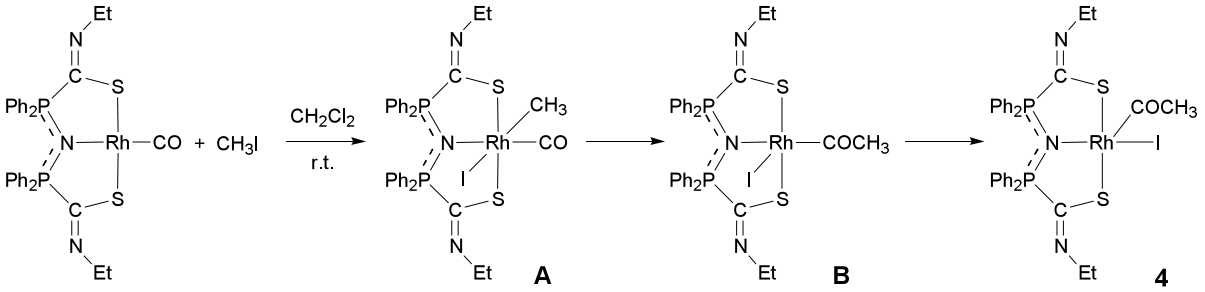

Scheme 2. Reactivity of complex **1** with CH_3I

The FTIR spectrum of the reacting solution (Figure 1) shown the decay of the intensity of the νCO stretching of **1** at 1967 cm^{-1}, accompanied by the formation of a new adsorption at 1712 cm^{-1}, assigned to the acetyl complex **4** (for *ca*. 30 mg of complex **1** the reaction was completed in *ca*. 8 minutes).

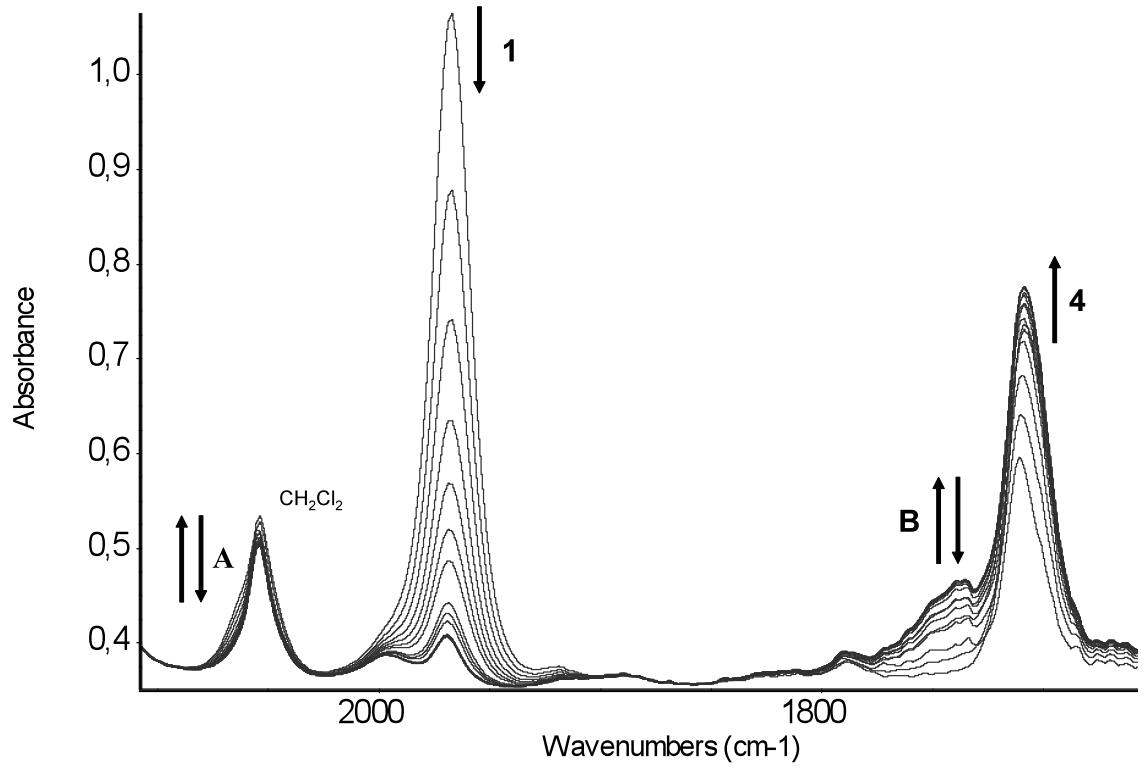

Figure 1. Superimposed FTIR spectra collected during the reaction of **1** with CH_3I in 1:1 ratio in CH_2Cl_2 at r.t.

The intensity of the νCO band of the methyl-carbonyl Rh^{III} intermediate **A** (2065 cm^{-1}, observed as a shoulder of the CH_2Cl_2 absorption at 2055 cm^{-1}) was very weak and absent at the end of the reaction. Another weak band started to form at 1736 cm^{-1} and then decayed after *circa* 5 minutes, finally disappearing at the end of the reaction. This band can be possibly assigned to isomer **B**. The intermediate **A** and isomer **B** were not evidenced in the ^1H NMR spectra at room temperature. The complex **A** could be observed by ^1H NMR only by slowing the reaction at 250 K ($\delta = 1.92$ $^2J_{Rh,H} = 2$ Hz, integral = 3% with respect to the integral of the CH_3 signal of the ligand ethyl groups). When the reaction was performed at 280 K, two sets of peaks with very close chemical shifts and different intensities were present (Figure 4, *vide infra*). They were assigned to the ethyl groups of **4** and, possibly, to the acetyl isomer **B** [**4** = 1.208 (t, -CH_2CH_3), 3.699 (m, -CH_2CH_3); **B** = 1.214 (t, -CH_2CH_3), 3.800 (m, -CH_2CH_3)]. The solution was then warmed from 280 to 300 K, and only the peaks of **4** were present. At r.t. the presence of the CO absorptions of **A** and **B** in the infrared spectra, at low relative concentrations not detectable by ^1H NMR, is probably due to a high infrared absorbitivity of these Rh^{III} complexes. The $^{31}P\{^1H\}$ NMR spectrum of the reacting solution shows the

formation of only one singlet at 27.4 ppm (**4**), and the complete decay of the signal of **1** (16.6 ppm).

Crystals of **4** were obtained at -20 °C by layering hexane on a CH_2Cl_2 solution. The ORTEP plot of the structure of **4** is depicted in Figure 2.

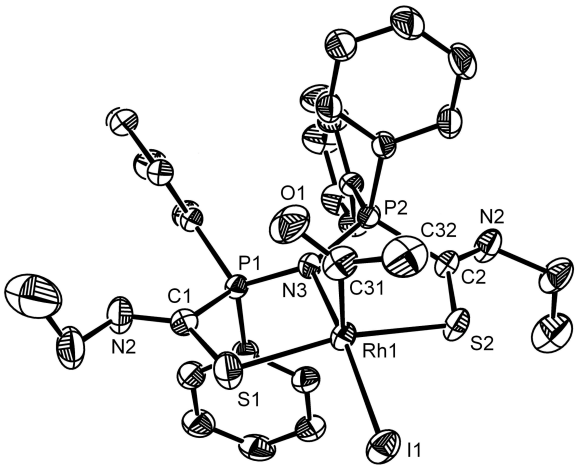

Figure 2. ORTEP plot of the structure of **4**. Thermal ellipsoids are drawn at 30% probability level. H atoms are omitted for clarity. Selected distances [Å] and angles (°): Rh1-S1 2.340(1), Rh1-S2 2.322(1), Rh1-I1 2.619(4), Rh1-N3 2.128(3), Rh1-C31 1.950(4), C31-O1 1.194(5), C31-C32 1.475(6), C1-S1 1.743(4), C2-S2 1.721(4), C1-N1 1.278(5), C2-N2 1.271(5), P1-N3 1.622(3), P2-N3 1.626(3); P1-N3-P2 133.8(1), S1-Rh1-N3 89.8(1), S1-Rh1-I1 89.7(1), S1-Rh1-C31 101.4(1), S2-Rh1-N3 91.8(1), S2-Rh1-I1 86.2(1), S2-Rh1-C31 91.5(1), S1-Rh1-S2 168.0(1), C31-Rh1-I1 98.9(1), C31-Rh1-N3 91.8(1), C32-C31-O1 122(4), I1-Rh1-N3 169.1(1).

The complex shows a slightly distorted square-pyramidal coordination geometry with the acetyl group occupying the apical position. The coordination around the metal involves the S1, N3 and S2 atoms of the ligand, in a *S*,*N*,*S*-κ^3 coordination fashion, the carbon atom of the acetyl and the iodine atom. The Rh atom lies at 0.24(1) Å from the mean plane defined by I1-S1-S2-N3. The oxidation to Rh^{III} causes a slight variation of the bond lengths and angles of the $EtSNS^-$ ligand with respect to the Rh^I complex **1**. In particular the Rh1-N3 [2.128(3) Å], Rh1-S1 [2.340(1) Å] and Rh1-S2 [2.322(1) Å] bond distances are slightly shorter than those observed in **1**.[13] The bond distances Rh1-I1 [2.619(4)Å] and Rh1-C31 [1.950(4)Å] are among the shortest found in the Cambridge Structural Database for similar fragments.[26] The acetyl group adopts a conformation that minimizes steric interactions with the close phenyl group of the EtSNS ligand, directing the methyl group between the I1 and S2 atoms (I1-Rh1-C31-C32 torsion angle 48.9°).

The ^{1}H-^{1}H 2D NOESY NMR spectrum of **4** (CD_2Cl_2 at 25 °C) displays cross-peaks between the acetylic CH_3 group and some of the phenylic hydrogens. This is consistent with the square-pyramidal coordination geometry with an apical acetyl ligand as found in the solid state (Figure 2).

In the solid state, **4** seems to partially transform in the methyl complex **A** as evidenced by FTIR-HATR. In the spectrum, a weaker νCO band at 2049 cm^{-1} is present, together with the stronger one at 1709 cm^{-1} assigned to the acetyl complex. When the solid is dissolved on the HATR crystal, by addition of few μL of dichloromethane, the spectrum shows only one band at 1712 cm^{-1}. By evaporating the solvent on the crystal, the band at 2049 cm^{-1} reappears. A similar behavior was already reported in the literature, with the acetyl complex undergoing reductive elimination reforming the parent Rh^{I} complex.[2,27]

A CP-MAS ^{13}C solid state NMR was collected on **4**, in order to verify the presence of **A**. Only the peaks of **4** were present, probably due to the very low concentration (< 3%) of **A** in the solid (< 3%, see Figure S1 and S2 of the Appendix 2).

3.3.2 Reaction of the mono-protonated complexes [Rh(HEtSNS)(CO)]X (2·X, X = PF_6, OTf, NO_3) with CH_3I.

The reaction of complexes **2**·X with CH_3I in 1:100 ratio (CH_2Cl_2 at 25 °C, Scheme 3) was monitored by FTIR, ^{1}H NMR and ^{31}P{^{1}H} NMR. In the infrared spectrum of the reacting solution of **2**·OTf (Figure 3, the same discussion applies for X = PF_6 and NO_3; see superimposed spectra in Figures S3 and S4 of the Appendix 2), the presence of a very weak band at 2066 cm^{-1} (PF_6 = 2068 cm^{-1}, NO_3 = 2061 cm^{-1}) indicated the formation of the methyl-Rh^{III} intermediate **A'**.

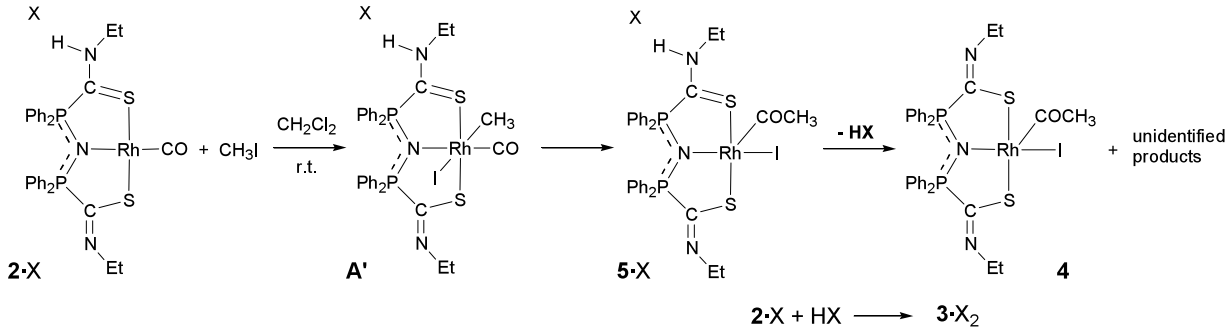

Scheme 3. Reactivity of **2**·X (X = PF_6, OTf, NO_3) with CH_3I in CH_2Cl_2.

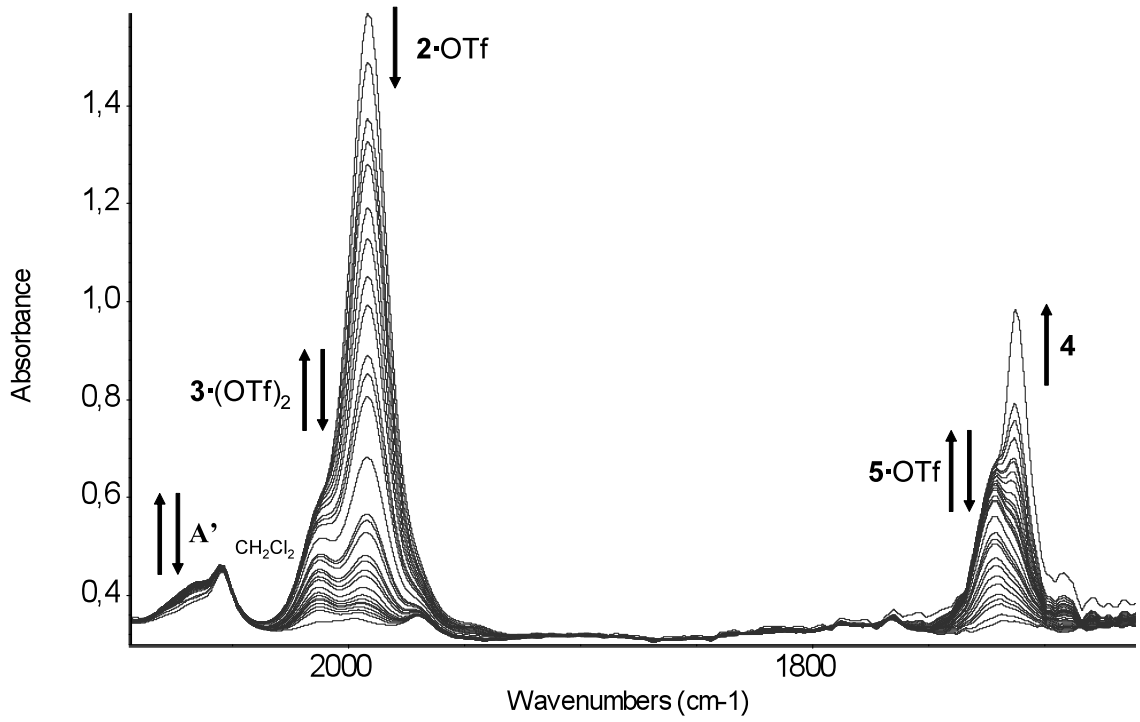

Figure 3. Superimposed FTIR spectra of the reaction of **2**·OTf with CH_3I in 1:100 ratio in CH_2Cl_2 at r.t.

The change in the intensity of this band was in agreement with a steady state intermediate and the band disappeared at the end of the reaction (after 48 hours). The formation of the acetyl complex [Rh(HEtSNS)($COCH_3$)I]OTf (**5**·OTf) was evidenced by the raising of a band at 1721 cm^{-1} (PF_6 = 1725 cm^{-1}, NO_3 = 1717 cm^{-1}). After *circa* 50 minutes, for all the three anions, a shoulder band at 1712 cm^{-1} was evident in the spectra and was ascribed to the deprotonated acetyl-complex **4**. At the end of the reaction, only this band was present (Figure S5 of the Appendix 2 for X = OTf). During the reaction, a weak shoulder band at 2013 cm^{-1} formed and then disappeared [2017 cm^{-1} for **3**·$(PF_6)_2$ and 2009 cm^{-1} for **3**·$(NO_3)_2$]. It could be due to the formation of the diprotonated complex **3**·$(OTf)_2$ by protonation of **2**·OTf.[14] In the ^1H NMR spectrum of the CD_2Cl_2 reacting solution, the methyl group of intermediate **A'** is not observable, due to the strong excess of CH_3I whose peak resonates in the same region. The -CH_2CH_3 groups of **2**·X and **5**·X (X = PF_6, OTf, NO_3) are broad, probably due to proton exchange, and resonate in the same range, resulting undistinguishable. Moreover, only one peak attributed to acetyl complexes is present.

In the $^{31}P\{^1H\}$ NMR spectrum of the reacting solution, a similar situation was observed. The intensity of the two peaks of **2**·OTf (Table 2) decreased along with the formation of two new

absorptions at lower field (44.6, 23.7 ppm) which were attributed to complex **5**·OTf. The methyl-Rh intermediate **A'** was not evidenced in the spectra. After *circa* 50 minutes, a new band at 27.4 ppm was starting to form and was attributed to complex **4**, obtained by deprotonation of **5**·OTf (see Figure S6 of the Appendix 2). After two days, the peak of **4** was still present in the $^{31}P\{^{1}H\}$ NMR spectrum. Other unidentified decomposition products, that were not observed in the carbonylic region of the FTIR spectrum, were also formed (see Figure S7 of the Appendix 2). The decomposition of the protonated complexes **5**·X can be due to the strong excess of CH_3I present in solution or to the intrinsic incompatibility of the acid with the acetyl group.[1d]

Compounds **5**·OTf and **4** could be separated by preparative TLC (in a test reaction that was stopped before completion, using silica plates and CH_2Cl_2/Hexane 8:2 as eluent). The $^{31}P\{^{1}H\}$ NMR spectra of the separated compounds confirmed the assignment. In the ^{1}H NMR spectrum, the acetyl group of complexes **5**·X and **4** resonates at the same chemical shift.

3.3.3 Reaction of the di-protonated complexes [Rh(H$_2$EtSNS)(CO)]X (3·X$_2$, X = PF$_6$, OTf, NO$_3$) with CH$_3$I.

The diprotonated complexes **3**·X_2 reacted very slowly with CH_3I in 1:100 ratio, the band of the starting reagents disappearing from the solution FTIR spectra only after 5 days. No Rh-methyl complexes were evidenced in the FTIR spectra and only the formation of the acetyl complex **4** was observed (FTIR absorption at 1712 cm^{-1} for all three complexes). This complex was separated by TLC, as in the case of the reactions of compounds **2**·X, and identified by $^{31}P\{^{1}H\}$ NMR. Unidentified decomposition compounds were also evidenced in the $^{31}P\{^{1}H\}$ NMR spectrum of the crude product, but no further investigation was performed.

3.3.4 Kinetics of the reaction of 1 and 2·X with CH$_3$I.

At the concentrations employed for the kinetic measurements for the oxidative addition of CH_3I on **1** and **2**·X (X = PF_6, OTf and NO_3), ^{1}H NMR spectra obtained by a single FID collection were of good resolution and good signal-to-noise ratios, and prompted us in the use of this technique for the determination of the reaction rates. For the **2**·X complexes, the experiments were performed in order to evaluate the effect of protonation and the role of the counterion.

In the case of **1** the reaction with CH_3I is quite fast and its constant could be determined at different temperatures under second-order conditions ([CH_3I] / [Rh] = 1 – 5). The calculation was performed by processing the integral of the signals of the CH_3 groups of CH_3I and -$C(O)CH_3$ as a function of time (Figure 4), using non-linear least-squares fitting functions.

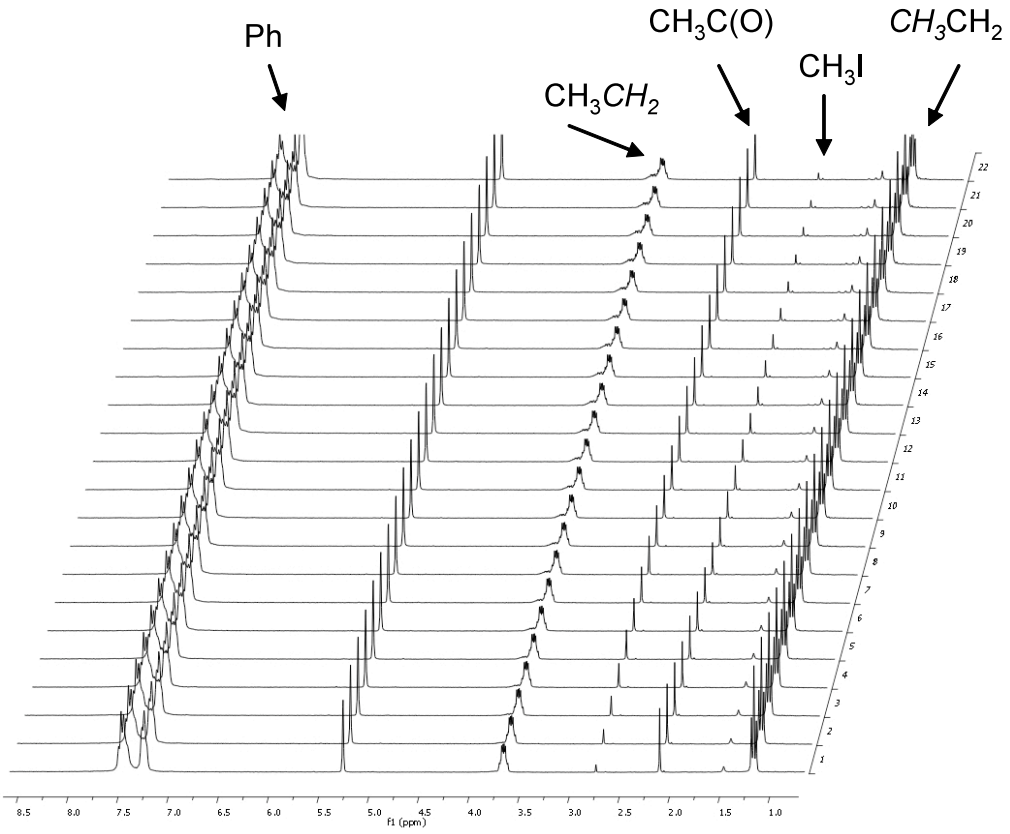

Figure 4. ^1H NMR stack plot spectra for the reaction of **1** with CH_3I (ratio 1:1) at 280 K in CD_2Cl_2.

On this ground, their integrals could be related to the concentrations of the species making use of appropriate equations as reported in the experimental section. At r.t. the migratory CO insertion is a very fast reaction compared with the oxidative addition of CH_3I. Only at 250 K the methyl intermediate **A** was detected, but its relative concentration was too low for the determination of the migratory insertion rate. Thus, it was not possible to determine the kinetic rate constants for both reaction steps, but only the reaction rate of the slowest one (oxidative addition) which was then approximated to the overall rate for the reaction: **1** + CH_3I → **4** with $v = k_1[\mathbf{1}][CH_3I]$. The rate constants determined at different temperatures for this reaction are reported in Table 4. They were employed for the calculation of the activation parameters $\Delta H^{\ddagger}$ [28(3) kJ mol-1; 6.7(7) kcal mol^{-1}] and $\Delta S^{\ddagger}$ [-173(10) J mol^{-1} K^{-1}; -41(2) cal

mol^{-1} K^{-1}] by means of the non-linearized Eyring function and using the least-square procedure (see Figure S8 of the Appendix 2). As expected, the oxidative addition of CH_3I on the Rh^I complex to reach the transition state is an endothermic process, to which corresponds a negative activation entropy, confirming an associative mechanism.[16]

Table 4. Second-order rate constants for the reaction of **1** with CH_3I at different temperatures (standard deviations are given in parentheses). The corresponding least-square sample standard deviations (σ) are also reported.

Temperature (K)	k (M^{-1} s^{-1})	σ[a]
273.16	1.53(3) x 10^{-2}	1.23 x 10^{-3}
278.16	2.31(3) x 10^{-2}	1.64 x 10^{-3}
286.16	3.56(7) x 10^{-2}	1.39 x 10^{-3}
298.16	5.48(7) x 10^{-2}	1.38 x 10^{-3}

[a] $\sigma = [\Sigma_i (I_i^o - I_i^c)^2/(n-m)]^{1/2}$, where I_i^o, I_i^c are the observed and calculated integral values, *i* is the number of the spectrum, *n* is the number of observations and *m* is the number of parameters refined.

For the monoprotonate complexes **2**·X (X = PF_6, OTf and NO_3) the reaction is slower than for **1** and pseudo-first-order conditions were used ([CH_3I] / [Rh] = 100). Under these conditions, both a second-order treatment and a pseudo-first-order treatment gave the same values for the second-order rate constants. Being CH_3I in large excess, the decrease in its ^1H NMR peak integral could not be observed, and only the increase of the CH_3 signal of the Rh acetyl complex **5**·X was considered in the calculations. We decided to take into account only the integral values at t < 15 min. During this time, as observed in the FTIR and $^{31}P\{^1H\}$ NMR spectra, **A'** and **5**·X are the only product observed. Taking into account a single reaction step under pseudo-first order conditions, a very good fitting of the intensity of the acetyl ^1H NMR signal *vs*. time was obtained, as evidenced by the very low standard deviations of the calculated rate constants, at 298.16 K, (Table 5). This suggested that, although in steady-state, under this approximation the concentration of the methyl complex **A'** is very low, as supported by the $^{31}P\{^1H\}$ NMR spectrum and as also found for the reaction of complex **1**.

Table 5. Second-order rate constants for the reaction **2**·X (X = PF_6, OTf and NO_3) with CH_3I at 298.16 K (standard deviations are given in parentheses). The corresponding least-square sample standard deviations (σ) are also reported.

Counterion	k_1 (M^{-1} s^{-1})	σ[a]
PF_6	2.50 (6) 10^{-5}	7.66 10^{-3}
OTf	12.7 (3) 10^{-5}	2.88 10^{-2}
NO_3	24.6 (6) 10^{-5}	1.67 10^{-2}

[a] $\sigma = [\Sigma_i (I_i^o - I_i^c)^2/(n-m)]^{1/2}$, where I_i^o, I_i^c are the observed and calculated integral values, *i* is the number of the spectrum, *n* is the number of observations and *m* is the number of parameters refined.

The $\Delta H^{\ddagger}$ and $\Delta S^{\ddagger}$ activation parameters were determined for the **2**·PF_6 complex and resulted 45(7) kJ mol^{-1} and -180(30) J mol^{-1} K^{-1}, respectively (see Table S1 of the supporting information for kinetic rate costants at different temperature for **2**·PF_6). The $\Delta H^{\ddagger}$ value is markedly higher than that determined for **1**, indicating, as expected, that the activation process for an oxidative addition of CH_3I on a positively charged complex is more endothermic. The $\Delta S^{\ddagger}$ value is similar to that of the neutral complex (-175 J mol^{-1} K^{-1}) but, due to the high standard deviation, is not possible any clear discussion on the entropic activation change during the reaction. It seems clear that the decreased reaction rate for the monoprotonate complexes might be due to enthalpic factors associated to the oxidative addition step.

A similar cationic tridentate *S,N,S*-κ^3 Rh^I monocarbonyl complex, namely [Rh(L)CO]PF_6 [νCO (CH_3CN) = 2015 cm^{-1}; L = 2,6-bis(benzylthiomethyl)piridine] was reported to react with CH_3I.[16h,16n] In this case, the kinetic costants of both the oxidative additon step (1.4 x 10^{-4} M^{-1} s^{-1}) and the migratory CO insertion (4 x 10^{-5} M^{-1} s^{-1}) were determined in CH_3CN at 31 °C. Under these conditions, the rate determining step of the reaction is apparently the migratory insertion while, in our case, is the oxidative addition. Nevertheless, the observed rate contant in CH_2Cl_2 is very close[16h] (5.9 x 10^{-5} M^{-1} s^{-1}; see Table 5 for **2**·X rate constants).

As expected taking into account the νCO stretching frequency of the complexes, the reactivity decreases in the order **1** >> **2**·NO_3 > **2**·OTf > **2**·PF_6 >> **3**·X_2. The effect of the protonation can be also seen in the energy of the gas phase DFT-calculated MOs. Assuming that the suitable MO for the nucleophilic attack of the Rh atom on the CH_3 group must be the one at the highest energy with a s-simmetry, the energies found for these MOs in **1**, **2** and **3** were -0.167 a.u., -0.278 a.u. and -0.393 a.u. respectively.

A similar situation can be found in the literature for b-aminovinylketonato complexes of formula {Rh[$R^1C(O)CHC(NH)R^2$](PPh_3)(CO)} where the R groups can be CH_3 or CF_3: it was observed that the presence of one or two electron-attractive fluorinated substituents in the ligand retards the oxidative addition. In this case, however, quantitative kinetic parameters were not determined.[28]

A correlation between the νCO stretching and the global kinetic constants for **1** and **2**·X (X = PF_6, OTf, NO_3) should be possible. This is only true for the **2**·X series, as depicted in Figure 5.

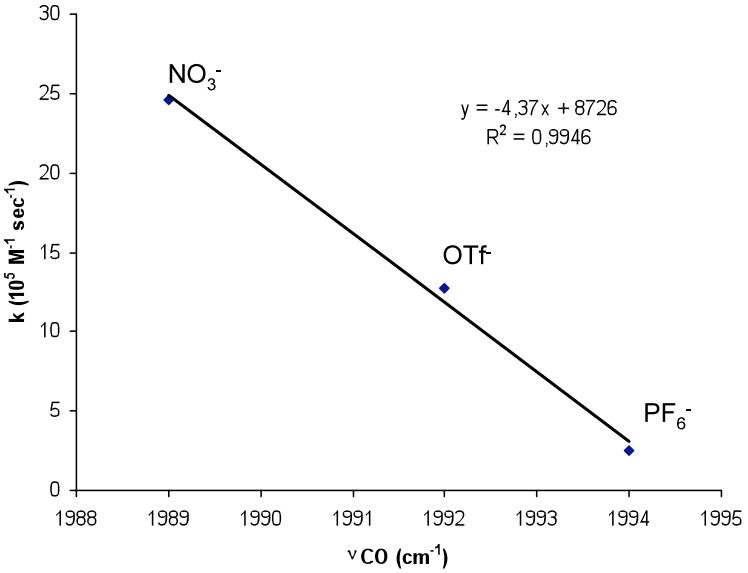

Figure 5. Linear regression function of the correlation between the frequency value of the CO stretching and the rate kinetic constants of the monoprotonated complexes **2**·X.

The experimental rate constant for complex **1** is one order of magnitude higher than the calculated one, (using the linear regression function obtained for the **2**·X series: experimental = 5.48 x 10^{-2} M^{-1} s^{-1}; calculated = 1.29 x 10^{-3} M^{-1} s^{-1}) pointing out that the monoprotonated complexes react more slowly than expected. Two simultaneous effects could be responsible of this behavior. A steric effect can be due to the variation in the geometry of the two penta-atomic chelation rings (Rh-S-C-P-N) when complex **1** is protonated, causing one axial phenyl ring to move towards the Rh metal centre [the distance of the Rh atom from the phenyl carbon atoms directly bonded to the P atoms of the PNP group are 3.92 for **1**, and 3.75 and 3.86 for **2**·PF_6]. A superposition of the solid state structures of **1**[13] and **2**·PF_6[14] is depicted in Figure 6 (the atoms used for superposing the structures were the Rh and the coordinated S, S', N and C).

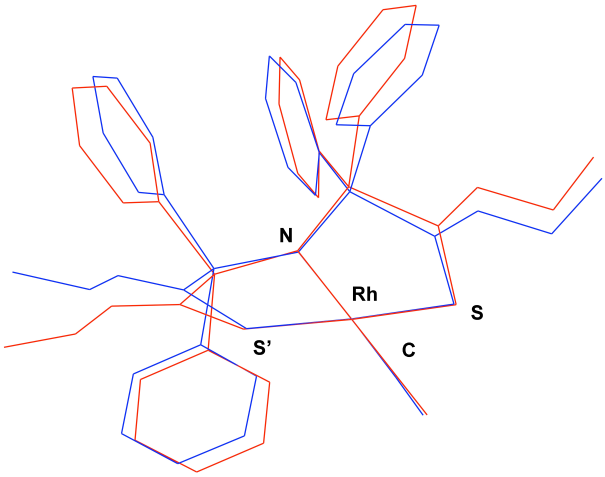

Figure 6. Superposition of **1** (red) and **2**·PF_6 (blue) [the atoms used for the superiposed were the Rh atoms and the coordinated S, N and C(O) atoms].

This higher steric hindrance would lower the rate of the oxidative addition but enhance the rate of the migratory insertion. As previously reported[3,9-11] the migratory CO insertion rate can be higher when a p-donor ligand is present, forming a molecular orbital of suitable energy in which the contribution of the methyl ligand is not negligible and is in-phase with Rh and CO(π^*), thus generating a continuous lobe that contains the three atoms involved in migratory CO insertion. A DFT calculation was performed to optimize the possible Rh^{III}-CH_3 intermediate for the reaction of complex **1** and complex **2** with CH_3I (**A** and **A'**, respectively). An octahedral geometry for the Rh-CH_3 complex was adopted, with the CH_3 group and the I atom in *trans* axial positions with respect to the S, N, S, C, Rh plane. Only in the case of the neutral complex **A** we found one MO spreading on the atoms involved in the migratory CO insertion, whereas no similar orbital was present in the cationic **A'**. This two effects, one reducing the oxidative addition rate and the other reducing the migratory CO insertion rate, could be responsible of the lower than expected reactivity of **2**·X (X = PF_6, OTf and NO_3).

3.4 Conclusions

The zwitterionic Rh^I monocarbonyl complex [Rh(EtSNS)(CO)] (**1**) can be mono- and bi-protonated affording cationic complexes [Rh(HEtSNS)(CO)]X (**2**·X) and [Rh(H_2EtSNS)(CO)]X_2 (**3**·X_2) (X = PF_6, OTf, NO_3). In these compounds, the electron density

on the Rh atom varies, as pointed out by the change of the IR stretching frequency of the coordinated CO, and confirmed by the DFT-calculated Mulliken atomic populations. The effect of the protonation was studied in the reaction with iodomethane. In the case of **1** and **2**·X the oxidative addition of CH_3I was followed by the migratory CO insertion, forming the acetyl-Rh^{III} complexes [Rh(EtSNS)($COCH_3$)I] (**4**) and [Rh(HEtSNS)($COCH_3$)I]X (**5**), respectively. Complex **4** was characterized in solution and its solid state structure was determined by X-Ray diffraction methods. Compounds **5**·X are stable in solution for a short time, undergoing deprotonation forming complex **4**, and also decomposing in unidentified products. The rate constants of the reaction were determined by means of ^1H NMR spectroscopy; in the case of complex **1**, second order conditions ([CH_3I] / [Rh] = 1) could be employed. The reactivity decreases in the order **1** [5.48(7) x 10^{-2} M^{-1} s^{-1}] >> **2**·NO_3 [24.6 (6) x 10^{-5} M^{-1} s^{-1}] > **2**·OTf [12.7 (3) x 10^{-5} M^{-1} s^{-1}] > **2**·PF_6 [2.50 (6) x 10^{-5} M^{-1} s^{-1}] >> **3**·X_2 at 25 °C in CH_2Cl_2. Complexes **3**·X_2 reacted too slowly, hindering the determination of the rate constants. The activation parameters $\Delta H^{\ddagger}$ and $\Delta S^{\ddagger}$ were determined for **1** and **2**·PF_6, confirming the nucleophilic addition mechanism. Calculations showed that the suitable MO for the nucleophilic attack of the Rh atom on the CH_3 group of iodomethane (that must be the one at the highest energy with a σ-simmetry), displayed a variation of its energy that paralleled to the reactivity trend of **1**, **2** and **3**. A good correlation was found between the rate constants, along the series **2**·NO_3, **2**·OTf and **2**·PF6, with the corresponding CO stretching frequency values. This correlation could be explained assuming that the different non metal-coordinated anions form a hydrogen bonding with the NH group of **2** (as evidenced by its ^1H NMR chemical shift), that in turn causes a variation of the electron density on the Rh centre (as observed by the change in the CO stretching frequency). In conclusion, the reactivity of complex **1** towards iodomethane could be tuned by protonation and fine-tuned by changing the counterion.

3.5 References

[1] (a) Feliz, M.; Freixa, Z.; van Leeuwent, P. W. N. M.; Bo, C., *Organometallics* **2005**, *24*, 5718-5723. (b) Doppiu, A.; Englert, U.; Salzer, A., *Chem. Commun.* **2004**, 2166-2167. (c) Kinnunen, T.; Laasonen, K., *J. Organomet. Chem.* **2003**, *665*, 150-155. (d) Chauby, V.; Daran, J. C.; Serra-Le Berre, C.; Malbosc, F.; Kalck, P.; Gonzalez, O. D.; Haslam, C. E.; Haynes, A., *Inorg. Chem.* **2002**, *41*, 3280-3290. (e) Ivanova, E. A.; Gisdakis, P.; Nasluzov, V. A.; Rubailo, A. I.; Rosch, N., *Organometallics* **2001**, *20*,

1161-1174. (f) Kinnunen, T.; Laasonen, K., *J. Mol. Struct. (THEOCHEM)* **2001**, *540*, 91-100. (g) Kinnunen, T.; Laasonen, K., *J. Mol. Struct. (THEOCHEM)* **2001**, *542*, 273-288. (h) Griffin, T. R.; Cook, D. B.; Haynes, A.; Pearson, J. M.; Monti, D.; Morris, G. E., *J. Am. Chem. Soc.* **1996**, *118*, 3029-3030. (i) Chock, P. B.; Halpern, J., *J. Am. Chem. Soc.* **1966**, *88*, 3511-3514.

[2] Martin, H. C.; James, N. H.; Aitken, J.; Gaunt, J. A.; Adams, H.; Haynes, A., *Organometallics* **2003**, *22*, 4451-4458.

[3] Gonsalvi, L.; Adams, H.; Sunley, G. J.; Ditzel, E.; Haynes, A., *J. Am. Chem. Soc.* **2002**, *124*, 13597-13612.

[4] (a) Haynes, A.; Mann, B. E.; Morris, G. E.; Maitlis, P. M., *J. Am. Chem. Soc.* **1993**, *115*, 4093-4100. (b) Haynes, A.; Mann, B. E.; Gulliver, D. J.; Morris, G. E.; Maitlis, P. M., *J. Am. Chem. Soc.* **1991**, *113*, 8567-8569.

[5] Gaunt, J. A.; Gibson, V. C.; Haynes, A.; Spitzmesser, S. K.; White, A. J. P.; Williams, D. J., *Organometallics* **2004**, *23*, 1015-1023.

[6] Moser, M.; Wucher, B.; Kunz, D.; Rominger, F., *Organometallics* **2007**, *26*, 1024-1030.

[7] Wilson, J. M.; Sunley, G. J.; Adams, H.; Haynes, A., *J. Organomet. Chem.* **2005**, *690*, 6089-6095.

[8] Gonsalvi, L.; Adams, H.; Sunley, G. J.; Ditzel, E.; Haynes, A., *J. Am. Chem. Soc.* **1999**, *121*, 11233-11234.

[9] Cavallo, L.; Sola, M., *J. Am. Chem. Soc.* **2001**, *123*, 12294-12302.

[10] Margl, P.; Ziegler, T.; Blochl, P. E., *J. Am. Chem. Soc.* **1996**, *118*, 5412-5419.

[11] Daura-Oller, E.; Poblet, J. M.; Bo, C., *Dalton Trans.* **2003**, 92-98.

[12] Chauvin, R., *Eur. J. Inorg. Chem.* **2000**, 577-591.

[13] Asti, M.; Cammi, R.; Cauzzi, D.; Graiff, C.; Pattacini, R.; Predieri, G.; Stercoli, A.; Tiripicchio, A., *Chem. Eur. J.* **2005**, *11*, 3413-3419.

[14] Delferro, M.; Cauzzi, D.; Pattacini, R.; Tegoni, M.; Graiff, C.; Tiripicchio, A., *Eur. J. Inorg. Chem.* **2008**, 2302-2312.

[15] (a) Delferro, M.; Pattacini, R.; Cauzzi, D.; Graiff, C.; Terenghi M.; Predieri G.; Tiripicchio A., *Dalton Trans.*, **2009**, DOI: 10.1039/b812050a. (b) Pattacini, R.; Barbieri, L.; Stercoli, A.; Cauzzi, D.; Graiff, C.; Lanfranchi, M.; Tiripicchio, A.; Elviri, L., *J. Am. Chem. Soc.* **2006**, *128*, 866-876.

[16] (a) Conradie, M. M.; Conradie, J., *Inorg. Chim. Acta* **2008**, *361*, 208-218. (b) Conradie, M. M.; Conradie, J., *Inorg. Chim. Acta* **2008**, *361*, 2285-2295. (c) Baber, R. A.; Haddow, M. F.; Middleton, A. J.; Orpen, A. G.; Pringle, P. G.; Haynes, A.; Williams, G. L.; Papp, R., *Organometallics* **2007**, *26*, 713-725. (d) Best, J.; Wilson, J. M.; Adams, H.; Gonsalvi, L.; Peruzzini, M.; Haynes, A., *Organometallics* **2007**, *26*, 1960-1965. (e) Conradie, J.; Lamprecht, G. J.; Roodt, A.; Swarts, J. C., *Polyhedron* **2007**, *26*, 5075-5087. (f) Dutta, D. K.; Woollins, J. D.; Slawin, A. M. Z.; Konwar, D.; Sharma, M.; Bhattacharyya, P.; Aucott, S. M., *J. Organomet. Chem.* **2006**, *691*, 1229-1234. (g) Freixa, Z.; Kamer, P. C. J.; Lutz, M.; Spek, A. L.; van Leeuwen, P. W. N. M., *Angew. Chem. Int. Ed.* **2005**, *44*, 4385-4388. (h) Bassetti, M.; Capone, A.; Salamone, M., *Organometallics* **2004**, *23*, 247-252. (i) Haynes, A.; Maitlis, P. M.; Stanbridge, I. A.; Haak, S.; Pearson, J. M.; Adams, H.; Bailey, N. A., *Inorg. Chim. Acta* **2004**, *357*, 3027-3037. (l) Kumari, N.; Sharma, M.; Chutia, P.; Dutta, D. K., *J. Mol. Cat. A* **2004**, *222*,

53-58. (m) Gonsalvi, L.; Gaunt, J. A.; Adams, H.; Castro, A.; Sunley, G. J.; Haynes, A., *Organometallics* **2003**, *22*, 1047-1054. (n) Bassetti, M.; Capone, A.; Mastrofrancesco, L.; Salamone, M., *Organometallics* **2003**, *22*, 2535-2538. (o) Steyn, G. J. J.; Roodt, A.; Leipoldt, J. G., *Inorg. Chem.* **1992**, *31*, 3477-3481.

[17] Bott, S. G.; Fleischer, H.; Leach, M.; Mingos, D. M. P.; Powell, H.; Watkin, D. J.; Watson, M. J., *J. Chem. Soc.-Dalton Trans.* **1991**, 2569-2578.

[18] *SAINT Software Users Guide*, Version 6.0; Bruker Analytical X-ray Systems: Madison, WI, **1999**.

[19] G. M. Sheldrick, *SADABS*; Bruker Analytical X-ray Systems, Madison, WI, **1999**. G. M. Sheldrick, *SHELXL-97*, Program for crystal structure refinement; University of Göttingen: Germany, **1997**.

[20] Binstead, R. A.; Jung, B.; Zuberbühler, A. D. SPECFIT Global Analysis System, Version 3.0, Spectrum Software Associates, Marlborough (MA, U.S.A.), **2004**.

[21] (a) Stephens, P. J.; Devlin, F. J.; Chabalowski, C. F.; Frisch, M. J., *J. Phys. Chem.* **1994**, *98*, 11623-7. (b) Becke, A. D., *J. Chem. Phys.* **1993**, *98*, 5648-5652. (c) Lee, C.; Yang, W.; Parr, R. G., *Phys. Rev. B: Condens. Matter* **1988**, *37*, 785-789.

[22] (a) Godbout, N.; Salahub, D. R.; Andzelm, J.; Wimmer, E., *Can. J. Chem.* **1992**, *70*, 560-71. (b) Sosa, C.; Andzelm, J.; Elkin, B. C.; Wimmer, E.; Dobbs, K. D.; Dixon, D. A., *J. Phys. Chem.* **1992**, *96*, 6630-6636.

[23] Reed, A. E.; Curtiss, L. A.; Weinhold, F., *Chem. Rev.* **1988**, *88*, 899-926.

[24] Frisch, M. J.; Trucks, G. W.; Schlegel, H. B.; Scuseria, G. E.; Robb, M. A.; Cheeseman, J. R.; Montgomery, J. A., Jr.; Vreven, T.; Kudin, K. N.; Burant, J. C.; Millam, J. M.; Iyengar, S. S.; Tomasi, J.; Barone, V.; Mennucci, B.; Cossi, M.; Scalmani, G.; Rega, N.; Petersson, G. A.; Nakatsuji, H.; Hada, M.; Ehara, M.; Toyota, K.; Fukuda, R.; Hasegawa, J.; Ishida, M.; Nakajima, T.; Honda, Y.; Kitao, O.; Nakai, H.; Klene, M.; Li, X.; Knox, J. E.; Hratchian, H. P.; Cross, J. B.; Adamo, C.; Jaramillo, J.; Gomperts, R.; Stratmann, R. E.; Yazyev, O.; Austin, A. J.; Cammi, R.; Pomelli, C.; Ochterski, J. W.; Ayala, P. Y.; Morokuma, K.; Voth, G. A.; Salvador, P.; Dannenberg, J. J.; Zakrzewski, V. G.; Dapprich, S.; Daniels, A. D.; Strain, M. C.; Farkas, O.; Malick, D. K.; Rabuck, A. D.; Raghavachari, K.; Foresman, J. B.; Ortiz, J. V.; Cui, Q.; Baboul, A. G.; Clifford, S.; Cioslowski, J.; Stefanov, B. B.; Liu, G.; Liashenko, A.; Piskorz, P.; Komaromi, I.; Martin, R. L.; Fox, D. J.; Keith, T.; Al-Laham, M. A.; Peng, C. Y.; Nanayakkara, A.; Challacombe, M.; Gill, P. M. W.; Johnson, B.; Chen, W.; Wong, M. W.; Gonzalez, C.; Pople, J. A., Gaussian 03, revision C.02; Gaussian, Inc.: Wallingford CT, **2004**.

[25] (a) Ernsting, J. M.; Gaemers, S.; Elsevier, C. J., *Mag. Reson. Chem.* **2004**, *42*, 721-736. (b) Donkervoort, J. G.; Buhl, M.; Ernsting, J. M.; Elsevier, C. J., *Eur. J. Inorg. Chem.* **1999**, 27-33.

[26] Allen, F. H., *Acta Cryst.* **2002**, B58, 380-388.

[27] (a) Frech, C. M.; Milstein, D., *J. Am. Chem. Soc.* **2006**, *128*, 12434-12435. (b) Kinnunen, T.; Laasonen, K., *J. Organomet. Chem.* **2001**, *628*, 222-232.

[28] Galding, M. R.; Cherkasova, T. G.; Osetrova, L. V.; Varshavsky, Y. S.; Roodt, A., *Rhodium Express* **1996**, *16*, 23-36.

4

Reactivity of the Zwitterionic Ligand $EtNHC(S)Ph_2P{=}NPPh_2C(S)NEt$ towards $[Ru_3(CO)_{12}]$. Sulfur Transfer and Ligand Fragmentation Leading to the Methideylamide *[-N(Et)-CH(R)-]* μ_3-Bridging Moiety.

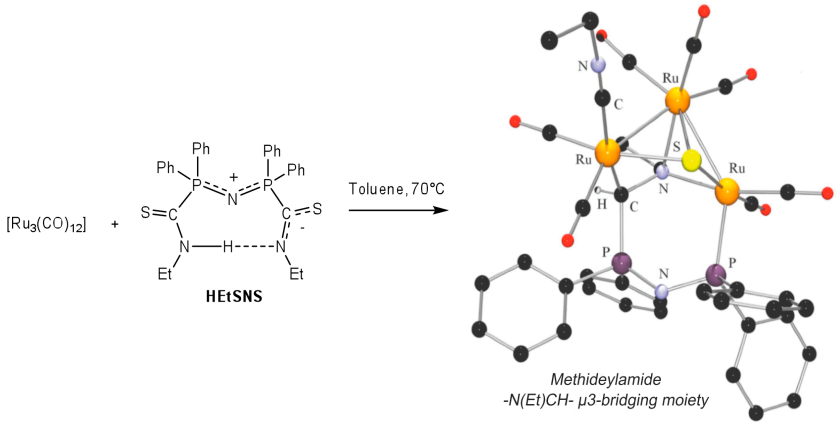

The reaction of $EtNHC(S)Ph_2PN{=}P^+Ph_2C(S)N^-Et$ (HEtSNS) with $[Ru_3(CO)_{12}]$ has been carried out under two different experimental conditions: in the first case $[Ru_3(CO)_{12}]$, previously turned into the labile intermediate $[Ru_3(CO)_{10}(CH_3CN)_2]$, afforded, at room temperature in dichloromethane, the trinuclear clusters $[Ru_3(CO)_{11}(CNEt)]$ (**1**), $\{Ru_3(CO)_9(\mu\text{-}H)[(\mu\text{-}S{:}k\text{-}P)Ph_2PN{=}PPh_2C(S)NEt]\}$ (**2**), $\{Ru_3(CO)_9(\mu\text{-}H)[(\mu\text{-}S{:}k\text{-}P)Ph_2PN{=}P(S)Ph_2]\}$ (**3**) and $\{Ru_3(CO)_{10}[(\mu\text{-}k^2P)Ph_2PNHPPh_2]\}$ (**4**). Ligand fragmentation occurs via loss of EtNC or EtNCS, without sulfur transfer to the cluster core. In the second case, $[Ru_3(CO)_{12}]$ reacted with HEtSNS in toluene at 70 °C, giving the trinuclear clusters **4**, $\{Ru_3(CO)_7(CNEt)(\mu_3\text{-}S)[(\mu_2\text{-}N{:}\eta^1\text{-}C{:}\kappa^1\text{-}P)Ph_2PN{=}PPh_2C(H)NEt]\}$ (**5**), $\{Ru_3(CO)_8(\mu_3\text{-}S)[(\mu_2\text{-}N{:}\eta^1\text{-}C{:}\kappa^1\text{-}P)Ph_2PN{=}PPh_2C(H)NEt]\}$ (**6**) and $\{Ru_3(CO)_6(\mu_3\text{-}CO)(\mu_3\text{-}S)(EtNC)[(\mu\text{-}\kappa^2P)Ph_2PNHPPh_2]\}$ (**7**). Cluster **5** shows an open triangle of Ru atoms capped by a μ_3-sulfide and by the unprecedented methideylamide –N(Et)CH(R)– μ_3-bridging moiety of the $Ph_2PN{=}PPh_2C(H)NEt$ ligand. It formally derives from cluster **6** by substitution of ethyl isonitrile with one CO molecule.

4.1 Introduction

This chapter deals with the results of a research work matching our longstanding interest in cluster chemistry[1-5] with our recent investigations on the coordination behaviour of the zwitterionic ligand $EtNHC(S)Ph_2P{=}NPPh_2NEt$ (HEtSNS).[6-8] It can be turned into the phosphine sulfide derivative $Ph_2(S)PN{=}PPh_2C(S)NHEt$ by moderate heating[6] (Scheme 1).

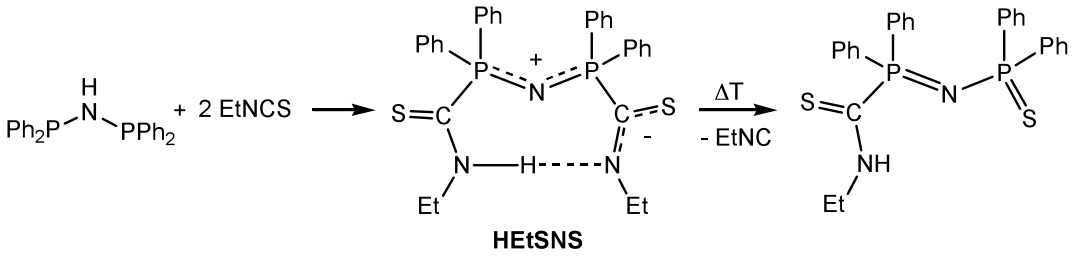

Scheme 1

The aim of this work was to investigate the reactivity of HEtSNS, towards the trinuclear cluster $[Ru_3(CO)_{12}]$. Two different experimental strategies were followed: HEtSNS was reacted with $[Ru_3(CO)_{10}(CH_3CN)_2]$ under mild conditions and with $[Ru_3(CO)_{12}]$ under pyrolitic conditions. These reactions led to novel ruthenium carbonyl clusters and gave insight into the fragmentation behaviour of HEtSNS. Their major products, in terms of yield, were isolated and characterized and the structure of the most significant ones are described herein.

4. 2 Experimental

4.2.1 General procedures.

Crystalline $[Ru_3(CO)_{12}]$ was a commercial product (Aldrich) and used as received. $EtNHC(S)Ph_2P{=}NPPh_2C(S)NEt$ (HEtSNS)[6] and $[Ru_3(CO)_{10}(CH_3CN)_2]$[9] were prepared according to published procedures. The solvents (J.T. Baker) were dried and distilled by standard techniques. Elemental analyses (C, H, N, S) were carried out on a Carlo Erba EA1108 microanalyzer. Solution FTIR spectra (4000-400 cm^{-1}, CaF_2 cell) were recorded on a Nicolet Nexus spectrophotometer. ^1H (300.13 MHz, TMS) and 2D ^1H-^1H COSY spectra in

$CDCl_3$ were recorder on a Bruker Avance 300; $^{31}P\{^1H\}$ NMR (161.98 MHz, external reference 85% H_3PO_4) spectra in $CDCl_3$ were recorder on a Bruker AMX400. The ^{31}P-^1H heterocorrelation NMR experiment (HETCOR) was recordered at room temperature in $CDCl_3$ on a Varian Inova-600 (600 MHz, ^1H; 125 MHz, ^{31}P). For the two-dimensional experiment phase-sensitive detection of the directly observed frequency (^{31}P) was achieved by the TPPI method. Multiplicity and coupling constants for ^1H NMR spectra of cluster **5** and **6** were simulated, in very good accordance with those observed experimentally, by using the MestRe-C program.[10] Experimental mass measurements were made on a LTQ XL (Thermo Electron Corporation) equipped with an ESI interface operating in positive ion (PI) mode, acquiring mass spectra over the scan range *m/z* 200-2000, using CH_3OH as solvent. The source introductions were carried on by a pneumatically assisted syringe (5 μL/min) flowing into a continum flow (200 μL/min) of pure methanol from an LC pump (Finningan Surveyor-Thermo Electron Corporation). Spray voltage were set to 4.5 KV and capillary temperature was 250°C. All other instrumental parameters were automatically tuned in order to achieve best ion trasmission to the analyzer.

4.2.2 Reaction of HEtSNS and $[Ru_3(CO)_{10}(CH_3CN)_2]$.

To a solution of $[Ru_3(CO)_{10}(CH_3CN)_2]$ (0.200 g, 0.30 mmol) in CH_2Cl_2 (40 mL) HEtSNS (0.168, 0.30 mmol) was added, resulting in an orange reaction mixture. After stirring for 2 h at room temperature, the volatiles were removed in vacuo. The residue was chromatographed by preparative TLC. Elution with CH_2Cl_2 : *n*-Hexane (3:2, v/v) developed four bands. The third yellow (Rf = 0.52) and the fourth orange (Rf = 0.38) bands gave the known compounds $\{Ru_3(CO)_9(\mu\text{-H})[(\mu\text{-S}:k\text{-P})Ph_2PN{=}PPh_2S]\}$[11] (**3**) (3%) and $\{Ru_3(CO)_{10}[(\mu\text{-}k^2\text{P})Ph_2PNHPPh_2]\}$[12] (**4**) (13%) respectively. The first yellow band (Rf = 0.73) gave the new compound $[Ru_3(CO)_{11}(CNEt)]$ (**1**) (18%) as a yellow powder. Anal. Calc. for $C_{14}H_5NO_{11}Ru_3$: C, 25.23; H, 0.76; N, 2.10. Found C, 25.17; H, 0.75; N, 2.08. FTIR (CH_2Cl_2, νCO, cm^{-1}): 2190w, 2094m, 2060s, 2044vs, 2008s. ^1H NMR (300 MHz, $CDCl_3$, 25°C): δ = 3.91(q, 2H, $-CH_2-$, $^3J_{H,H}$ = 7.7 Hz), 0.88 (t, 3H, $-CH_3$, $^3J_{H,H}$ = 7.7 Hz) ppm. The second red band (Rf = 0.62) gave the new compound $\{Ru_3(CO)_9(\mu\text{-H})[(m\text{-S}:k\text{-P})Ph_2PN{=}PPh_2C(NEt)S]\}$ (**2**) (25%) as red crystals after recrystallization from hexane/CH_2Cl_2 at –4 °C. Anal. Calc. for $C_{36}H_{26}N_2O_9P_2Ru_3S$: C, 42.07; H, 2.55; N, 2.73; S, 3.12. Found C, 41.89; H, 2.51; N, 2.69; S, 3.09. FTIR (CH_2Cl_2, νCO, cm^{-1}): 2085s, 2048s,

2009s, 1958sh. ^{1}H NMR (300 MHz, $CDCl_3$, 25°C): δ = 8.20-7.26 (m, 20H, Ph), 4.10 (m, br, 1H, -C*H*H-), 3.85 (m, br, 1H, -CH*H*-), 1.36 (t, 3H, -CH_3, $^{3}J_{H,H}$ = 7.2 Hz), -14.7 (d, 1H, μ-H, $^{2}J_{P,H}$ = 9.0 Hz) ppm. ^{31}P{^{1}H} NMR (161.98 MHz, $CDCl_3$, 25°C): δ = 10.42 (s), 54.09 (s) ppm.

*4.2.3 Thermal treatment at 50 °C of cluster **2**; conversion in cluster **3** in a sealed tube.*

A solution of cluster **2** (0.154 g, 0.15 mmol) in toluene (20 mL) was heated at 50°C for 1 h in a sealed tube. Conversion in cluster **3** was detected by ^{1}H NMR, ^{31}P{^{1}H} NMR, FTIR (Yield 92% by NMR peak integration).

4.2.4 Pyrolitic reaction between HEtSNS and [$Ru_3(CO)_{12}$].

To a solution of [$Ru_3(CO)_{12}$] (0.200 g, 0.31 mmol) in CH_2Cl_2 (40 mL) HEtSNS (0.175, 0.31 mmol) was added, resulting in an orange reaction mixture. After stirring for 2 h at 70°C, the solvent was removed in vacuo. The residue was chromatographed by preparative TLC (CH_2Cl_2 : *n*-Hexane = 3:2) and the four resulting bands collected.

The third yellow band (Rf = 0.56) gave the known compound **4** (9%).

The first yellow band (Rf = 0.81) gave the new compound {$Ru_3(CO)_7$(CNEt)(μ_3-S)[(μ_2-N:η^1-C:κ^1-P)Ph_2PN=PPh_2CHNEt]} (**5**) (14%) as yellow crystals after recrystallization by layering *n*-hexane on a dichloromethane solution of **5**. Anal. Calc. for $C_{37}H_{31}N_3O_7P_2Ru_3S$: C, 43.28; H, 3.04; N, 4.09; S, 3.12. Found C, 43.21; H, 3.01; N, 4.02; S, 3.08. FTIR (CH_2Cl_2, νCO, cm^{-1}): 2186s, 2054m, 2005vs, 1993sh, 1972sh. ^{1}H NMR (300 MHz, $CDCl_3$, 25°C): δ = 8.02-7.14 (m, 20H, Ph), 4.16 (d, 1H, -RuCH-, $^{2}J_{P,H}$= 7.5 Hz), 3.73 (q, 2H, CH_3CH_2NCRu, $^{3}J_{H,H}$ = 7.2 Hz), 2.60 (observed multiplicity: m, simulated (line width 1 Hz), qdd, 2H, -CH_2-, $^{3}J_{H,H}$ = 6.9 Hz, $^{4}J_{H,P}$ = 3.20 Hz, $^{4}J_{H,P}$ = 3.80 Hz), 1.40 (t, 3H, CH_3CH_2NCRu, $^{3}J_{H,H}$ = 7.2 Hz), 0.86 (t, 3H, CH_3CH_2NRu, $^{3}J_{H,H}$ = 6.9 Hz) ppm. ^{31}P{^{1}H} NMR (161.98 MHz, $CDCl_3$, 25°C): δ = 77.6 (d, $^{2}J_{P,P}$ = 37 Hz), 35.5 (d, $^{2}J_{P,P}$ = 37 Hz) ppm.

The second yellow band (Rf = 0.75) gave the new compound {$Ru_3(CO)_8$)(μ_3-S)[(μ_2-N:η-C:κ-P)Ph_2PN=PPh_2CHNEt]} (**6**) (26%) as yellow powder. Anal. Calc. for $C_{35}H_{26}N_2O_8P_2Ru_3S$: C, 42.05; H, 2.62; N, 2.80; S, 3.21. Found C, 41.93; H, 2.58; N, 2.74; S, 3.18. FTIR (CH_2Cl_2, νCO, cm^{-1}): 2070vs, 2034s, 2016m, 1997sh, 1981sh, 1961m. ^{1}H NMR (300 MHz, $CDCl_3$, 25°C): δ = 8.1-7.15 (m, 20H, Ph), 4.23 (d, 1H, -RuCH-, $^{2}J_{P,H}$= 6.3 Hz), 2.59 (observed multiplicity: m, simulated (line width 1 Hz), qdd, 2H, -CH_2-, $^{3}J_{H,H}$ = 6.6 Hz,

$^4J_{H,P}$ = 3.0 Hz, $^4J_{H,P}$ = 3.0 Hz), 0.91 (t, 3H, *CH*$_3$CH$_2$NRu, $^3J_{H,H}$ = 6.6 Hz) ppm. $^{31}P\{^1H\}$ NMR (161.98 MHz, $CDCl_3$, 25°C): δ = 68.54 (d, $^2J_{P,P}$ = 35 Hz), 34.80 (d, $^2J_{P,P}$ = 35 Hz) ppm.
The fourth yellow band (Rf = 0.41) gave the new compound $\{Ru_3(CO)_6(\mu_3\text{-}CO)(\mu_3\text{-}S)(EtNC)[(\mu\text{-}\kappa^2P)Ph_2PNHPPh_2]\}$ (**7**) as yellow crystals of **7**·CH_3OH after recrystallization by layering methanol on a dichloromethane solution (21%). Anal. Calc. for $C_{34}H_{26}N_2O_7P_2Ru_3S$: C, 42.02; H, 2.70; N, 2.88; S, 3.30. Found C, 41.95; H, 2.67; N, 2.84; S, 3.27. FTIR (CH_2Cl_2, νCO, cm^{-1}): 2055m, 2037s, 2009vs, 1975s, 1652br. ^1H NMR (300 MHz, $CDCl_3$, 25°C): δ = 7.62-7.22 (m, 20H, Ph), 4.02 (t, 1H, NH, $^2J_{P,H}$ = 6 Hz), 3.63 (q, 2H, -CH_2-, $^3J_{H,H}$ = 7.5 Hz), 1.35 (t, 3H, -CH_3, $^3J_{H,H}$ = 7.5 Hz) ppm. $^{31}P\{^1H\}$ NMR (161.98 MHz, $CDCl_3$, 25°C): δ = 82.1 (s) ppm.

*4.2.5 Thermal treatment at 80 °C of cluster **2**; conversion in cluster **7**.*

A solution of cluster **2** (0.154 g, 0.15 mmol) in toluene (20 mL) was heated at 80°C for 1 h. Conversion in cluster **7** was detected by ^1H NMR, $^{31}P\{^1H\}$ NMR, FTIR (Yield 82% by NMR peak integration).

*4.2.6 X-Ray data collection, structure solution and refinement of **2**, **5** and **7**·CH_3OH.*

The intensity data of **2**, **5** and **7**·CH_3OH were collected at room temperature with a Bruker AXS Smart 1000[13] single crystal diffractometer equipped with an area detector, using a graphite monochromated Mo-K_α radiation (λ = 0.71073 Å). Crystallographic and experimental details of the structures are summarized in Table 1. The structures were solved by direct methods and refined by full-matrix least-squares procedures (based on F_o^2) [14] first with isotropic thermal parameters and then with anisotropic thermal parameters in the last cycles of refinement for all the non-hydrogen atoms. The hydrogen atoms, introduced into the geometrically calculated positions, were refined riding on the corresponding parent atoms, except for the hydride in **2**, H1 in **5** and H1N in **7**·CH_3OH that were found in the ΔF maps and refined isotropically.

Table 1 Crystal Data and Structure Refinement for **2**, **5** and **7**·CH_3OH

	2	**5**	**7**·CH_3OH
formula	$Ru_3SP_2N_2O_9C_{36}H_{26}$	$Ru_3SP_2N_3O_7C_{37}H_{31}$	$Ru_3SP_2N_2O_7C_{34}H_{26}$·$CH_3OH$
FW	1027.80	1026.86	1003.82
crystal system	monoclinic	monoclinic	monoclinic
space group	$P2_1/c$	$C2/c$	$P2_1/a$
a, Å	10.737(3)	33.751(5)	20.304(5)
b, Å	21.612(4)	10.518(2)	9.910(5)
c, Å	34.138(5)	22.346(2)	20.779(5)
β, deg	91.58(5)	97.27(3)	110.97(5)
V, Å^3	7919(3)	7869(2)	3904(2)
Z	8	8	4
D_{calcd}, g cm^{-3}	1.724	1.734	1.708
F(000)	4048	4064	1984
crystal size (mm^3)	0.09 x 0.10 x 0.12	0.07 x 0.08 x 0.12	0.09 x 0.11 x 0.14
μ cm^{-1}	13.17	13.22	13.31
rflns collected	69593	23146	22882
rflns unique	23041 (R_{int} = 0.0597)	8602 (R_{int} = 0.0570)	8397 (R_{int} = 0.0687)
rflns observed [I>2σ(I)]	16946	4311	5080
parameters	963	482	464
R indices [I>2σ(I)]	R1 = 0.0506; wR2 = 0.1008	R1 = 0.0423; wR2 = 0.0628	R1 = 0.0421; wR2 = 0.0941
R indices (all data)	R1 = 0.0925; wR2 = 0.1175	R1 = 0.1091; wR2 = 0.0740	R1 = 0.0745; wR2 = 0.1129

4.3 Results and Discussion

4.3.1 Reaction between $Ru_3(CO)_{10}(MeCN)_2$ and HEtSNS

In CH_2Cl_2, the 1:1 room temperature reaction between the labile $[Ru_3(CO)_{10}(MeCN)_2]$ and the zwitterionic ligand HEtSNS, gives rise to four main products, as depicted in Scheme 2. Ligand fragmentation is observed, without sulfur transfer to the metal core.

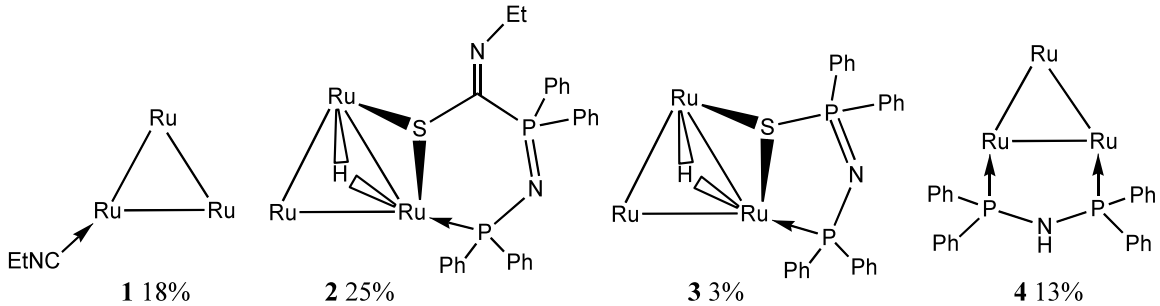

1 18% **2** 25% **3** 3% **4** 13%

Scheme 2

Clusters $\{Ru_3(CO)_9(\mu\text{-H})[(\mu\text{-S}:k\text{-P})Ph_2PN{=}PPh_2S]\}$[10] (**3**) and $\{Ru_3(CO)_{10}[(\mu\text{-}k^2\text{P})Ph_2PNHPPh_2]\}$[11] (**4**) were identified by comparison of their spectroscopical data with those reported in the literature. Cluster $[Ru_3(CO)_{11}(CNEt)]$ (**1**) was identified by ^{1}H NMR spectrum, in which only the coordinated ethyl isonitrile peaks were present, and by comparison of its FTIR spectrum with that of published $[Ru_3(CO)_{11}(CN^tBu)]$.[15] Cluster **1**, **3** and **4** can be seen as the products of the reaction of $[Ru_3(CO)_{10}(MeCN)_2]$ with CNEt, $PPh_2NHP(S)Ph_2$ and dppa respectively, that are degradation products of HEtSNS.

The cluster $\{Ru_3(CO)_9(\mu\text{-H})[(\mu\text{-S}:k\text{-P})Ph_2PN{=}PPh_2C(NEt)S]\}$ (**2**) is a new compound and it has been recognized by X-ray diffraction analysis. In the crystals, two crystallographically, but very similar, independent molecules are present (A and B). An ORTEP view of molecule A is reported in Figure 1.

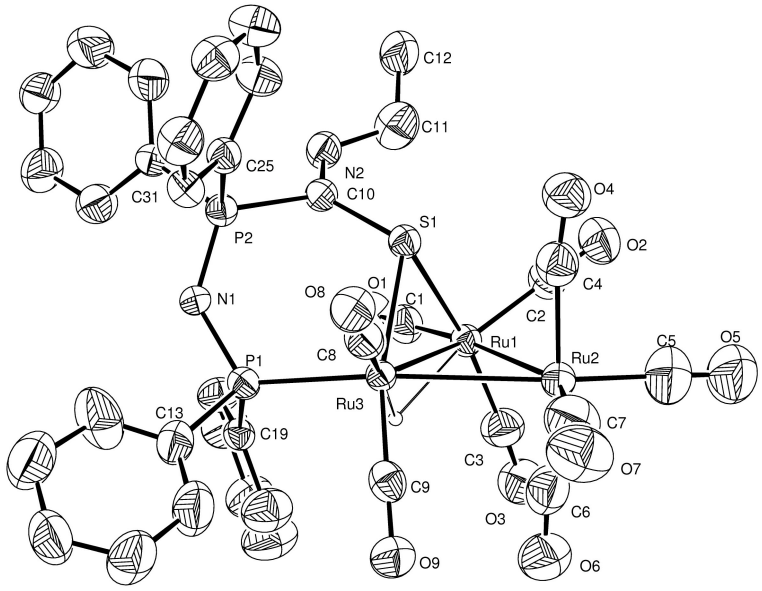

Figure 1. ORTEP plot of the structure of cluster **2** (molecule A). Thermal ellipsoids are drawn at the 30% probability level. H atoms, except the hydride, are omitted for clarity. Selected bond distance (Å) and angle (°) (Values for molecule B are given in parenthesis): Ru1A-S1A 2.433(1) [2.417(2)], Ru1A-Ru3A 2.828(1) [2.849(1)], Ru1A-Ru2A 2.850(1) [2.834(1)], Ru2A-Ru3A 2.876(1) [2.877(1)], Ru3A-P1A 2.341(1) [2.342(1)], Ru3A-S1A 2.419(1) [2.409(1)]; Ru2A-Ru1A-Ru3A 60.87(2) [60.82(2)], Ru1A-Ru2A-Ru3A 59.18(1) [59.83(1)], Ru1A-Ru3A-Ru2A 59.95(2) [59.34(2)], P2A-N1A-P1A 131.1(2) [133.5(3)].

In the structure of cluster **2** the metal centres form a triangle showing Ru-Ru distances consistent with metal-metal bonds [spanning from 2.828(1) to 2.876(1) Å]. The anionic ligand $Ph_2PN{=}PPh_2C(S)NEt$ chelates the Ru3 atom through the phosphorus and sulfur atoms, giving

rise to a six-membered chelation ring. The phosphorus is approximatively *trans* to the Ru3-Ru2 bond, while the sulfur further coordinates to Ru1, thus bridging a triangle edge [Ru1-S1 and Ru3-S1 distances: 2.433(1) [2.417(2)] and 2.419(1) [2.409(1)] Å, respectively]. The C-S (S1A-C10A 1.793(5) [1.788(6)]) and C-N 8 N2A-C10A 1.252(5) [1.278(6)]) distances suggest for these bonds single and double characters, respectively. The P-N-P group is asymmetric, P-N distances confirming, for P1 and P2, oxidation states III and V respectively (P1A-N1A 1.620(4) [1.638(5)], P2A-N1A 1.581(4) [1.548(5)]). The Ru1-Ru3 bond is bridged by the hydride. Nine terminal CO ligands complete the coordination over the metal centres (two for Ru3, four for Ru2 and three for Ru1). An analogous ligand arrangement was observed for a similar 2-(diphenylphosphanyl)thiophenolate derivative.[16,17]

Cluster **2** derives formally from the reaction of $Ph_2PNPPh_2CSNHEt$, formed by HEtSNS *via* loss of a molecule of isothiocyanate (EtNCS), with $[Ru_3(CO)_{10}(MeCN)_2]$ (Scheme 3).

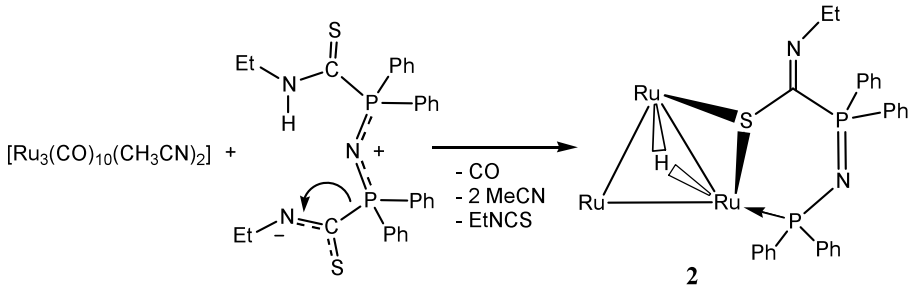

Scheme 3

The fragmentation could be facilitated by the metal centre, shifting the reaction to the right side, by forming the Ru-P bond. The PC(S)NHEt moiety could then react in its thiolic form [PC(SH)NEt] by oxidative addition of the SH group to the metal triangle with hydride transfer from the thiolic group to the cluster core, as observed in the case of thiols and thioureas.[18-20]

In the ^1H NMR spectrum, the hydride resonates at δ = -14.7 (d, $^2J_{P,H}$ = 9.0 Hz) ppm, as typically found for bridging hydrides. In the $^{31}P\{^1H\}$ NMR spectrum two singlets are present at δ = 10.42 (s) and 54.09 (s) ppm, assigned respectively to P2 and to the P1 atoms. Noteworthy, the $Ph_2PNPPh_2C(S)NHEt$ ligand is the non-isolable intermediate in the preparation reaction of HEtSNS between dppa and EtNCS.[6]

The thermal treatment at 50 °C of cluster **2** in closed vessel affords cluster **3** in a quantitative yield by elimination of EtNC, as observed by ^1H and $^{31}P\{^1H\}$ NMR spectroscopy.

4.3.2 Pyrolitic reaction between $Ru_3(CO)_{12}$ and HEtSNS.

When $[Ru_3(CO)_{12}]$ and HEtSNS were reacted at 70°C in toluene, several products, some of them present in trace amount, were detected. The isolated clusters are depicted in Scheme 4. The multi-component crude mixture results from the tendency of the ligand to fragment in various ways at high temperature.

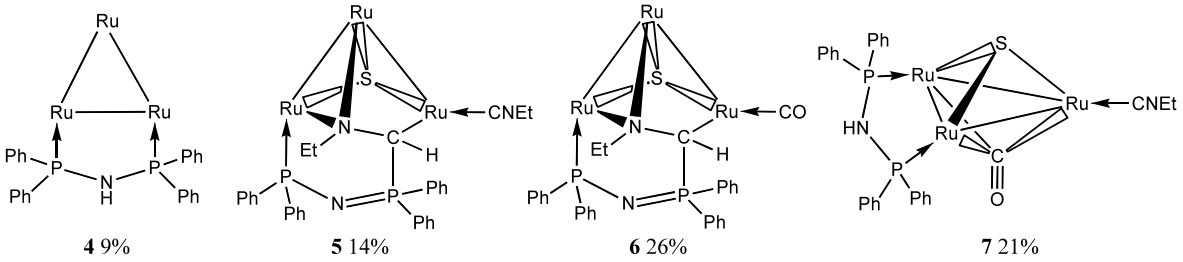

Scheme 4

The product corresponding to the first yellow TLC band (Rf = 0.81) was identified as $\{Ru_3(CO)_7(CNEt)(\mu_3\text{-}S)[(\mu_2\text{-}N{:}\eta^1\text{-}C{:}\kappa^1\text{-}P)Ph_2PN{=}PPh_2CHNEt]\}$ (**5**) by X-ray diffraction methods; an ORTEP view of its structure is shown in Figure 2.

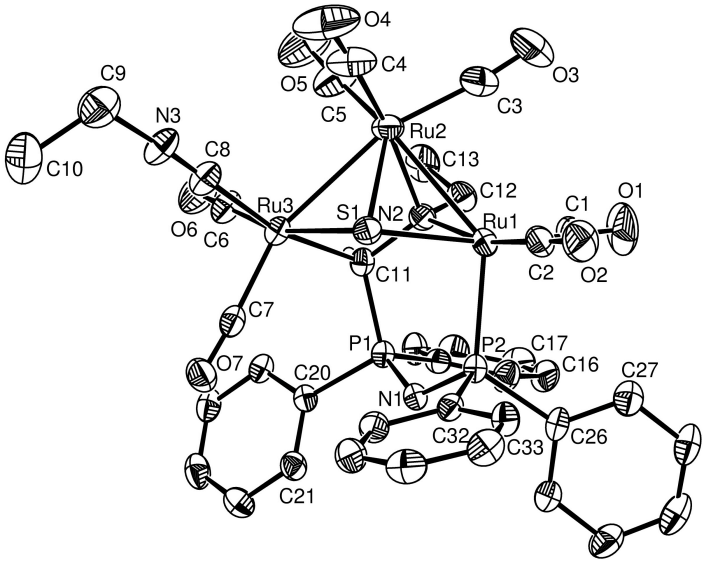

Figure 2. ORTEP plot of the structure of cluster **5**. Thermal ellipsoids are drawn at the 30% probability level. H atoms are omitted for clarity. Selected bond distance (Å) and angle (°): Ru1-N2 2.130(4), Ru1-P2 2.286(1), Ru1-S1 2.366(1), Ru1-Ru2 2.775(1), Ru2-N2 2.170(3), Ru2-S1 2.407(1), Ru2-Ru3 2.790(1) Ru3-C11 2.176(4), Ru3-S1 2.366(1), P1-N1 1.587(4), P2-N1 1.613(3); P2-Ru1-Ru2 135.07(4), Ru1-Ru2-Ru3 88.51(2), C11-Ru3-Ru2 72.5(1), S1-Ru3-Ru2 54.92(3), Ru1-S1-Ru3 110.30(5), Ru1-S1-Ru2 71.11(4), Ru3-S1-Ru2 71.52(4), P1-N1-P2 127.7(2), Ru1-N2-Ru2 80.4(1).

The structure of cluster **5** shows an open Ru_3 triangle with Ru1-Ru2 and Ru2-Ru3 distances of 2.775(1) and 2.789(1) Å respectively. The cluster is capped by a triple bridging sulphide and by the -N(Et)CH(R)- moiety of the $PPh_2NPPh_2C(H)NEt$ fragment. The carbon atom is η^1 bound to Ru3 [Ru3-C11 2.176(4) Å] while the nitrogen atom is bridging Ru1 and Ru2 [Ru1-N2 2.130(4), Ru2-N2 2.170(3) Å]. Ligand PPh_2NPPh_2CHNEt further coordinates to Ru1 atom through the tertiary P atom [Ru1-P2 2.286(1) Å], forming a six-membered chelation ring around Ru1 and adopting a chair conformation. The two P-N bond distances in the P-N-P moiety are similar being 1.587(4) (P1-N1) and 1.613(3) Å (P2-N1). The coordination around the ruthenium atoms of the cluster core is completed by seven terminal carbonyls and one ethyl isonitrile. To our knowledge the -N(Et)CH(R)- bridging moiety is unprecedented in coordination chemistry. Nevertheless, this coordination mode resembles that of an h^2-formimidoyl ligand (RN=CH) obtained through step by step coordination and fragmentation (sulfur transfer) of *p*-fluoro-phenylisothiocyanate on a tri-osmium hydrido-carbonyl cluster.[21] Another similar coordinating group is the triple bridging 1-(methylamino)-2,3-diphenylallyl fragment of a μ-N(Me)C(H)C(Ph)CPh ligand also found on a tri-osmium cluster.[22] In this case, however, the allyl PhC(Ph)CC(H) fragment is π-bonded to an Os atom.

In order to reach the 50 electrons required for an open triangular cluster, the -N(Et)CH(R)- group should donate four electrons to the metal centres, suggesting that the N atom participates to the electron count with three electrons, through one σ-bond and one coordination bond. Following the Mingos-Wade's rules,[23-29] cluster **5** is to be considered a *nido*-square pyramidal cluster with five apices: three RuL_3 fragments (two electrons), one sulfur (four electrons) and one -N(Et)CH(R)- group (four electrons) permit to attain seven skeletal electron pairs (s.e.p.'s).

The solution spectroscopic data (^1H and $^{31}P\{^1H\}$ NMR, FTIR) for **5** are consistent with the solid state structure. The $^{31}P\{^1H\}$ NMR spectrum shows two doublets at δ = 77.6 ($^2J_{P,P}$ = 37 Hz) and 35.5 ($^2J_{P,P}$ = 37 Hz) ppm, assigned, respectively, to P2 (directly coordinated to Ru atom) and P1. This was confirmed by 2D ^{31}P-^1H Hetcor NMR. Besides, in the FTIR spectrum (CH_2Cl_2) the coordinated isonitrile characteristic absorption is observed at 2186 cm^{-1}.

The cluster generating the second yellow TLC band (Rf = 0.75) has been recognized as $\{Ru_3(CO)_8)(\mu_3\text{-}S)[(\mu_2\text{-}N{:}\eta\text{-}C{:}\kappa\text{-}P)Ph_2PN{=}PPh_2CHNEt]\}$ (**6**). The coordination around the Ru_3 core is the same found in cluster **5**, CNEt being replaced by a CO molecule as confirmed by ^1H NMR, FTIR and positive ion ESI-MS experiments (Figure 3).

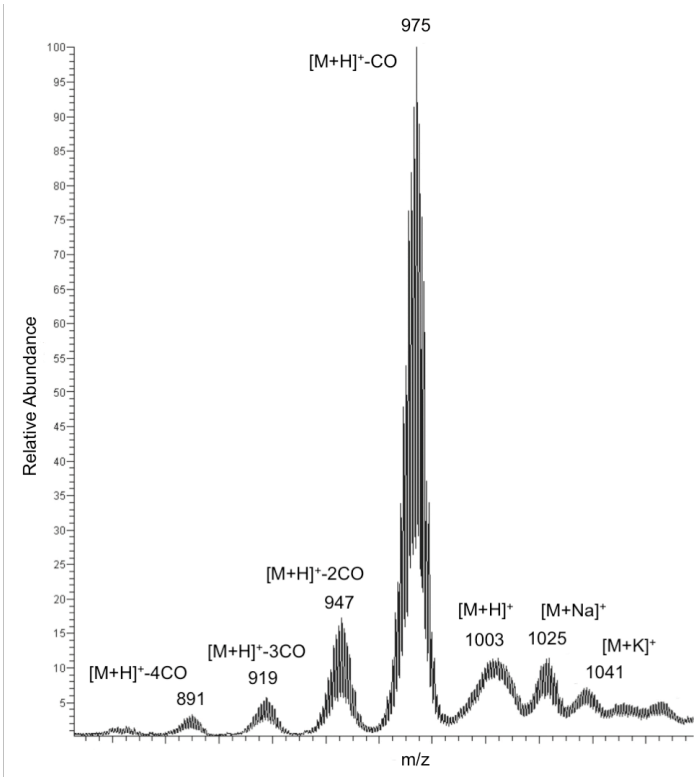

Figure 3. Positive ion ESI-MS of cluster **6** in CH_3OH.

The $^{31}P\{^1H\}$ NMR spectrum shows the relevant peak of the coordinated P2 at δ = 68.54 ppm upfield with respect to the same atom signal in cluster **5**. Negligible shift was observed for the P1 atom. The significant increase in chemical shift of the P2 atoms resonances, could be explained with a change in the coordination around the Ru1 atom. In fact, the P2 atom could be coordinated by the Ru1 in equatorial position. This behaviour was observed for the $[Ru_3(CO)_7(\mu_3\text{-}Se)_2[(\mu\text{-}\kappa^2P)dppf]$ (dppf = diphenylphosphine ferrocene),[30,31] where a shift of ~17 ppm was present between the P_{ax} and P_{eq}. The flexibility of the ligand can allow the coordination either in axial or equatorial position. Unfortunately, we were not able to produce single crystals of **6**.

Clusters **5** and **6** can be regarded to the products of sulfur migration from the thioamidic group on the cluster core, by the rupture of the C-S bond, as observed with various thioureas.[32]

From the same reaction, $\{Ru_3(CO)_6(\mu_3\text{-}CO)(\mu_3\text{-}S)(EtNC)[(\mu\text{-}\kappa^2P)Ph_2PNHPPh_2]\}$ (**7**) was also isolated and structurally characterized. An ORTEP view of its crystal structure is shown in Figure 4.

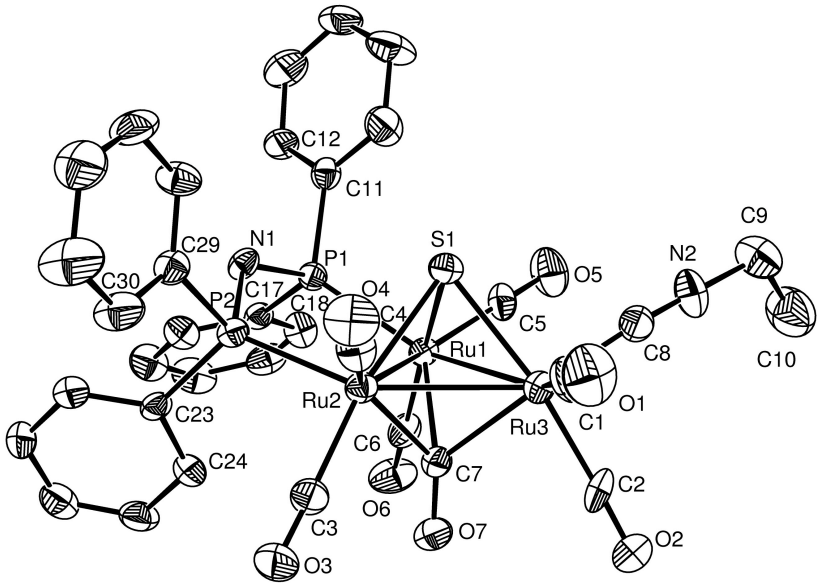

Figure 4. ORTEP plot of the structure of cluster **7** in **7**·CH_3OH. Thermal ellipsoids are drawn at the 30% probability level. H atoms and MeOH are omitted for clarity. Selected bond distance (Å) and angle (°): Ru1-C7 2.176(6), Ru1-P1 2.331(2), Ru1-S1 2.364(2), Ru1-Ru2 2.809(1), Ru1-Ru3 2.815(1), Ru2-C7 2.138(6), Ru2-P2 2.289(2), Ru2-S1 2.366(2), Ru2-Ru3 2.793(1), Ru3-C7 2.165(5), Ru3-S1 2.367(2), P1-N1 1.670(5), P2-N1 1.692(5); Ru2-Ru1-Ru3 59.55(3), C7-Ru2-Ru1 49.96(15), C7-Ru2-Ru3 49.95(14), C7-Ru3-Ru2 49.12(15), Ru3-Ru2-Ru1 60.33(4), Ru2-Ru3-Ru1 60.13(4), Ru1-S1-Ru2 72.87(5), Ru1-S1-Ru3 73.02(5), Ru2-S1-Ru3 72.33(5), N1-P1-Ru1 111.13(18), N1-P2-Ru2 114.43(19), P1-N1-P2 122.6(3).

The structure of cluster **7** contains a Ru_3S nido core (6 s.e.p's). The sulfide is bound in a μ_3 modality to the metal triangle with the sulfur atom lying at a distance of 1.724(1) Å from the Ru_3 plane. The dppa ligand coordinates through the tertiary P atoms to Ru1 and Ru2 metal [Ru1-P1 2.331(2) and Ru2-P2 2.289(2) Å]. The two P-N bond distances are similar [1.670(5) and 1.692(5) Å]. A triple-bridging carbonyl, seven terminal carbonyls and an isonitrile group complete the coordination around the ruthenium atoms of the cluster core. The isonitrile ligand is attached to the ruthenium atom not coordinated by the phosphorous. The short O7···O1S separation, 2.762(3) Å, suggests an hydrogen bond between the oxygen of μ_3-CO bridging molecule and the hydroxy group of methanol.

The spectroscopic data (FTIR, ^1H NMR, $^{31}P\{^1H\}$ NMR) for **7** agree with the solid state structure. The FTIR spectrum in solution (CH_2Cl_2) shows a characteristic absorption at 1652 cm^{-1}, attribuited to a μ_3-CO bridging molecule. The $^{31}P\{^1H\}$ NMR spectrum contains one singlet at δ = 82.1 ppm, indicating the magnetic equivalence of the phosphorus atoms. Sulfido clusters analogue to cluster **7** are well know and can easily be prepared upon reaction of phosphano sulfides with $[Ru_3(CO)_{12}]$.[32-37]

4.4 Conclusions

This chapter gave further insight into the chemistry of the zwitterionic ligand HEtSNS. In particular it enabled us to understand its fragmentation behaviour in the reaction with $[Ru_3(CO)_{12}]$. Under room temperature condition only fragmentation *via* loss of EtNC or EtNCS, without sulfur transfer to the cluster core is observed. On the other hand, under pyrolitic condition sulfur transfer on the cluster core occurs with unprecedented formation of the methideylamide -N(Et)CH(R)- μ_3-bridging ligating moiety.

4.5 References

[1] C. Graiff, G. Predieri, A. Tiripicchio, *Eur. J. Inorg. Chem.,* **2003**, *9*, 1659.

[2] D. Belletti, C. Graiff, C. Massera, A. Minarelli, G. Predieri, A. Tiripicchio, D. Acquotti, *Inorg. Chem.,* **2003**, *42*, 8509.

[3] D. Belletti, C. Graiff, R. Pattacini, G. Predieri, A. Tiripicchio, *Eur. J. Inorg. Chem.,* **2004**, *17*, 3564.

[4] D. Belletti, C. Graiff, R. Pattacini, G. Predieri, A. Tiripicchio, F. Fabrizi de Biani, P. Zanello, *Inorg. Chim. Acta*, **2005**, *358*, 161.

[5] D. Cauzzi, C. Graiff, C. Massera, G. Predieri, A. Tiripicchio, *Eur. J. Inorg. Chem.*, **2001**, *3*, 721.

[6] M. Asti, R. Cammi, D. Cauzzi, C. Graiff, R. Pattacini, G. Predieri, A. Stercoli, A. Tiripicchio, *Chem. Eur. J.*, **2005**, *11*, 3413.

[7] R. Pattacini, L. Barbieri, A. Stercoli, D. Cauzzi, C. Graiff, M. Lanfranchi, A. Tiripicchio, L. Elviri*, J. Am. Chem. Soc.,* **2006**, *128*, 866.

[8] M. Delferro, D. Cauzzi, R. Pattacini, M. Tegoni, C. Graiff, A. Tiripicchio, *Eur. J. Inorg. Chem.,* **2008**, *14*, 2302.

[9] P. Grenouillet, C. de Bellefon, *J. Organomet. Chem.,* **1996**, *513*, 5786.

[10] MestRe-C: J. C. Cobas Gomez, F. J. Sardina Lòpez, Mestrelab Research, Acoruna, Spain, **2004**.

[11] M. I. Bruce, D. Schultz, R. C. Wallis, A. D. Redhouse, *J. Organomet. Chem.,* **1979**, *169*, C15-C18.

[12] G. Sanchez-Cabrera, E. V. Garcia-Baez, M. J. Rosales-Hoz, *J. Organomet. Chem.,* **2000**, *599*, 313.

[13] SMART Software Users Guide, Version 5.1, Bruker Analytical X-ray Systems: Madison, WI, **1999**; SAINT Software Users Guide, Version 6.0, Bruker Analytical X-ray Systems: Madison, WI, **1999**; Sheldrick, G. M. SADABS, Bruker Analytical X-ray Systems, Madison, WI, **1999**.

[14] Sheldrick, G. M. SHELXL-97, Program for crystal structure refinement, University of Göttingen: Germany, **1997**.

[15] E. V. Garcia-Baez, M. J. Rosales-Hoz, H. Nöth, I. Haiduc, C. Silvestru, *Inorg. Chem. Comm.,* **2000**, *3*, 173.

[16] J. A. Cabeza, M. A. Martínez-García, V. Riera, D. Ardura, S. García-Granda, *Eur. J. Inorg. Chem.,* **2000**, *3*, 499.

[17] J. A. Cabeza, M. A. Martınez-Garcıa, V. Riera, S. Garcıa-Granda, J. F. Van der Maelen, *J. Organomet. Chem.*, **1996**, *514*, 197.

[18] G. R. Crooks, B. F. G. Johnson, J. Lewis, *J. Chem. Soc. (A)*, **1969**, *5*, 797.

[19] U. Bodensiek, H. Stoeckli-Evans, G. Suess-Fink, *Chem. Ber.*, **1990**, *123*, 1603.

[20] E. Boroni, G. Predieri, A. Tiripicchio, M. Tiripicchio-Camellini, *Organometallics*, **1992**, *11*, 3456.

[21] R. D. Adams, Z. Dawoodi, *J. Am. Chem. Soc.,* **1981**, *103*, 6510.

[22] R.D. Adams, G. Chen, *Organometallics*, **1992**, *11*, 837.

[23] K. Wade, *Chem. Commun.*, **1971**, 792.

[24] D. M. P. Mingos, *Nature Phys. Sci.,* **1972**, *236*, 99.

[25] K. J. Wade, *Adv. Inorg. Chem. Radiochem.,* **1976**, *18*, 1.

[26] J. W. Lauher, *J. Am. Chem. Soc.,* **1978***, 100*, 5305.

[27] M. A. Cavanaugh, T. P. Fehlner, R. Stramel, M. E. O'Neill, K. Wade, *Polyhedron*, **1985**, *4*, 687.

[28] E. D. Jemmis, M. M. Balakrishnarajan, P. D. Pancharatna*, J. Am. Chem. Soc.* **2001**, *123*, 4313.

[29] M. M. Balakrishnarajan, R. Hoffman, *J. Am. Chem. Soc.*, **2004**, *126*, 13119.

[30] D. Cauzzi, C. Graiff, C. Massera, G. Predieri, A. Tiripicchio, D. Acquotti, *J. Chem. Soc., Dalton Trans.*, **1999**, 3515.

[31] F. Fabrizi de Biani, C. Graiff, G. Opromolla, G. Predieri, A. Tiripicchio, P. Zanello, *J. Organomet. Chem.*, **2001**, *637-639*, 586.

[32] G. Suess-Fink, U. Bodensiek, L. Hoferkamp, G. Rheinwald, H. Stoeckli-Evans, *J. Cluster Science*, **1992**, *3*, 469.

[33] S. E. Kabir, S. J. Ahmed, M. I. Hyder, M. A. Miah, D. W. Bennett, D. A. Haworth, T. A. Siddiquee, E. Rosenberg, *J. Organomet. Chem.*, **2004**, *689*, 3412.

[34] R. D. Adams, G. Chen, J. T. Tanner, J. Yin, *Organometallics*, **1990**, *9,* 595.

[35] R. D. Adams, J. E. Babin, P. Mathur, K. Natarajan, J. G. Wang, *Inorg. Chem.*, **1989**, *28*, 1440.

[36] R. D. Adams, J. E. Babin, M. Tasi, T. A. Wolfe, *Organometallics*, **1987**, *6*, 2228.

[37] P. Fompeyrine, G. Lavigne, J. J. Bonnet, *J. Chem. Soc., Dalton Trans.*, **1987**, 91.

5

Synthesis, characterization and reactivity of zwitterionc metallates of Palladium (II)

The reaction of $Ph_2PNHPPh_2$ with EtNCS in 1:2 molar ratio leads to the formation of the zwitterionic ligand $EtNHC(S)PPh_2NPPh_2C(S)NEt$ (HEtSNS). This ligand is amphoteric, forming by protonation the cation H_2EtSNS^+ and, when deprotonated, dianion-cation $EtSNS^-$. All the three forms can coordinate to metal centres. Reaction of $[Pd(CH_3CN)_2Cl_2]$ with HEtSNS affords [Pd(HEtSNS)Cl]Cl (**1**). When a base is added, [Pd(EtSNS)Cl] **(3)** is obtained as an orange powder. The reaction of **2** with AgOTf in 1:1 molar ratio affords the trimeric complex $[Pd(EtSNS)]_3(OTf)_3$ (**5a**). When **3** reacts with three eq. of $K[Ag(CN)_2]$, a yellow powder of [Pd(EtSNS)(CN)] **(6)** is produced. The presence of a terminal cyano-group can afford the formation of a bridge with other metal. In fact, when **5b** reacts with **3** in CH_2Cl_2, in the presence of one eq. of $AgPF_6$, a dark orange powder of $[Pd(EtSNS)_2(\mu\text{-}CN)]PF_6$ (**5**) is obtained. Moreover, **6** reacts with $[Rh(cod)(CH_3CN)_2]OTf$ to give $[Rh(cod)(\mu\text{-}CN)_2(PdEtSNS)_2]OTf$ (**8**).

5.1 Introduction

Pincer complexes of transition metal have recentely attracted much attention in catalysis and material science.[1] In particular, N-heterocyclic carbenes (NHCs)[2] have been used in different field as homogeneous catalysis,[3] polymer and dendrimer chemistry[4] and sensing application.[5] These symmetrical pincer type structures are XCX, where X = N, P, S, O, but in last years the asymmetrical pincer complexes with mixed donor atoms or ring sizes have been studied.[6]

In this chapter are described on the synthesis, reactivity, spectroscopic and structural characterization of the novel pincer-type complexes of Pd(II) with the zwitterionic ligand HRSNS [RNHC(S)Ph_2P=NPPh_2C(S)NR, R = Et,[7] (*R*)-Ph(CH_3)CH].

5.2 Experimental

5.2.1 General procedures.

All manipulations were carried out at room temperature under nitrogen atmosphere by standard Schlenk techniques; *t*-BuOK, $PdCl_2$, K[Ag$(CN)_2$], $AgPF_6$, AgOTf (OTf = CF_3SO_3), (R)-[(C_6H_5)$CH_3$$CHNH_2$] and $CSCl_2$ were purchased from Aldrich and Fluka. The solvents was dried and distilled by standard techniques. dppa,[8] HEtSNS and H_2EtSNSCl,[7a,b,c] [Pd$(CH_3CN)_2Cl_2$],[9] [Pd(CH_3)Cl(cod)][10] (cod = 1,5-cyclooctadiene) and [Rh(cod)$(CH_3CN)_2$]OTf[11] and were prepared as described elsewhere. Elemental analyses were carried out on a Carlo Erba EA1108 microanalyzer. FTIR spectra (4000-400 cm^{-1}) were recorded on a Nicolet Nexus spectrophotometer equipped with a Smart Orbit HATR (diamond or ZnSe crystals). ^{1}H NMR (300.13 MHz, TMS) and ^{31}P{^{1}H} NMR (161.98 MHz, external reference 85%-H_3PO_4) spectra were recorder on Bruker instruments (AC300 Avance and AMX400, respectively) using deuterated solvents ($CDCl_3$, CD_2Cl_2, dmso-d_6 and MeOD-d_4).

*5.2.2 Preparation of (R)-[(C_6H_5)CH_3CHNCS] (**χNCS**)*

A mixture of thiophosgene (1.4 mL, 81.1 mmol) and CH_2Cl_2 (50 mL) were cooled to – 5°C after which a water solution of K_2CO_3 (50 mL, 0.33 M) was added. A solution of (R)-

[$(C_6H_5)CH_3CHNH_2$] (2.13 mL, 16.5 mmol) was added dropwise over a period of 15 min with vigorous stirring and maintaining of the temperature beween 0 and 5°C. After an additional 10 min a cold (0°C) 100 ml of water solution of KOH (50 mL, 0.1 M) was added in one portion with cooling below 0°C. The organic layer and three extracts (30 mL x 3) of ethyl ether were dried over $MgSO_4$. The solution was concentrated under reduced pressure and a yellow-orange oil of (R)-[$(C_6H_5)CH_3CHNCS$] was obtained (Yield 85%). E.A. % calcd. for: C_9H_9NS (*M* = 163.24): C 66.22; H 5.56; N 8.58. Found: C 66.10; H 5,51; N 8.53. ^{1}H NMR: ($CDCl_3$): δ = 7.33-7.15 (m, 5H, Ph); 4.90 (q, 1H, -*CH*-, $^3J_{H,H}$ = 6.9 Hz), 1.67 (d, 3H, -*CH*$_3$, $^3J_{H,H}$ = 6.9 Hz) ppm.

*5.2.3 Preparation of (R)-PhCH$_3$CHNHC(S)Ph$_2$P=NPPh$_2$C(S)N-(R)-CHCH$_3$Ph (**HχSNS**)*

A solution of $HN(PPh_2)_2$ (1.387 g, 3.86 mmol) in CH_2Cl_2 (15 mL) was added to a stirred solution of ***K*NCS** (1.021 g, 2.6 mmol) in CH_2Cl_2 (10 mL) and left at room temperature for 4 h under stirring. The volatile was removed and the resulting rubbery yellow products was re-crystallized in EtOH (5 mL, 96%) giving (*R*)-PhCH$_3$CHNHC(S)Ph$_2$P=NPPh$_2$C(S)N-(*R*)-CHCH$_3$Ph (**HχSNS**) as yellow crystals (Yield 92 %). E.A. % calcd. for: $C_{42}H_{39}N_3P_2S_2$ (*M* = 711.87): C 70.86; H 5.52; N 5.90; S 9.01. Found: C 70.53; H 5.45; N 5.82; S 8.96. ^{1}H NMR: ($CDCl_3$): δ = 13.0 (s, br, 1H, NH); 7.62-7.15 (m, 40H, Ph); 5.62 (qd, 2H, -*CH*-, $^3J_{H,H}$ = 6.9 Hz, $^4J_{H,P}$ = 2.4 Hz), 1.49 (d, 6H, -CH_2CH_3, $^3J_{H,H}$ = 6.9 Hz) ppm. $^{31}P\{^1H\}$ NMR ($CDCl_3$): δ = 7.29 (s) ppm.

*5.2.4 Preparation of [Pd(HEtSNS)Cl]Cl (**1**)*

Solid [$Pd(CH_3CN)_2Cl_2$] (0.100 g, 0.385 mmol) was dissolved in 10 mL of CH_2Cl_2. To this, solid HEtSNS (0.215 g, 0.385 mmol) was added and the reaction mixture stirred for 30 min. Evaporation of the solvent afforded complex [Pd(HEtSNS)Cl]Cl **(1)** as brown powder. The complex can be recristalized by layering hexane onto a CH_2Cl_2 solution, affording dark red crystals of **1**·$(CH_2Cl_2)_2$. E.A. % calcd. for: $C_{30}H_{31}Cl_2N_3PdP_2S_2$ (*M* = 736.99): C 48.89; H 4.24; N 5.70; S 9.62. Found: C 48.78; H 4.21; N 5.66; S 9.58. ^{1}H-NMR: (MeOD-d_4): δ = 7.84-7.57 (m, 20H, Ph); 3.80 (qd, 4H, -CH_2CH_3, $^3J_{H,H}$ = 3.0 Hz, $^4J_{H,P}$ = 7.5 Hz), 1.28 (t, 6H, -CH_2CH_3, $^3J_{H,H}$ = 7.50 Hz) ppm. $^{31}P\{^1H\}$ NMR (MeOD-d_4): δ = 43.5 (s) ppm.

*5.2.5 Preparation of [Pd(EtSNS)Cl] (**2**)*

Solid $[Pd(CH_3CN)_2Cl_2]$ (0.100 g, 0.385 mmol) was dissolved in 10 mL of CH_2Cl_2. To this, solid HEtSNS (0.215 g, 0.385 mmol) was added. A solution of *t*-BuOK (0.043 g, 0.385 mmol) in 2 mL of MeOH was then added and the reaction mixture stirred for 30 min. The volatiles were evaporated and the resulting dark yellow powder was redissolved in 5 mL of CH_2Cl_2. KCl was removed via filtration. Evaporation of the solvent afforded complex [Pd(EtSNS)Cl] **(2)** as orange powder. The complex can be recristalized by layering hexane onto a CH_2Cl_2 solution, affording orange crystals of **2**. E.A. % calcd. for: $C_{30}H_{30}ClN_3PdP_2S_2$ (*M* = 700.53): C 51.44; H 4.32; N 6.00; S 9.15. Found: C 51.35; H 4.29; N 5.96; S 9.11. ^{1}H NMR: ($CDCl_3$): δ = 7.64-7.38 (m, 20H, Ph), 3.67 (qd, 4H, -*CH*$_2$CH$_3$, $^3J_{H,H}$ = 7.50 Hz, $^4J_{H,P}$ = 3.00 Hz), 1.22 (t, 6H, -CH$_2$*CH*$_3$, $^3J_{H,H}$ = 7.50 Hz) ppm. ^{31}P{^{1}H} NMR ($CDCl_3$): δ = 25.8 (s) ppm.

*5.2.6 Preparation of [Pd(H*χ*SNS)Cl]Cl (**3**)*

Solid $[Pd(CH_3CN)_2Cl_2]$ (0.036 g, 0.14 mmol) was dissolved in 10 mL of CH_2Cl_2. To this, solid H*K*SNS (0.100 g, 0.14 mmol) was added and the reaction mixture stirred for 30 min. Evaporation of the solvent afforded complex [Pd(Hχ*K*SNS)Cl]Cl **(3)** as brown powder. E.A. % calcd. for: $C_{42}H_{39}Cl_2N_3PdP_2S_2$ (*M* = 889.19): C 56.73; H 4.42; N 4.72; S 7.21. Found: C 56.65; H 4.41; N 4.69; S 7.19. ^{1}H-NMR: (MeOD-d$_4$): δ = 8.05 (m, 10H, Ph$_{isothio}$), 7.75-7.06 (m, 40H, Ph), 5.36 (q, 2H, CH, $^3J_{H,H}$ = 4.8 Hz), 1.51 (d, 6H, CH$_3$, $^3J_{H,H}$ = 4.8 Hz) ppm. ^{31}P{^{1}H} NMR (MeOD-d$_4$): δ = 42.8 (s) ppm.

*5.2.7 Preparation of [Pd(*χ*SNS)Cl] (**4**)*

Solid $[Pd(CH_3CN)_2Cl_2]$ (0.036 g, 0.14 mmol) was dissolved in 10 mL of CH_2Cl_2. To this, solid HEtSNS (0.100 g, 0.14 mmol) was added. A solution of *t*-BuOK (0.016 g, 0.14 mmol) in 2 mL of MeOH was then added and the reaction mixture stirred for 30 min. The volatiles were evaporated and the resulting dark yellow powder was redissolved in 5 mL of CH_2Cl_2. KCl was removed via filtration. Evaporation of the solvent afforded complex [Pd(χSNS)Cl] **(4)** as orange powder. E.A. % calcd. for: $C_{42}H_{38}ClN_3PdP_2S_2$ (*M* = 852.74): C 59.16; H 4.49; N 4.93; S 7.52. Found: C 59.08; H 4.45; N 4.89; S 7.49. ^{1}H NMR: ($CDCl_3$): δ = 7.96 (m, 10H, Ph$_{isothio}$), 7.67-6.98 (m, 20H, Ph), 5.32 (q, 2H, CH, $^3J_{H,H}$ = 6.6 Hz), 1.32 (d, 6H, CH$_3$, $^3J_{H,H}$ = 6.6 Hz) ppm. ^{31}P{^{1}H} NMR ($CDCl_3$): δ = 28.4 (s) ppm.

*5.2.8 Preparation of [Pd(EtSNS)]$_3$(X)$_3$ [X = OTf (**5a**), PF$_6$ (**5b**)]*

Complex **2** (0.200 g, 0.285mmol) was dissolved in 10 mL of CH_2Cl_2. To this, AgX (X = OTf, PF_6, 0.285 mmol) was added and the reaction mixture stirred for 1 h. The volatile was evaporated and the resulting orange powder was redissolved in 5 mL of CH_2Cl_2. AgCl was removed via filtration. Evaporation of the solvent afforded complex $[Pd(EtSNS)]_3(OTf)_3$ (**5a**) as orange powder. Suitable crystals for the X-ray analysis for complexe **5a** were obtained by layering hexane onto dichloromethane solutions (Yield 91%). E.A. % calcd. for: $C_{93}H_{90}F_9N_9O_9P_6Pd_3S_9$ (**5a**, *M* = 2442.45): C 45.73; H 3.71; N 5.16; S 11.82. Found: C 45.68; H 3.69; N 5.15; S 11.78. ^{1}H NMR: (CD_2Cl_2): δ = 8.37-6.64 (m, 60H, Ph), 4.17-3.53 (4 multi., 12H, -*CH*$_2$CH$_3$), 1.24 (2 trip., 18H, -CH$_2$*CH*$_3$) ppm. ^{31}P{^{1}H} NMR ($CDCl_3$): δ = 37.5 [d, $^2J_{P,P}$ = 9.7 Hz], 35.4 [d, $^2J_{P,P}$ = 9.7 Hz] ppm.

*5.2.9 Preparation of [Pd(CN)(EtSNS)] (**6**)*

(a) Complex **5** (0.110 g, 0.045 mmol) was dissolved in 10 mL of CH_2Cl_2. To this, a solution of K[Ag(CN)$_2$] (0.027 g, 0.135 mmol) in 5 mL of methanol was added and the reaction mixture stirred for 1h. The volatiles were evaporated and the resulting yellow powder was redissolved in 5 mL of CH_2Cl_2. AgCN and KOTf were removed via filtration. Evaporation of the solvent afforded complex [PdEtSNS(CN)] (**6**) as lemon-yellow solid (Yield 88 %).

(b) Complex **2** (0.200 g, 0.285 mmol) was dissolved in 10 mL of CH_2Cl_2. To this, a solution of K[Ag(CN)$_2$] (0.057 g, 0.285 mmol) in 5 mL of methanol was added and the reaction mixture stirred for 1h. The volatiles were evaporated and the resulting yellow powder was redissolved in 5 mL of CH_2Cl_2. KCl and AgCN were removed via filtration. Evaporation of the solvent afforded complex [PdEtSNS(CN)] (**6**) as lemon-yellow solid. Suitable crystals for the X-ray analysis of complex **6** were obtained by layering hexane onto dichloromethane solution (Yield 93 %). E.A. % calcd. for: $C_{31}H_{30}N_4P_2PdS_2$ (*M* = 691.10): C 53.88; H 4.38; N 8.11; S 9.28. Found: C 53.80; H 4.35; N 8.05; S 9.24. ^{1}H NMR: ($CDCl_3$): δ = 7.58-7.33 (m, 20H, Ph); 3.74 (qd, 4H, -*CH*$_2$CH$_3$, $^3J_{H,H}$ = 7.15 Hz, $^4J_{H,P}$ = 4.2 Hz), 1.12 (t, 6H, -CH$_2$*CH*$_3$, $^3J_{H,H}$ = 7.15 Hz) ppm. ^{31}P{^{1}H} NMR ($CDCl_3$): δ = 24.4 (s) ppm. FTIR (ZnSe HATR, cm^{-1}): ν_{CN} = 2131.

*5.2.10 Preparation of [(PdEtSNS)$_2$(μ-CN)]X [X = OTf (**7a**), PF$_6$ (**7b**)]*

Complex **2** (0.152 g, 0.217 mmol) and **6** (0.150 g, 0.217 mmol) were dissolved in 15 mL of CH_2Cl_2. To this, a solution of AgX (X = OTf, PF_6, 0.217 mmol) in 5 mL of THF was added and the reaction mixture stirred for 4 h. The volatiles were evaporated and the resulting orange powder was redissolved in 5 mL of CH_2Cl_2. AgCl was removed via filtration. Evaporation of the solvent afforded complex [(PdEtSNS)$_2$(μ-CN)]PF_6 (**7b**) as dark-orange powder (Yield 95 %). Suitable dark-orange crystals for the X-ray analysis of complex **7b** were obtained by evaporation of a CH_2Cl_2/pentane solution. E.A. % calcd. for: $C_{61}H_{60}F_6N_7P_5Pd_2S_4$ (**7b**, *M* = 1501.14): C 48.81; H 4.03; N 6.53; S 8.54. Found: C 48.75; H 3.99; N 6.47; S 8.48. ^{1}H NMR: ($CDCl_3$): δ = 7.75-7.40 (m, 40H, Ph); 3.68 (qd, 8H, -*CH*$_2$CH$_3$, $^3J_{H,H}$ = 7.15 Hz, $^4J_{H,P}$ = 4.2 Hz), 1.24 (t, 12H, -CH$_2$*CH*$_3$, $^3J_{H,H}$ = 7.15 Hz) ppm. ^{31}P{^{1}H} NMR ($CDCl_3$): δ = 32.14 (s), 27.52 (s), -145 (sept, PF_6, $^1J_{F,P}$ = 704 Hz) ppm. FTIR (ZnSe ATR, cm^{-1}): νCN = 2326.

*5.2.11 Preparation of {[Rh(cod)][PdEtSNS(μ-CN)]$_2$}OTf (**8**)*

A solution of [Rh(cod)(CH_3CN)$_2$]OTf_3 (0.100 g, 0.226 mmol) in CH_3CN (10 mL) was added dropwise to a solution of complex **6** (0.312 g, 0.452 mmol) in CH_3CN (10 mL). The orange reaction mixture was stirred for 1 h. Evaporation of the volatile yielded compound {[Rh(cod)][PdEtSNS(μ-CN)]$_2$}OTf (**8**) as a purple powder (Yield 87%). E.A. % calcd. for: $C_{71}H_{72}F_3N_8O_3P_4Pd_2RhS_5$ (*M* = 1742.35): C 48.94; H 4.16; N 6.43; S 9.20. Found: C 48.89; H 4.12; N 6.39; S 9.16. ^{1}H NMR: (CD_2Cl_2): δ = 7.66-7.41 (m, 40H, Ph); 4.14 (br, 4H; -CH=CH-, cod), 3.72 (qd, 8H, -*CH*$_2$CH$_3$, $^3J_{H,H}$ = 7.2 Hz, $^4J_{H,P}$ = 3.9 Hz), 2.35 (br, 8H; -C*H*H-, cod), 1.79 (m, 8H; -CH*H*-, cod), 1.27 (t, 12H, -CH$_2$*CH*$_3$, $^3J_{H,H}$ = 6.6 Hz) ppm. ^{31}P{^{1}H} NMR (CD_2Cl_2): δ = 29.37 (s) ppm. FTIR (ZnSe HATR, cm^{-1}): 2165.

*5.2.12 Preparation of [Pd(CH$_3$)(EtSNS)] (**9**)*

To a solution of [PdCl(CH_3)(cod)] (0.100 g, 0.377 mmol) of CH_2Cl_2 (20 mL) was added HEtSNS (0.211 g, 0.377 mmol) in CH_2Cl_2 (10 mL) and *t*-BuOK (0.042 g, 0.377 mmol) in MeOH (2 mL). The red mixture was left for 3h. The solvents were evaporated and a reddish powder was obtained. This was redissolved in 20 ml of CH_2Cl_2. KCl was removed via filtration. Evaporation of the solvent afforded complex [Pd(CH_3)EtSNS] (**9**) as light orange powder. Suitable orange crystals for the X-ray analysis of complex **9** were obtained by

layering hexane onto dichloromethane solution (Yield 93%). E.A. % calcd. for: $C_{31}H_{33}N_3P_2PdS_2$ (*M* = 680,11): C, 54.75; H, 4.89; N, 6.18; S, 9.43. Found: C, 54.67; H, 4.85; N, 6.13; S, 8.14. ^{1}H-NMR: ($CDCl_3$): δ = 7.49-7.23 (m, 40H, Ph), 3.76 (qd, 4H, -CH_2-, $^3J_{H,H}$ = 7.25 Hz, $^4J_{H,P}$ = 2.2 Hz), 1.25 (t, , 6H, -CH_3, $^3J_{H,H}$ = 7.25 Hz), 0.54 (s, 3H, Pd-CH_3) ppm. ^{31}P{^{1}H} NMR ($CDCl_3$): δ = 14.1 (s) ppm.

5.2.13 Preparation of [Pd(COCH$_3$)(EtSNS)] (10)

Compuond **9** (g, mmol) was dissoled in THF (10 mL). CO was then bubbled through this solution for 15 minutes at 60 Atm. The solution was concentrated and *n*-penatne (20 mL) was added. Red powder of [Pd(COCH$_3$)(EtSNS)] (**10**) was obtained (Yield 92 %). Suitable red crystals for the X-ray analysis of complex **10** were achieved by layering *n*-pentane onto dichloromethane solution. E.A. % calcd. for: $C_{32}H_{33}N_3OP_2PdS_2$ (*M* = 707.06): C, 54.28; H, 4.70; N, 5.93; S, 9.06. Found: C, 54.12; H, 4.67; N, 5.89; S, 9.00. ^{1}H NMR: ($CDCl_3$): δ = 7.64-7.23 (m, 40H, Ph), 3.74 (qd, , 4H, -*CH_2*CH_3, $^3J_{H,H}$ = 6.88 Hz), 2.36 (s, 3H, Pd-$COCH_3$), 1.20 (t, 6H, -CH_2*CH_3*, $^3J_{H,H}$ = 6.88 Hz) ppm. ^{31}P{^{1}H} NMR ($CDCl_3$): δ = 12.98 (s) ppm. FTIR (ZnSe ATR, cm^{-1}): ν$COCH_3$ = 1689.

*5.2.14 X-Ray data collection, structure solution and refinement of **1**·(CH_2Cl_2)$_2$, **2**, **5b**, **6**, **7b**, **9** and **10***

The intensity data of all compounds were collected at room temperature with a Bruker AXS Smart 1000[12] single crystal diffractometer equipped with an area detector, using a graphite monochromated Mo-K$_\alpha$ radiation (λ = 0.71073 Å). Crystallographic and experimental details of the structures are summarized in Table 1. The structures were solved by direct methods and refined by full-matrix least-squares procedures (based on F_o^2)[13] first with isotropic thermal parameters and then with anisotropic thermal parameters in the last cycles of refinement for all the non-hydrogen atoms. The hydrogen atoms were introduced into the geometrically calculated positions and refined riding on the corresponding parent atoms, except for the amidic hydrogen atoms in **1** which was localized in the 2Fo-Fc map and refined isotropically.

Table 1 Crystal Data and Structure Refinement for **1**·$(CH_2Cl_2)_2$, **2**, **5b**, **6**, **7b**, **9** and **10**

	1·$(CH_2Cl_2)_2$	**2**	**5b**	**6**
formula	$C_{32}H_{35}Cl_6N_3PdP_2S_2$	$C_{30}H_{30}ClN_3PdP_2S_2$	$C_{90}H_{90}F_{18}N_9P_9Pd_3S_6$	$C_{31}H_{30}N_4P_2PdS_2$
FW	906.86	700.53	2430	691.10
crystal system	monoclinic	monoclinic	rhombohedral	monoclinic
space group	$P2_1/a$	$C2/c$	$R\bar{3}$	$C2/c$
a, Å	13.850(3)	13.66(1)	29.008(5)	13.529(3)
b, Å	16.840(5)	14.94(2)	29.008(5)	15.209(5)
c, Å	16.481(5)	15.80(2)	10.732(3)	15.582(5)
a, deg	-	-	-	
β, deg	99.54(5)	106.26(7)	-	105.38(5)
γ, deg	-	-	120.00(6)	
V, Å^3	3791(2)	3096(2)	7821(3)	3091(2)
Z	2	4	3	4
D_{calcd}, g cm^{-3}	1.512	1.503	1.548	1.485
F(000)	1742	1424	3672	1408
crystal size (mm^3)	0.09 x 0.10 x 0.12	0.07 x 0.08 x 0.12	0.09 x 0.09 x 0.10	0.07 x 0.08 x 0.11
μ mm^{-1}	1.063	0.949	0.850	0.867
rflns collected	22594	2714	19240	18435
rflns unique	9449 (R_{int} = 0.0597)	2714 (R_{int} = 0.0568)	10016 (R_{int} = 0.0672)	3906 (R_{int} = 0.0804)
rflns observed	4235	1966	8788	2722
parameters	428	196	415	201
R indices [I>2σ(I)]	R1 = 0.0483; wR2 = 0.0987	R1 = 0.0509; wR2 = 0.1623	R1 = 0.0320; wR2 = 0.0656	R1 = 0.0326; wR2 = 0.0741
R indices (all data)	R1 = 0.1069; wR2 = 0.1095	R1 = 0.0788; wR2 = 0.1930	R1 = 0.0383; wR2 = 0.0672	R1 = 0.0554; wR2 = 0.0804

	7b	**9**	**10**
formula	$C_{61}H_{60}F_6N_7Pd_2P_5S_4$	$C_{31}H_{33}N_3PdP_2S_2$	$C_{32}H_{33}ON_3PdP_2S_2$
FW	1501.1	680.1	708.1
crystal system	monoclinic	monoclinic	triclinic
space group	$P2_1/m$	$C2/c$	$P\bar{1}$
a, Å	8.609(6)	13.609(2)	10.034(1)
b, Å	38.955(3)	15.038(3)	15.038(1)
c, Å	11.256(8)	15.983(3)	15.983(2)
a, deg	-	-	96.15(2)
β, deg	106.66(2)	106.93(3)	99.13(2)
g, deg	-	-	98.43(2)
V, Å^3	3616(5)	3129(2)	1650(3)
Z	2	4	2
D_{calcd}, g cm^{-3}	1.378	1.444	1.425
F(000)	1520	1392	724
crystal size (mm^3)	0.07 x 0.08 x 0.12	0.07 x 0.08 x 0.10	0.09 x 0.10 x 0.12
μ mm^{-1}	0.779	0.854	0.815
rflns collected	36422	16431	18686
rflns unique	8486 (R_{int} = 0.1136)	4347 (R_{int} = 0.1179)	7336 (R_{int} = 0.1698)
rflns observed [I>2σ(I)]	4700	3558	4688
parameters	400	180	379
R indices [I>2σ(I)]	R1 = 0.0483; wR2 = 0.1013	R1 = 0.0385; wR2 = 0.1080	R1 = 0.0577; wR2 = 0.1585
R indices (all data)	R1 = 0.0987; wR2 = 0.1136	R1 = 0.0498; wR2 = 0.1179	R1 = 0.0904; wR2 = 0.1698

5.3 Results and discussion

The chiral isotiocianate was obtained by reaction of the parent amine with $CSCl_2$ in presence of a base (Scheme 1).

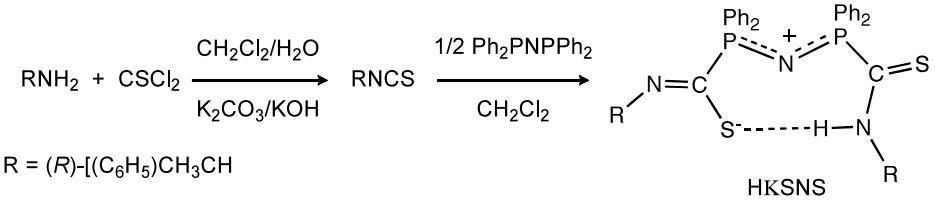

Scheme 1

The chiral isotionaciante was reacted with Ph_2PNPPh_2 in CH_2Cl_2 solution in a 2.1 : 1 ratio. Yellow crystals of (*R*)-$PhCH_3CHNHC(S)Ph_2P{=}NPPh_2C(S)N$-(*R*)-$CHCH_3Ph$ (**HχSNS**) were obtained.

5.3.1 Synthesis and characterization of chloro complexes.

The $[Pd(CH_3CN)_2Cl_2]$ precursor was reacted with HRSNS (R = Et, (*R*)-$[(C_6H_5)CH_3CH]$, Scheme 2) in CH_2Cl_2, affording chloro-palladium complex [Pd(HRSNS)Cl]Cl (R = Et, **1**; R = (*R*)-$[(C_6H_5)CH_3CH]$, **2**) (or ([Pd(RSNS)Cl] · HCl) as dark red solids.

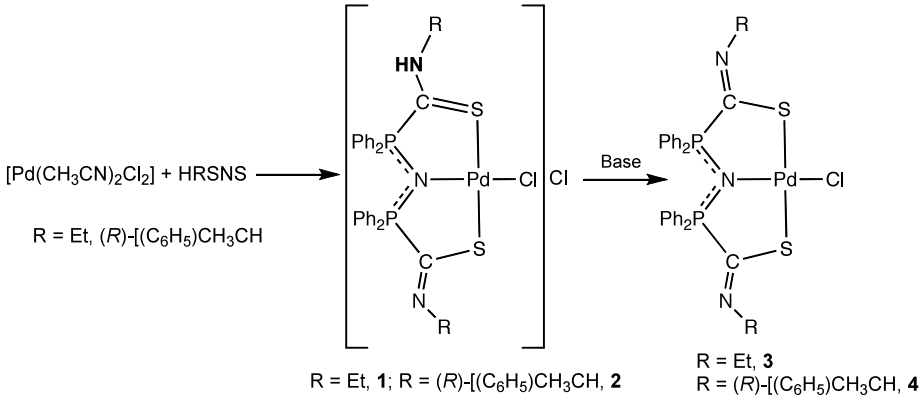

Scheme 2

The $^{31}P\{^1H\}$ NMR spectrum (MeOD-d_4, 25 °C) of **1** exhibit a singlet at 43.5 ppm; instead in $CDCl_3$ solution at the same temperature, a broad band was observed (*ca*. 33 ppm), probably due to the lowest rate exchange of the counter anion in this solvent. This behaviour was also

observed in the zwitterionic complexes of Rh(I) with the same ligand with different counter anion (PF_6, OTf, NO_3, TFA).[14]

Red single crystals of **1** · 2 (CH_2Cl_2) were obtained by layering hexane on a CH_2Cl_2 solution. View of the crystal structure of **1** in **1** · 2 (CH_2Cl_2) is reported in Figure 1.

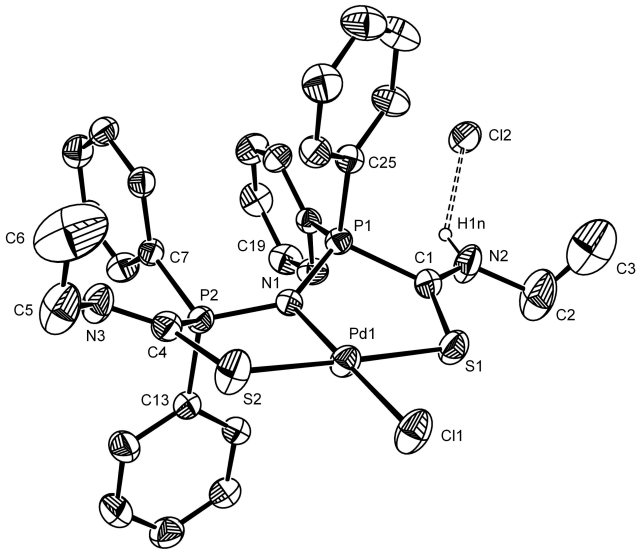

Figure 1. ORTEP plot of the molecular structure of **1** in **1** · 2(CH_2Cl_2). Thermal ellipsoid are drawn at 30% probability level. H atoms and CH_2Cl_2 molecules are omitted for clarity, except for the H1n. Selected distances [Å] and angles [°]: P1-N1 1.61(2), P2-N1 1.64(2), P1-C1 1.83(3), P2-C4 1.82(3), C1-S1 1.68(3), C4-S2 1.74(3), C1-N2 1.29(4), C4-N3 1.26(3), S1-Pd1 2.303(9), S2-Pd1 2.288(9), Cl1-Pd1 2.294(8), N1-Pd1 2.08(2), P1-N1-P2 133.1(14), P1-N1-Pd1 113.3(11), P2-N1-Pd1 112.1(11), N1-Pd1-S2 91.9(6), N1-Pd1-Cl1 179.6(7), S2-Pd1-Cl1 88.4(3), N1-Pd1-S1 88.9(6), S2-Pd1-S1 177.4(4), Cl1-Pd1-S1 90.8(3).

In the solid state structure, the ligand coordinates in a *S,N,S*-κ^3 modality to the Pd atom, which is found in a slightly distorted square-planar environment. The coordination around the metal center is completed by a chlorine atom (Cl1). An N2H1n···Cl2 intraction is present, in order to neutralize the remaining positive charge of the HEtSNS ligand. Distances P1-N1 and P2-N2 have approximately equal values, as should be expected for a delocalized P-N-P system and therefore that the positive charge is distributed on the two P atoms. The P1-C1 and P2-C4 bonds are of similar lengths, while variations can be evidenced in the C-S and C-N distances. The proton on the thioamidyl group causes the lengthening of the C1-N2 bond; in turn, the C1-S1 distance decreases, resulting in an improved double bond character. Similar behaviour was observed for Pd complexes of thioamidic *S,N,S* pincer ligands.[15]

When **1** and **2** were reacted with a base (*t*-BuOK, NEt_3) an orange powder of [Pd(EtSNS)Cl] (**3**) or [Pd(KSNS)Cl] (**4**) were obtained, respectively (Scheme 2). As evidenced *in situ* by

$^{31}P\{^{1}H\}$ NMR spectroscopy, when *t*-BuOK was added to a solution of **1**, it was quickly and completely consumed in few minutes, and it was accompanied by formation of **3** (singlet at 25.8 ppm). This fast reactivity is in agreement with the proposed structure of **1** whose formula can be written as [Pd(EtSNS)Cl] · HCl. View of molecular structure of **3**, obtained by single crystal X-ray diffraction, is reported in Figure 2.

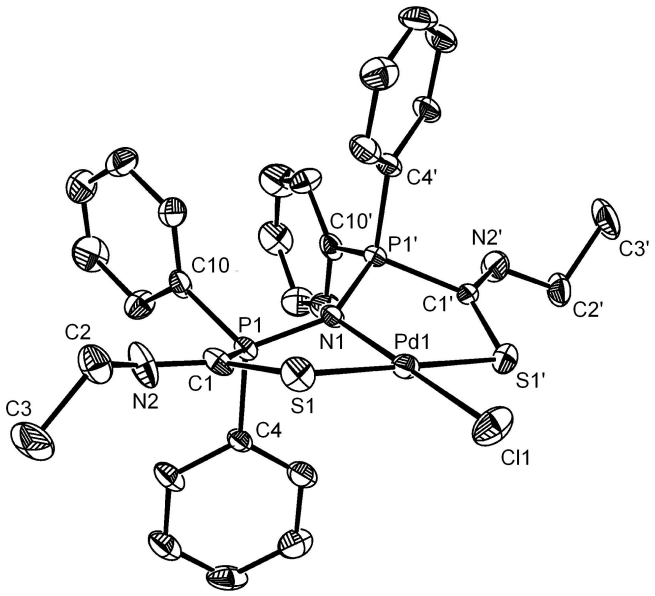

Figure 2. ORTEP plot of the molecular structure of **3**. Thermal ellipsoid are drawn at 30% probability level. H atoms are omitted for clarity. Selected distances [Å] and angles [°]: P1-N1 1.619(3), P1-C1 1.823(6), C1-S1 1.739(7), C1-N2 1.263(9), S1-Pd1 2.323(3), Cl1-Pd1 2.296(4), N1-Pd1 2.078(8), P1-N1-P1' 134.0(5), P1-N1-Pd1 113.0(2), N1-Pd1-Cl1 180.000(1), N1-Pd1-S1 89.76(5), S2-Pd1-S1 179.52(9), Cl1-Pd1-S1 90.24(5). (symmetry transformation used to generate equivalent atoms:' = x + 1, y, z + 1/2).

In the solid state**,** the coordination geometry of **3**, is almost identical to that of **1**. The complex has a crystallographically imposed C_2 simmetry. Molecules all oriented in the same direction are disposed in layers in a head-to-tail fashion. Adjacent layers contain molecules with opposite orientations. The shortest intermolecular Pd···Pd separation, between two molecules with different orientations in two adjacent layers in the same column, is 8.883 Å. The shortest Pd···Pd separation between two equally oriented molecules in the same layer is 11.804 Å, as found in [Rh(CO)EtSNS].[7a] Deprotonation of the thioamidic group causes the decrease of C1-N1 bond, resulting in a double bond, in turn the C1-S1 increase, becoming a single bond.

5.3.2 Synthesis and characterization of trinuclear complexes.

The reaction of **3** with a stoichiometric amount of AgX (X = OTf, PF_6) in CH_2Cl_2 solution results in the quantitative formation of $[Pd(EtSNS)]_3(X)_3$ (X = OTf, **5a**; X = PF_6, **5b**). A view of the molecular structure of **5b** is depicted in Figure 3.

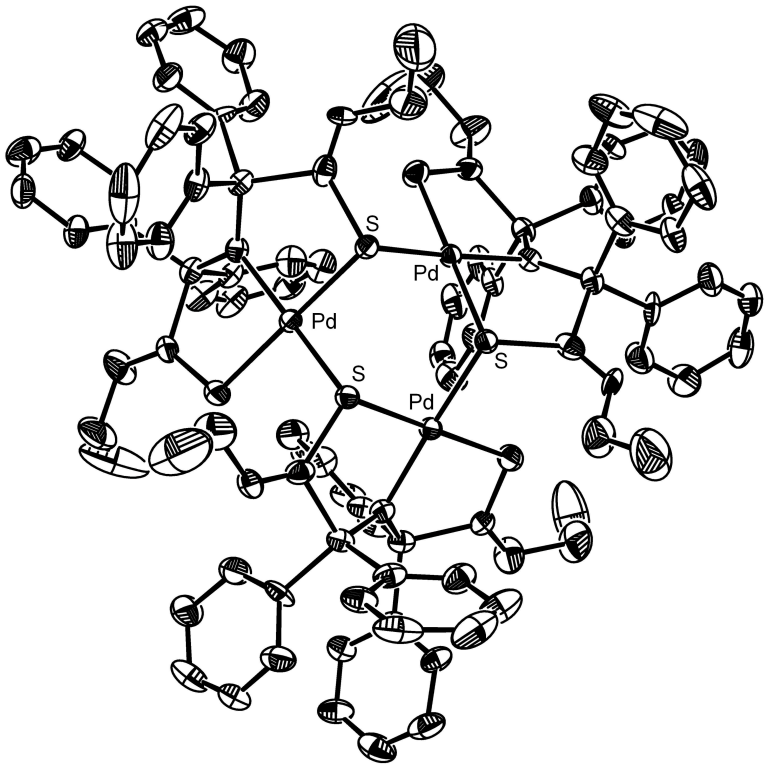

Figure 3. ORTEP plot of the molecular structure of **5b**. Thermal ellipsoid are drawn at 30% probability level. H atoms and PF_6 are omitted for clarity. Selected distances [Å] and angles [°]: C1-N1 1.255(4), C1-S1 1.756(3), C2-N2 1.242(4), C2-S2 1.808(3), N3-P2 1.637(2), N3-P1 1.591(2), N3-Pd1 2.092(2), Pd1-S1 2.291(1), Pd1-S2' 2.299(1), Pd1-S2 2.340(1); P2-N3-P1 130.10(14), N3-Pd1-S1 90.27(7), N3-Pd1-S2' 173.63(6), S1-Pd1-S2' 92.06(2), N3-Pd1-S2 90.46(6), S1-Pd1-S2 179.11(3), S2-Pd1-S2' 87.16(3), Pd1-S2-Pd1' 106.60(3).

The tri-anionic Pd(II) trimer consists of a Pd_3S_3 core in a chair configuration. This type of core has been reported previously for group 10 (Ni, Pd, Pt) complexes.[16] The trimer has a crystallographic threefold symmetry. The Pd(II) atom is coordinated by three S atoms and one N atom in a approximately square planar arrangement. Two of these three S atoms and N atoms belong to the same zwitterionic ligand and the other S atom comes from to adjacent complex, forming a six member-ring of alternating Pd-S atoms. The bridging S atoms is bonded to two Pd(II) atoms and one C atoms located at the apex of a pyramidal structure. The torsion angle of S1-Pd1-S2'-C4' are within 12.65°. The dihedral angles between monocomplex planes (S1-Pd1-N1-S2-S2') in the trimeric unit is 68.89(3)°. The distance between the Pd(II) centres is 3.721(6) Å forming a equilater triangle. This distance indicates that there is not bonding between the metals [the maximum reported value for weak

interaction in Pd(II)-Pd(II) is 3.539(1) Å]. The angles involving bridging sulfur atoms are for Pd1-S2'-Pd1' 106.60(3) Å and for S2-Pd1-S2' 87.16(3) Å. The formation of a trimer changes considerably the distances with respect to **2**. The Pd1-S1 and S1-C1 bond distances decrease, 2.291(1) and 1.756(3), respectively. The P1-N3 and P2-N3 bonds are 1.591(2) and 1.637(2) respectively. In $^{31}P\{^{1}H\}$ NMR spectrum two doublets are presente [δ =37.5 (d, $^{2}J_{P,P}$ = 9.7 Hz) and 35.4 (d, $^{2}J_{P,P}$ = 9.7 Hz) ppm]. The resonance at low fields is attribuited at the quaternarium phosphorous (P2). The Pd1-S2 bond lenghts are almost equal to **3** while a variations is presente in C2-S2 distances. This is due to the formation of bridge between two palladium atoms. Interesting, it is the higher decrease of C1-N1 bond distance [1.255(4)], strengthening the the character of double bond (CSD, December 2008, mean = 1.271 Å). The angle of the P-N-P system decrease [130.10(14)] with a lengthening of the Pd1-N3 bond.

The ESI-MS analysis confirms the formation of the Pd_3S_3 cluster also in methanol solution, indicating the stability of the trinuclear molecule.

5.3.3 Synthesis and characterization of cyano complexes

When **5** was reacted with 3 equivalents of $K[Ag(CN)_2]$, a lemon yellow microcrystalline product of [Pd(CN)(EtSNS)] (**6**) was achieved. The same product was obtained reacting **3** with 1 equivalent of $K[Ag(CN)_2]$. A view of its molecular structure is depicted in Figure 4.

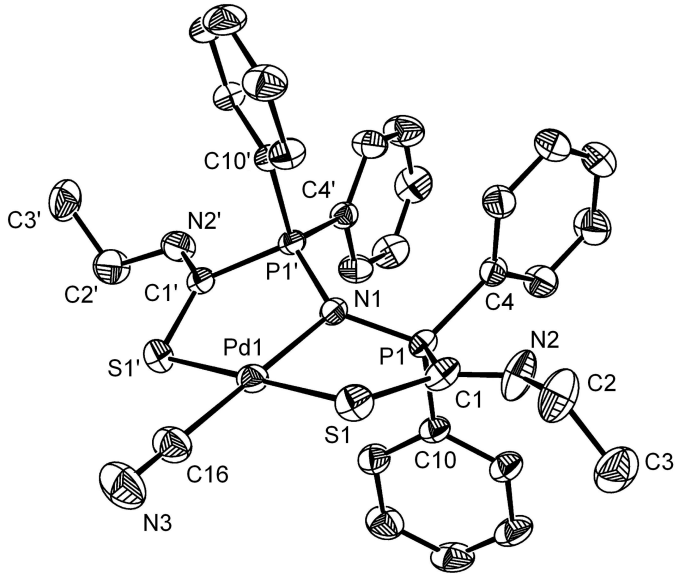

Figure 4. ORTEP plot of the molecular structure of **6**. Thermal ellipsoid are drawn at 30% probability level. H atoms are omitted for clarity. Selected distances [Å] and angles [°]: P1-N1 1.6113(11), P1-C1 1.818(2), C1-S1 1.742(2), C1-N2 1.251(3), S1-Pd1 2.3101(11), N1-Pd1 2.093(2), C16-Pd1 1.944(4), C16-N3 1.143(5), P1-N1-P1' 134.70(16), P1-N1-Pd1 112.65(8), N1-Pd1-S1 90.001(15), N1-Pd1-C16 180.0(1), Pd1-C16-N3 180.0(1),S1-Pd1-C16 89.999(15), S1-Pd1-S1' 180,00(3) (symmetry transformation used to generate equivalent atoms:'= x + 1, y, z + 1/2).

Complex **6** is isostructural to **3** and displays analogous geometrical parameters. The bond distances Pd1-C16 [1.944(4)] and C16-N3 [1.143(5)] are in agreement with those found in CSD. In the FTIR spectrum, a characteristic absorbtion at 2130 cm^{-1} was visible and it was ascribed to the CN group, coordinated to the metal centre.

The present of a terminal cyano group can afford the formation of bridge with other metal. In fact, when **6** was reacted with **3** in dichloromethane solution, in the presence of 1 equivalent of $AgPF_6$, a dark orange powder of $[Pd(EtSNS)_2(\mu\text{-}CN)]PF_6$ (**7a**) was obtained (Scheme 3).

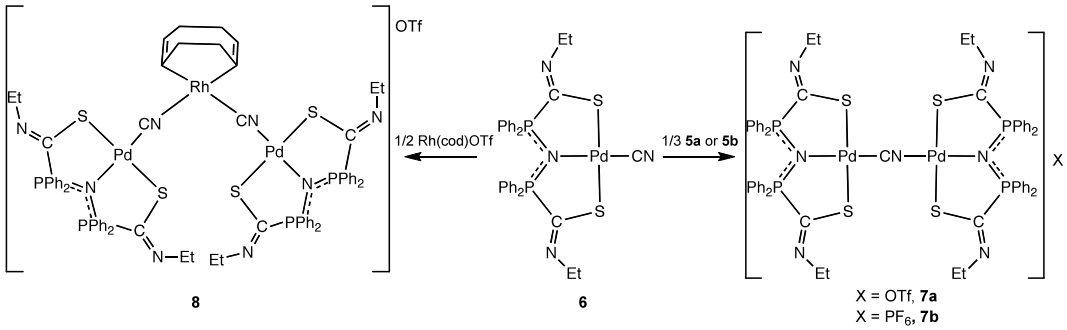

Scheme 3

View of the crystal structure of **5** is reported in Figure 5.

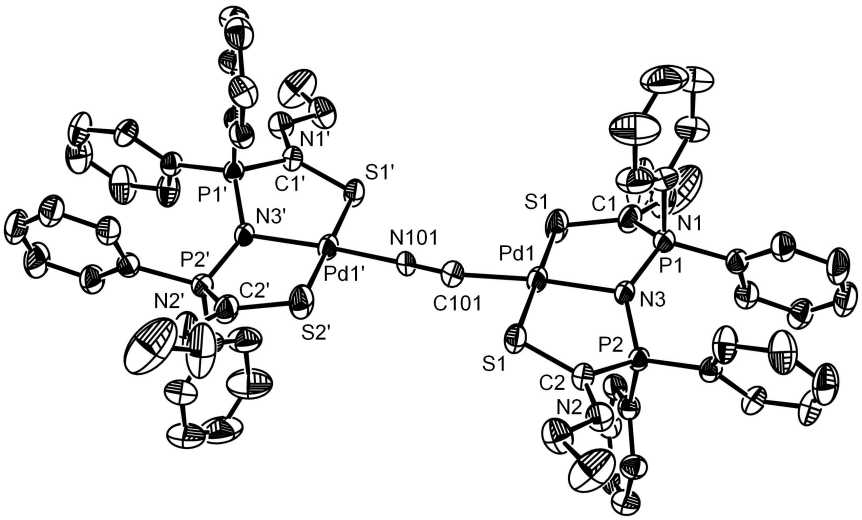

Figure 5. ORTEP plot of the molecular structure of **7a**. Thermal ellipsoid are drawn at 30% probability level. H atoms and PF_6 are omitted for clarity. Selected distances [Å] and angles [°]: C1-N1 1.252(5), C1-S1 1.739(4), C2-N2 1.263(4), C2-S2 1.747(3), N3-P1 1.616(3), N3-P2 1.623(2), N3-Pd1 2.056(2), Pd1'-N101 1.96(2), Pd1-C101 1.97(3), Pd1-S1 2.309(1), Pd1-S2 2.317(1) C101-N101 1.147(3); P1-N3-P2 133.44(15), N101-Pd1'-N3' 174.2(3), C101-Pd1-N3 172.9(4), N101-Pd1'-S1' 83.5(3), N101-Pd1'-S2' 96.0(3), C101-Pd1-S2 83.1(4), N3-Pd1-S2 89.77(7), Pd1-C101-N101 166.7(2), Pd1'-N101-C101 179.3(3) (symmetry transformation used to generate equivalent atoms:'= x + 1, y, z + 1/2).

In the solid state, two unit of [Pd(EtSNS)] are held together by a CN bridge. The coordination around the Pd(II) atoms is the same found in **6** and displays anologues geometrical parameters. The distance C101-N101 [1.147(3)] is in line with the reported for similar complexes. In the structure a disorder is present in the CN group, and is not possible clarify which atom is coordinate to the metal centre. Note that the Pd1-C101-N101 [166.7(2)] are not co-linear, but a slight deviation are present [166.7(2)], probably due to the steric hindrance of the two units. The coordination planes (Pd1-S1-S2-N3-N101 and Pd1'-S1'-S2'-N3'-C101) of the two unit lie in the same plane and no torsions are present.

In order to obtain novel cyano bridge with different metals, the reaction of **6** with a cationic Rh(I) precursor affords the quantitatively formation of {[Rh(cod)][PdEtSNS(μ-CN)]$_2$}OTf (**8**) (Scheme 3). Any attempt to obatin single crystals failed. In the FTIR spectrum a not negligible shift of the CN stretching frequency was observed and indicating the formtion of **8** (2130 cm^{-1} for **6**, 2165 cm^{-1} for **8**). The $^{31}P\{^{1}H\}$ NMR spectrum of the reacting solution shown the decady of the intensity of the chemical shift of **6** at 24.7 pppm accompanied by the formation of a new peak at 29.4 ppm assigned to the eteronuclear compound **8**.

5.3.4 Synthesis and characterization of methyl and acetyl complexes

The reaction of HEtSNS with [Pd(CH$_3$)Cl(cod)] in the presence of 1 equivalent of *t*-BuOK in dichloromethane solution afforded compound [Pd(CH$_3$)(EtSNS)] (**9**) as reddish powder in good yield (Scheme 4).

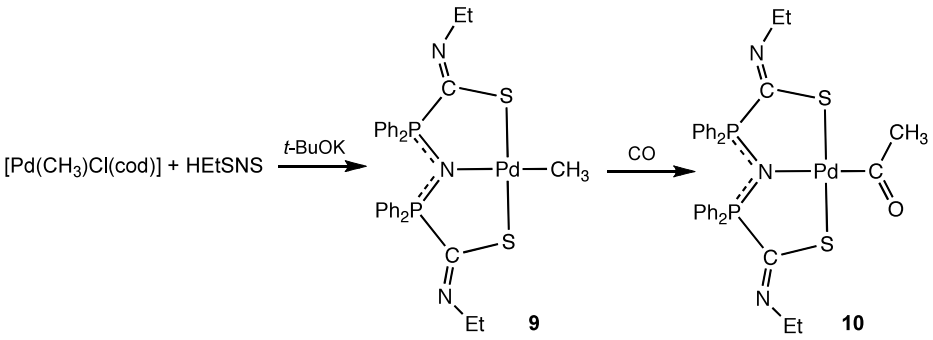

Scheme 4

In ^{1}H NMR spectrum a characteristic signal at 0.54 ppm of methyl palladium is presented. The molecular structure of **9** was confirmed by single-crystal X-ray structure anaysis. A view of its molecular structure is depicted in Figure 6.

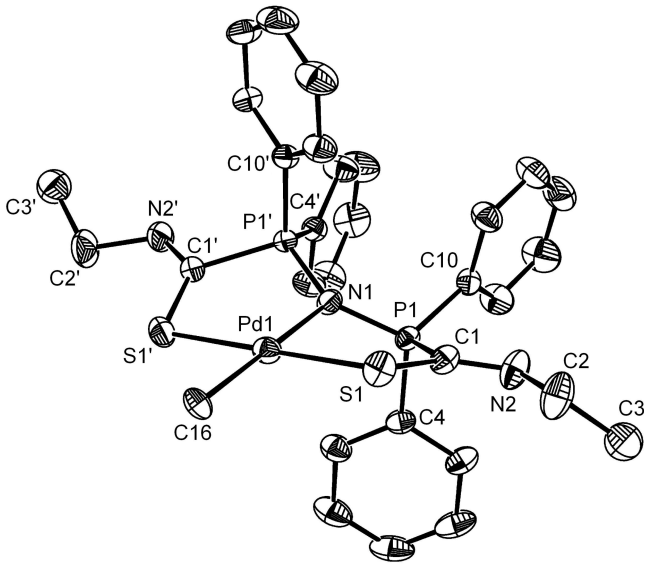

Figure 6. ORTEP plot of the molecular structure of **9**. Thermal ellipsoid are drawn at 30% probability level. H atoms are omitted for clarity. Selected distances [Å] and angles [°]: P1-N1 1.6039(13), P1-C1 1.825(3), C1-S1 1.731(3), C1-N2 1.266(4), S1-Pd1 2.3107(9), C16-Pd1 2.178(3), N1-Pd1 2.140(3), P1-N1-P1' 136.4(2), P1-N1-Pd1 111.8(1), N1-Pd1-S1 89.572(19), N1-Pd1-C16 180.0(1), S1-Pd1-C16 90.428(19), S1-Pd1-S1' 179.14(4) (symmetry transformation used to generate equivalent atoms:'= x+1, y, z+1/2).

In the solid state of **9,** the palladium atom adopts a square-planar geometry. Ligand coordinated by means of *S,N,S* atoms as in the other complexes descripted before and methyl group completed the coordination around the palladium atom. In addition, complex **9** has a crystallographically imposed C_2 simmetry, that implies the magnetic equivalence of phosphorus atoms, as confirmed by the presence in $^{31}P\{^1H\}$ NMR spectrum of a singlet at 14.1 ppm.

On bubbling CO for a few minutes at 60 Atm throught THF solution of complex **9** no palladium black was formed and [Pd($COCH_3$)(EtSNS)] (**10**) was obtained as red powder after precipitation with *n*-pentane (Scheme 4). Red crystals of **9** were achieved. Its structure is depicted in Figura 7.

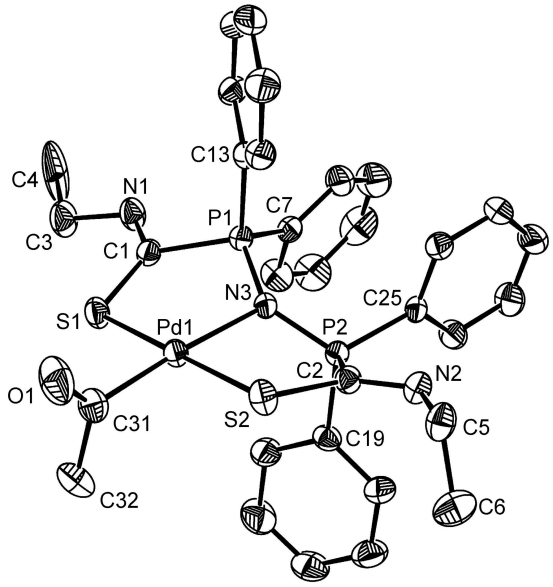

Figure 7. ORTEP plot of the molecular structure of **10**. Thermal ellipsoid are drawn at 30% probability level. H atoms are omitted for clarity. Selected distances [Å] and angles [°]: P1-N3 1.610(4), P2-N3 1.607(4), P1-C1 1.846(5), P2-C4 1.827(5), C1-S1 1.732(6), C2-S2 1.757(5), C1-N2 1.290(7), C2-N2 1.274(7), S1-Pd1 2.3513(15), S2-Pd1 2.3519(15), C31-Pd1 1.963(6), C31-C32 1.489(8), C31-01 1.195(7), N3-Pd1 2.211(4), P1-N1-P2 137.6(3), P1-N3-Pd1 113.3(2), P2-N3-Pd1 109.0(2), , N3-Pd1-C31 175.3(2), S1-Pd1-C31 91.62(12), S2-Pd1-C31 89.64(18), N3-Pd1-S1 89.45(12), N3-Pd1-S2 90.21(12), S1-Pd1-S2 178.36(6), C32-C31-Pd1 113.6(5), O1-C31-C32 121.6(6), O1-C31-Pd1 124.8(5).

The CO insertion is demostered by ^{1}H NMR spectroscopy; the disappearance of the Pd-CH_3 signal of **9** is fellowed of a new singlet at 2.36 ppm. This value is typical for an acetyl group σ bonded to Pd. The formation of acetyl complex **10** is also confirmed by ^{31}P {^{1}H} NMR. The singlet of **9** is replaced by a singlet at 12.98 ppm. In FTIR-HATR spectrum is presented the νCO stretching frequency of the acetyl group at 1689 cm^{-1}.

In solid state, **9** is coordinated in *S,N,S*-κ^3 coordination fashion. The square planar coordination around the metal is completed by the acetyl group. The plane of acetyl group is tilted by *ca*. 83° with respect to the mean plane (Pd1-S1-N3-S2) of the complex. This value is in agreement as found in Cambridge Structural Database (from 68° to 90°).

5.4 Conclusions

This chapter gave further insight into the coordination chemistry of the zwitterionic ligand HRSNS, in particular with respect to the Pd(II) atom. Novel zwitterionic metallate are obtained and are fully charaterized.

5.5 References

[1] For reviews see: Dupont, J.; Consorti, C. S.; Spencer, J. *Chem. Rev.* **2005**, *105*, 2527. Beletskaya, I. P.; Cheprakov, A. V. *J. Organomet. Chem.* **2004**, *689*, 4055. Bedford, R. B. *Chem. Commun.* **2003**, 1787. van der Boom, M. E.;Milstein, D. *Chem. Rev.* **2003**, *103*, 1759. Milstein, D. *Pure Appl. Chem.* **2003**, *75*, 2003. Albrecht, M.; van Koten, G. *Angew. Chem., Int. Ed.* **2001**, *40*, 3750. Dupont, J.; Pfeffer, M.; Spencer, J. *Eur. J. Inorg. Chem.* **2001**, 1917. Vigalok, A.; Milstein, D. *Acc. Chem. Res.* **2001**, *34*, 798. Beletskaya, I. P.; Cheprakov, A.V. *Chem. Rev.* **2000**, *100*, 3006.

[2] Herrmann, W. A. *Angew. Chem., Int. Ed.* **2002**, *41*, 1290. Bourisou, D.; Guerret, O.; Gabbai, F. P.; Bertrand, G. *Chem. Re*V. **2000**, *100*, 39. Nolan, S. P., Ed. *N-Heterocyclic Carbenes in Synthesis;* Wiley-VCH: Weinheim, Germany, **2006**. Scott, N. M.; Nolan, S. P. *Eur. J. Inorg. Chem.* **2005**, 1815.

[3] Selected recent applications of pincer complexes: Sebelius, S.; Ollson, V. J.; Szabo´, K. J. *J. Am. Chem. Soc.* **2005**, *127*, 10478. Kjellgren, J.; Sunde´n, H.; Szabo´, K. J. *J. Am. Chem. Soc.* **2005**, *127*, 1787. Solin, N.; Wallner, O. A.; Szabo´, K. J. *Org. Lett.* **2005**, *7*, 689. Solin, N.; Kjellgren, J.; Szabo´, K. J. *J. Am. Chem. Soc.* **2004**, *126*, 7026. Kjellgren, J.; Sunde´n, H.; Szabo´, K. J. *J. Am. Chem. Soc.* **2004**, *126*, 474. Wallner, O. A.; Szabo´, K. J. *Org. Lett.* **2004**, *6*, 1829. Solin, N.; Kjellgren, J.; Szabo´, K. J. *Angew. Chem., Int. Ed.* **2003**, *42*, 3656. Göttker-Schnetmann, I.; Brookhart, M. *J. Am. Chem. Soc.* **2004**, *126*, 9330. Göttker-Schnetmann, I.; White, P.; Brookhart, M. *J. Am. Chem. Soc.* **2004**, *126*, 1804. (j) Go¨ttker-Schnetmann, I.; White, P.; Brookhart, M. *Organometallics* **2004**, *23*, 1766. Zhao, J.; Goldman, A. S.; Hartwig, J. F. *Science* **2005**, *307*, 1080. Zhang, X.; Emge, T. J.; Ghosh, R.; Goldman, A. S. *J. Am. Chem. Soc.* **2005**, *127*, 8250. Kanzelberger, M.; Zhang, X.; Emge, T. J.; Goldman, A. S.; Zhao, J.; Incarvito, C.; Hartwig, J. F. *J. Am. Chem. Soc.* **2003**, *125*, 13644. Kanzelberger, M.; Singh, B.; Czerw, M.; Krogh-Jespersen, K.; Goldman, A. S. *J. Am. Chem. Soc.* **2000**, *122*, 11017. Amoroso, D.; Jabri, A.; Yap, G. P. A.; Gusev, D. G.; dos Santos, E. N.; Fogg, D. E. *Organometallics* **2004**, *23*, 4047. Gagliardo, M.; Dijkstra, H. P.; Coppo, P.; De Cola, L.; Lutz, M.; Spek, A. L.; van Klink, G. P. M.; van Koten, G. *Organometallics* **2004**, *23*, 5833. Eberhard, M. R. *Org. Lett.* **2004**, *6*, 2125. Yao, Q.; Kinney, E. P.; Zheng, Z. *Org. Lett.* **2004**, *6*, 2997. Cohen, R.; Milstein, D.; Martin, J. M. L. *Organometallics* **2004**, *23*, 2342. Kozhanov, K. A.; Bobnov, M. P.; Cherkasov, V. K.; Fukin, G. K.; Abakumov, G. A. *Dalton Trans.* **2004**, 2957. Chase, P. A.; Gagliardo, M.; van Klink, G. P. M.; Lutz, M.; Spek, A. L.; van Koten, G. *Organometallics* **2005**, *24*, 2016. Kossoy, E.; Iron, M. A.; Rybtchinski, B.; Ben-David, Y.; Shimon, L. J. W.; Konstantinovski, L.; Martin, J. M. L.; Milstein, D. *Chem.-Eur. J.* **2005**, *11*, 2321.

[4] Knapen, J. W. J.; van der Made, A. W.; De Wilde, J. C.; van Leeuwen, P. W. N. M.; Wijkens, P.; Grove, D. M.; van Koten, G. *Nature* **1994**, *372*, 659**.** Kleij, A. W.; Gossage, R. A.; Jastrzebski, J. T. B. H.; Boersma, J.; van Koten, G. *Angew. Chem., Int. Ed.* **2000**, *39*, 176. Kleij, A. W.; Gossage, R. A.; Klein Gebbink, R. J. M.; Brinkmann, N.; Reijerse, E. J.; Kragl, U.; Lutz, M.; Spek, A. L.; van Koten, G. *J. Am. Chem. Soc.* **2000**, *122*, 12112. Albrecht, M.; Hovestad, N. J.; Boersma, J.; van Koten, G. *Chem. Eur. J.* **2001**, *7*, 1289. Dahan, A.; Weissberg, A.; Portnoy, M. *Chem. Commun.* **2003**, 1206. Huck, W. T. S.; van Veggel, F. C. J. M.; Reinhoudt, D. N. *Angew.Chem., Int. Ed.* **1996**, *35*, 1213. Huck, W. T. S.; Hulst, R.; Timmerman, P.; van Veggel, F. C. J. M.; Reinhoudt, D. N. *Angew. Chem., Int. Ed.* **1997**, *36*,

1006. Huck, W. T. S.; van Veggel, F. C. J. M.; Reinhoudt, D. N. *New J. Chem.* **1998**, *22*, 165. van Manen, H.-J.; Fokkens, R. H.; van Veggel, F. C. J. M.; Reinhoudt, D. N. *Eur. J. Org. Chem.* **2002**, *18*, 3189. van de Coevering, R.; Kuil, M.; Klein Gebbin k, R. J. M.; van Koten, G. *Chem. Commun.* **2002**, 1636.

[5] Albrecht, M.; Lutz, M.; Spek, A. L.; van Koten, G. *Nature* **2000**, *406*, 970. Albrecht, M.; Schlupp, M.; Bargon, J.; van Koten, G. *Chem. Commun.* **2001**, 1874. Robitzer, M.; Sirlin, C.; Kyritsakas, N.; Pfeffer, M. *Eur. J. Inorg. Chem.* **2002**, 2312. Robitzer, M.; Bouamaï¨ed, I.; Sirlin, C.; Chase, P. A.; van Koten, G.; Pfeffer, M. *Organometallics* **2005**, *24*, 1756.

[6] See, for example: Rybtchinski, B.; Oevers, S.; Montag, M.; Vigalok, A.; H. Rozenberg, J. M. L. Martin and D. Milstein, *J. Am. Chem. Soc.*, **2001**, *123*, 9064–9077; E. Poverenov, Gandelman, M.; Shimon, L. J. W.; Rozenberg, H.; Ben-David, Y.; Milstein, D., *Chem.–Eur. J.*, **2004**, *10*, 4673–4684. Poverenov, E.; Gandelman, M.; Shimon, L. J. W.; Rozenberg, H.; Ben-David, Y.; Milstein, D., *Organometallics*, **2005**, *24*, 1082–1090; Poverenov, E.; Leitus, G.; Ben-David, Y.; Milstein, D., *Organometallics*, **2005**, *24*, 5937–5944; Fischer, J.; Schürmann, M.; Mehring, M.; Zachwieja U.; Jurkschat, K., *Organometallics*, **2006**, *25*, 2886–2893 and references therein.

[7] (a) Asti, M.; Cammi, R.; Cauzzi, D.; Graiff, C.; Pattacini, R.; Predieri, G.; Stercoli, A.; Tiripicchio, A., *Chem. Eur. J.* **2005**, *11*, 3413-3419. (b) Pattacini, R.; Barbieri, L.; Stercoli, A.; Cauzzi, D.; Graiff, C.; Lanfranchi, M.; Tiripicchio, A.; Elviri, L., *J. Am. Chem. Soc.* **2006**, *128*, 866-876. (c) Delferro, M.; Cauzzi, D.; Pattacini, R.; Tegoni, M.; Graiff, C.; Tiripicchio, A., *Eur. J. Inorg. Chem.* **2008**, 2302-2312. (d) Delferro, M.; Pattacini, R.; Cauzzi, D.; Graiff, C.; Terenghi M.; Predieri G.; Tiripicchio A., *Dalton Trans.*, **2009**, *3*, 544-549.

[8] Bhattacharyya, P.; Woollins, J. D., *Polyhedron* **1995**, *14* (23/24), 3367–3388.

[9] Wayland, B. B.; Schrammz R. F., *Inorg. Chem.*, **1969**, *8*, 971-976.

[10] Rülke, R. E.; Ernsting, J. M.; Spelt, A. L.; Elsevier, C. J.; van Leeuwen P. W. N. M.; Vrieze, K., *Inorg. Chem.,* **1993**, *32*, 5769-5778.

[11] Osborn, J. A.; Schrock, R., *J. Am. Chem. Soc.* **1971**, *93* (12), 3089–3091.

[12] *SAINT Software Users Guide*, Version 6.0; Bruker Analytical X-ray Systems: Madison, WI, **1999**.

[13] G. M. Sheldrick, *SADABS*; Bruker Analytical X-ray Systems, Madison, WI, **1999**. G. M. Sheldrick, *SHELXL-97*, Program for crystal structure refinement; University of Göttingen: Germany, **1997**.

[14] Delferro, M.; Cauzzi, D.; Tegoni, M.; Verdolino, V.; Graiff, C.; Tiripicchio, A., **2009**, submitted.

[15] Begum, R. A.; Powell, D.; Bowman–James, K., *Inorg. Chem,* **2006**, *45* (3), 964-966.

[16] Kovala-Demertzi, D.; Kourkoumelis, N.; Demertzis, N. A.; Miller, J. R.; Frampton, C. S.; Swearingen, J. K.; West, D. X., *Eur. J. Inorg. Chem.* **2000**, 727-734 and references therein.

[17] (a) Siedle, G.; Kersting, B., *Dalton Trans.*, **2006**, 2114-2126.

6

Enchainment Cooperativity Effects in Neutrally Charged Bimetallic Nickel (II) Phenoxyiminato Polymerization Catalysts, and Enhanced Selectivity for Polar Comonomer Enchainment

The synthesis and characterization of the bimetallic 2,7-di-[(2,6-diisopropylphenyl)imino]-1,8-naphthalenediolato group 10 metal polymerization catalysts {[Ni(CH_3)]$_2$[1,8-(O)$_2$$C_{10}H_4$-2,7-[CH=N(2,6-^{i}Pr$_2$$C_6H_3$)](PMe$_3$)$_2$} ([**FI^2-Ni$_2$-A**]) and {[Ni(Naphthyl)]$_2$[1,8-(O)$_2$$C_{10}H_4$-2,7-[CH=N(2,6-^{i}Pr$_2$$C_6H_3$)](PPh$_3$)$_2$} (Naphthyl = $C_{10}H_7$) [**FI^2-Ni$_2$-B**] are presented, along with the synthesis and characterization of the mononuclear analogues {Ni(CH_3)[3-^{t}Bu-2-(O)C_6H_3CH=N(2,6-^{i}Pr$_2$$C_6H_3$)](PMe)$_3$} ([**FI-Ni-A**]) and {Ni(Naphtyl)[3-^{t}Bu-2-(O)C_6H_3CH=N(2,6-^{i}Pr$_2$$C_6H_3$)](PPh)$_3$} ([**FI-Ni-B**]). Monometallic Ni catalysts were also prepared by functionalizing one ligation center of the bimetallic ligand with a trimethylsilyl group (TMS), yielding {Ni(CH_3)[1,8-(O)(TMS-O)$C_{10}H_4$-2,7-[CH=N(2,6-^{i}Pr$_2$$C_6H_3$)](PPh$_3$)} [**TMS-FI^2-Ni-(PPh$_3$)**]. The **FI^2-Ni$_2$** catalysts exhibit significant increases in ethylene homopolymerization activity versus the monometallic analogues, as well as increased branching and methyl branch selectivity, even in the absence of a [Ni(cod)$_2$] cocatalyst. Increasing ethylene concentrations significantly suppresses branching and branch morphology. **FI^2-Ni$_2$**-mediated copolymerizations with ethylene + polar-functionalized norbornenes exhibit a four-fold increase in comonomer incorporation versus **FI-Ni**, yielding copolymers with up to 10% norbornene copolymer incorporation. **FI^2-Ni$_2$**-catalyzed copolymerizations with ethylene + methylacrylate or methyl methacrylate incorporate up to 11% acrylate comonomer, while the corresponding mononuclear **FI-Ni** catalysts incorporate negligible amounts. Furthermore, the **FI^2-Ni$_2$**-mediated polymerizations exhibit appreciable polar solvent tolerance, turning over in the presence of ethyl ether, acetone, and even water. The mechanism by which the present cooperative effects take place is investigated, as is the nature of the copolymer microstructures produced.

6.1 Introduction

Over the past few years much research attention has focused on discovering more efficient and selective homogeneous catalytic processes made possible by cooperative effects between proximate active centers in multinuclear metal complexes.[1] In some cases, these complexes mimic the capabilities of enzymes in enforcing conformational control and preogranization to promote selectivity.[1] Research from this laboratory in the field of single-site[2] bimetallic olefin polymerization catalysis has shown that in group 4 constrained geometry[3,4] and aryloxyiminato[5] catalytic systems, exhibit increased activity, branch formation and comonomer enchainment versus their mononuclear analogues (Chart 1).

Chart 1. Group 4 Mononuclear and Bimetallic Olefin Polymerization Catalysts

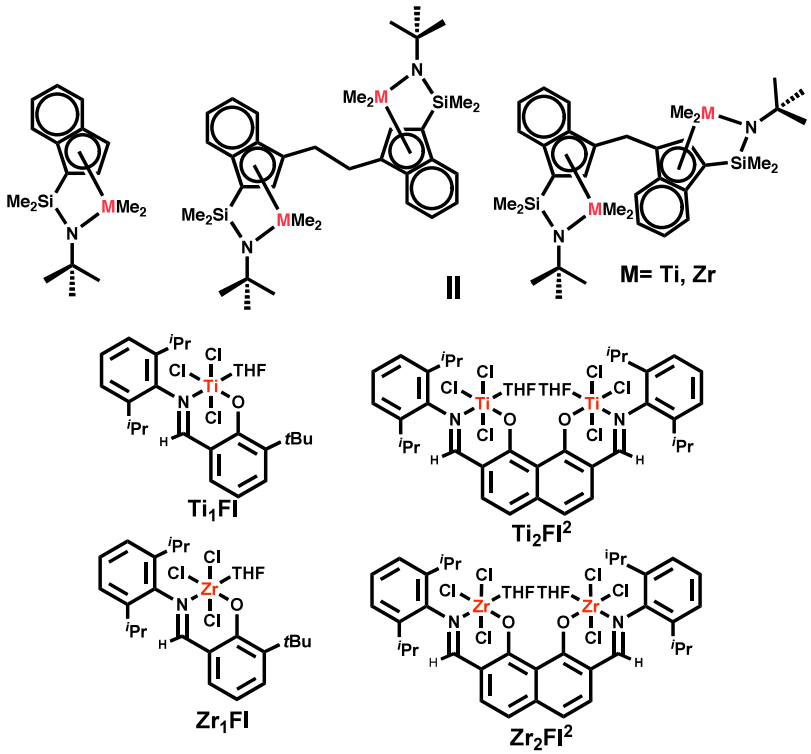

The origin of these effects is proposed to include non-negligible comonomer secondary binding to weakly basic groups on the olefin which modifies relative chain transfer rates and facilitates comonomer enchainment at the second, proximate metal center, as shown in **A**.[4,5] An excellent example of this is observed in polystyrene homopolymerizations with the binuclear CGC catalysts[4] (**II**).

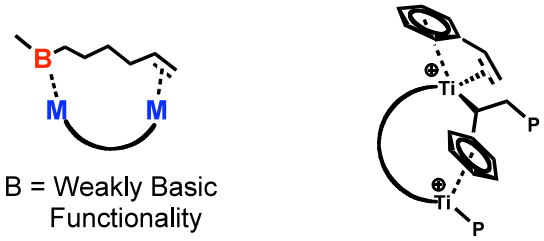

A **B**

Here binuclear cooperative Ti···arene interactions significantly enhance styrene homopolymerization rates, modify enchainment regioselectivity, and greatly increase comonomer enchainment selectivity (e.g., **B**).[4] The group 4 studies indicate that the degree of cooperativity between the two catalytic centers in these catalysts scales roughly inversely with intermetallic distance.[6]

Although very high olefin polymerization and copolymerization activities can be achieved with the group 4 catalysts, be it *via* the CGC ligation or otherwise, the electrophilicity of these metal centers greatly depresses their activity in the presence of polar comonomers or solvents. Desirable properties arising from the incorporation of polar functionalities into polyolefins include precise control over polymer characteristics such as mechanical toughness, rheology, and surface functionalization properties,[7] while the ability of the catalyst to withstand polar solvents allows bypassing the need for rigorous drying of polymerization solvent. In order to develop single-site catalysts capable of achieving these properties, our attention turned from the oxophilic group 4 metals towards catalyst systems with more electron-rich catalyst centers, such as the group 10 metals. The cationic and neutrally-charged group 10 systems pioneered by Brookhart, Johnson and Ittel[8,9] (Chart 2, **C** and **D**) demonstrated that coordinative enchainment of polar monomers such as acrylates is indeed possible in highly branched polyethylenes or polypropylenes, where the enchained acrylate units cap the branch ends.

Chart 2. Ni(II) Mononuclear Olefin Polymerization Catalysts

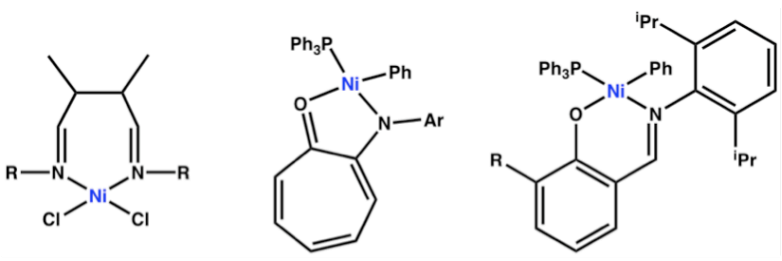

A **B** **C**

Contemporaneously, Grubbs *et al*[10,11] demonstrated that neutrally-charged Ni catalytic system **E** mediates ethylene copolymerization with functionalized norbornenes while producing very highly branched polymers. Controlled branching in polyolefins is desirable to depress the glass transition and melting temperatures, thus enhancing processability.[8-12] Also of note is that the group 10 catalysts are active in the presense of polar solvent additives, with only minor reductions in activity,[11] bypassing the need for hyperpurification of polymerization media. Although polar comonomers can be introduced into polyolefins via radical and other polymerization methods, single-site catalysts offer the attraction of greater control over polymer microstructure, polydispersity, and tunability of comonomer content.[8-13] The ability to effect these polymerizations *via* a coordinative/insertive pathway instead of the typically used free-radical processes also circumvents the need for expensive reactors and extremely high pressures. The above Ni catalyst systems are capable of introducing over 50 branches /1000 C into the polymer chain, yielding polymers with lower melting points than those produced by their group 4 counterparts, although typically with lower molecular weight. The group 10 systems typically incorporate 2-4 mol % of functionalized and non-functionalized norbornenes, further depressing the melting point and serving as an interesting starting point for determining what comonomers can be incorporated and to what extent.

The above results raise the intriguing question of whether the advantageous characteristics of binuclear polymerization catalysts (Chart 1) might be applied to group 10 catalytic systems. Attractions include the possibility of modifying polymerization rates and selectivites while enhancing selectivity for monomers having basic substituents, as in structures **A** and **B**, above, and tolerance to polar media, which is not possible for the group 4 catalysts. A group 10 binuclear catalyst would also allow probing the full scope of the bimetallic cooperativity effects first demonstrated with the aforementioned group 4 catalysts by providing a broader spectrum of polymerization conditions and monomers to be explored.

We recently communicated[14] the synthesis of binuclear phenoxyiminato Ni(II) catalysts [**FI^2-Ni_2-A**] and [**FI^2-Ni_2-B**] in which the rigid ligation ensures that the metal centers are bound in close spatial proximity (Chart 3).

Chart 3. Group 10 Mononuclear and Bimetallic Olefin Polymerization Catalysts

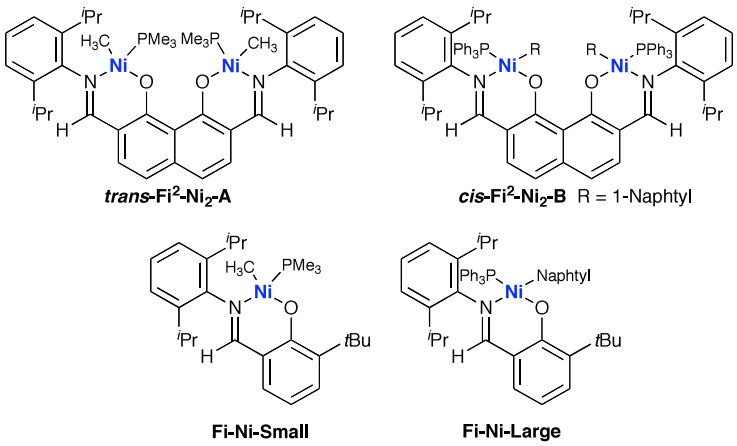

In initial ethylene homopolymerizations mimicking the reaction conditions of the previous monometallic group 10 work,[10,11] the **FI²-Ni₂** systems exhibited a doubling in catalytic activity for ethylene homopolymerizations and introduced significantly more alkyl branches than the mononuclear **FI** catalysts, and exhibited a strong selectivity for methyl-only branch formation (>99%). Intriguing preliminary binuclear copolymerization effects were observed with norbornene, including a four-fold increase of enchainment selectivity over the monometallic catalyst. In the present contribution, we present a detailed study of **FI²-Ni₂** synthetic, solid-state and solution structural, and olefin polymerization catalytic chemistry. Using the monometallic Ni analogues as controls, we show that: 1) Ethylene hompolymerizations in the presence of the **FI²-Ni₂** exhibit significantly increased activity to produce different product microstructures than the mononuclear **FI-Ni** catalysts. 2) This enhanced activity is maintained in the presence of polar cosolvents, while concurrently retaining the selectivity for large branch densities. 3) Substantial cooperativity effects operate in the **FI²-Ni₂**-mediated copolymerizations of ethylene with functionalized norbornenes, and 4) Ethylene copolymerizations with normally unresponsive acrylate esters achieve up to 11% comonomer incorporation in reactions catalyzed by **FI²-Ni₂**, versus negligible enchainment by **FI-Ni** catalysts. As supported by structural, in situ NMR spectroscopic, and product polymer microstructure studies, these results are in accord with strong Ni···Ni mediated cooperative effects in the enchainment process.

Recent complimentary binuclear group 10 catalyst studies by Hu, *et al*[15b] (Chart 4, **F**) and Mecking, *et al*[15e] (Chart 4, **G**), report enhancements in non-cocatalyzed polymerization

activity vis-à-vis the mononuclear analogues as well as differences in polyolefin microstructure. The degree to which these observations reflect cooperative effects is not obvious, especially in view of the ligand conformational flexibility and/or the sizable metal-metal distances.[15]

Chart 4. Ni(II) Binuclear Olefin Polymerization Catalysts

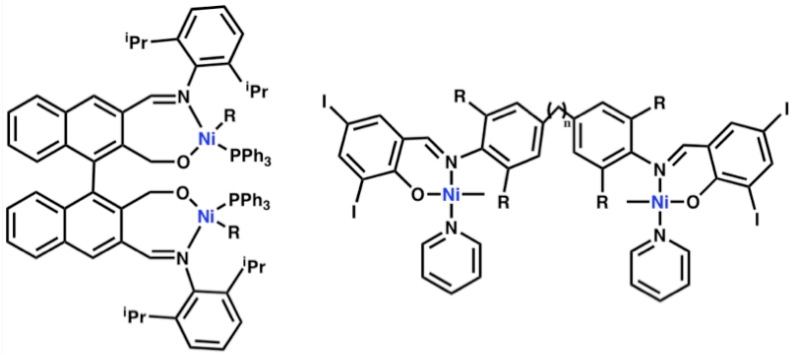

D **E**

6. 2 Experimental

6.2.1 General procedures.

All manipulations of air-sensitive materials were performed with rigorous exclusion of oxygen and moisture in flamed Schlenk-type glassware on a dual manifold Schlenk line, or interfaced to a high-vacuum line (10^{-5} Torr), or in a nitrogen-filled Vacuum Atmospheres glove box with a high capacity recirculator (<1 ppm O_2). Argon and ethylene (Matheson, polymerization grade) were purified by passage through a supported MnO oxygen-removal column and an activated Davison 4A molecular sieve column. Ether solvents were purified by distillation from Na/K alloy/benzophenone ketyl. Hydrocarbon solvents (*n*-pentane and toluene) were dried using activated alumina columns according to the method described by Grubbs,[16] and were additionally vacuum-transferred from Na/K alloy immediately before vacuum line manipulations. All solvents for high-vacuum line manipulations were stored *in vacuo* over Na/K alloy in Teflon-valve sealed bulbs. Deuterated solvents were obtained from Cambridge Isotope Laboratories (all ≥ 99 atom %D), were freeze pump- thaw degassed, dried over Na/K alloy and were stored in resealable flasks. Other non-halogenated solvents were dried over Na/K alloy, and halogenated solvents were distilled from CaH_2 and stored over

activated Davison 4A molecular sieves. The reagents *trans*-[Ni(CH_3)Cl(PMe_3)$_2$],[17] *trans*-[Ni(Naphtyl)Cl(PPh_3)$_2$] (Naphtyl = $C_{10}H_7$),[18] 2,7-di(2,6-diisopropylphenyl)imino-1,8-dihydroxynaphthalene,[5,14] salicylaldimine and salicylaldiminate sodium salt[10,11] were prepared according to literature procedures. [Ni(cod)$_2$] (cod = 1,5-cyclooctadiene) was purchased from Aldrich.

6.2.2 Physical and Analytical Measurements.

NMR spectra were recorded on Bruker AVANCEIII (FT, 600 MHz, ^{1}H; 150 MHz ^{13}C), Varian ^{UNITY}Inova-500 (FT, 500 MHz, ^{1}H; 125 MHz, ^{13}C), ^{UNITY}Inova-400 (FT, 400 MHz, ^{1}H; 100 MHz, ^{13}C) and Mercury-400 (FT 400 MHz, ^{1}H; 100 MHz, ^{13}C; 162 MHz, ^{31}P). Chemical shifts (δ) for ^{1}H and ^{13}C spectra were referenced using internal solvent resonances and are reported relative to tetramethylsilane. Chemical shifts (δ) for ^{31}P spectra were reported relative to an external 85% H_3PO_4 standard. NMR experiments on air-sensitive samples were conducted in Teflon valve-sealed sample tubes (J.Young). Elemental analyses were performed by Midwest Microlab, Indianapolis, Indiana. ^{1}H and ^{13}C NMR spectra of polymers were collected in either 1,1,2,2-tetrachloroethane-d_2 at 130°C and $CDCl_3$ at 25°C at 400 or 600 MHz, as specified in each spectrum. In ethylene polymerizations, spectral assignments were made as described in the literature,[19] with extra care taken to ensure that peak widths of the methyl branch signal are representative of the true branch density. In copolymerizations, the additional product resonances were assigned to the corresponding comonomer functional groups as determined by the literature.[13,19] In each of the copolymerizations, ^{13}C NMR integration of the cononomer resonances versus those in the PE backbone was used to determine the density of incorporation. Signals were assigned according to the literature for the polyethylene part.[19] FTIR spectra were collected on a Bio-Rad FTS spectrophotometer (KBr pellet). Melting temperatures of polymers were measured by DSC (DSC 2920, TA Instruments, Inc.) from the second scan with a heating rate of 10 °C/min. GPC-RI measurements were performed on a Polymer Laboratories PL-GPC 220 instrument using 1,2,4-trichlorobenzene solvent (stabilized with 125 ppm BHT) at 150 °C. A set of three PLgel 10 μm mixed columns was used. Samples were prepared at 160 °C. GPC-UV measurements were performed on a Waters GPC 484 instrument using chloroform at 35 °C using two linear 500 X 10mm columns. Molecular weights determined by GPC used narrow polystyrene standards and are not corrected. NMR, DSC, GPC-RI and GPC-UV measurements were

performed as explained above, on both product copolymers and on control physical mixtures of the corresponding homopolymers.

6.2.3 X-Ray crystallography.

The intensity data of **[FI^2-Ni-(OPMe$_3$)]$_2$·**(OPMe$_3$) was collected collected at 173 K on a Bruker AXS Smart 1000[20] single crystal diffractometer equipped with an area detector using a graphite monochromated Mo K_α radiation (λ = 0.71073 Å). Crystallographic and experimental details of the structures are summarized in Table 1. An empirical absorption correction were applied to the data. The structure was solved by direct methods and refined by full-matrix least-squares procedures (based on F_o^2)[20] first with isotropic thermal parameters and then with anisotropic thermal parameters in the last cycles of refinement for all the non-hydrogen atoms. The hydrogen atoms were introduced into the geometrically calculated positions and refined *riding* on the corresponding parent atoms.

Table 1. Crystallographic data and structure refinement details for **[FI^2-Ni-(OPMe$_3$)]$_2$·**(OPMe$_3$).

	$Ni_2Fi_2(OPMe_3)_3$
Empirical formula	$C_{84}H_{116}N_4Ni_2O_8P_4$
FW	1551.11
Temperature, K	173(2)
Wavelength, Å	0.71073
crystal system	monoclinic
space group	*P21/c*
a, Å	10.4373(3)
b, Å	14.2123(4)
c, Å	27.5727(7)
α, deg	90
β, deg	92.476(1)
γ, deg	90
V, Å^3	4086.3(2)
Z	2
D_{calcd}, g cm^{-3}	1.261
F(000)	1656
crystal size, mm^3	0.07 x 0.08 x 0.10
μ, cm^{-1}	0.595
θ range (deg)	2.06 to 30.00
rflns collected	90633
rflns unique	11819 [R(int) = 0.0553]
Data / restraints / parameters	11819 / 0 / 460
Final R indices [I>2sigma(I)]	R1[a] = 0.0570, wR2[b] = 0.1422
R indices(all data)	R1[a] = 0.0746, wR2[b] = 0.1664

[a] $R1 = \Sigma||F_o|-|F_c||/\Sigma|F_o|$; [b] $wR2 = [\Sigma[w(F_o^2-F_c^2)^2]/\Sigma[w(F_o^2)^2]]$

*6.2.4 Synthesis of 2,7-Di-[(2,6-diisopropylphenyl)imino]-1,8-naphthalenediolate disodium salt (**1**).*

To a solution of 2,7-di(2,6-diisopropylphenyl)imino-1,8-dihydroxynapthalene (1.0g, 1.87 mmol) in THF dry (30 mL) was added NaH (0.224, 9.35 mmol). The resulting mixture was

stirred at 25°C for 1 h, filtered, and the filtrate evaporated. The yellow residue was washed with pentane (30 mL) and dried *in vacuo*. This product was immediately used without further purification for the synthesis of Ni complexes. Yield, 83%. ^{1}H NMR ($CDCl_3$, 25°C, 500 MHz): δ = 8.13 (s, 2H, *H*C=N), 7.53-6.75 (m,10H, Ph) 3.07 (sept, 4H, $^{3}J_{HH}$ = 6.8 Hz, C*H*Me$_2$), 1.34 (s, 12H, CH*Me*$_2$) ppm.

*6.2.5 Synthesis of {[Ni(CH$_3$)]$_2$[1,8-(O)$_2$C$_{10}$H$_4$-2,7-[CH=N(2,6-^{i}Pr$_2$C$_6$H$_3$)](PMe$_3$)$_2$} (**[FI^2-Ni$_2$-A]**).*

A solution of **1** (0.900 g, 1.55 mmol) in Et_2O (25 mL) was added dropwise at 25°C to a stirring solution of *trans*-[Ni(CH$_3$)Cl(PMe$_3$)$_2$] (0.815 g, 3.12 mmol) in benzene (25 mL). A rapid color change from yellow to dark red was observed, and after 1 h the mixture became dark orange. After this time, the reaction mixture was filtered by cannula. The volatiles were then removed from the filtrate *in vacuo* and the residue was washed with pentane. A light orange powder of {[Ni(CH$_3$)]$_2$[1,8-(O)$_2$C$_{10}$H$_4$-2,7-[CH=N(2,6-^{i}Pr$_2$C$_6$H$_3$)](PMe$_3$)$_2$} (**[FI^2-Ni$_2$-A]**) was obtained. Yield, 73%. ^{1}H NMR (C_6D_6, 25°C, 500 MHz): δ = 7.65 (d, $^{4}J_{PH}$ = 8.0 Hz, 2H, *H*C=N), 7.13-6.43 (m, 10H, Ph), 4.13 (sept, 2H, $^{3}J_{HH}$ = 6.5 Hz, C*H*Me$_2$), 3.73 (sept, 2H, $^{3}J_{HH}$ = 6.5 Hz, C*H*Me$_2$), 1.56 (d, $^{3}J_{HH}$ = 6.5 Hz, 6H, CH*Me*$_2$), 1.31 (d, $^{3}J_{HH}$ = 6.5 Hz, 6H, CH*Me*$_2$), 1.15 (d, $^{3}J_{HH}$ = 6.5 Hz, 6H, CH*Me*$_2$), 1.08 (d, $^{3}J_{HH}$ = 6.5 Hz, 6H, CH*Me*$_2$), 1.06 (d, $^{2}J_{PH}$ = 9.5 Hz, 18H, PMe$_3$), -1.15 (d, $^{3}J_{PH}$ = 7.3 Hz, 6H, NiMe) ppm. ^{13}C NMR (C_6D_6, 25°C, 125 MHz): δ = 170.33, 163.93, 150.17, 145.26, 141.96, 133.50, 125.96, 123.91, 123.02, 115.97, 113.51, 28.47, 24.45, 14.15, -12.23 ppm. ^{31}P NMR (C_6D_6, 25°C, 162 MHz): δ = -7.58 ppm. Anal. Found: C, 63.12; H, 7.71; N, 3.29. Calcd. for $C_{44}H_{64}N_2Ni_2O_2P_2$: C, 63.49; H, 7.75; N, 3.37.

*6.2.6 Synthesis of {[Ni(CH$_3$)]$_2$[1,8-(O)$_2$C$_{10}$H$_4$-2,7-[CH=N(2,6-^{i}Pr$_2$C$_6$H$_3$)](PPh$_3$)$_2$} (**[FI^2-Ni$_2$-B]**).*

A solution of **1** (0.800 g, 1.38 mmol) in Et_2O (25 mL) was added dropwise at 25°C to a stirring solution of *trans*-[Ni(Naph)Cl(PPh$_3$)$_2$] (2.06 g, 2.76 mmol) in benzene (25 mL). A rapid color change from yellow to dark pink was observed, and after 2 h the mixture became dark purple. After this time, the reaction mixture was filtered by cannula. The volatiles were next removed *in vacuo* from the filtrate and the residue was washed with pentane. Compound {[Ni(CH$_3$)]$_2$[1,8-(O)$_2$C$_{10}$H$_4$-2,7-[CH=N(2,6-^{i}Pr$_2$C$_6$H$_3$)](PPh$_3$)$_2$} (**[FI^2-Ni$_2$-B]**) was isolated as a

purple powder. Yield, 74%. ^{1}H-NMR (C_6D_6, 25°C, 500 MHz): δ = 11.07 (d, $^{3}J_{PH}$ = 14.0 Hz, 2H, Naph-H), 10.16 (d, $^{4}J_{PH}$ = 8.0 Hz, 2H, Naph-H), 8.90 (d, $^{4}J_{PH}$ = 8.0 Hz, 2H, Naph-H), 7.88 (d, $^{4}J_{PH}$ = 6.6 Hz, 2H, *H*C=N), 7.53-6.24 (m, 48H, Ph), 3.09 (sept, 2H, $^{3}J_{HH}$ = 6.9 Hz, C*H*Me$_2$, 1.22 (d, $^{3}J_{HH}$ = 6.9 Hz, 6H, CH*Me*$_2$) ppm. ^{13}C NMR (C_6D_6, 25°C, 125 MHz): δ = 177.47, 159.34, 152.28, 144.14, 140.62, 137.41, 134.14, 130.37, 129.91, 123.86, 122.50, 118.79, 113.20, 28.08, 22.96 ppm. ^{31}P NMR (C_6D_6, 25°C, 162 MHz): δ = 33.2 ppm. Anal. Found: C, 77.16; H, 6.01; N, 2.11. Calcd. for $C_{92}H_{86}N_2Ni_2O_2P_2$: C, 77.33; H, 5.92; N, 1.96.

*6.2.6 Synthesis of {Ni(Naph)[1,8-(O)(TMS-O)C$_{10}$H$_4$-2,7-[CH=N(2,6-^{i}Pr$_2$C$_6$H$_3$)](PPh$_3$)} (**[TMS-FI^2-Ni-(PPh$_3$)]**).*

A solution of **1** (0.800 g, 1.38 mmol) in Et_2O (25 mL) was added dropwise at rt to a stirring solution of *trans*-[Ni(Naph)Cl(PPh_3)$_2$] (1.03 g, 1.38 mmol) in benzene (25 mL). A rapid color change from yellow to dark pink was observed, and after 2 h the mixture became dark red. After this time, 1 equivalent of trimethylsilane-chloride was added to react with the second Na^+ site. The reaction mixture was then filtered by cannula. The volatiles were next removed from the filtrate *in vacuo* from the filtrate and the residue was washed with pentane. A red powder of {Ni(Naph)[1,8-(O)(TMS-O)$C_{10}H_4$-2,7-[CH=N(2,6-$^{i}Pr_2C_6H_3$)](PPh$_3$)} (**[TMS-FI^2-Ni-(PPh$_3$)]**) was obtained. Yield, 78%. ^{1}H NMR ($CDCl_3$, 25°C, 500 MHz): δ = 11.07 (d, $^{4}J_{PH}$ = 14.0 Hz, 1H, Naph-H), 10.16 (d, $^{5}J_{PH}$ = 8.0 Hz, 1H, Naph-H), 8.90 (d, $^{4}J_{PH}$ = 8.0 Hz, 2H, Naph-H) 8.13-8.22 (d, 2H, *H*C=N), 7.53-6.75 (m, 30H, Ph) 3.07 (m, 4H, $^{3}J_{HH}$ = 6.8 Hz, C*H*Me$_2$), 1.34 (s, 12H, CH*Me*$_2$), 0.04 (s, 9H, $SiMe_3$) ppm. ^{31}PNMR (C_6D_6, 25°C, 162 MHz): δ = 31.0. Anal. Found: C, 75.16; H, 5.98; N, 2.96. Calcd. for $C_{59}H_{56}NiN_2O_2PSi$: C, 75.16; H, 5.99; N, 2.97.

*6.2.7 Synthesis of {Ni(CH$_3$)[3-^{t}Bu-2-(O)C$_6$H$_3$CH=N(2,6-^{i}Pr$_2$C$_6$H$_3$)](PMe)$_3$} (**[FI-Ni-A]**).*

A solution of the appropriate salicylaldiminate sodium salt (0.400 g, 1.11 mmol) in Et_2O (30 mL) was added dropwise at 25°C to a solution of *trans*-[Ni(CH_3)Cl(PMe_3)$_2$] (0.290 g, 1.11 mmol) in Et_2O (25 mL). The orange mixture was stirred for 2 h at 25°C. After this time, the reaction mixture was filtered by cannula. The filtrate was then evaporated *in vacuo* and the solid residue was washed with pentane. A yellow-orange microcrystalline powder of {Ni(CH_3)[3-^{t}Bu-2-(O)C$_6$H$_3$CH=N(2,6-^{i}Pr$_2$C$_6$H$_3$)](PMe)$_3$} (**[FI-Ni-B]**). was obtained. Yield, 74%. ^{1}H NMR (C_6D_6, 25°C, 500 MHz): δ = 7.84 (d, $^{4}J_{PH}$ = 8.8 Hz, 1H, *H*C=N), 7.42-6.56 (m,

6H, Ph), 3.96 (sept, 1H, $^3J_{HH}$ = 6.7 Hz, C*H*Me$_2$), 1.51 (s, 9H, C*Me$_3$*), 1.32 (d, $^3J_{HH}$ = 6.7 Hz, 6H, CH*Me$_2$*), 0.97 (d, $^3J_{HH}$ = 6.7 Hz, 6H, CH*Me$_2$*), 0.95 (d, $^2J_{PH}$ = 9.1 Hz, 9H, PMe$_3$), -1.10 (d, $^3J_{PH}$ = 7 Hz, 3H, NiMe) ppm. ^{13}C NMR (C_6D_6, 25°C, 125 MHz): δ = 166.25, 149.49, 141.45, 140.62, 133.690, 126.220, 123.45, 120.19, 35.23, 29.80, 28.32, 22.45, 14.15, -17.32 ppm. ^{31}P NMR (C_6D_6, 25°C, 162 MHz): δ = -12.57 ppm. Anal. Found: C, 66.53; H, 8.63; N, 2.91. Calcd. for $C_{27}H_{42}NNiOP$: C, 66.69; H, 8.71; N, 2.88.

*6.2.8 Synthesis of {Ni(Naphtyl)[3-^{t}Bu-2-(O)C_6H_3CH=N(2,6-^{i}Pr$_2C_6H_3$)](PPh)$_3$} (**[FI-Ni-B]**).*

A solution of the appropriate salicylaldiminate sodium salt (0.500 g, 1.39 mmol) in benzene (30 mL) was added dropwise at 25°C to a stirring solution of *trans*-[Ni(Naph)Cl(PPh$_3$)$_2$] (1.037 g, 1.39 mmol) in benzene (25 mL). The orange mixutre was stirred for 2 h at 25°C. After this time, the reaction mixture was filtered by cannula filtration. The filtrate was then evaporated *in vacuo* and the solid residue was washed with ethanol. A yellow-orange microcrystalline powder of {Ni(Naphtyl)[3-^{t}Bu-2-(O)C_6H_3CH=N(2,6-^{i}Pr$_2C_6H_3$)](PPh)$_3$} (**[FI-Ni-B]**) was obtained. Yield, 75%. ^{1}H NMR (C_6D_6, 25°C, 500 MHz): δ = 10.47 (d, $^4J_{PH}$ = 8.8 Hz, 1H, NiC-C*H*$_{naph}$), 7.96 (d, $^4J_{PH}$ = 8.8 Hz 1H, *H*C=N), 7.69-6.55 (m, 24H, Ph), 5.56 (sept, 1H, $^3J_{HH}$ = 6.5 Hz, C*H*Me$_2$), 2.98 (sept, 1H, $^3J_{HH}$ = 6.5 Hz, C*H*Me$_2$),1.68 (d, $^3J_{HH}$ = 6.6 Hz, 3H, CH*Me$_2$*), 1.10 (d, $^3J_{HH}$ = 6.6 Hz, 3H, CH*Me$_2$*), 0.90 (s, 9H, CMe$_3$), 0.85 (d, $^3J_{HH}$ = 6.6 Hz, 3H, CH*Me$_2$*), -0.07 (d, $^3J_{HH}$ = 6.6 Hz, 3H, CH*Me$_2$*) ppm.^{13}C NMR (C_6D_6, 25°C, 125 MHz): δ = 167.11, 165.13, 150.59, 141.56, 140.51, 136.42, 134.82, 133.42, 132.16, 131.73, 129.55, 127.51, 125.79, 123.71, 122.18, 121.56, 120.70, 114.20, 34.67, 30.02, 28.45, 24.45, 21.43 ppm. ^{31}P NMR (C_6D_6, 25°C, 162 MHz): δ = 24.21 ppm. Anal. Found: C, 77.78; H, 6.81; N, 1.86. Calcd. for $C_{51}H_{52}NNiOP$: C, 78.07; H, 6.68; N, 1.79.

*6.2.9 Synthesis of {[Ni(n-butyl)]$_2$[1,8-(O)$_2C_{10}H_4$-2,7-[CH=N(2,6-^{i}Pr$_2C_6H_3$)](PPh$_3$)$_2$} (**[FI^2-Ni$_2$-(n-butyl)$_2$]**) and in situ NMR studies.*

One equivalent of a solution of **1** in benzene (30 mL) was added dropwise at -78°C to a stirring solution of *trans*-[NiCl$_2$(PPh$_3$)$_2$] in benzene (25 mL). After stirring for 4 h, two equivalents of *n*-BuLi (2.5M) was added dropwise and allowed to stir at -78°C for an additional 4 h. The resulting salt is filtered off via cannula and the thermally unstable dinickel complex is dried via evaporation at 0°C. The dinickel complex is loaded into an NMR tube along with two equivalents of [Ni(cod)$_2$] and dissolved in d_8-toluene. Due to the instability of

the complex, the NMR is cooled to -80°C beforehand. Spectra are collected on a Varian ^{UNITY}Inova-400 (FT, 400 MHz, ^{1}H; 100 MHz, ^{13}C) at -80°C, -60°C, -40°C, and -20°C to monitor the presence of any agostic interactions.

6.2.10 General procedure for Ethylene Polymerization by Ni complexes.

A 200 mL glass pressure vessel (dried in 120°C oven overnight prior to use) was equipped with a large magnetic stirbar, and was heated to the required temperature by oil bath, with the temperature monitored by thermocouple. At no time was the temperature allowed to deviate more than 2°C. Next, 25 mL of toluene was injected via syringe into the reactor and the reactor was pressurized with ethylene to 1.0 atm. For trias without cocatlyst, 20 μmol of catalyst solution was then injected and the pressure brought to 7.0 atm for 2 h with rapid stirring. For cocatalyst-activated trials, a solution of 10 μmol of catalyst in [Ni(cod)$_2$] was injected, after which the pressure was increased to 7.0 atm and rapid stirring maintained for 40 min. After the desired run time, the reactor was vented, and the reaction mixture was quenched with 10% HCl in ethanol. The precipitated polymer was stirred overnight, collected by filtration, and dried under vacuum at 80°C overnight.

6.2.11 General procedure for Ethylene Polymerization by Ni complexes in Polar Solvents.

A 200 mL glass pressure vessel (dried in 120°C oven overnight prior to use) was equipped with a large magnetic stirbar and heated to the required temperature by oil bath. Next, 25 mL of toluene was injected into the reactor along with 1500 eq. of the desired rigorously degassed polar solvent additive. The reactor was then pressurized with ethylene to 1.0 atm. 10 μmol of catalyst solution was then injected and the pressure brought to 7.0 atm for 1 h with rapid stirring. After the desired run time, the reactor was vented, and the reaction mixture was quenched with 10% HCl in ethanol. The precipitated polymer was stirred overnight, collected by filtration, and dried under vacuum at 80°C overnight.

6.2.12 General procedure for Ethylene Co-polymerization by Ni complexes with Acrylates or Functionalized Norbornenes.

A 200 mL glass pressure vessel (dried in 120°C oven overnight prior to use) was equipped with a large magnetic stirbar and heated to the required temperature by oil bath. Next, 25 mL of toluene was injected via syringe into the reactor along with 225 eq. of the desired polar

comonomer. The reactor was then pressurized with ethylene to 1.0 atm. 20 μmol of catalyst solution was then injected and the pressure brought to 7.0 atm for 1.5 h with rapid stirring. After the desired run time, the reactor was vented, and the reaction mixture was quenched with 10% HCl in ethanol. The precipitated polymer was stirred overnight, collected by filtration, and dried under vacuum at 80°C overnight.

6.3 Results

The goal of this study was to explore the scope and mechanism of Ni center- Ni center cooperative enchainment effects in polymerizations mediated by binuclear **FI^2-Ni$_2$**-derived catalysts. This included defining the scope of this cooperativity in ethylene homopolymerizations and in ethylene copolymerizations with polar functionalized norbornenes and acrylates. Here rigorous copolymer microstructure analysis is carried out to differentiate copolymers from mixtures of the corresponding homopolymers. Ethylene homopolymerizations were also carried out in the presence of polar additives to assess the stability of the binuclear cooperativity effects in the presence of coordinating and protic media. Finally, the pathway by which this cooperativity takes place is explored by means of product polymer microstructure analysis, and structural characterization of the catalytic species in the solid state and in solution via *in situ* low temperature NMR studies.

6.3.1 Synthesis and Characterization of Bimetallic Catalysts

The sodium salt of ligand **FI^2-H$_2$**[5] was obtained by treating 2,7-di(2,6-diisopropylphenyl)imino-1,8-dihydroxy-naphthalene with NaH in THF. The bimetallic catalysts **FI^{2-}Ni$_2$-A** and **FI^2-Ni$_2$-B** were then prepared as shown in Scheme 1. All new compounds were characterized by standard analytical and spectroscopic techniques. The imine protons in the **FI^{2-}Ni$_2$-A** ^{1}H NMR spectrum exhibit a characteristic $J_{PH} \approx 9$ Hz, corresponding to PMe_3 coordination *trans* to the ketimine (confirmed by ^{1}H NOESY and ^{1}H COSY). Close proximity of the Ni-CH_3 group and the methyls of one ^{i}Pr group is also detected in the NOESY spectrum. In contrast, $J_{PH} \approx 6$ Hz and the ^{1}H NOESY spectrum indicate *cis*-PPh_3 binding[8c] in **FI^2-Ni$_2$-B**. The ^{1}H-decoupled ^{31}P singlets in both complexes are consistent with the proposed **FI^{2-}Ni$_2$-A** and **FI^2-Ni$_2$-B** symmetries. Upon standing at elevated

temperatures (≥35 °C), the presence of free phosphine is also detected in the ^{31}P NMR along with a dimeric phosphine-free complex (see more below). For polymerization control experiments, mononuclear complexes **FI-Ni-A** and **FI-Ni-B** were synthesized *via* reaction of the corresponding mono-salicylaldiminate sodium salt[10,11] with the aforementioned Ni(II) precursors. A monometallic control complex with one Ni site replaced by a bulky TMS group was prepared by reaction of 1.0 equiv. of the Ni(II) precursor with the disodium salt of **FI^2-H$_2$**, followed by addition of TMS-Cl *in situ* to yield **[TMS-FI^2-Ni-(PPh$_3$)]** (Scheme 1).

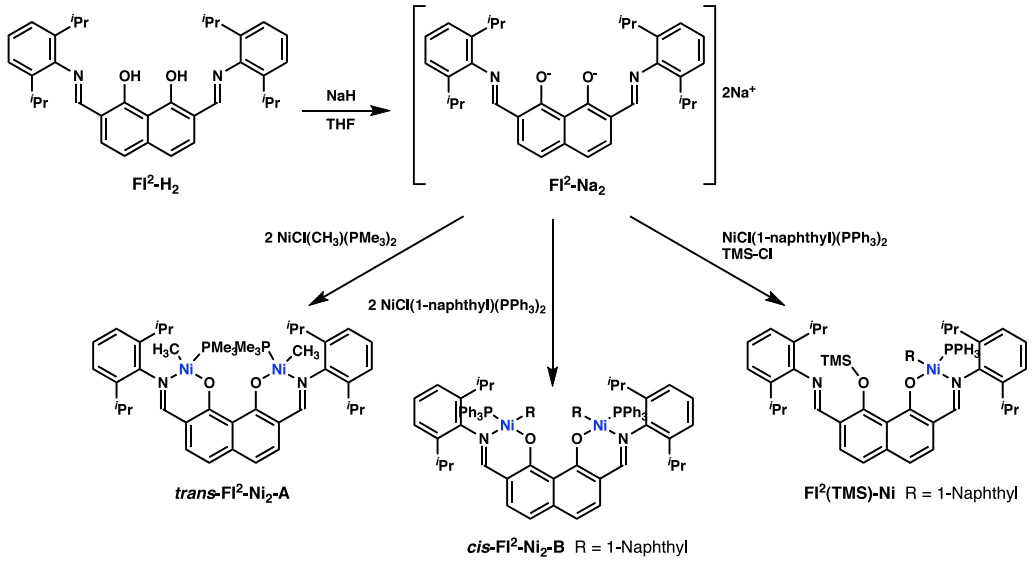

Scheme 1. Synthesis of binuclear **FI^2-Ni$_2$-A**, **FI^2-Ni$_2$-B** and mononuclear **FI^2(TMS)-Ni** catalysts.

Stepwise Ni incorporation can be monitored by integration of the now inequivalent *i*-propyl and imine ^{1}H NMR resonances. This monometallic complex was designed to probe the nature and extent of Ni···Ni cooperativity effects on polymerization and to verify that the effects observed are not the result of simple steric crowding, but are due to the presence of two active metal sites.

Any attempt to obatined single crystals of **FI^2-Ni$_2$-A/B** failed. Otherwise, bischelating complex **[FI^2-Ni-(OPMe$_3$)]$_2$**·(OPMe$_3$) was achieved. The ORTEP plot of the structure of **[FI^2-Ni-(OPMe$_3$)]$_2$** in **[FI^2-Ni-(OPMe$_3$)]$_2$**·(OPMe$_3$) is depicted in Figure 2. Selected bond distances (Å) and angles (°) are given in Table 2.

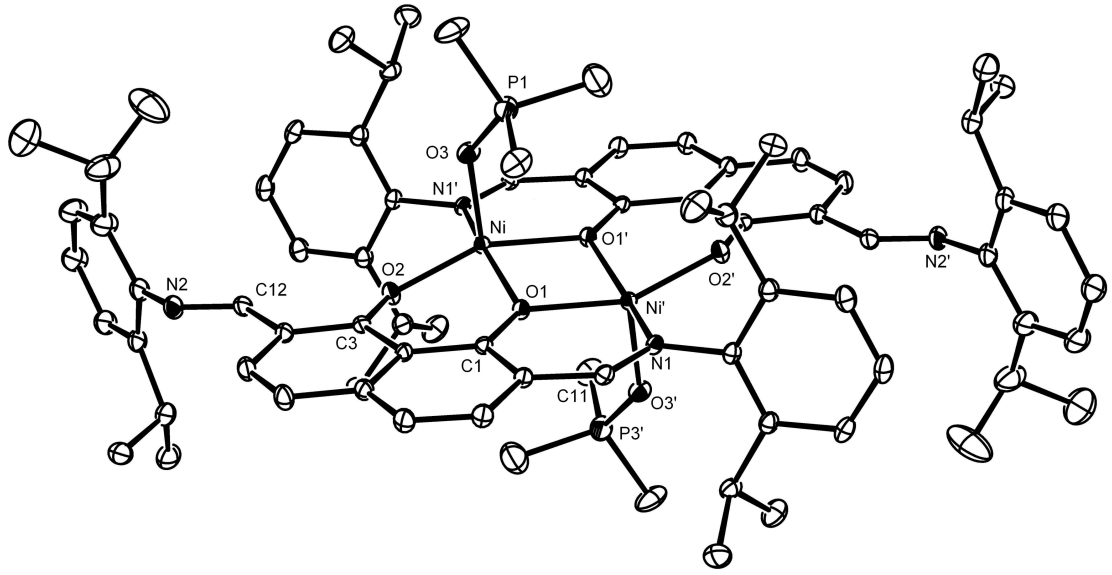

Figure 1. ORTEP plot of the molecular structure of **[FI^2-Ni-(OPMe$_3$)]$_2$**·(OPMe$_3$). Thermal ellipsoids are drawn at the 30 % probability level. H atoms are omitted for clarity. The OPMe$_3$ molecules are not involved in interactions with the complex are omitted for clarity. Symmetry transformation used to generate equivalent atoms: ' = - x, - y, - z.

Table 2. Selected distances [Å] and angles [°] for **[FI^2-Ni-(OPMe$_3$)]$_2$**·(OPMe$_3$)

C1-O1	1.317(3)	Ni1-O3	1.982(2)
C3-02	1.302(3)	Ni1'-O1	2.008(3)
C11-N1	1.288(3)	Ni1-O1	2.013(2)
C12-N2	1.282(3)	O3-P1	1.502(2)
N1-Ni1	2.014(2)	Ni1···Ni1'	3.092(3)
Ni1-O2	1.924(2)		
O1-Ni1-O2	88.5(1)	N1-Ni1'-O1	90.4(1)
O1-Ni1-O1'	79.5(1)	N1-Ni1'-O2'	94.9(1)
Ni1-O1-Ni1'	100.5(1)	N1-Ni1'-O3	97.0(1)
O1-Ni1-O3	98.3(1)	P1-O3-Ni1	138.1(1)

The resultant dimer is catalytically inactive due to the absence of a free coordination site and is of a type well documented in the literature,[8d,11a,21] several of which are derived from redistribution of monometallic polymerization catalysts. Each nickel is coordinated by two FI_2^- ligands in a square-planar fashion with a *trans*-NO_3 arrangement of the donor atoms. In addition, the phenol oxygen atoms (O1 and O1') bridge both Ni metal. The double O-bridge give rise to a Ni_2O_2 metallacycle, with interatomic Ni1···Ni1' separation of 3.092(3) and Ni1-O1-Ni1' angle of 100.5(1). The Ni···Ni distance is shorter than the sum of the Ni(II) atomic van der Waals radii (3.3 Å) and the chemical interaction may be considered to be

significant.[22] There exists an inversion center at the center of the four-membered ring formed by the two Ni atoms and the two phenolic O atoms. The Ni1-O1-Ni1' and O1-Ni1-O1' angles are 100.5(1) and 79.5(1), respectively. The coordination sphere of the nickel centres are completed by the oxygen atom [Ni-O3 1.982(2)] of dimethyl phosphine oxide, yielding the five-coordinate species and causing an offset binding of the ligands and a deviation in planarity of the metals, each being pulled away from the ligand plane. The Ni-O_{bridge} distances span from 2.008(3) to 2.013(2) (Ni'-O1 and Ni-O1, respectively), while the Ni1-O2' and Ni1'-O2 distances are 1.924(2). The Ni1-N2 and Ni1'-N2' distances are 1.924(2). The Ni-O and the Ni-N distances in **[FI^2-Ni-($OPMe_3$)]$_2$** are slightly longer than those found in the bis[(*N*-2,6-diisopropylphenyl)salicyclaldiminate]Ni(II) complex,[10,11] probably due to the steric hindrance around the metals. In the crystal, other two molecules of O=PMe_3 are presented and they are not involved in interaction with the complex.

6.3.2 Polymerization Experiments and Polymer Characterization. General Remarks.

All olefin polymerizations were performed as described in the Experimental Section. Polymeric products were characterized by ^{1}H and ^{13}C NMR spectroscopy, gel permeation chromatography, FT-IR spectroscopy, and differential scanning calorimetry as required. To determine the density of alkyl group branching in polyethylene homo- and copolymers, integration of the ^{1}H NMR spectra yields the relative density of methyl and other groups versus the polymer backbone resonances.[19] For other copolymerizations, the comonomer incorporation density is determined by integration of the ^{13}C NMR spectra using standard procedures.[19] Characterization of the ethylene + acrylate copolymerization products included NMR spectroscopy (^{1}H, ^{13}C, and ^{1}H-^{1}H COSY) and DSC to differentiate copolymers from simple physical mixtures. Similarly, both the copolymers and representative physical mixtures were subjected to selective solvent extraction experiments to verify that a heterogeneous polyethylene + polyacrylate physical mixture could be cleanly separated, while a random ethylene + acrylate copolymer would remain homogeneous. Furthermore, GPC with UV detection was also performed in addition to GPC with RI detection to allow more accurate detection of acrylate containing polymers.[23] Utilizing both refractive index and ultraviolet GPC detection aids in differentiating mixtures of homopolymers from acrylate-containing random copolymers.

6.3.3 Ethylene Homopolymerization Experiments.

Room temperature ethylene homopolymerizations using the present catalysts were carried out in the presence of the phosphine scavenger/cocatalyst [$Ni(cod)_2$] under conditions minimizing mass transport and exotherm effects.[3,4] It can be seen in Table 3 that bimetallic **FI^2-Ni_2-A** and **FI^2-Ni_2-B** catalysts afford polyethylenes with molecular weights comparable to those produced by the analogous monometallic **FI-Ni_1-A, FI-Ni_1-B,** and **[TMS-FI^2-Ni_1-(PPh_3)]** controls, having polydispersities consistent with single-site processes.

Table 3. Ethylene Homopolymerization Data with and without Cocatalyst Using Mono and Binuclear Ni Aryloxyiminato Catalysts.

Entry	Catalyst	Cocatalyst	Yield (g)	M_w[a]	M_w/M_n	Branches/ 1000C[b]	m.p °C[c]	Activity[d]
1	**FI^2-Ni_2-A**[e]	$Ni(cod)_2$	0.663	10300	2.6	80	68	7.1
2	**FI^2-Ni_2-B**[e]	$Ni(cod)_2$	0.684	10100	2.6	93	66	7.4
3	**FI^2-Ni_2-B**[f]	$Ni(cod)_2$	0.631	10700	2.6	92	68	6.8
4	**FI^2-Ni_2-B**[g]	$Ni(cod)_2$	0.566	10900	2.6	86	68	6.2
5	**FI-Ni-A**[e]	$Ni(cod)_2$	0.167	11700	2.5	52	93	3.6
6	**FI-Ni-B**[e]	$Ni(cod)_2$	0.175	10500	2.5	54	97	3.7
7	**[TMS-FI^2-Ni_1-(PPh_3)]**[e]	$Ni(cod)_2$	0.141	11200	2.6	40	98	3.3
8	**FI^2-Ni_2-A**[h]	-	0.103	6000	2.7	102	60	0.2
9	**FI^2-Ni_2-B**[h]	-	0.196	7000	2.7	105	61	0.4
10	**FI-Ni-A**[h]	-	i	-	-	-	-	-
11	**FI-Ni-B**[h]	-	i	-	-	-	-	

[a]Determined by GPC vs polyethylene standards, uncorrected. [b]Determined by ^1H NMR. [c]Melting temperature determined by DSC. [d]Kg polyethylene/ (mol of Ni·h·atm). [e]Polymerizations carried out with 10 μmol catalyst and 2.0 equiv. cocatalyst / Ni center at 25°C for 40 min in 25 mL toluene at 7.0 atm ethylene pressure. [f]Polymerizations carried out with 10 μmol catalyst and 2.0 equiv cocatalyst / Ni at 25°C for 60 min in 25 mL toluene at 7.0 atm ethylene. [g]Polymerizations carried out with 10 μmol catalyst and 2.0 equiv cocatalyst / Ni at 25°C for 90 min in 25 mL of toluene at 7.0 atm ethylene. [h]Polymerizations carried out with 20 μmol of catalyst at 25°C for 2 h in 25 mL toluene at 7.0 atm ethylene. [i]Negligable polymer obtained.

Note however that the bimetallic catalysts exhibit an approximately two-fold greater polymerization activity along with increased methyl branch density. The branch density assayed by ^1H NMR[19] is ~ 2x that achieved by the mononuclear catalysts under identical reaction conditions, with the greater branch density also supported by depressed DSC-determined melting points. Interestingly, no branches longer than methyl are detected under these reaction conditions in the **FI^2-Ni_2**-mediated polymerization products. The polymerizations mediated by the PMe_3 and PPh_3-containing catalysts exhibit similar activities,

regardless of the phosphine, reflecting the role of the [$Ni(cod)_2$] cocatalyst as an effective phosphine-abstracting "sponge".[8-13] When no cocatalyst is used in the bimetallic polymerizations, modest activity is still exhibited, presumably due to nonbonded repulsions of the proximate phosphine groups, favoring dissociation and catalyst self-activation. Not surprisingly, this effect is slightly more pronounced in the PPh_3 complex than in the PMe_3 analogue (compare Table 3, entries 8 and 9). In contrast, negligible catalytic activity is observed with the monometallic catalysts in the absence of the phosphine-abstracting cocatalyst. Attempts to conduct polymerizations with the bimetallic catalysts at higher temperatures yield negligible polyolefin product and formation of coordinatively saturated **[FI^2-Ni-(OPMe$_3$)]$_2$** species, as described above. This result is reminiscent of the Ni dimers reported by Grubbs *et al*[11d,21] and Brookhart *et al*[8d] for other classes of mononuclear Ni catalysts. Furthermore, variable-temperature ^{31}P NMR spectroscopy was performed on the present binuclear catalyst solutions to examine the phosphine dissociation characteristics of **FI^2-Ni$_2$-A** and **FI^2-Ni$_2$-B.** On warming solutions of **FI^2-Ni$_2$-B** from 25 to 35°C, a free triphenylphosphine signal is observed at δ = 4 ppm in addition to that for **FI^2-Ni$_2$-B**, the intensity of which declines as the free PPh_3 resonance grows in. No other ^{31}P resonances are observed. Furthermore, cooling the solution back to room temperature does not result in re-coordination of the free phosphine to the Ni centers.

6.3.4 Ethylene Homopolymerizations at Varying Ethylene Pressure

One distinctive characteristic of the **FI^2-Ni$_2$** catalysts is the nearly exclusive formation of methyl branches under our standard reaction conditions (7.0 atm ethylene), while significant densities of longer branching are produced in the present monometallic control experiments, as well as with monometallic catalysts investigated by other groups.[10-13,15] As has been previously shown regarding branch formation in other Ni(II)-mediated polymerization processes, the degree and length of branching obtained is highly dependent on the ethylene concentration during the polymerization,[13] a consequence of so-called "chain-walking" processes[8] (Scheme 2) in which incoming monomer activation/enchainment (k_{insert}) competes with β-H elimination/isomerization (k_{elim}).

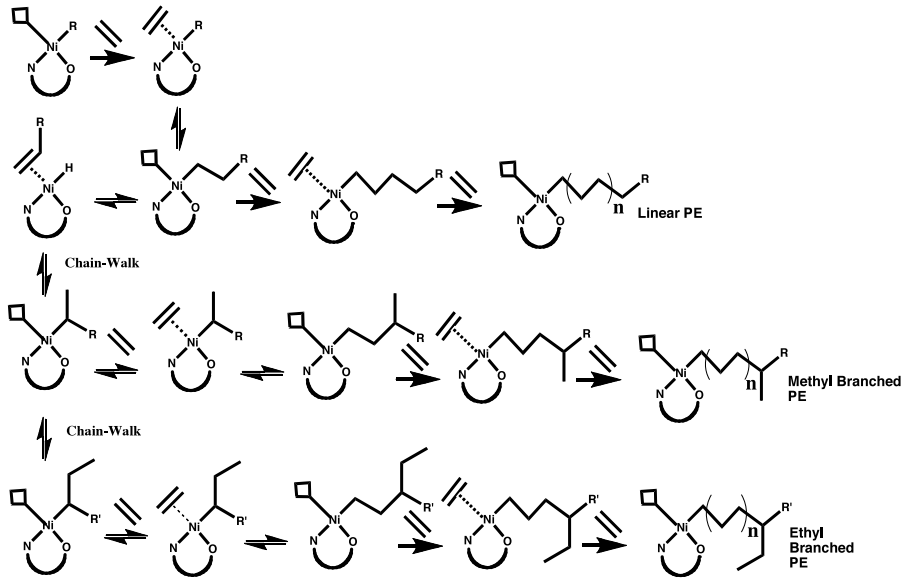

Scheme 2. Chain-Walking Mechanism in Ethylene Polymerizations.

To determine whether similar processes are operative in the present bimetallic systems, polymerizations were carried out over a range of ethylene pressures. As shown in Table 4 and Figure 3, when the ethylene pressure is increased from 3.0 atm to 5.0 to 7.0 atm, ^{13}C signals representative of ethyl branching are suppressed. Polymerizations carried out with the present monometallic catalysts parallel previously reported trends[8d] in polyethylene microstructure, as do the **FI^2-Ni$_2$** bimetallic systems, with a direct proportionality between ethylene concentration and polymerization activity, and suppression of branch formation with increasing ethylene concentration. Note in Figure 3 the relative intensities of the signals corresponding to the α, β, and γ carbons proximate to a methyl branch compared to the polyethylene backbone. These results are in agreement with the pressure dependence trends observed previously by Brookhart.[8d] Long branches are the result of the competing rates of ethylene coordination/insertion versus Ni-alkyl isomerization, where long branches are formed via multiple chain-walks prior to olefin (Scheme 2). In the case of the bimetallic catalyst systems, no more than one isomerization takes place (See Discussion section for additional remarks).

Table 4. Ethylene Homopolymerization at Varying Ethylene Pressure Using Mono and Binuclear Catalysts.

Entry	Catalyst	P (atm)	Yield (g)	Activity[a]	M_w[b]	M_w/M_n	m.p °C[c]	Branches/ 1000C[d]
1	**FI^2-Ni_2-A**	3.0	0.113	7.5	8400	2.4	52	107
2	**FI-Ni-A**	3.0	0.027	3.9	8200	2.5	88	71
3	**FI^2-Ni_2-B**	3.0	0.108	7.2	8200	2.5	53	115
4	**FI-Ni-B**	3.0	0.022	3.9	7900	2.5	82	68
5	**FI^2-Ni_2-A**	5.0	0.292	19.7	9200	2.4	64	99
6	**FI-Ni-A**	5.0	0.070	10.5	9100	2.6	92	62
7	**FI^2-Ni_2-B**	5.0	0.286	19.7	9700	2.4	66	101
8	**FI-Ni-B**	5.0	0.069	10.0	9600	2.5	91	66
9	**FI^2-Ni_2-A**	7.0	0.703	46.9	10100	2.6	68	80
10	**FI-Ni-A**	7.0	0.167	25.2	11700	2.5	93	52
11	**FI^2-Ni_2-B**	7.0	0.711	47.6	10000	2.6	68	92
12	**FI-Ni-B**	7.0	0.175	25.6	10500	2.5	97	54

Polymerizations carried out with 10 μmol catalyst and 2 equiv cocatalyst / Ni center at 25°C for 90 min in 25 mL toluene. [a]Kg of polyethylene/ (mol of Ni·h) Not normalized for atm to illustrate the change in activity. [b]Determined by GPC vs polyethylene standard, uncorrected. [c]Melting temperature determined by DSC. [d]Determined by ^{1}H NMR.

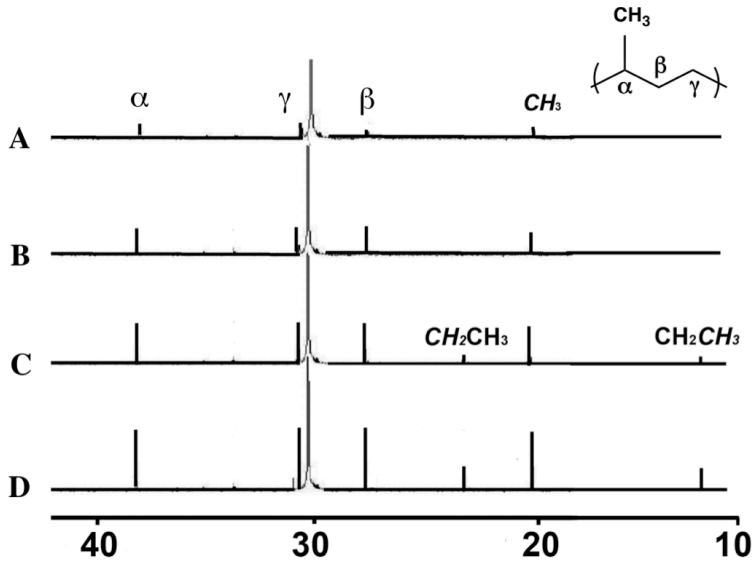

Figure 3. ^{13}C NMR spectra in $CDCl_3$ at 100MHz of PE polymer produced by (a) monometallic catalyst **FI-Ni** at 7.0 atm (b) bimetallic catalyst **FI^2-Ni_2** at 7.0 atm, (c) 5.0 atm, and (d) 3.0 atm ethylene pressure. Note the increase in relative intensity of branches compared to the polymer backbone resonance with decreasing ethylene concentration. Spectral assignments are as indicated.

6.3.5 Ethylene Homopolymerizations in Presence of Polar Additives

Previous work has shown that in the presence of polar co-solvents such as water, the Ni (II) phenoxyiminato catalysts exhibit activity, but it is severely diminished, as are branch densities.[11] In view of the bimetallic *vs*. monometallic catalyst enchainment selectivity differences identified above, it was of interest to investigate the polymerization characteristics of the **FI^2-Ni$_2$** systems versus their **FI-Ni$_1$** analogues in the presence of 225 eq. of various polar additives. Thus, ethylene homopolymerizations were carried out in toluene solutions containing polar additives. As shown in Figure 4 and Table 5, polymerization activities decline in the order, toluene > diethyl ether > acetone > water.

Table 5. Ethylene Homopolymerization Data in Presence of 5% Polar Additives with Mono and Bimetallic Ni Catalysts.

Entry	Catalyst	Cocatalyst	Polar Additive	Yield (g)	M_w[a]	M_w/M_n	Branches/ 1000C[b]	m.p °C[c]	Activity[d]
1	**FI^2-Ni$_2$-A**	Ni(cod)$_2$	Et. Ether	0.299	12700	5.4	86	71	2.2
2	**FI^2-Ni$_2$B**	Ni(cod)$_2$	Et. Ether	0.314	13200	5.2	81	72	2.3
3	**FI-Ni-A**	Ni(cod)$_2$	Et. Ether	0.077	12800	2.4	18	98	1.2
4	**FI-Ni-B**	Ni(cod)$_2$	Et. Ether	0.060	12000	2.4	13	98	0.9
5	**FI^2-Ni$_2$-A**	Ni(cod)$_2$	Acetone	0.067	20200	5.6	82	80	0.5
6	**FI^2-Ni$_2$-B**	Ni(cod)$_2$	Acetone	0.074	21100	5.8	90	78	0.5
7	**FI-Ni-A**	Ni(cod)$_2$	Acetone	0.010	21000	2.9	h	122	0.1
8	**FI-Ni-B**	Ni(cod)$_2$	Acetone	0.009	19100	2.9	h	122	0.1
9	**FI^2-Ni$_2$-A**	Ni(cod)$_2$	Water	e	-	-	-	-	-
10	**FI^2-Ni$_2$B**	Ni(cod)$_2$	Water	0.036	23700	3.9	39	103	0.3
11	**FI-Ni-A**	Ni(cod)$_2$	Water	e	-	-	-	-	-
12	**FI-Ni-B**	Ni(cod)$_2$	Water	0.006	21800	3.1	f	122	0.1

Polymerizations carried out with 10 μmol catalyst and 2.0 equiv cocatalyst / Ni center at 25°C and 1500 equiv. polar additive for 40 min in 25 mL toluene at 7.0 atm ethylene pressure. [a]Determined by GPC vs polyethylene standards, uncorrected. [b]Determined by ^{1}H NMR. [c]Melting temperature determined by DSC. [d]Kg of polyethylene/ (mol of Ni·h·atm). [e]Negligable polymer obtained. [f]Insufficient sample.

While the polar additives significantly reduce polymerization activity, it can be seen that the binuclear catalysts remain ~ 3x more active than the mononuclear analogues and achieve far greater branch densities (~6x for Table 5 entry 2 vs. 4). Note that polymer molecular weights are greatly increased as the polarity of the co-solvent is increased, both in the case of the monometallic and bimetallic catalysts.

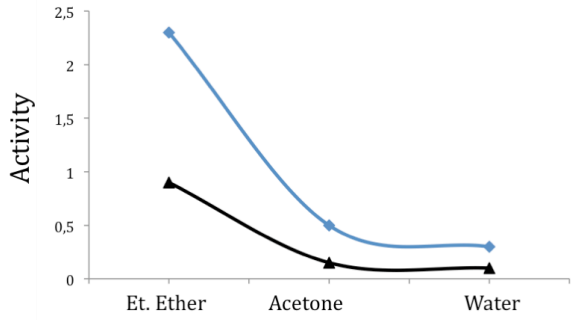

Figure 4. Ethylene Polymerization Activity in kg PE/mol Ni·h·atm in toluene with the Indicated Cosolvents, Mediated by Mononuclear and Binuclear Ni Phenoxyiminato Catalysts.

6.3.6 Ethylene-Norbornenes Copolymerizations

As alluded to in the introduction, previous reports[11b] indicate that norbornene incorporation in mononuclear Ni(II)-catalyzed ethylene copolymerizations is possible but at very low levels. To investigate the comonomer enchainment selectivity of the new **FI^2-Ni$_2$** catalysts, ethylene + norbornene copolymerizations were investigated with the present mono and bimetallic catalysts, using a diversity of norbornenes bearing polar substituents (Figure 5).

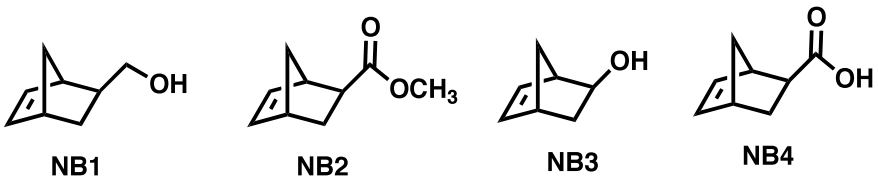

Figure 5. Functionalized Norbornenes Used as Comonomers for Ethylene Copolymerizations.

It is found that modest comonomer enchainment levels are achieved with the present monometallic **FI-Ni$_1$** catalysts (Table 6), in accord with the results reported for comparable mononuclear catalysts systems.[11b] In marked contrast, ethylene + norbornene copolymerizations mediated by binuclear **FI^2-Ni$_2$-A** and **FI^2-Ni$_2$-B** proceed with 3-4 x greater activity and with 3-4 x greater selectivity for comonomer enchainment than the **FI-Ni** mediated processes under identical reaction conditions. Note that product molecular weights are comparable to those in the homopolymerization experiments discussed above. Despite somewhat increased polydispersities, both **FI^2-Ni$_2$-A** and **FI^2-Ni$_2$-B** produce polymers with microstructures and with molecular weights similar to those of the monometallic catalysts. Attempts to carry out ethylene copolymerizations in the presence of monomer **NB4** yielded

negligible polymeric product. This result likely reflects the acidity of this comonomer, since ^{1}H NMR spectra show that the ligand has been protonated at the hydroxyl functionality.

Table 6. Ethylene Copolymerization Data in the Presence of Norbornene and Functionalized Norbornenes **NB1-4** Using Mono- and Bimetallic Ni Phenoxyiminato Catalysts.

Entry	Catalyst	Comonomer	Yield (g)	M_w[b]	M_w/M_n	Branches/ 1000C[c]	m.p °C[d]	Activity[e]	% Incorp.[f]
1	**FI^2-Ni$_2$-A**[a]	NB	0.558	66400	5.2	34	107	1.3	9
2	**FI^2-Ni$_2$-B**[a]	NB	0.504	65800	4.5	38	106	1.2	11
3	**FI-Ni-A**[a]	NB	0.072	63200	2.3	9	124	0.3	3
4	**FI-Ni-B**[a]	NB	0.066	64000	2.1	11	124	0.3	3
5	**FI^2-Ni$_2$-A**[a]	NB1	0.488	62600	4.6	39	105	1.2	8
6	**FI^2-Ni$_2$B**[a]	NB1	0.502	63500	4.8	33	109	1.2	9
7	**FI-Ni-A**[a]	NB1	0.067	64900	2.0	9	122	0.3	≤ 2
8	**FI-Ni-B**[a]	NB1	0.059	63800	2.1	9	122	0.3	3
9	**FI^2-Ni$_2$-A**[a]	NB2	0.444	61800	5.2	33	112	1.1	8
10	**FI^2-Ni$_2$-B**[a]	NB2	0.450	67300	4.8	37	110	1.1	8
11	**FI-Ni-A**[a]	NB2	0.054	65400	2.2	8	122	0.2	≤ 2
12	**FI-Ni-B**[a]	NB2	0.058	62000	2.6	8	126	0.3	2
13	**FI^2-Ni$_2$-A**[a]	NB3	0.398	66100	4.4	33	120	0.9	7
14	**FI^2-Ni$_2$-B**[a]	NB3	0.411	64200	4.6	29	112	0.9	8
15	**FI^2-Ni$_2$-A**[a]	NB3	0.029	64100	2.2	8	122	0.1	≤ 2
16	**FI-Ni-B**[a]	NB3	0.033	62900	2.5	8	124	0.1	≤ 2

[a]Polymerizations carried out with 10 μmol catalyst and 2.0 equiv. cocatalyst / Ni center at 25°C and 225 equiv. of comonomer for 60 min in 25 mL toluene at 7.0 atm ethylene pressure. [b]Determined by GPC vs polyethylene standard, uncorrected. [c]Determined by ^{1}H NMR. [d]Melting temperature determined by DSC. [e]Kg of polyethylene/ (mol of Ni·h·atm). [f]Molar percentage determined by ^{13}C NMR.

6.3.7 Ethylene-Acrylate Copolymerizations

Up to this point, we have focused on determining whether a second catalytic center might enhance the enchainment characteristics that make neutrally charged monometallic Ni catalytic systems distinctive. However, there are also polar comonomers of interest that are only minimally responsive to the monometallic **FI-Ni** systems, such as methylacrylate or methyl methacrylate. It was therefore of interest to investigate the copolymerization characteristics of the present **FI^2-Ni$_2$** catalysts. Thus, ethylene + methylacrylate (**MA**) and methylmethacrylate (**MMA**) copolymerizations mediated by the **FI^2-Ni$_2$** and **FI-Ni$_1$** catalytic systems were studied in detail. While the present monometallic catalysts co-enchain

negligible **MA** or **MMA**, as assayed by ^{1}H and ^{13}C NMR spectroscopy, the bimetallic catalysts incorporate up to 8% methyl methylacrylate and up to 11% methacrylate in the polyethylene (Table 7).

Table 7. Ethylene Copolymerizations in the Presence of Methylacrylate (MA) and Methylmethacrylate (MMA)

Entry	Catalyst[a]	Comon.	Yield (g)	M_w[b]	M_w/M_n	Br/ 1000C[c]	m.p °C[d]	Activity[e]	% Incorp.[f]
1	**FI^2-Ni_2-A**	MMA	0.700	8000	1.4	48	106	1.7	8
2	**FI^2-Ni_2-B**	MMA	0.690	7900	1.7	39	106	1.6	9
3	**FI-Ni-A**	MMA	g	-	-	-	-	-	-
4	**FI-Ni-B**	MMA	g	-	-	-	-	-	-
5	**FI^2-Ni_2-A**	MA	0.722	6300	1.6	36	108	1.8	11
6	**FI^2-Ni_2B**	MA	0.741	6700	1.7	37	108	1.8	11
7	**FI-Ni-A**	MA	g	-	-	-	-	-	-
8	**FI-Ni-B**	MA	g	-	-	-	-	-	-

[a]Polymerizations carried out with 10 μmol catalyst and 2.0 equiv. cocatalyst / Ni center at 25°C and 225 equiv. of polar additive for 60 min in 25 mL toluene at 7.0 atm ethylene pressure. [b]Determined by GPC vs polyethylene standard, uncorrected. [c]Determined by ^{1}H NMR. [d]Melting temperature determined by DSC. [e]Kg of polyethylene/ (mol of Ni·h·atm). [f]Molar percentage determined by ^{13}C NMR. [g]Negligible polymer obtained.

In both cases, the copolymers produced yield physical and NMR characteristics similar to random ethylene-acrylate copolymers reported in the literature[24,25] prepared using other transition metal catalysts and/or completely different polymerization pathways (Figure 6).

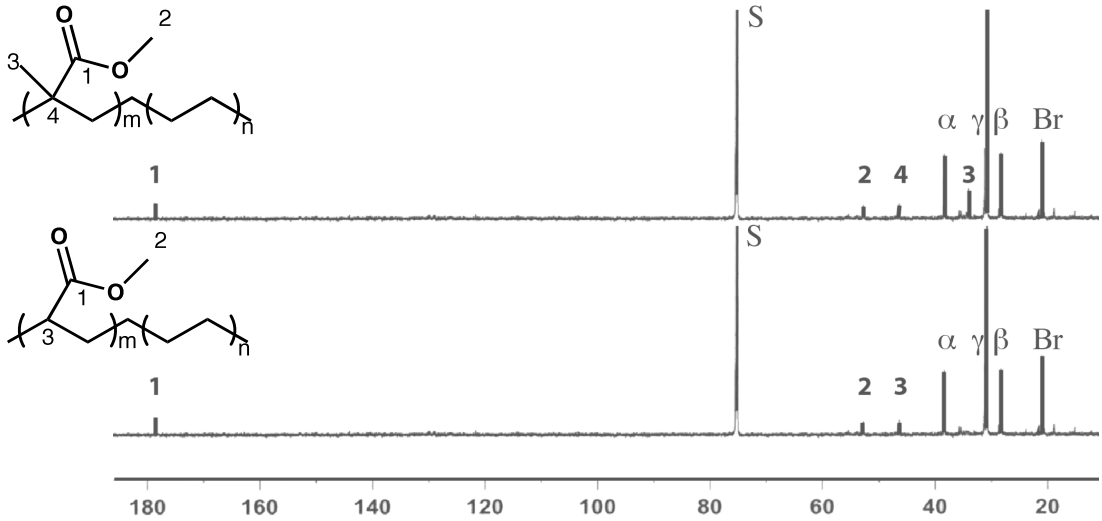

Figure 6. ^{13}C NMR spectra at 100 MHz in $CDCl_3$ of (top) the ethylene + MMA copolymer and (bottom) ethylene + MA copolymer produced by binuclear catalyst **FI^2-Ni_2-A**.

In the present copolymers, the absence of significant ^{13}C NMR resonances at δ = 120 (a) and 149 (b) ppm rule out the possibility of significant methylenoate terminated branching end groups.[25d]

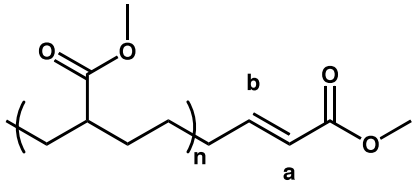

Therefore, essentially all of the MMA units incorporated into the copolymer are enchained in the polymer backbone. In addition, we find that the monometallic catalyst **[TMS-FI^2-Ni-(PPh$_3$)]** is also incapable of mediating ethylene + acrylate copolymerizations, further supporting a bimetallic enchainment pathway. All product polymer NMR spectra were assigned according to the literature for the products of cationic, monometalic Ni catalysts competent to copolymerize acrylates + ethylene, and are in complete agreement.[25]

Additional selective extraction, GPC, and NMR experiments were conducted to establish that the products of these **FI^2-Ni$_2$**-mediated copolymerizations are indeed random copolymers and not simple physical mixtures of polyethylene and polymethylcrylate or polymethylmethacrylate. These experiments included selective extraction of the copolymers with hot dichloromethane, which dissolves commercially available MMA homopolymers (M_w = 120,000) but not PE (M_w = 21,000; Sample of Table 5, entry 6); results are shown in Figures 7 (^{13}C NMR) and 8 (RI-GPC), which indicate that the physically mixed homopolymers are readily separated by extraction.

These results are obtained by selective extracting 10:1 of PE:PMMA physical mixture of two homopolymers. While the homopolymers could be completely separated, in the case of the copolymer, no separation is achieved.

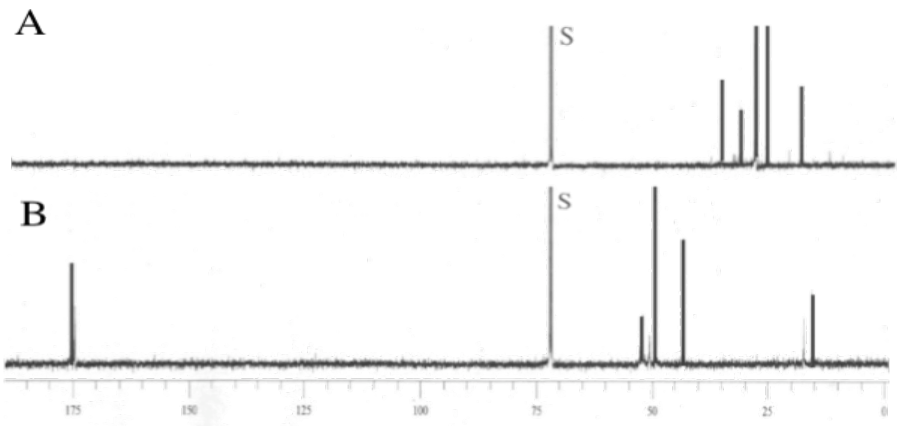

Figure 8. ^{13}C NMR of at 100MHz in $CDCl_3$ of (a) the solid highly-branced PE phase and (b) the wash commercially available PMMA extract after extracting a physical mixture of the homopolymers with hot CH_2Cl_2. Note the resulting spectra show complete separation of homopolymers, as determined by the presence or absence of carbonyl resonance at 175 ppm and the PE backbone resonance at 30 ppm.

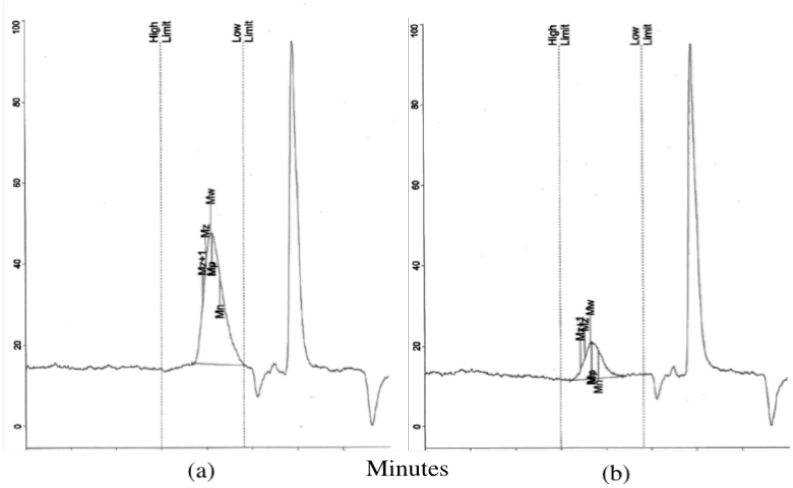

Figure 8. GPC with RI detection of (a) the residual solid PE phase and (b) the PMMA extract after extracting a physical mixture of homopolymers with hot CH_2Cl_2.

In addition to the above evidence, the monomodal traces in the RI-detected GPC (Figure 8) for the isolated pure PE phase and the pure PMMA extract, in conjunction with the NMR spectra, demonstrate that the physical mixture can be separated. To further distinguish the copolymer from its homopolymer mixture, UV detected GPC was also performed to demonstrate that the **FI^2-Ni_2**-derived MMA + PE copolymer is monomodal and distinct from a PMMA homopolymer. As shown in Figure 9, ethylene + acrylate copolymer (blue) is clearly monomodal and distinguishable from the PMMA homopolymer (red). DSC was also

performed on the MMA + ethylene copolymer and the same physical mixture of homopolymers.

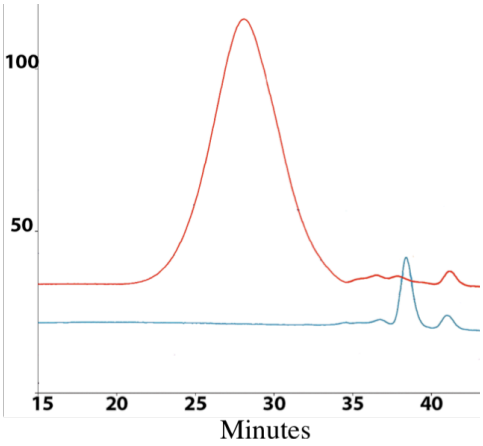

Figure 9. GPC with UV detection at 210 nm from polymer samples of (red) PMMA homopolymer (Mw= 120,000) and (blue) **FI^2-Ni$_2$**- derived ethylene + MMA copolymer (Entry 1, Table 7). Note the distinct retention time of each sample.

As seen in Figure 10, two distinct thermal transitions are observed in the case of the physical mixture, whereas a single transition is evident for the copolymer at 108°C, in agreement with the literature.

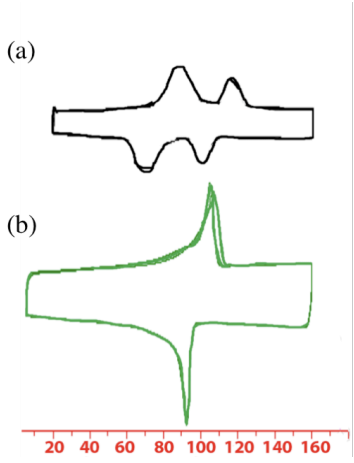

Figure 10. Second scan DSC of (a) physical mixture of PMMA and PE homopolymers (b) the ethylene + PMMA copolymer (Entry 1, Table 7). Note the single T_g obtained in the copolymer as opposed to the individual T_g values observed in the polymer mixture

Additional copolymer characterization was carried out by IR spectroscopy. The FT-IR spectrum, shown in Figure 11 exhibit characteristic MMA $\nu_{C=O}$ mode at 1738 cm^{-1} and two PE

modes at 1480 and 718 cm^{-1}, corresponding to the scissoring and rocking vibrations of the ethylene co-units.[13b,26]

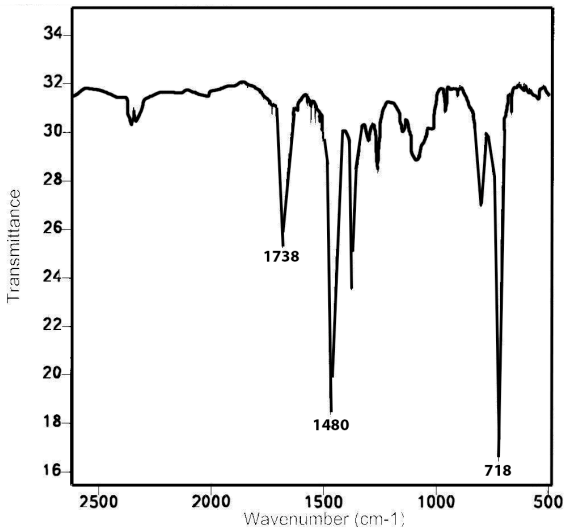

Figure 11. IR spectra of the ethylene + PMMA copolymer copolymer in a KBr pellet produced by bimetallic catalyst **FI^2-Ni_2**. The band at 1738 cm^{-1} corresponds to MMA and two bands at 1480 and 718 cm^{-1} correspond to a polyethylene chain.

Finally, ^{1}H-^{1}H COSY NMR spectroscopy was performed on both homopolymers and the result compared to that on the ethylene + MMA copolymer. The PMMA homopolymer exhibits no discernable cross-peaks as expected, and the PE spectrum exhibits a single cross-peak indicating branch proton interactions with the backbone protons, as expected. In contrast, the ethylene + MMA copolymer exhibits new cross-peaks absent in the homopolymer spectra at δ = 1.4 and 1.8 ppm (Figure 12, circled), corresponding to the proximate enchained acrylate (**A-CH_2**) andethylene units (**PE-CH_2**). This crosspeak is relatively weak compared to the **PE-CH_3** to **PE-CH_2** interaction, since the copolymer is very highly branched and contains far more methyl branches than enchained acrylate units (the acrylate content is only 8%). The results of this experiment, in conjunction with the ^{13}C NMR chemical shift arguments, FT-IR, and DSC data, show definitively that this material is a true random copolymer.

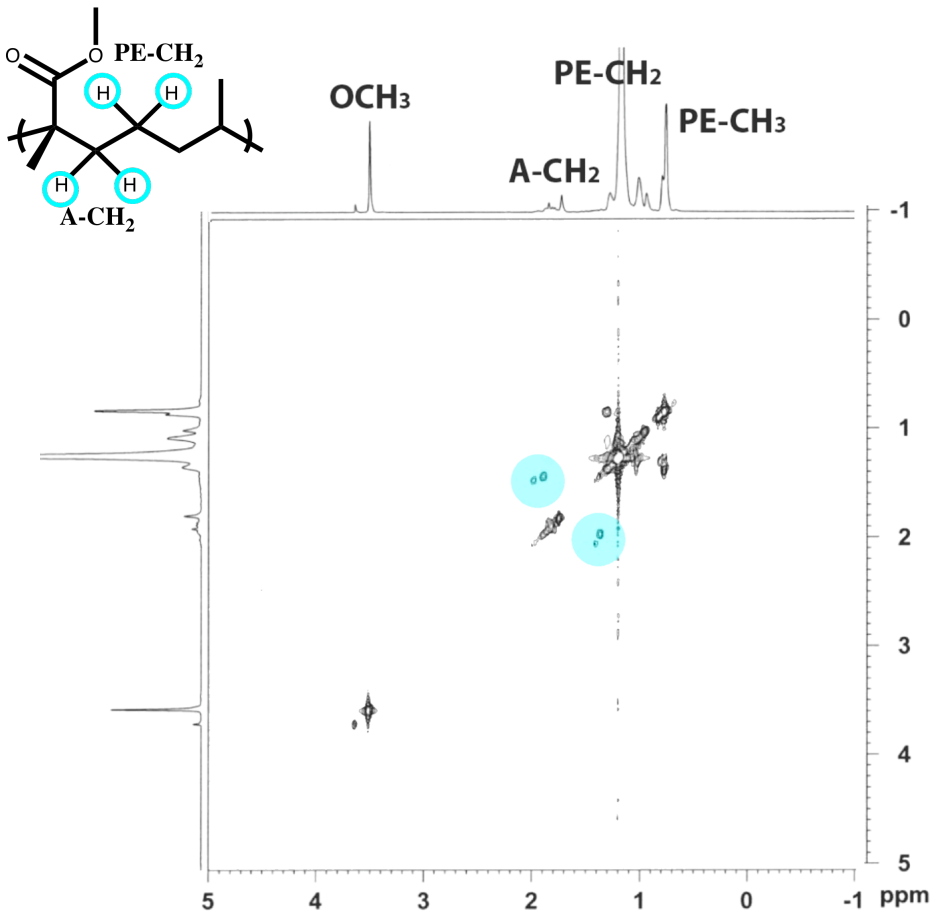

Figure 12. COSY at ^{1}H-^{1}H NMR in $CDCl_3$ at 600MHz of PE+PMMA Copolymer Produced by Binuclear Catalyst **FI^{2}-Ni$_2$.**

6.3.8 Ethylene-Acrylate Copolymerization Mechanism

With the identity of the **FI^{2}-Ni$_2$**-derived ethylene + acrylate copolymers confirmed, the next question that arises regards the pathway leading to their formation. To date, the vast majority of group 10 catalysts that produce ethylene + acrylate copolymers are either cationic Ni systems proceeding *via* a coordinative/insertive pathway, or Pd systems which initiate *via* a radical pathway.[27] It is therefore important to establish the pathway traversed in the present bimetallic catalysts. To explore the possibility of radical pathways, CH_3OD was employed as a radical trap.[28] In the case of metal complex-mediated radical polymerization, it has been shown that the weaker methanol C-H bond is abstracted by radical species, whereas for ionic polymerization systems, the more acidic methanol OD is abstracted to yield deuterated acrylate monomer.[28] In the present case, CH_3OD (0.02 mmol) was added to a solution of **FI^{2}-Ni$_2$-B** (0.01 mmol), [Ni(cod)$_2$] (0.02 mmol), and MMA (0.04 mmol) under an ethylene atmosphere. ^{1}H and ^{2}D NMR spectroscopic analysis of the reaction solution shows that the

CH_3OD remains unreacted, ruling out the possibility of either predominant cationic or radical copolymerization pathways.

To further probe the nature of the of **FI^2-Ni_2-**mediated copolymerization process, ethylene and methylmethacrylate reactivity ratios were determined for the present copolymer formation process. The analysis was performed using the Mayo-Lewis equation[29] (eq, 1), and compared to published reactivity ratios.[30] In eq. 1, ϑm_i is the mole fraction of monomer i incorporated into the copolymer, M_i is number of moles of monomer i present in the reaction solution, and r_i is the reactivity ratio.

$$\frac{\vartheta m_1}{\vartheta m_2} = \frac{M_1(r_1 M_1 + M_2)}{M_2(r_2 M_2 + M_1)} \tag{1}$$

Under the present polymerization reaction conditions, the radical copolymerization of ethylene + MMA should yield $r_{ethylene}$= 0.2 and r_{mma}= 17.[28] Calculating the same r values for the **FI^2-Ni_2**-mediated copolymerizatons, as determined by the NMR assay, yields $r_{ethylene}$= 0.34 and r_{mma}= 12.2. Likewise, under the present reaction conditions, the radical copolymerization of ethylene + MA would yield an $r_{ethylene}$= 0.2 and r_{mma}= 11. In contrast, the r values for the present **FI^2-Ni_2**-mediated copolymerizatons, as determined by the NMR assay are $r_{ethylene}$= 0.33 and r_{mma}= 12.9. These results argue strongly against significant radical pathway contributions to product formation.

6.3.8 Low Temperature Catalyst NMR Studies

In neutral Ni aryloximinato coordinative polymerization catalysts, an agostic interaction can be identified by ^{1}H NMR at low temperatures[8d] involving the vacant Ni coordination site and a β C-H unit on the growing polymer chain (Complex **R**, Scheme 3). It was therefore of interest to determine whether similar interactions take place in the present bimetallic catalysts or whether the presence of a second Ni center might offer additional possibilities. To this end, low temperature ^{1}H NMR studies were undertaken on *in situ* generated **FI-Ni_1** and **FI^2-Ni_2** alkyl derivatives. Thus, $[NiCl_2(PMe_3)_2]$[17] was reacted with the sodium salt of ligand **FI^2-H_2**, affording **[FI^2-Ni_2-$Cl_2(PMe_3)_2$]** (complex **K** in Scheme 3). Next, *n*-butyl Grignard was used to generate the very thermally unstable Ni-alkyl species.

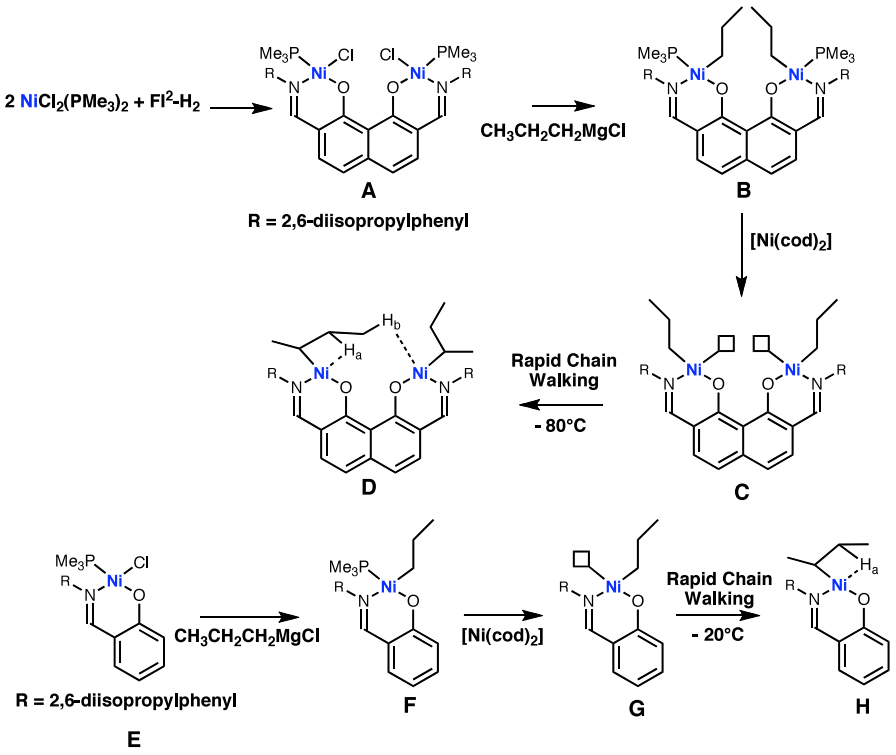

Scheme 3. Synthesis and Possible Agostic Interactions in Model *n*-Butyl Derivatives of Catalysts **FI-Ni$_1$** and **FI^2-Ni$_2$**.

This solution was rapidly transferred to a cold NMR tube containing [Ni(cod)$_2$] and maintained at -20°C until spectroscopic experiments could be performed. The same procedure was then used to produce an **FI-Ni$_1$** *n*-butyl derivative of the mononuclear Ni catalyst. Note that instead of the *n*-propyl derivative originally investigated by Brookhart in mononuclear complexes,[8d] the longer *n*-butyl group was chosen to provide a branch more capable of simultaneously acessing both Ni sites. This is evidenced in molecular modeling[31] where a doubly-bond *n*-propyl chain would have an C-H···Ni bond length of ~3.5 Å at lowest energy (Figure 13a), as opposed to a C-H···Ni bond distance of ~2.8 Å in the butyl species (Figure 13b).

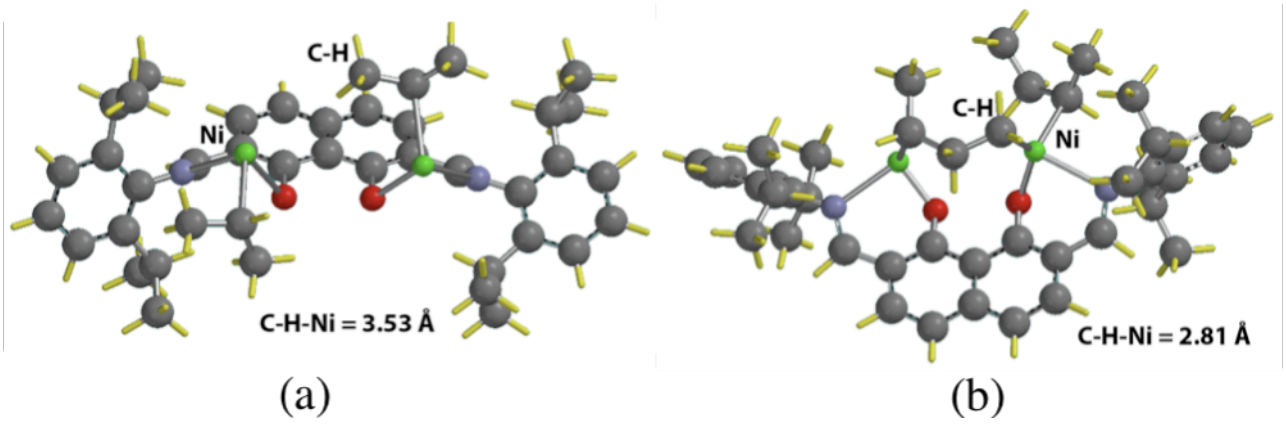

Figure 12. Molecular models of (a) *sec*-Propyl branched model compound and (b) Butyl branched model compound.

The ^{1}H NMR spectrum of the **FI-Ni$_1$** alkyl complex at -20°C suggests that *n*-alkyl isomerization has already taken place, similar to that observed by Brookhart, *et al*[8d] for *n*-propyl complexes, yielding here complex **R** (Scheme 3) and exhibiting a Ni-CH resonance as a very broad singlet at –2.2 ppm. Lowering the temperature to -80 °C reveals a broad signal at –9.9 ppm, assignable to a Ni agostic species, similar to that of a previously reported example where Brookhart, *et al*[8d] installed an *n*-propyl group and observed an agostic signal at -13.9 ppm.

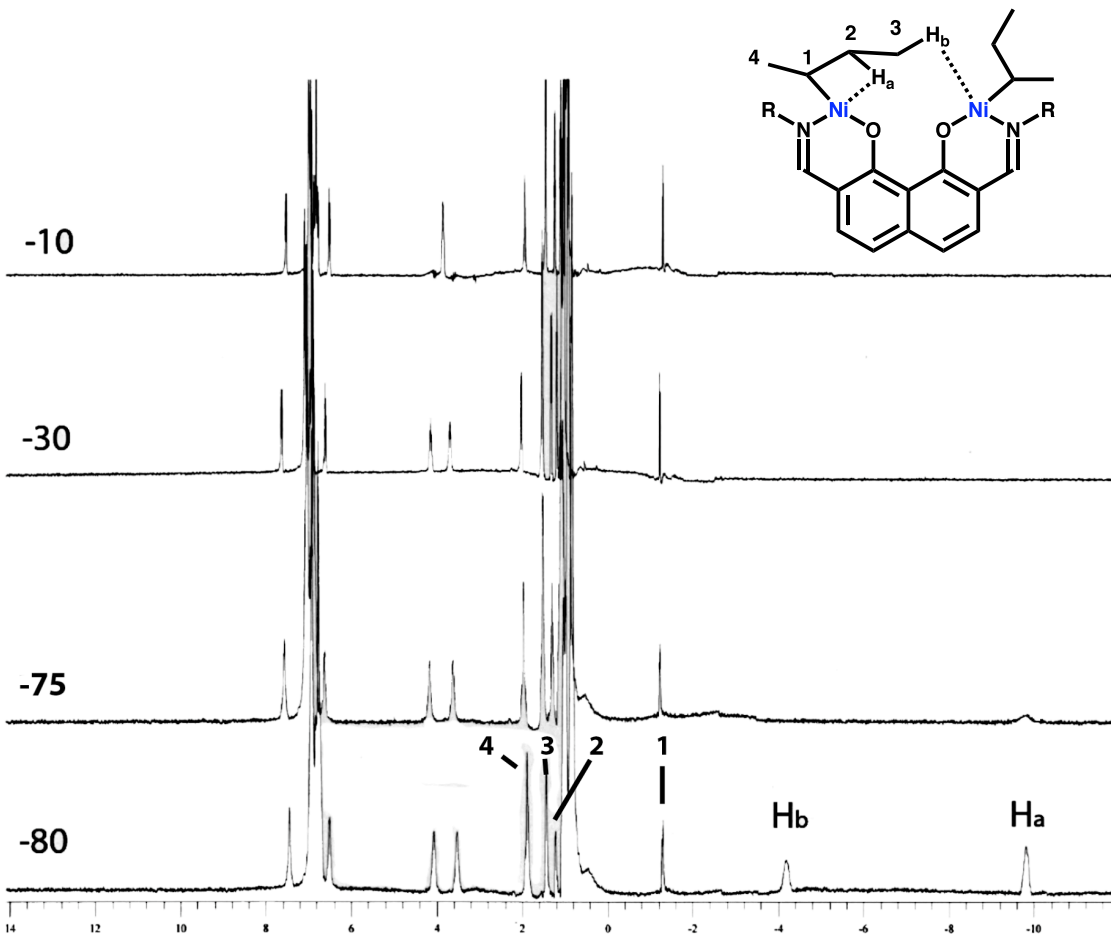

Figure 13. Variable Temperature ^{1}H NMR at 500 MHz in toluene-d_8 going from -80 to 10 ºC of the Bimetallic **FI^{2}-Ni$_2$** di-butyl.

At the same low temperatures, the bimetallic **FI^{2}-Ni$_2$** dibutyl complex exhibits a similar agostic resonance, as shown in Figure 14. However, solely in the binuclear case is a second resonance is observed at –4.1ppm. The ^{1}H-^{1}H COSY NMR spectrum of **[FI^{2}-Ni$_2$-(*n*-butyl)$_2$]** at -80°C (Figure 15) exhibits two separate alkyl chains- one chain bond to a Ni participating in no agostic interaction, and another chain participating in two agostic interactions (Scheme 3). These two alkyl chains can readily be distinguished by the localized interactions between the agostic protons at -4.1 ppm, and -9.9 ppm with the protons on the CH_2 between them, at 1.9 ppm, as well as with other proximate protons. The non-agostic chain exhibits a separate group of alkyl proton interactions within the -1.0 ÷ 1.9 ppm region, which can only be tentatively assigned.

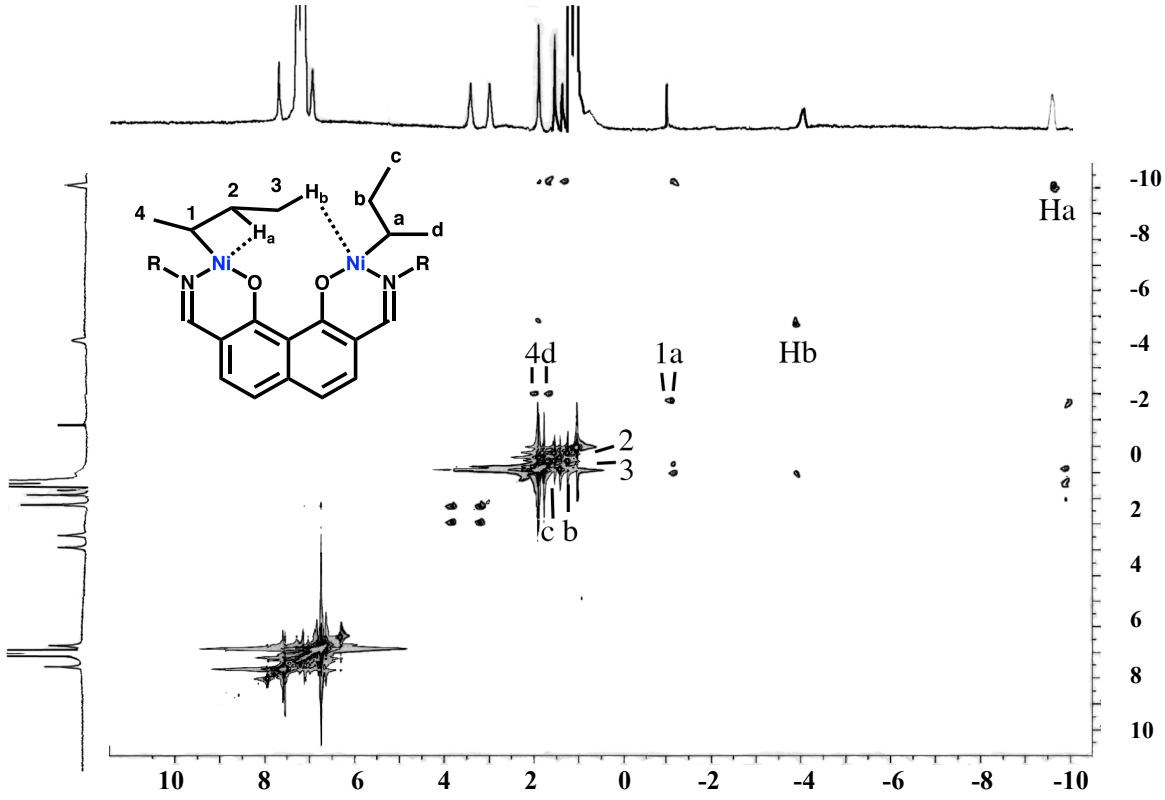

Figure 14. ^{1}H-^{1}H COSY NMR spectrum of at 400MHz and -80°C in toluene d_8 of the Bimetallic Model Complex.

6.4 Discussion

6.4.1 Ethylene Homopolymerizations

Comparing the ethylene homopolymerization characteristics of the monometallic **FI-Ni$_1$-** and **[TMS-FI^2-Ni$_1$]-**derived catalysts with the **FI^2-Ni$_2$**-derived bimetallic systems reveals significant differences which are most plausibly attributed to cooperative effects involving both Ni centers. The **FI^2-Ni$_2$-A/B** catalyst activity and product polyethylene branch density and architecture determined by ^{1}H NMR[19] is ~ 2x that achieved by the mononuclear catalysts under identical reaction conditions, and is confirmed by depressed DSC-determined melting points. As noted above, the branching in the **FI^2-Ni$_2$**-derived polyethylenes is more emthyl-rich. Moreover, [**TMS-FI^2-Ni$_1$-(PPh$_3$)**] polymerization properties show both activity and polymer microstructure similar to that of the present **FI-Ni** and other monometallic catalysts,[8-11] verifying that the increased activity and methyl-rich branch density is exclusive

to catalysts bearing a second, adjacent catalytic Ni center. Interestingly, product molecular weights and polydispersities are essentially indistinguishable for the monometallic and bimetallic polymerization systems.

In the absence of a cocatalyst, the present mononuclear systems do not produce significant polyethylene, in agreement with previous observations for similar mononuclear catalysts,[8-11] In contrast, the present bimetallic catalysts produce essentially the same polyethylenes but with increased branch densities and concurrently depressed melting points, albeit at somewhat reduced activities versus the cocatalyzed polymerizations (Table 1, entries 8-11). This particular cocatalyst-related productivity difference between **FI^2-Ni$_2$-A**, **FI^2-Ni$_2$-B**, and the mononuclear analogues may reflect previously reported phosphine dissociation-related steric and electronic factors.[14] Typically, equilibria between such phosphine-coordinated and uncoordinated species heavily favor the former, however the proximate bulky phosphine ligands in **FI^2-Ni$_2$-A** and **FI^2-Ni$_2$-B** likely favor phosphine dissociation, as indicated by both ^{31}P NMR and x-ray diffraction results.

The distinctive ethylene homopolymerization characteristics of the **FI^2-Ni$_2$**-based catalysts doubtless reflect a complex interplay of kinetics and thermodynamics. In regard to those factors underlying the relative importance of propagation and chain walking rates versus the mononuclear analogues, it is clear that any cooperative effects such as enhanced substrate binding/preorganization (e.g. structure **A**) as proposed for bimetallic group 4 polymerization catalysts, do not influence the overall propagation/chain transfer rate ratios in a way that significantly alters the product polyethylene M_w or the polydispersity. However, significant differences in product macromolecule architecture are observed, with higher branch densities and the greater selectivity for methyl branch formation in the **FI^2-Ni$_2$-**mediated homopolymerizations (Tables 3,4; Figure 3) indicating that the presence of the second Ni center enhances chain walking but suppresses ethyl branch formation versus FI-Ni-mediated processes: 1) by intercepting species such as **S** in Scheme 4 prior to isomerization to species such as **T** ($k_{PropagationMe}$)[ethylene] >> $k_{EtBranch}$, 2) because the equilibrium to form **T** is for steric and/or electronic reasons unfavorable, or 3) because ($k_{PropagationEt}$)[ethylene] is for steric and/or electronic reasons slower than ($k_{PropagationMe}$)[ethylene].

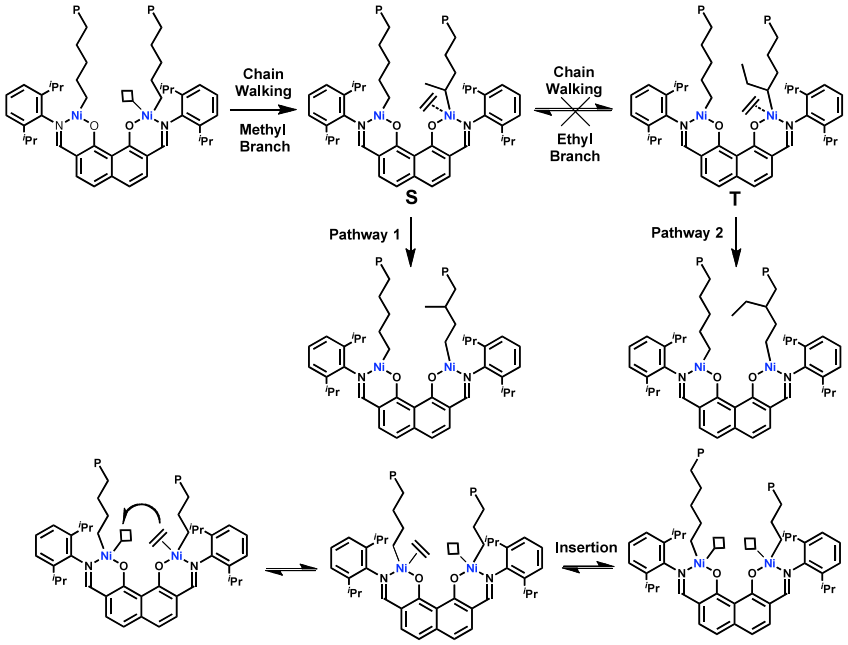

Scheme 4. Methyl Branch Formation Pathways in **FI^2-Ni$_2$-**Mediated Ethylene Homopolymerization.

From the low temperature NMR studies of **[FI^2-Ni$_2$-(*n*-butyl)$_2$]** (Figures 14, 15) implicate binuclear agnostic interactions, it is conceivable that secondary agnostic binding as in **U** may influence the β-H elimination/-readdition kinetics of the chain walking processes, while increased propagation kinetics may reflect monomer binding to the neighboring Ni center, thereby increasing local concentrations (Scheme 5).

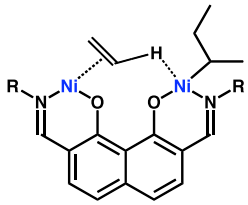

U

The predominance of methyl branch formation likely suggests that the presence of the second Ni center suppresses insertion pathway 2 versus pathway 1 (Scheme 4) via the rapid switching of the ethylene monomer from one catalyst center to the other before a second chain-walk can take place, in addition to the amount of monomer coordinated from solution. When the ethylene concentration is increased, the propagation rate is greatly increased and the competing rate of chain-walking reduced, suppressing ethyl branch formaton, indicating that pathway 1 takes place faster than β-H/rearrangment.

In both this and our previously reported work[14] the **FI^2-Ni$_2$-B** catalysts adhere to the same trends in activity and polydispersity as the **FI^2-Ni$_2$-A** analogues: polymerizations exhibit comparable activities between large and small phosphine bearing complexes in all cases, except when water is added. Note also that while significant increases in activity and branching are observed for the bimetallic catalysts, the molecular weights of the polyethylene produced by the mono and binuclear systems are similar.

6.4.2 Copolymerizations with Polar Comonomers

In copolymerizations with functionalized norbornenes (Figure 5), the present mononuclear catalysts produce copolymers with relatively small levels of polar commoner incorporation, in agreement with literature results for similar mononuclear Ni(II) catalysts.[8-11] In marked contrast, the bimetallic **FI^2-Ni$_2$**-derived catalysts exhibit 3-4x enhanced enchainment selectivities and polymerization activities (Table 6) versus the mononuclear analogues, regardless of the polar norbornene substituent, as assayed by NMR spectroscopy. Minimal influence of **NB** polar substituent skeletal position is observed, similar to previous reports with other mononuclear Ni(II) catalysts.[11b] **FI^2-Ni$_2$-A** and **FI^2-Ni$_2$-B** enchain significant quantities of polar-functionalized norbornene (7-9%) while simultaneously maintaining high methyl branch densities (~ 8-10 x the level of the mononuclear catalysts) in the oligoethylene blocks. This is likely due to rapid re-insertion of the growing polymer onto the second metal site after it has undergone elimination by the first.

In the case of ethylene copolymerizations with methylacrylate or methylmethacrylate as comonomers, the present monometallic Ni(II) catalysts are incapable of significant comonomer co-enchainment. However, in the case of the bimetallic **FI^2-Ni$_2$**-derived systems, 8-11% incorporation is achieved as determined by NMR spectroscopic assay. As expected from the ethylene homopolymerizations, once again the [**TMS-FI^2-Ni$_1$-(PPh$_3$)**] exhibits reduced activity and minimal polar comonomer enchainment, similar to that of the conventional monometallic phenoxyiminate systems. To explain selectivity for co-enchainment of a previously unresponsive comonomer, we consider the insertion pathway and its potential modification when two metal centers are in close proximity. It has been proposed[25] that acrylate enchainment in the mononickel polymerization systems is impeded by the formatin of a relatively stable/inert six-membered resting state that occupies the

otherwise vacant Ni site used for subsequent ethylene binding/ insertion (Scheme 2, Figure 16a).

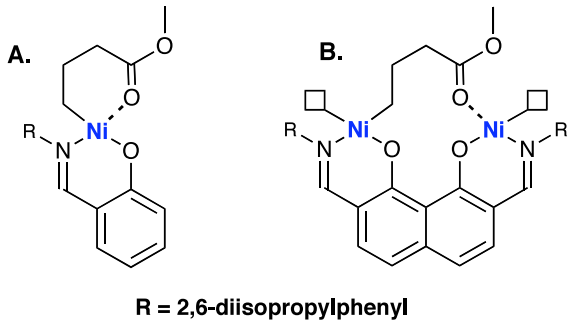

Figure 16. Proposed Resting States of Mono and Binuclear Catalysts After Acrylate Insertion

Interestingly, it was recently argued that in the case of styrene polymerizations with monometallic organotitanium CGC catalysts,[3,4] an analagous "back-biting" occurs, in which a styreneic arene group binds to the cationic metal catalytic center and effectively blocks the monomer (Structure **B**). However, in the case of bimetallic CGC Ti_2 catalytic systems, the styrene π-system is proposed to be pulled away from one Ti center by the second, proximate Ti, resulting in far greater monomer access, enhanced propagation rate and altered insertion regiochemisry.[3] We therefore suggest that an analogous process is operative in the present bimetallic group 10 systems, wherein a second catalytic site 'peels' the acrylate away from the insertion site and therefby facilitates macromolecule propagation subsequent to acrylate activation/enchainment (Figure 16B). The wide array of characterization techniques applied confirm that the resulting copolymer is a genuine random copolymer rather than a physical mixture of the homopolymers. The copolymer can differentiated from a physical admixture by DSC, GPC, FT-IR, and selective extraction. Furthermore, ^{1}H-^{1}H COSY NMR experiments evidence distinctive spin-spin interactions within the copolymer structure, not present in the homopolymers, corresponding to neighboring enchained acrylate and ethylene units, seen in Figure 11 as cross-peaks at δ = 1.8 and 1.4 ppm. Note that polymerizations activities are reduced approximately four-fold in copolymerizations of acrylate with ethylene compared to ethylene homopolymerizations under the same reaction conditions. While the present density of acrylate incorporation is by no means the highest possible for all transition metal catalysts capable of producing PE + acrylate copolymers under all polymerization conditions,[25] it is the highest, to our knowledge, of all neutrally-charged catalytically systems.

6.4.3 Bimetallic Influence on Olefin Polymerization Pathways

The pathway by which the present bimetallic catalyst olefin enchainment cooperativity effects take place is the central interest in this investigation: What is the nature of the catalytic interaction between the two Ni centers? Radical trapping via CH_3OD was performed to test for radical polymerization pathways, as alternatives to a coordinative polymerization process. The deuterated methanol probe argues that no significant concentrations of radical species are present.[29] However, since radical traps can potentally modify the catalyst under investigation influence subsequent polymerization pathways, ethylene + acrylate reactivity ratios were also analyzed for the **FI^2-Ni$_2$**-mediated copolymerizations. For a radical polymerization process the ethylene + MMA reactivity ratios under the present reaction conditions should be approximately: $r_{ethylene}$= 0.2 and r_{MMa}= 17[28] whereas values for **FI^2-Ni$_2$**-mediated copolymerizatons are: $r_{ethylene}$= 0.34 and r_{MMa}= 12.2. For ethylene and MA, a radical copolymerization mechanism would give: $r_{ethylene}$= 0.2 and r_{MA}= 11 whereas the measured values for the present copolymerizatons are: $r_{ethylene}$= 0.33 and r_{MA}= 12.9. In fact, solving for the incorporation ratio ($\vartheta m_{ethylene}$ / ϑm_{MMA}) in the Mayo-Lewis equation for a radical process yields an ethylene/MMA incorporation ratio of 1.7 under the present conditions. Because the moles of monomer incorporated into the copolymer is known, solving for the expected MMA incorporation were this a radical process under the same reaction conditions yields a predicted MMA incorporation level of over 30 mol%, a value in large excess of that observed in the present copolymer, 9 mol%.

Low temperature ^{1}H and 2D NMR spectroscopy of the thermally labile [**FI^2-Ni$_2$-(*n*-butyl)$_2$**] derivative provides evidence for an agostic species at δ = -9.9 ppm. However, a second agostic interaction is observed in the bimetallic complex at δ = -4.2 ppm (Figure 14). The exclusivity of this peak to the bimetallic system suggests a second agostic interaction of an alkyl coordinated to one Ni communicating with a second Ni, suggested to be H_b, the γ-proton of a *sec*-Bu ligand (Scheme 3, Figure 14). Furthermore, the methyl branch signal at δ = 1.9 ppm remains unchanged with temperature, while the protons corresponding to those on the ß and γ carbons are both shifted slightly upfield and decrease in intensity as temperature is decreased. This observation, in conjunction with the exclusivity of the second peak to the bimetallic complex, also rules out the possibility of an equilibrium between species such as **V** and **W**, as this would also be present in the mononuclear complex NMR spectrum.

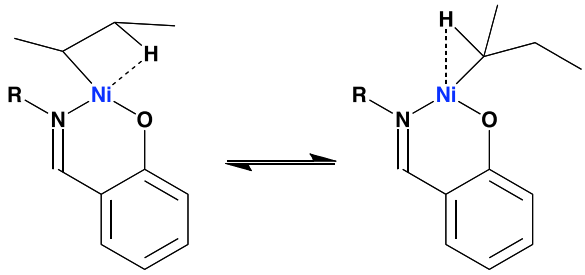

V **W**

Instead we confirm that the secondary agostic interaction involves a proton from the terminal carbon of the alkyl chain. Warming the NMR tube results in complete degradation of the complex by -10 °C. Furthermore, low temperature ^{1}H-^{1}H COSY NMR (Figure 15) shows definitively that one Ni-alkyl group has no agostic interactions, while another has agostic protons occupying both of the open coordination sites provided by the metal centers. Thus, the agostic proton on the γ C shows a cross peak with the protons on the β carbon and with no other. The β agostic proton shows two cross peaks, one with the adjacent α C-H at δ = -1.6 ppm and the other with γ C-H at δ = 1.5 ppm. The intensity of these crosspeaks suggest that this secondary agostic interaction (H_b) is somewhat weaker than that of the primary agostic interaction (H_a), possibly because of the increased degree of rotational freedom at the end of the *sec*-butyl chain. These experiments provide strong evidence that the vacant coordination site provided by the second Ni center during polymerizations is structurally/mechanistically communicating with the growing polymer on the first, and that this interaction is crucial for the reported increases polymerization activity and comonomer enchainment selectivity.

6. 5 Conclusion

The synthesis and characterization of two structurally rigid, neutrally charged bimetallic phenoxyiminato Ni(II) polymerization catalysts and their monometallic analogues is presented. The bimetallic catalysts evidence significant active center-active center cooperative effects in ethylene homopolymerization versus their mononuclear analogues. This cooperativity reflects that a rigid ligation environment that binds the Ni centers in close enough proximity. Evidence for the Ni···Ni communication includes agostic interactions which span both metal centers. Cooperative bimetallic catalytic interactions are associated with the doubling of the ethylene homopolymerization activity, as well as an increased polar

comonomer enchainment selectivity for functionalized norbornenes (4x) and for acrylates (~10-100x). The selectivity of the bimetallic systems for incorporating higher densities of comonomer, as well as their significantly higher oligo/polyethylene branch content, affords substancially altered polymer microstructures, with lowered melting points and greater solubility. Furthermore, the bimetallic catalysts exhibit significantly higher activities than the monometallic catalysts in the presence of polar solvents, while concurrently achieving higher molecular weights and branch densities. This feature permits using less rigorously dried media for polymerization while preserving the desired product microstructure. Mechanistic studies confirm that, as in the monometallic species,[8-11] polymerizations follow a coordinative insertion process, with enhanced monomer enchainment facilitated by the second catalytic center.

The point of greatest interest here is not the polymerization activities or levels of incorporation alone. It is instead that the cooperativity between group 10 catalytic centers, as shown with the present model complexes, affording both substancial enhancements in the catalyst/polymer properties that make the monometallic analogs of interest, while also expanding the scope of polymerizations possible.

6. 6 References

[1] (a) Esswein, A. J.; Veige, A. S.; Piccoli, P. M. B.; Schultz, A. J.; Nocera, D. G. *Organometallics* **2008**, *27,* 1073–1083. (b) Li, C.; Chen, L.; Garland, M. *J. Am. Chem. Soc.* **2007**, *129*, 13327-13334. (c) Weng, Z.; Teo, S.; Liu, Z.; Hor, T. S. A. *Organometallics* **2007**, *26*, 2950-2952. (d) Sammis, G. M.; Danjo, H.; Jacobsen, E. N. *J. Am. Chem. Soc.* **2004**, *126*, 9928-9929. (e) Collman, J. P.; Boulatov, R.; Sunderland, C. J.; Fu, L. *Chem. Rev.* **2004**, *104*, 561-588. (f) Krishnan, R.; Voo, J. K.; Riordan, C. G.; Zahkarov, L.; Rheingold, A. L. *J. Am. Chem. Soc.* **2003**, *125*, 4422-4423. (g) Moore, D. R.; Cheng, M.; Lobkovsky, E. B.; Coates, G. W. *J. Am. Chem. Soc.* **2003**, *125*, 11911-11924. (h) Trost, B. M.; Mino, T. *J. Am. Chem. Soc.* **2003**, *125*, 2410-2411. (i) Jacobsen, E. N. *Acc. Chem. Res.* **2000**, *33*, 421-431. (j) Molenveld, P.; Engbersen, J. F. J.; Reinhoudt, D. N. *Chem. Soc. Rev.* **2000**, *29*, 75-86. (k) Konsler, R. G.; Karl, J.; Jacobsen, E. N. *J. Am. Chem. Soc.* **1998**, *120*, 10780-10781. (l) Molenveld, P.; Kapsabelis, S.; Engbersen, J. F. J.; Reinhoudt, D. N. *J. Am. Chem. Soc.* **1997**, *119*, 2948-2949. (m) Mathews, R. C.; Howell, D. H.; Peng, W.-J.; Train, S. G.; Treleaven, W. D.; Stanley, G. G. *Angew. Chem., Int. Ed. Engl.* **1996**, *35*, 2253-2256. (n) Sawamura, M.; Sudoh, M.; Ito, Y. *J. Am. Chem. Soc.* **1996**, *118*, 3309-3310

[2] For recent reviews of single-site olefin polymerization, see: (a) Amin, S.B.; Marks, T.J. *Angew. Chem. Int. Ed.* **2008**, *47*, 2006-2025. (b) Marks, T.J., ed., *Proc. Nat. Acad. Sci. USA* **2006**, *103*, 15288-15354, and contributions therein (special feature on polymerization). (c) Suzuki, N. *Top. Organomet. Chem.*

2005, *8*, 177-216. (d) Alt, H. G. *Dalton T*. **2005**, *20,* 3271-3276. (e) Kaminsky, W. J. *Polym. Sci. Pol. Chem*. **2004**, *42*, 3911-3921. Wang, W.; Wang, L. *J. Polym. Mater*. **2003**, *20*, 1-8. (f) Delacroix, O.; Gladysz, *J. A. Chem. Comm*. **2003**, *6*, 665-675. (g) Kaminsky, W.; Arndt-Rosenau, M. *Applied Homogeneous Catalysis with Organometallic Compounds (2nd Edition)* Wiley-VCH Verlag GmbH, Weinheim, Germany 2002 (h) Lin, S.; Waymouth, R. M. *Accts. Chem. Res*. **2002**, *35*, 765-773. (i) Chen, E. Y-X.; Marks, T. J. *Chem. Rev*. **2000**, *100*, 1391-1434. (j) Gladysz, J. A. *Chem. Rev*. **2000**, *100*, and contributions therein. (k) Schweier, G.; Brintzinger, H-H. *Macromol. Symp*. **2001**, *173* 89-103. (l) Kaminsky, W. *Catal. Today* **2000**, *62*, 23-34. (l) Kaminsky, W. *Adv. Catal*. **2001**, *46*, 89-159.

[3] (a) Review: Li, H.; Marks, T. J. *Proc. Nat. Acad. Sci*. **2006**, *103*, 15295-15302, and references therein. (b) Li, H.; Stern, C. L.; Marks, T. J. *Macromolecules* **2005**, *38*, 9015-9027. (c) Li, H.; Li, L.; Schwartz, D.J.; Stern, C.L.; Marks, T.J. *J. Am. Chem. Soc*. **2005**, *127*, 14756-14768. (d) Li, H.; Li, L.; Marks, T.J. *Angew. Chem. Int. Ed*. **2004**, *43*, 4937-4940. (e) Guo, N.; Li, L.; Marks, T.J. *J. Am. Chem. Soc*. **2004**, *126*, 6542-6543. (f) Li, H.; Li, L.; Marks, T. J.; Liable-Sands, L.; Rheingold, A. L. *J.Am. Chem. Soc*. **2003**, *125*,10788-10789.

[4] (a) Guo, N.; Stern, C.L.; Marks, T.J. *J. Am. Chem. Soc*. **2008**, *130* (7),2246–2261. (b) Amin, S.; Marks, T.J., *J.Am.Chem.Soc*. **2007**, *129(10)*, 2938-2953. (c) Amin, S.; Marks, T.J., *J.Am.Chem.Soc*. **2006**, *128(14)*, 4506-4507. (d) Guo, N.; Li, L.; Marks, T.J., *J.Am.Chem.Soc*. **2004**, *126(21),* 6542-6543.

[5] (a) Salata, M.R.; Marks, T.J. *J. Am. Chem. Soc*. **2008**, *130*, 12-13. (b) Salata, M.R.; Marks, T.J. *Macromolecules*, In press.

[6] DFT computation: Motta, A.; Fragalá, I.; Marks, T.J., **2008**, *130*, 16533–16546.

[7] (a) Yanjarappa, M. J.; Sivaram, S. *Prog. Polym. Sci*. **2002**, *27*, 1347 and references therein. (b) Boffa, L. S.; Novak, B. M. *Chem. Rev*. **2000**, *100*, 1479 and references therein.

[8] (a) Domski, G.J.; Rose, J.M.; Coates, G.W.; Bolig, A.D.; Brookhart, M. *Prog. Polym. Sci*. **2007**, *32*, 30-92. (b) McCord, E.F.; McLain, S.J.; Nelson, L.T.J.; Ittel, S.D.; Tempel, D.; Killian, C.M.; Johnson, L.K.; Brookhart, M. *Macromolecules* **2007**, *40*, 410-420. (c) Zhang, L.; Brookhart, M.; White, P.S. *Organometallics* **2006**, *25*, 1868-1874. (d) Jenkins, J.C; Brookhart, M. J. *J. Am. Chem. Soc*. **2004**, *126*, 5827-5842. (e) Gibson, V.C.; Spitzmesser, S.K. *Chem. Rev*. **2003**, *103*, 283-316. (f) Ittel, S. D.; Brookhart, M. *Chem. Rev*. **2000**, *100*, 1169-1203. (g) Desjardins, S. Y.; Cavell, K. J.; Hoare, J. L.; Skelton, B. W.; Sobolev, A. N.; White, A. W.; Keim, W. *J. Organomet. Chem*. **1997**, *544*, 163. (h) Kurtev, K.; Tomov, A. *J. Mol. Catal*. **1994**, *88*, 141. (i) Klabunde, U.; Ittel, S. D. *J. Mol. Catal*. **1987**, *41*, 123. (j) Klabunde, U.; Mülhaupt, R.; Herskovitz, T.; Janowicz, A. H.; Calabrese, J.; Ittel, S. D. *J. Polym. Sci., Part A: Polym. Chem*. **1987**, *25*, 1989.

[9] Hicks, F. A.; Brookhart, M. *Organometallics* **2001**, *20*, 3217-3219

[10] Connor, E. F.; Younkin, T, R.; Henderson, J. I.; Hwang, S.; Grubbs, R. H.; Roberts, W. P.; Litzau, J. J., *J. Polym. Sci. Part A: Polymer Chem*. **2002,** *40*, 2842-2854.

[11] (a) Waltman, A.; Younkin, T.; Grubbs, R.H. *Organometallics* **2004**, *23*, 5121-5123. (b) Connor, E. F.; Younkin, T, R.; Henderson, J. I.; Hwang, S.; Grubbs, R. H.; Roberts, W. P.; Litzau, J. J., *J. Polym. Sci. Part A: Polymer Chem*. **2002,** *40*, 2842-2854. (c) Younkin, T. R.; Connor, E. F.; Henderson, J. I.; Friedrich, S. K.; Grubbs, R. H.; Bansleben, D. A. *Science* **2000**, *287*, 460. (d) Wang, C.; Friedrich, S.

K.; Younkin, T. R.; Li, R. T.; Grubbs, R. H.; Bansleben, D. A.; Day, M. W. *Organometallics* **1998**, *17*, 3149.

[12] (a) Cotts, P.M.; Guan, Z.; McCord, E. F.; McLain, S. *Macromolecules* **2000**, *33*, 6945 (b) Kang, M.; Sen, A. *Organometallics* **2005**, *24*, 3508-3515.

[13] (a) Hu, T.; Li, Y.; Li, Y.; Hu, N. *J. Polym. Sci. Part A: Polymer Chem.* **2006,** *253* 155-164. (b) Li, X.; Li, Y.; Li, Y.; Chen, Y.; Hu, N. *Organometallics* **2005**, *24*, 2502-2510. (c) Sujith, S.; Joe, D. J.; Na, S. J.; Park, Y.; Choi, C. H.; Lee, B. Y. *Macromolecules* **2005**, 38, 10027-10033. (d) Jenkins, J. C.; Brookhart, M. *J. Am. Chem. Soc.* **2004**, *126*, 5824-5827. (e) Johnson L.; Bennett, A.; Dobbs, K.; Hauptman, E.; Ionkin, A.; Ittel, S.; McCord, E.; McLain, S.; Radzewich, C.; Yin, Z.; Wang, L.; Wang, Y.; Brookhart, M. *PMSE-Preprints of the 22 ACS National Meeting, Orlando, FL* **2002**, 319(86). (f) Wang, L.; Hauptman, E.; Johnson, L. K.; McCord, E. F.; Wang Y. Ittel, S. D.; Radzewich, C. E.; Kunitsky, K.; Ionkin, A. S. *PMSE-Preprints of the 22 ACS National Meeting, Orlando, FL* **2002**, 319(86). (g) Johnson, L., Bennett, A.; Dobbs, K.; Haupman, A.; Ionkin, A.; Ittel, S.; McCord, E.; McLain, S.; Radsewich, C.; Yin, Z.; Wang, L.; Wang, Y.; Brookhart, M., *PMSE-Preprints of the 22 ACS National Meeting, Orlando, FL* **2002**, 319(86), (h) Johnson, L.; Bennett, A.; Dobbs, K., Hauptman E.; Ionkin, A.; Ittel, S.; McCord, E.; McLain, S.; Radzewich, C.; Yin, Z.; Wang, L.; Wang, Y.; Brookhart, M. *PMSE-Preprints of the 22 ACS National Meeting, Orlando, FL* **2002**, 319(86). (i) McCord, E. F. ; McLain, S. J.; Nelson, L. T. J.; Arthur, S. D.; Coughlin, E. B.; Ittel S. D.; Johnson, L. K.; Tempel D.; Killian, C. M.; Brookhart, M. *Macromolecules* **2001**, *34*, 362-371. (j) Bauers, F. M.; Mecking, S. *Macromolecules* **2001**, *34*, 1165-1171.

[14] Rodriguez, B.A.; Delferro, M.: Marks, T.J., *Organometallics* **2008**, *27,* 2166-2168.

[15] (a) Chen, Q.; Yu, J.; Huang, J. *Organometallics* **2007**, *26,* 617-625. (b) Hu, T.; Tang, L.; Li, X.; Li, Y.; Hu, N. *Organometallics* **2005**, *24*, 2628-2632. (c) Zhang, D.; Jin, G. *Organometallics*, **2003**, *22*, 2851-2854. (d) Akitsu, T.; Einaga, Y. *Polyhedron*, **2005**, *24*, 1869-1877. (e) Wehrmann, P.; Mecking, S. *Organometallics*, **2008**, *27*, 1399-1408 and references therein.

[16] Pangborn, A. B.; Giardello, M. A.; Grubbs, R. H.; Rosen, R. K.; Timmers F. J., *Organometallics*, **1996**, *15*, 1518-1520.

[17] Carmona, E.; Marin, Jose M.; Paneque, M.; Poveda, M. L. *Organometallics*, **1987**, *6*, 1757-1765.

[18] Van Soolingen, J.; Verkruijsse, H. D.; Keegstra, M. A.; Brandsma, L., *Synth. Commun.*, **1990**, *20*, 3153.

[19] Assay procedure from : (a) Gates, D. P.; Svejda, S. A.; Onate, E.; Killian, C. M.; Johnson, L. K.; White, P. S.; Brookhart, M. *Macromolecules* **2000**, *33*, 2320. (b) Polyethylene methyl branching densities were determined by ^{1}H NMR spectroscopy using the ratio of the integral of methyl groups to the overall number of carbons (methyl + methylene + methine), and are reported as branches per 1000 carbons. (c) Chen, Q., Yu, J, Huang, J *Organometallics*, **2007**, *26,* 617-625. (d) Hu, T.; Tang, L.; Li, X.; Li, Y.; Hu, N. *Organometallics*, **2005**, *24*, 2628-2632. (e) Zhang, D.; Jin, G. *Organometallics*, **2003**, *22*, 2851-2854. (f) Liu, W.; Ray D. G. III; Rinaldi, P. L. *Macromolecules* **1999**, *32*, 3817-3819. (g) Jurkiewicz, A.; Eilberts, N. W.; Hsieh, E. T., *Macromolecules* **1999**, *32*, 5471-5476.

[20] *SAINT Software Users Guide*, Version 6.0; Bruker Analytical X-ray Systems: Madison, WI, **1999**. G. M. Sheldrick, *SADABS*; Bruker Analytical X-ray Systems, Madison, WI, **1999**. G. M. Sheldrick, *SHELXL-97*, *Program for Crystal Structure Refinement*; University of Göttingen: Germany, **1997**.

[21] Connor, E. F.; Younkin, T. R.; Henderson, J. I.; Waltman, A. W.; Grubbs, R. H., *Chem. Commun.*, **2003**, 2272-2273.

[22] D. V. Soldatov, A. T. Henegouwen, G. D. Enright, C. I. Ratcliffe, J. A. Ripmeester, *Inorg. Chem.* **2001**, 40, 1626-1636.

[23] (a) Diaz-Requejo, M.; Werhmann, P.; Leatherman, M. D.; Trofimenko, S.; Mecking, S. Brookhart, M.; Perez, P. J. *Macromolecules* **2005**, *38*, 4966-4969. (b) Strbrany, R. T.; Schulz, D. N.; Kacker, S.; Patil, A. O.; Baugh, L. S.; Rucker, S. P.; Zushma, S.; Berluche, E.; Sissano, J. A. *Macromolecules* **2003**, *26*, 8584-8586. (c) Johnson, L. K.; Mecking, S.; Brookhart, M. *J. Am. Chem. Soc.* **1996**, *118*, 267-268.

[24] (a) Borkar, S.; Yennawar, H.; Sen, A. *Organometallics* **2007**, *26*, 4711-4714. (b) Sen, A.; Borkar, S. *J. of Organomet. Chem.* **2007**, *692*, 3291-3299.

[25] (a) Skupov, K. M.; Marella, P. R.; Simard, M.; Yap, G. A.; Allen, N.; Conner, D.; Goodall, B. L.; Claverie, J. P., *Macromol. Rapid. Commun,* **2007**, *28,* 2033-2038. (b) Ydens, I.; Degee, P.; Haddleton D. M.; Dubois, P. *Eur. Polymer Journal*, **2005**, *41*, 2255-2263. (c) Elia, C.; Elyashiv-Barad, S.; Sen, A. *Organometallics,* **2002**, *21,* 4249-4256, (d) Drent, E.; van Dijk, R.; van Ginkel, R.; van Oort, B.; Pugh, R. I. *Chem. Commun.*, **2002**, 744-745.

[26] Kuptsov, A. H.; Zhizhan, G. N., *Handbook of FT Raman and Infrared Spectra of Polymers*, Elsevier, *New York*, **1998**.

[27] (a) Tian, G.; Boone, H. W.; Novak, B. M. *Macromolecules* **2001**, *34*, 7656-7663. (b) Elia, C.; Elyashiv-Barad, S.; Sen, A.; Lopez-Fernandez, R.; Albéniz, A. C.; Espinet, P. *Organometallics* **2002**, *21*, 4249-4256. (c) Sen, A.; Borkar, S. *J. Organomet. Chem.* **2007** *692*, 3291-3299. (d) Kang, M.; Sen, A. *Organometallics* **2005**, *24*, 3508-3515.

[28] (a) Hughes, R. P.; Laritchev, R. B.; Zakharov, L. V.; Rheingold, A. L. *Organometallics* **2005,** *24,* 4845-4848. (b) Toscano, P. J.; Brand, H.; Liu, S.; Zubieta, *J. Inorg. Chem.* **1990**, *29*, 2101-2105 and references therein. (c) Kerr, J. A. *A. Chem Rev.* **1966** *66* 465.

[29] (a) Ydens, I.; Degee, P.; Haddleton, D. M.; Dubois, P. *Eur. Polymer Journal* **2005**, *41*, 2255-2263. (b) Buback, M.; Dietzsch, H. *Macrol. Chem. Phys.* **2001**, *202*, 1173-1181. (c) Mayo, F. R.; Lewis, F. M. *J. Am. Chem. Soc.* **1944**, *66*, 1594-1601.

[30] (a) *Polymer Handbook 2nd ed* Brandrup, J.; Immergut, E. H.; *John Wiley & Sons, Inc.* New York **1975**. (b) *Introduction to Polymers* Young, R. J. *Chapman and Hall Ltd* London **1981**.

[31] *Spartan '06*; Wavefunction, Inc.: Irvine, CA, **2006.**

7

Appendix

Appendix 1

A study on the coordinative versatility of the zwitterionic *S,N,S* ligand $EtNHC(S)Ph_2P{=}NPPh_2C(S)NEt$ in its anionic, neutral and cationic forms. Determination of absolute pK_a values in CH_2Cl_2 of Rh^I complexes.

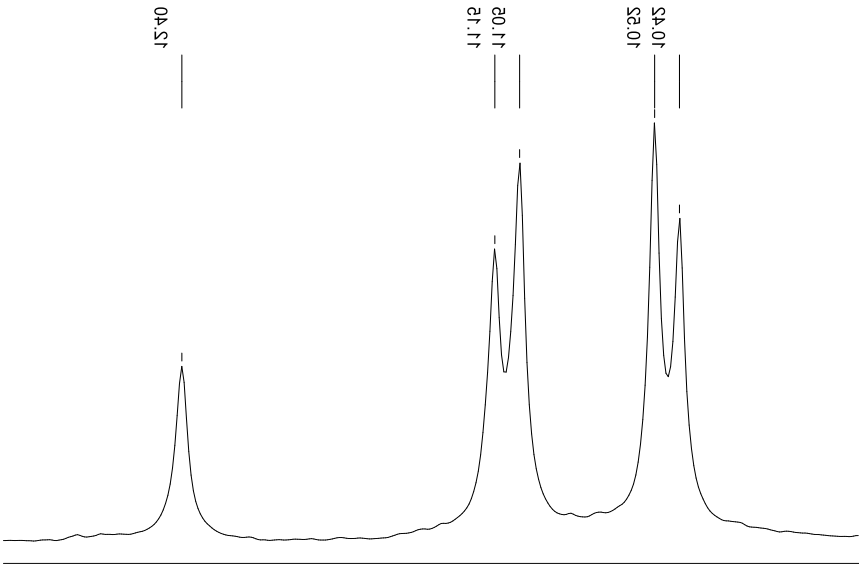

Figure S1. *In situ* $^{31}P\{^1H\}$ NMR spectrum of the reaction $[Rh(cod)_2Cl]_2$ + 2HEtSNS in $CDCl_3$.

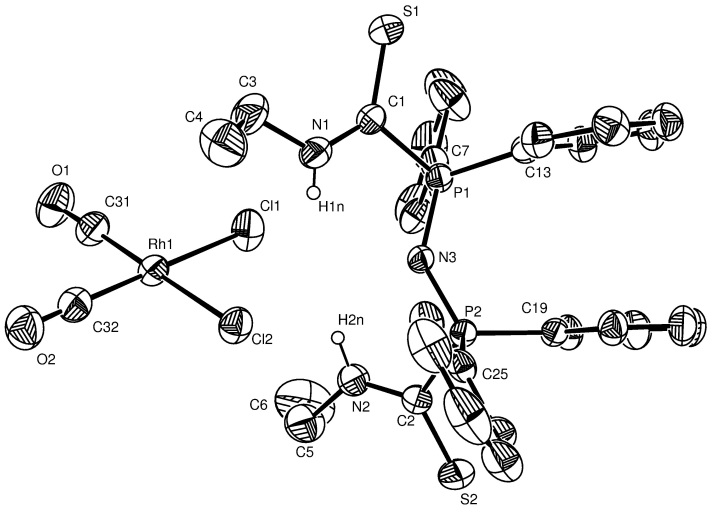

Figure S2. ORTEP plot of the molecular structure of **5**. Thermal ellipsoid are drawn at 30% probability level

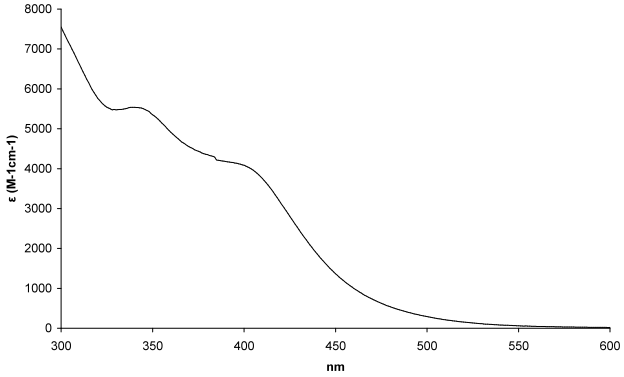

Figure S3. UV-Visible spectra (300-600 nm) of [Rh(CO)(EtSNS)] (C_{Rh} = 1x10^{-3} M, λ_{max} = 397 nm).

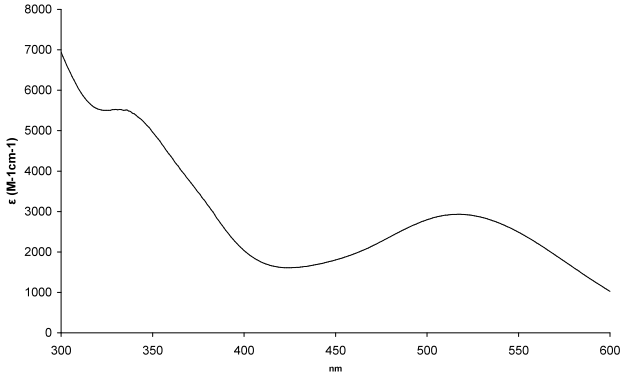

Figure S4. UV-Visible spectra (300-600 nm) of [Rh(CO)(HEtSNS)]OTf (C_{Rh} = 1x10^{-3} M, λ_{max} = 517 nm).

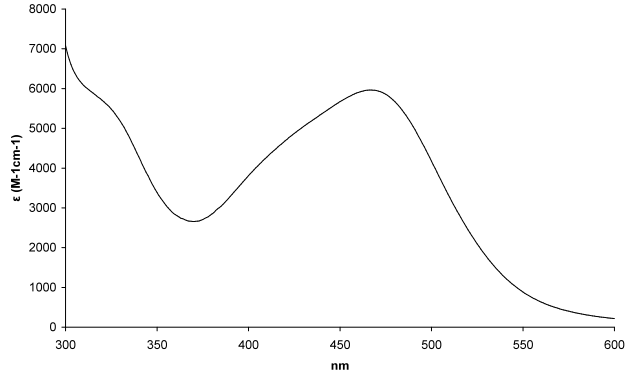

Figure S5. UV-Visible spectra (300-600 nm) of [Rh(CO)(H_2EtSNS)]$(OTf)_2$ (C_{Rh} = 1x10^{-3} M, λ_{max} = 467 nm).

Appendix 2

Oxidative Addition of Iodomethane to Charge-tuned Rh^I Complexes

Table S1. Mulliken populations in gas phase and solution (PCM, CH_2Cl_2) for **1**, **2** and **3**. Only the relevant atoms are reported. For compound **2**, the protonation is on the atom N1 [B3LYP/BS-I//B3LYP/BS-I; BS-I = 6-31g** + DGDZVP (Rh)]

					Gas					
	Rh	**S1**	**S2**	**N1**	**N2**	**N3**	**P1**	**P2**	**C**	**O**
1	-0,217	-0,093	-0,093	-0,382	-0,382	-0,833	0,926	0,926	0,341	-0,289
2	-0,191	0,062	-0,039	-0,413	-0,355	-0,838	0,897	0,925	0,340	-0,249
3	-0,151	0,101	0,101	-0,406	-0,406	-0,846	0,894	0,894	0,335	-0,215
					CH_2Cl_2					
	Rh	**S1**	**S2**	**N1**	**N2**	**N3**	**P1**	**P2**	**C**	**O**
1	-0,229	-0,164	-0,165	-0,364	-0,364	-0,858	0,927	0,927	0,347	-0,327
2	-0,193	0,046	-0,112	-0,408	-0,360	-0,861	0,896	0,926	0,343	-0,295
3	-0,158	0,079	0,078	-0,401	-0,406	-0,862	0,896	0,896	0,338	-0,264

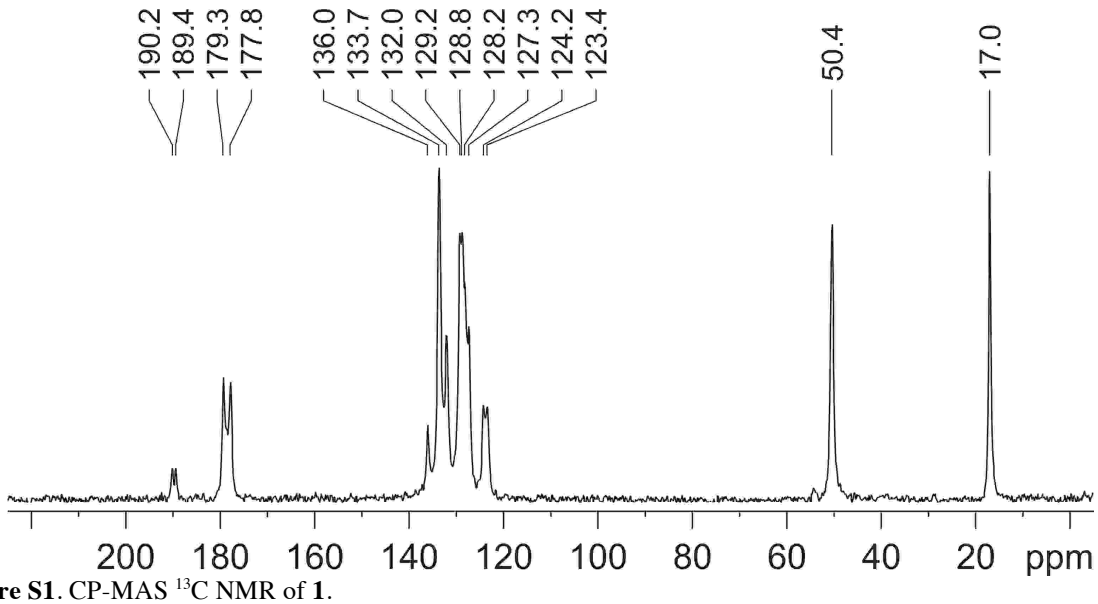

Figure S1. CP-MAS ^{13}C NMR of **1**.

CP-MAS ^{13}C NMR: δ = 189.8 (d, $^1J_{C,Rh}$ = 80.5 Hz, CO), 178.5 (d, $^1J_{C,P}$ = 151 Hz, C=N), 136.0-123.4 (m, Ph), 50.4 (s, -$CH_2$$CH_3$), 17.0 (s, -$CH_2$$CH_3$) ppm.

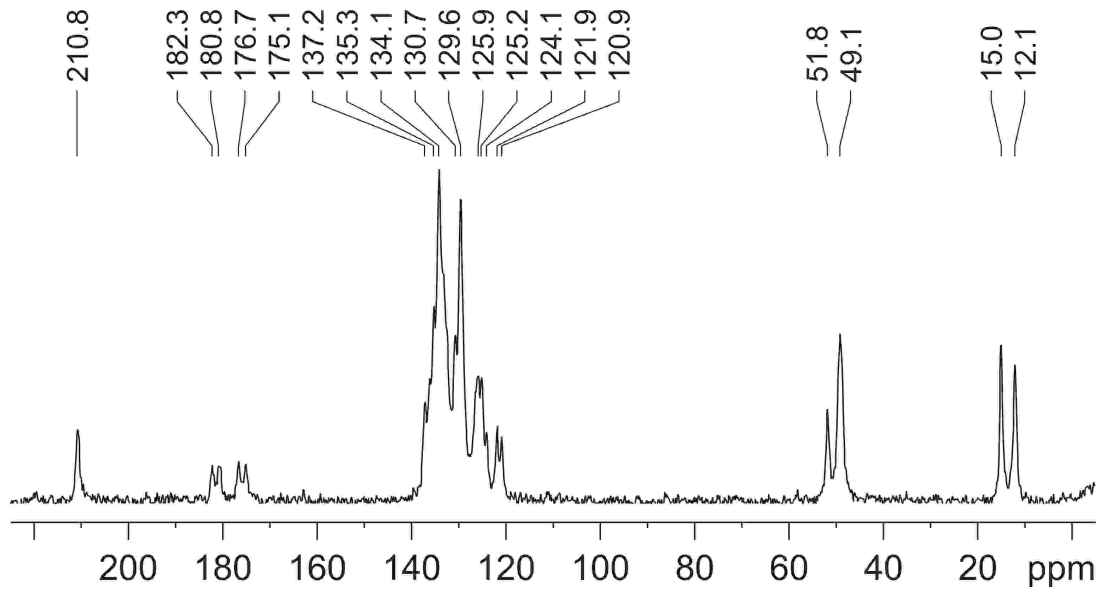

Figure S2. CP-MAS ^{13}C NMR of **4**.

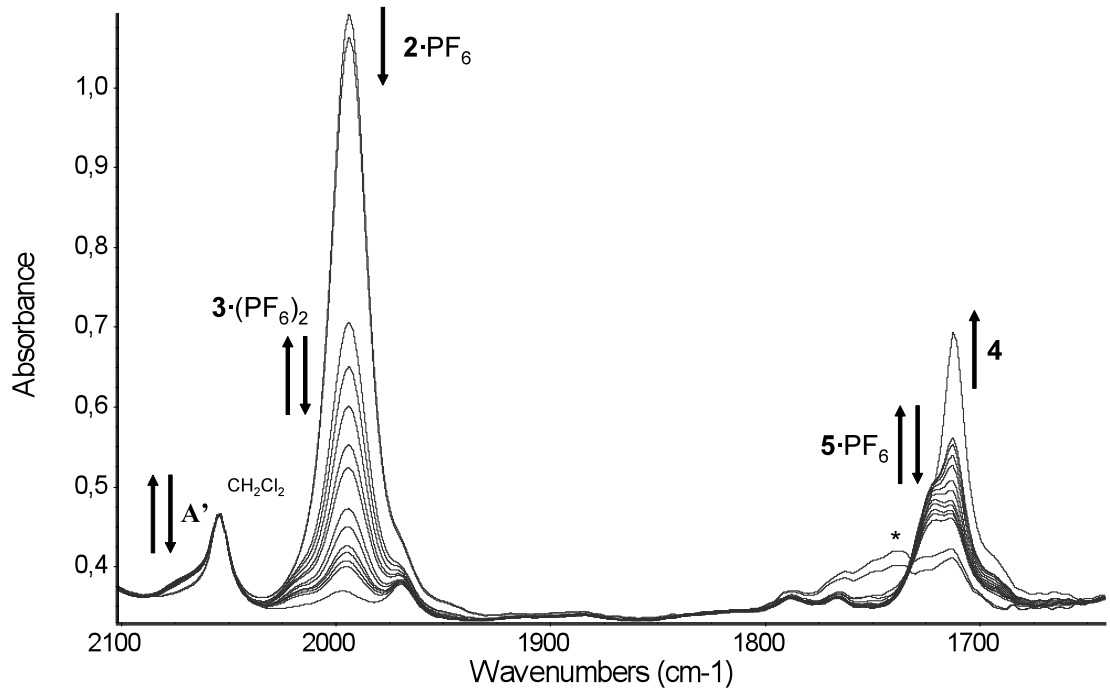

Figure S3. Superimposed FTIR spectra in CH_2Cl_2 solution of **2**·PF_6 + CH_3I. (* = possible isomer of **5**·PF_6)

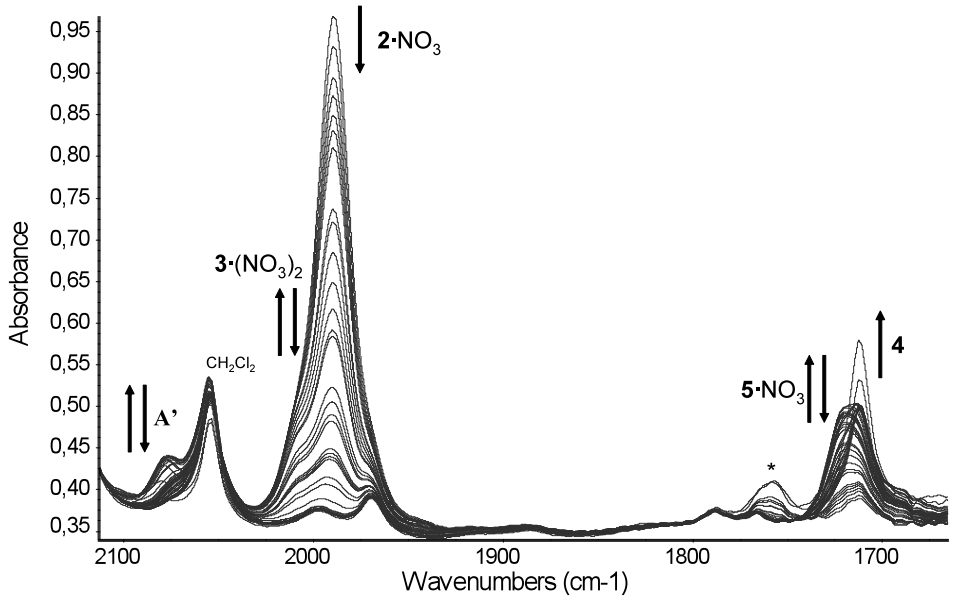

Figure S4. Superimposed FTIR spectra in CH_2Cl_2 solution of **2**·NO_3 + CH_3I. (* = possible isomer of **5**·NO_3)

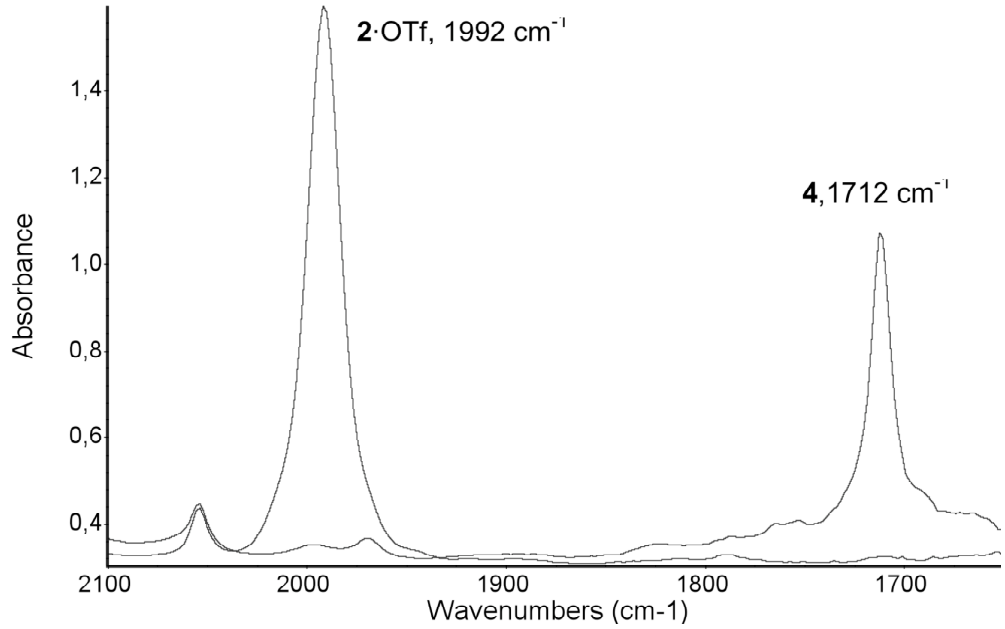

Figure S5. Superimposed FTIR spectra in CH_2Cl_2 solution of **2**·OTf + CH_3I at the beginning (1992 cm^{-1}) and at the end (1712 cm^{-1}) of the reaction.

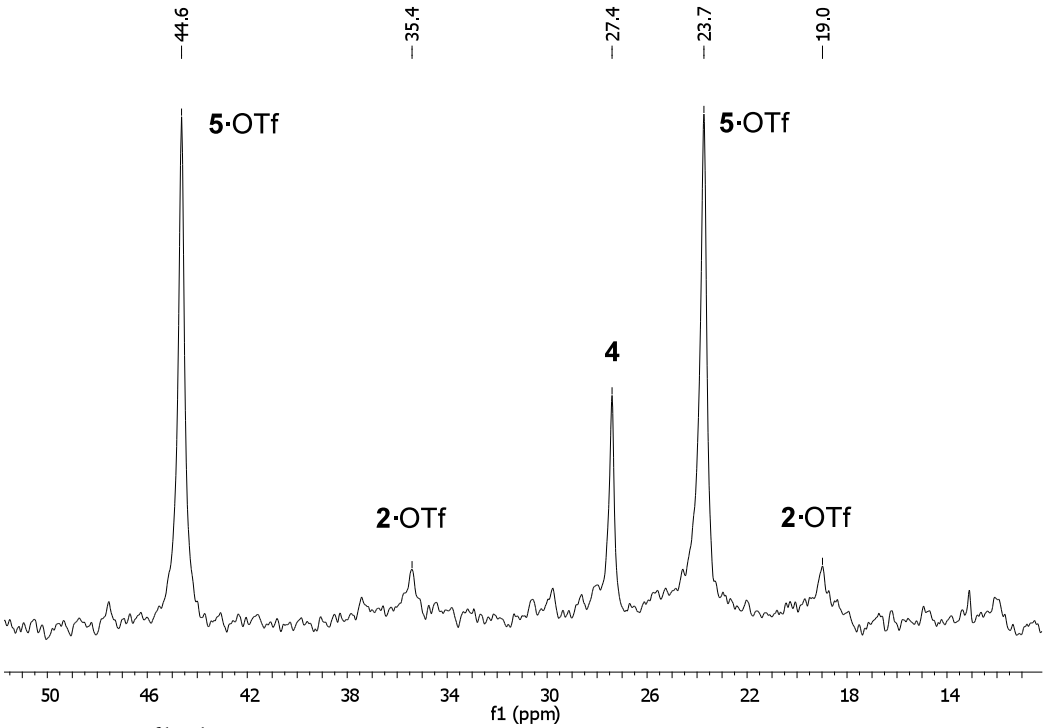

Figure S6. $^{31}P\{^{1}H\}$ NMR spectrum of the reaction of **2**·OTf + CH_3I in CD_2Cl_2 after 2 hours.

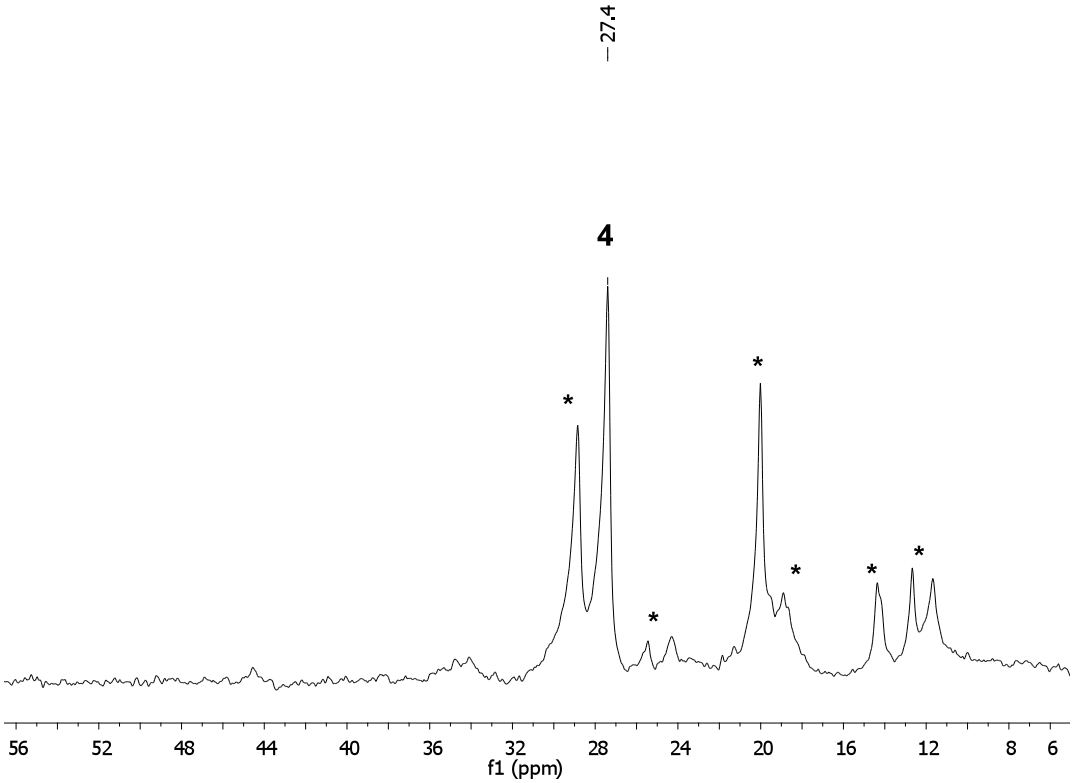

Figure S7. $^{31}P\{^{1}H\}$ NMR spectrum of the reaction of **2**·OTf + CH_3I in CD_2Cl_2 after 2 days; * corresponds to unidentified decomposition products.

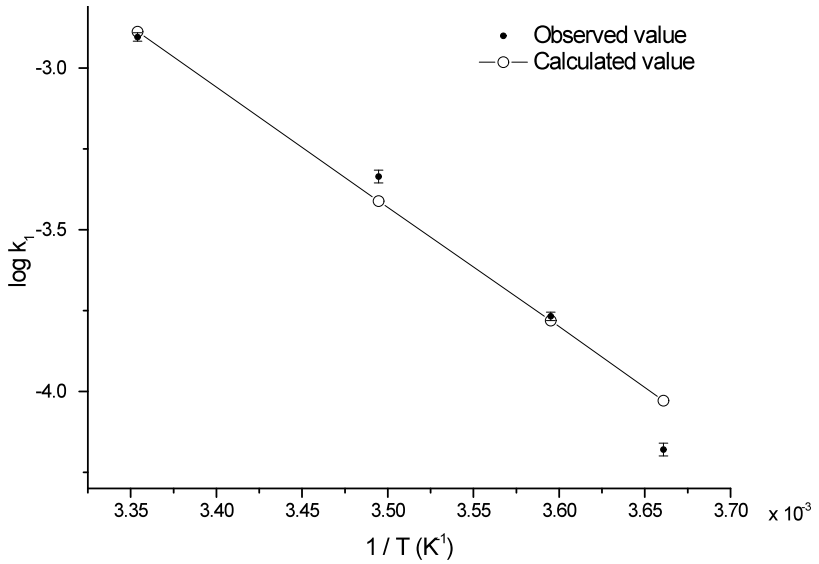

Figure S8. Linearized Eyring plot [log (k_1/T) *vs.* 1/T] for the reaction of **1** with CH_3I

Table S2. Second-order rate constants for the reaction **2**·PF_6 + CH_3I at different temperatures (standard deviations are given in parentheses). The corresponding least-square sample standard deviations (σ) are also reported.

Temperature (K)	k (M^{-1} s^{-1})	σ
280.16	0.64(3) x 10^{-5}	1.02 x 10^{-3}
291.16	1.71(2) x 10^{-5}	3.07 x 10^{-3}
298.16	2.56(6) x 10^{-5}	7.66 x 10^{-3}

[a] $\sigma = [\Sigma_i (I_i^o - I_i^c)^2/(n-m)]^{1/2}$, where I_i^o, I_i^c are the observed and calculated integral values, *i* is the number of the spectrum, *n* is the number of observations and *m* is the number of parameters refined.

Acknowledgments

Vorrei prima di tutto ringraziare i miei genitori per avermi aiutato spiritualmente, ma soprattutto economicamente in questi anni. Questo lavoro è dedicato a voi.
Un doveroso grazie al mio *"mentore"* Prof. Daniele Cauzzi. Posso dire di aver trovato un amico con la A maiuscola con i suoi pregi e i suoi tanti difetti. Tutto quello che ho imparato in questi tre anni lo devo a lui e alle tante cene e aperitivi che abbiamo fatto!!!
Un ringraziamento particolare al Prof. Tiripicchio, Prof. Predieri e alla Prof.ssa Graiff per tutto quello che hanno fatto per me.
A special thanks to Prof. Tobin J. Marks of the Northwestern University, Evanston, Illinois, USA for allowing me to work in his laboratory for six months.
Grazie a tutti i "personaggi" che ho incontrato in dipartimento e fuori...in particolare al Genna, Tego, Lucio, Beppe, Gardella, Panama, Nicoletta, Mattia e chi più ne ha ne metta!!!!
Un saluto e un grazie a tutti i miei amici, in particolare al Moss. Ti porterò sempre nel mio cuore.
Un ringraziamento particolare al mio amico Vincenzo, con il quale ho condiviso tanti anni insieme (superiori, università, dottorato e post-doc) e che ancora passeremo anche se a 10 mila miglia da casa!!!
Infine vorrei dire a Carlotta che torno (almeno spero) e che sei molto importante!!!

Massimiliano Delferro